

Synthesis and evaluation of sesamol derivatives as inhibitors of monoamine oxidase

I Engelbrecht
21639159

Dissertation submitted in fulfilment of the requirements for the degree *Magister Scientiae* in Pharmaceutical Chemistry at the Potchefstroom Campus of the North-West University

Supervisor: Dr A Petzer
Co-Supervisor: Prof JP Petzer

November 2014



The financial assistance of the National Research Foundation (DAAD-NRF) towards this research is hereby acknowledged. Opinions expressed and conclusions arrived at, are those of the author and are not necessarily to be attributed to the DAAD-NRF.

TABLE OF CONTENT

LIST OF ABBREVIATIONS	vii
LIST OF FIGURES	ix
LIST OF TABLES	xiii
LIST OF KEYWORDS	xiii
ABSTRACT	xiv
UITTREKSEL	xvi
CHAPTER 1: Introduction and rationale	1
1.1. Introduction and overview	1
1.2. Rationale	3
1.3. Hypothesis of this study	5
1.4. Objectives of this study	6
CHAPTER 2: Literature Overview	7
2.1. Parkinson's disease	7
2.1.1. General background	7
2.1.2. Etiology	8
2.1.3. Neurochemical and neuropathological features of Parkinson's disease	9
2.1.4. Pathogenesis and genetics of Parkinson's disease	10
2.1.4.1. Pathogenesis	10
2.1.4.2. Genetics	11
2.1.5. Treatment of Parkinson's disease	13
2.1.5.1. Symptomatic treatment of Parkinson's disease	13
2.1.5.2. Drugs for neuroprotection	16

2.2. Animal models of Parkinson's disease	18
2.2.1. 1-Methyl-4-phenyl-1,2,3,6-tetrahydropyridine	18
2.2.2. 6-Hydroxydopamine	21
2.2.3. Rotenone	24
2.2.4. Paraquat	24
2.3. Monoamine oxidase	25
2.3.1. General background and tissue distribution	25
2.3.2. Mechanism of action of MAO	27
2.3.3. Biological function of MAO-A	30
2.3.4. The potential role of MAO-A in Parkinson's disease	31
2.3.5. Inhibitors of MAO-A	32
2.3.6. The three dimensional structure of MAO-A	33
2.3.7. Biological function of MAO-B	34
2.3.8. The potential role of MAO-B in Parkinson's disease	34
2.3.9. Inhibitors of MAO-B	35
2.3.10. The three dimensional structure of MAO-B	37
2.3.11. <i>In vitro</i> measurements of MAO activity	39
2.4. Copper-containing amine oxidases	42
2.4.1. General background and classification	42
2.4.2. Substrates and known inhibitors of copper-containing amine oxidases	43
2.4.3. Biological function and mechanism of action of SSAOs	44
2.4.4. The three-dimensional structure of the copper-containing amine oxidases	46
2.5. Conclusion	46

CHAPTER 3: Preparation of synthetic targets	48
3.1. Introduction	48
3.2. Synthesis of target compounds	50
3.2.1. Literature method	50
3.2.2. Materials and instrumentation	51
3.2.3. Detailed synthetic procedures	52
3.2.3.1. Procedure for the synthesis of C5-substituted sesamol derivatives	52
3.2.3.2. Procedure for the synthesis of 6-Hydroxy-1,4-benzodioxane	53
3.2.3.3. Procedure for the synthesis of C6-substituted benzodioxane derivatives	54
3.3. Physical characterisation results	55
3.3.1. NMR-spectra	55
3.3.2. Interpretation of mass spectra	73
3.3.3. Interpretation of HPLC analyses	74
3.4. Conclusion	75
CHAPTER 4: Enzymology	76
4.1. Introduction	76
4.2. MAO activity measurements	76
4.2.1. General background	76
4.2.2. Materials and instrumentation	77
4.2.3. Experimental method for IC ₅₀ determination	77
4.2.3.1. Method	78
4.2.3.2. Results	81

4.2.4. Experimental method for the determination of the reversibility of inhibition	89
4.2.4.1. Method	89
4.2.4.2. Results	92
4.2.5. Experimental method for construction of Lineweaver-Burk plots	92
4.2.5.1. Method	93
4.2.5.2. Results	94
4.3. Conclusion	95
CHAPTER 5: Conclusion	97
BIBLIOGRAPHY	103
APPENDIX	107
Section 1: $^1\text{H-NMR}$ and $^{13}\text{C-NMR}$ spectra	107
Section 2: Mass spectra	139
Section 3: HPLC chromatograms	148

LIST OF ABBREVIATIONS

5-HT 5-Hydroxytryptamine/ serotonin

6-OHDA 6-Hydroxydopamine

A

ADH Aldehyde dehydrogenase

APCI Atmospheric-pressure chemical ionization

C

C-terminal Carboxy-terminal

Cys Cysteine

D

DAT Dopamine transporter

DMF N,N-Dimethylformamide

F

FAD Flavin adenine dinucleotide

G

GDNF Glial-derived neurotrophic factor

H

HPLC High pressure liquid chromatography

I

Ile Isoleucine

iNOS Inducible nitric oxide synthase

L

L-dopa Levodopa

Leu Leucine

LRRK-2 Leucine rich repeat kinase 2

M

MAO	Monoamine oxidase
MAO-A	Monoamine oxidase type A
MAO-B	Monoamine oxidase type B
mCPBA	<i>meta</i> -Chloroperoxybenzoic acid
MMDP ⁺	1-Methyl-4-(1-methylpyrrol-2-yl)-2,3-dihydropyridinium
MMTP	1-Methyl-4-(1-methylpyrrol-2-yl)-1,2,3,6-tetrahydropyridine
MPDP ⁺	1-Methyl-4-phenyl-2,3-dihydropyridinium
MPP ⁺	1-Methyl-4-phenylpyridinium
MPPP	1-Methyl-4-phenyl-4-propionpiperidine
MPTP	1-Methyl-4-phenyl-1,2,3,6-tetrahydropyridine
MS	Mass spectrometry

N

NMDA	N-Methyl-D-aspartate
NMR	Nuclear magnetic resonance
NO	Nitric oxide

P

Phe	Phenylalanine
-----	---------------

S

SET	Single electron transfer
SNpc	Substantia nigra pars compacta
SSAO	Semicarbazide-sensitive amine oxidase

T

TLC	Thin layer chromatography
TPQ	Topa-quinone
Tyr	Tyrosine

U

UCH-L1	Ubiquitin C-terminal hydrolase-L1
--------	-----------------------------------

LIST OF FIGURES

Figure 1.1.	The chemical structures of phthalide (1), sesamol (2) and benzodioxane (3)	3
Figure 1.2.	A proposed pharmacophore for MAO-B inhibition with 4a and 5a mapped	4
Figure 2.1.	The various pathological and genetic mechanisms leading up to neurodegeneration in Parkinson's disease	11
Figure 2.2.	Drugs frequently used in an <i>L</i> -dopa regime for the symptomatic treatment of Parkinson's disease	13
Figure 2.3.	Chemical structures of drugs frequently used in the symptomatic treatment of Parkinson's disease	15
Figure 2.4.	Chemical structures of agents for potential neuroprotective therapeutic use in Parkinson's disease	18
Figure 2.5.	The chemical structures of MPPP and MPTP	19
Figure 2.6.	The MAO-B catalysed oxidation of MPTP to MPDP ⁺ and the pyridinium metabolite, MPP ⁺	20
Figure 2.7.	Schematic representation of the detailed pathological mechanism of MPTP	21
Figure 2.8.	The oxidation of 6-OHDA	23
Figure 2.9.	The potential pathological mechanism of 6-OHDA toxicity	23
Figure 2.10.	The chemical structure of the insecticide rotenone	24
Figure 2.11.	The chemical structures of the MPTP metabolite, MPP ⁺ , and paraquat to demonstrate the structural similarities between these compounds	25
Figure 2.12.	The mechanism leading up to the potentially fatal 'cheese reaction'	26
Figure 2.13.	The simplistic oxidative deamination reaction catalysed by MAO	28

Figure 2.14.	A schematic representation of the catalytic reaction pathway followed by MAO-A and MAO-B	28
Figure 2.15.	The polar nucleophilic mechanism of MAO catalysis	29
Figure 2.16.	The SET mechanism of MAO catalysis	30
Figure 2.17.	The chemical structures of several MAO-A inhibitors	32
Figure 2.18.	A ribbon diagram representing the structure of human MAO-A	33
Figure 2.19.	The chemical structure of the selective irreversible MAO-B inhibitor, ladostigil	36
Figure 2.20.	The chemical structures of several reversible MAO-B inhibitors	37
Figure 2.21.	Ribbon diagram representing the structure of human MAO-B in monomeric form	38
Figure 2.22	Comparison of the active site cavities of rat MAO-A and human MAO-B with the selective inhibitors clorgyline and rasagiline, respectively, bound	38
Figure 2.23.	The peroxidase-linked continuous assay for amine oxidase enzymes	40
Figure 2.24.	The MAO-B catalysed oxidation of MMTP to the corresponding dihydropyridinium product	41
Figure 2.25.	The MAO-B catalysed oxidation of benzylamine	41
Figure 2.26.	The MAO-A/B catalysed oxidation of kynuramine to the fluorescent metabolite, 4-hydroxyquinoline	42
Figure 2.27.	A schematic illustration of the different classes of amine oxidases	42
Figure 2.28.	The chemical structures of several substrates of copper-containing amine oxidases	43
Figure 2.29.	The chemical structures of several SSAO inhibitors	44
Figure 2.30.	Simplified reaction of the oxidative deamination of primary amines to yield the resulting aldehydes via SSAOs	44
Figure 2.31.	The mechanism of action of SSAO, demonstrating the Schiff base	45

	formation	
Figure 2.32.	The most important structural motifs of SSAOs	46
Figure 3.1.	The chemical structures of phthalide (1), sesamol (2) and benzodioxane (3)	48
Figure 3.2.	The general synthetic route for the synthesis of C5-substituted sesamol derivatives (4a–h)	50
Figure 3.3.	The general synthetic route for the synthesis of C6-substituted benzodioxane derivatives (5a–h)	51
Figure 3.4.	The general synthetic route for the synthesis of 6-hydroxy-1,4-benzodioxane (7)	51
Figure 3.5.	Experimental setup for the synthesis of C5-substituted sesamol derivatives (4a–h)	53
Figure 3.6.	Experimental setup for the synthesis of 6-hydroxy-1,4-benzodioxane (7)	54
Figure 3.7.	Experimental setup for the synthesis of the C6-substituted benzodioxane (5a–h)	55
Figure 4.1.	The oxidation of kynuramine by MAO-A and MAO-B to yield 4-hydroxyquinoline	77
Figure 4.2.	An example of a calibration curve routinely constructed in this study	79
Figure 4.3.	Flow diagram summarising the experimental method for IC ₅₀ determination	80
Figure 4.4.	Comparison between sesamol (4a) and benzodioxane (5a) derivatives to establish the most suitable scaffold for MAO-B inhibition	83
Figure 4.5.	Comparison of the effect of the side chain length of sesamol derivatives (4a vs. 4d and 4e) on MAO-B inhibition potency	84
Figure 4.6.	Comparison of the effect of the side chain length of benzodioxane	85

	derivatives (5a vs. 5d and 5e) on MAO-B inhibition potency	
Figure 4.7.	The effect that halogen substitution on the benzyloxy phenyl ring of benzodioxane derivatives has on MAO-B inhibition potency	85
Figure 4.8.	The effect of the phenoxyethoxy side chain on the MAO-B inhibitory potencies of sesamol and benzodioxane derivatives	86
Figure 4.9.	The effect that halogen substitution on the phenoxyethoxy phenyl ring of sesamol and benzodioxane derivatives has on MAO-B inhibition potency	87
Figure 4.10.	Comparison of the MAO-B inhibition potencies of 5-benzyloxyphthalide with those of 4a and 5a	88
Figure 4.11.	Comparison of the MAO-A inhibition potencies of 5-benzyloxyphthalide to those of the sesamol and benzodioxane derivatives	89
Figure 4.12.	Flow diagram summarising the experimental method for the determination of the reversibility of inhibition by dialysis	91
Figure 4.13.	Histogram depicting the reversibility of inhibition of MAO-B by compound 5c	92
Figure 4.14.	Flow diagram summarising the experimental method for constructing Lineweaver-Burk plots	94
Figure 4.15.	Lineweaver-Burk plots of the human MAO-B activities in the absence and presence of various concentrations of 5c ($IC_{50} = 0.045 \mu M$)	95

LIST OF TABLES

Table 1.1.	The sesamol (4a–h) and benzodioxane (5a–h) analogues that will be synthesised	5
Table 2.1.	Strategies for neuroprotection in Parkinson’s disease	16
Table 3.1.	The chemical structures of the sesamol and benzodioxane derivatives that will be synthesised in this study	49
Table 3.2.	The calculated and experimentally determined high resolution masses of the various synthesised sesamol derivatives (4a–h)	73
Table 3.3.	The calculated and experimentally determined high resolution masses of the various synthesised benzodioxane derivatives (5a–h)	73
Table 3.4.	HPLC analysis results of the synthesised sesamol derivatives (4a–h)	74
Table 3.5.	HPLC analysis results of the synthesised benzodioxane derivatives (5a–h)	74
Table 4.1.	IC ₅₀ values of the synthesised sesamol derivatives (4a–h) for the inhibition of human MAO-A and MAO-B	81
Table 4.2.	IC ₅₀ values of the synthesised benzodioxane derivatives (5a–h) for the inhibition of human MAO-A and MAO-B	81
Table 5.1.	The synthesised sesamol (4) derivatives which were evaluated as MAO inhibitors	98
Table 5.2.	The synthesised benzodioxane (5) derivatives which were evaluated as MAO inhibitors	99

LIST OF KEYWORDS

Parkinson’s disease; substantia nigra pars compacta (SNpc); dopamine; monoamine oxidase (MAO); MAO-A; MAO-B; levodopa (*L*-dopa); phthalide; sesamol; benzodioxane; MAO-B inhibitors; inhibition potencies; IC₅₀ values; dialysis; reversibility; Lineweaver-Burk plots; competitive mode of inhibition.

ABSTRACT

Parkinson's disease is an age-related neurodegenerative disorder. The major symptoms of Parkinson's disease are closely linked to the pathology of the disease. The main pathology of Parkinson's disease consists of the degeneration of neurons of the substantia nigra pars compacta (SNpc), which leads to reduced amounts of dopamine in the brain. One of the treatment strategies in Parkinson's disease is to conserve dopamine by inhibiting the enzymes responsible for its catabolism. The monoamine oxidase (MAO) B isoform catalyses the oxidation of dopamine in the central nervous system and is therefore an important target for Parkinson's disease treatment. Inhibition of MAO-B provides symptomatic relief for Parkinson's disease patients by increasing endogenous dopamine levels as well as enhancing the levels of dopamine after administration of levodopa (*L-dopa*), the metabolic precursor of dopamine.

Recent studies have shown that phthalide can be used as a scaffold for the design of reversible MAO inhibitors. Although phthalide is a weak MAO-B inhibitor, substitution on the C5 position of phthalide yields highly potent reversible MAO-B inhibitors. In the present study, sesamol and benzodioxane were used as scaffolds for the design of MAO inhibitors. The structures of sesamol and benzodioxane closely resemble that of phthalide, which suggests that these moieties may be useful for the design of MAO inhibitors. This study may be viewed as an exploratory study to discover new scaffolds for MAO inhibition. Since substitution at C5 of phthalide with a benzyloxy side chain yielded particularly potent MAO inhibitors, the sesamol and benzodioxane derivatives possessed the benzyloxy substituent in the analogous positions to C5 of phthalide. These were the C5 and C6 positions of sesamol and benzodioxane, respectively.

The sesamol and benzodioxane derivatives were synthesised by reacting sesamol and 6-hydroxy-1,4-benzodioxane, respectively, with an appropriate alkyl bromide in the presence of potassium carbonate (K_2CO_3) in *N,N*-dimethylformamide (DMF). 6-Hydroxy-1,4-benzodioxane, in turn, was synthesised from 1,4-benzodioxan-6-carboxaldehyde. The structures of the compounds were verified with nuclear magnetic resonance (NMR) and mass spectrometry (MS) analyses, while the purities were estimated by high-pressure liquid chromatography (HPLC). Sixteen sesamol and benzodioxane derivatives were synthesised.

To determine the inhibition potencies of the synthesised compounds the recombinant human MAO-A and MAO-B enzymes were used. The inhibition potencies were expressed as the corresponding IC₅₀ values. The results showed that the sesamol and benzodioxane derivatives are highly potent and selective inhibitors of MAO-B and to a lesser extent MAO-A. The most potent MAO-B inhibitor was 6-(3-bromobenzyloxy)-1,4-benzodioxane with an IC₅₀ value of 0.045 µM. All compounds examined displayed selectivity for the MAO-B isoform over MAO-A. Generally the benzodioxane derivatives were found to be more potent inhibitors of human MAO-A and MAO-B than the sesamol derivatives.

The reversibility and mode of MAO-B inhibition of a representative derivative, 6-(3-bromobenzyloxy)-1,4-benzodioxane, was examined by measuring the degree to which the enzyme activity recovers after dialysis of enzyme-inhibitor complexes, while Lineweaver-Burk plots were constructed to determine whether the mode of inhibition is competitive. Since MAO-B activity is completely recovered after dialysis of enzyme-inhibitor mixtures, it was concluded that 6-(3-bromobenzyloxy)-1,4-benzodioxane binds reversibly to the MAO-B enzyme. The Lineweaver-Burk plots constructed were linear and intersected on the y-axis. Therefore it may be concluded that 6-(3-bromobenzyloxy)-1,4-benzodioxane is a competitive MAO-B inhibitor.

To conclude, the C6-substituted benzodioxane derivatives are potent, selective, reversible and competitive inhibitors of human MAO-B. These compounds are therefore promising leads for the future development of therapy for Parkinson's disease.

UITTREKSEL

Parkinson se siekte is 'n neurodegeneratiewe siektetoestand. Die mees algemene simptome van Parkinson se siekte kan toegeskryf word aan die patologie van die siekte. Parkinson se siekte ontstaan as gevolg van die degenerasie van die neurone van die substantia nigra pars compacta, wat aanleiding gee tot verlaagde konsentrasies dopamien in die brein. 'n Belangrike behandelingstrategie vir Parkinson se siekte is om die werkingsduur van dopamien te verleng deur die ensieme wat verantwoordelik is vir die katabolisme van dopamien te inhibeer. Monoamienoksidase B (MAO-B) is die ensiem wat verantwoordelik is vir die oksidasie van dopamien in die sentrale senuweestelsel en hierdie ensiem is dus 'n belangrike teiken vir die behandeling van Parkinson se siekte. Inhibisie van MAO-B lei tot simptomatiese verligting vir pasiënte met Parkinson se siekte deur endogene dopamienvlakke te verhoog asook dopamienvlakke na toediening van levodopa (*L*-dopa), die metaboliese voorganger van dopamien.

Onlangse studies het getoon dat ftalied as leidraadverbinding aangewend kan word vir die ontwerp van omkeerbare MAO-inhibeerders. Alhoewel ftalied 'n swak MAO-B-inhibeerder is, is C5-gesubstitueerde ftaliedanaloeë potente omkeerbare MAO-B-inhibeerders. In die huidige studie word sesamol en bensodioksaan as leidraadverbindinge aangewend vir die ontwerp van MAO-inhibeerders. Aangesien die strukture van sesamol en bensodioksaan verwant is aan dié van ftalied, kan sesamol en bensodioksaan aangewend word vir die ontwerp van MAO-inhibeerders. Hierdie studie kan gesien word as 'n verkenningsstudie om nuwe leidraadverbindinge te identifiseer vir MAO-inhibisie. Aangesien C5 bensieloksie-substitusie van ftalied potente MAO-inhibeerders oplewer, sal sesamol en bensodioksaan in die ooreenstemmende posisies met die bensieloksie-substituent gesubstitueer word. Hierdie posisies is die C5- en C6-posisies van sesamol en bensodioksaan, onderskeidelik.

Die sesamol- en bensodioksaananaloeë is gesintetiseer deur sesamol en 6-hidroksie-1,4-bensodioksaan, onderskeidelik, te reageer met 'n toepaslike alkielbromied in die teenwoordigheid van kaliumkarbonaat (K_2CO_3) in *N,N*-dimetielformamied (DMF). 6-Hidroksie-1,4-bensodioksaan is gesintetiseer deur 1,4-bensodioksaan-6-karboksaldehyd as uitgangstof te gebruik. Die chemiese strukture van die analoeë is bevestig deur kernmagnetieseresonansiespektroskopie en massaspektrometrie, terwyl die suiwerhede van die analoeë deur hoëdrukvlouistofchromografie bepaal is.

Die potensie waarmee die gesintetiseerde verbindings MAO-A en MAO-B inhibeer is bepaal deur van die rekombinante mens ensieme gebruik te maak. Die potensie van inhibisie is uitgedruk as die IC_{50} waardes. Die resultate toon dat die sesamol- en bensodioksaananalöë potente selektiewe inhibeerders van MAO-B is. Die analöë was ook inhibeerders van MAO-A. Die mees potente MAO-B inhibeerder van die reeks is 6-(3-bromobensieloksie)-1,4-bensodioksaan wat 'n IC_{50} waarde van $0.045 \mu\text{M}$ teenoor MAO-B besit. Al die verbindings was selektiewe MAO-B-inhibeerders, en oor die algemeen was die bensodioksaananalöë meer potente inhibeerders van MAO-A en MAO-B as die sesamolanalöë.

Die omkeerbaarheid en meganisme van MAO-B inhibisie van 'n verteenwoordigende verbinding, 6-(3-bromobensieloksie)-1,4-bensodioksaan, is geëvalueer deur dialise van die ensiem-inhibeerder kompleks uit te voer, terwyl Lineweaver-Burk grafieke aangewend is om vas te stel of die meganisme van inhibisie van die verbinding kompetitief is. Aangesien ensiemaktiwiteit herstel na dialise, kan die gevolgtrekking gemaak word dat 6-(3-bromobensieloksie)-1,4-bensodioksaan omkeerbaar aan die ensiem bind. Die stel Lineweaver-Burk grafieke is lineêr en sny op 'n enkele punt op die y-as. Dit dui daarop dat 6-(3-bromobensieloksie)-1,4-bensodioksaan 'n kompeterende MAO-B-inhibeerder is.

Uit hierdie studie kan afgelei word dat C6-gesubstitueerde bensodioksaananalöë potente, selektiewe, omkeerbare en kompeterende inhibeerders van mens MAO-B is. Hierdie verbindings is dus belowende leidraadverbindinge vir die toekomstige ontwikkeling van nuwe geneesmiddels vir die behandeling van Parkinson se siekte.

CHAPTER 1

Introduction and rationale

1.1. Introduction and overview

Parkinson's disease is an incurable and progressive disorder that is characterised by involuntary motor symptoms and balance impairment (Dauer & Przedborski, 2003). Although the initial responsible cause for developing Parkinson's disease is not known, several causes have been investigated including environmental, pathological and genetic factors (Lees *et al.*, 2009). Since Parkinson's disease is commonly associated with old age (Dauer & Przedborski, 2003; Lees *et al.*, 2009), many symptoms are attributed to ageing rather than disease and thus are overlooked. Cognitive changes appear to develop with the progression of Parkinson's disease, with patients exhibiting symptoms of depression and dementia (Dauer & Przedborski, 2003). The main pathological hallmark present in Parkinson's disease is the depletion of dopamine due to the loss of dopaminergic neurons situated in the SNpc (Przedborski, 2005). Current treatment options for Parkinson's disease focus on the replenishment of dopamine rather than the prevention of further progression of the disease (Yacoubian & Standaert, 2009). Although these replenishment therapies are of value, L-dopa, the precursor of dopamine and mostly used drug in Parkinson's disease, causes adverse effects and eventually dyskinesia (Dauer & Przedborski, 2003). Thus, L-dopa is usually given in conjunction with other symptomatic anti-parkinsonian drugs. Among the alternative symptomatic anti-parkinsonian drugs are MAO inhibitors. The goal of this study is to discover novel MAO inhibitors as potential anti-parkinsonian agents.

MAO exists as two isoforms, namely MAO type A and MAO type B (Youdim & Bakhle, 2006). Although these two isoforms are ~70% identical at the amino acid sequence level, they are encoded by different genes (Edmondson *et al.*, 2009) and have different pH optima and heat inactivation sensitivity (Youdim & Bakhle, 2006). The MAOs are flavin adenine dinucleotide (FAD) containing enzymes (Youdim & Bakhle, 2006), which primary functions are to catalyse the oxidation of neurotransmitters as well as the oxidation of xenobiotic amines such as dietary tyramine (Inoue *et al.*, 1999). Thus, the MAOs are considered drug targets for the treatment of psychiatric and neurological disorders (Strydom *et al.*, 2013). Since MAO-A is the predominant isoform in the periphery (Youdim & Bakhle, 2006), the oxidation of dietary amines is usually due to MAO-A thus preventing their entry into the systemic circulation (Youdim *et al.*, 2006). MAO-A inhibitors are frequently used therapeutically as antidepressants in Parkinson's disease and other depressive illnesses

(Youdim *et al.*, 2006). With the inhibition of MAO-A, an increased amount of dietary amines, especially tyramine, can enter the systemic circulation leading to sympathomimetic effects and a severe hypertensive response commonly referred to as the 'cheese reaction'. This reaction is the major cause of the restricted therapeutic use of MAO-A inhibitors for the treatment of depression (Youdim & Bakhle, 2006).

Since MAO-B is the main isoform present in the basal ganglia (Youdim *et al.*, 2006), and contributes to the oxidation and subsequent toxicity of dopamine (Edmondson *et al.*, 2009), it is a target for Parkinson's disease treatment. Selective MAO-B inhibitors increase the concentrations of both endogenous dopamine and *L*-dopa-derived dopamine in the brain, and can thus be used as monotherapy or as adjunctive therapy in patients with *L*-dopa induced dyskinesia (Lees, 2005). Furthermore, MAO-B inhibitors may exert neuroprotective effects by inhibiting the formation of toxic byproducts of MAO-B-catalysed oxidation of neurotransmitters (Strydom *et al.*, 2103). Selegiline [(R)-deprenyl] and rasagiline are examples of MAO inhibitors. These drugs are irreversible MAO-B inhibitors, which delay the initiation of dopaminergic treatment when used as monotherapy. These two inhibitors may also exhibit disease-modifying effects in Parkinson's disease, thus delaying the progression of the disease (LeWitt & Taylor, 2008). After treatment with irreversible MAO inhibitors, return of enzyme activity requires *de novo* synthesis of the MAO-B protein, a process which may require several weeks (Vlok *et al.*, 2006). In contrast, after treatment with reversible inhibitors, enzyme activity is regained immediately after the inhibitor is eliminated from the tissue. Reversible inhibition is thus considered to be safer than irreversible inhibition and potential side effects that may occur with MAO inhibition can be terminated quicker with reversible inhibition (Van den Berg *et al.*, 2007). Since dopamine is also metabolised by MAO-A in the human brain, the design of non-selective MAO inhibitors may also represent an attractive strategy for the enhancement of central dopamine levels in Parkinson's disease. As mentioned above, the inhibition of MAO-A may also alleviate depression which is commonly associated with Parkinson's disease (Strydom *et al.*, 2013). Based on the significant role that MAO inhibitors play in the treatment of Parkinson's disease, the design and development of new reversible MAO-inhibitors are of importance. The goal of this study is to design and synthesise novel MAO inhibitors that are highly potent and reversible with selectivity towards MAO-B. Such drugs may possess antisymptomatic and potential neuroprotective properties, which may be used in the future treatment of Parkinson's disease. Compounds that are non-selective may, however, also be of value in Parkinson's disease since MAO-A inhibition may further protect against dopamine depletion, and may offer relief of the symptoms of depression.

1.2. Rationale

Phthalide (1) has previously been used as a scaffold for the design of reversible MAO inhibitors. Phthalide itself proved to be a weak MAO-B inhibitor (IC_{50} value of 28.6 μ M). Substitution on the C5 position of phthalide, however, yields highly potent reversible MAO-B inhibitors. For example, 5-benzyloxyphthalide exhibits an IC_{50} value of 0.23 μ M for the inhibition of human MAO-B (Strydom *et al.*, 2013). It was found that a wide variety of substituents at position C5 of phthalide yields potent MAO-B inhibitors. This is advantageous since structural modifications made to improve drug properties would be less likely to affect the MAO inhibition activity of these compounds. Thus, C5-substituted phthalides are good lead compounds for the design of new MAO inhibitors. Furthermore, phthalide also exhibits MAO-A inhibitory activity, making phthalide analogues dual inhibitors of MAO-A and MAO-B (Strydom *et al.*, 2013). As discussed above, the reversible inhibition of MAO exhibited by substituted phthalides is a desirable property from a safety point of view. In addition, since MAO-A inhibitors may also elevate central dopamine levels, dual inhibitors of MAO-A and MAO-B may be of enhanced value when designing anti-parkinsonian therapies (Strydom *et al.*, 2013). In addition, MAO-A inhibition may alleviate depression, which is frequently associated with Parkinson's disease.

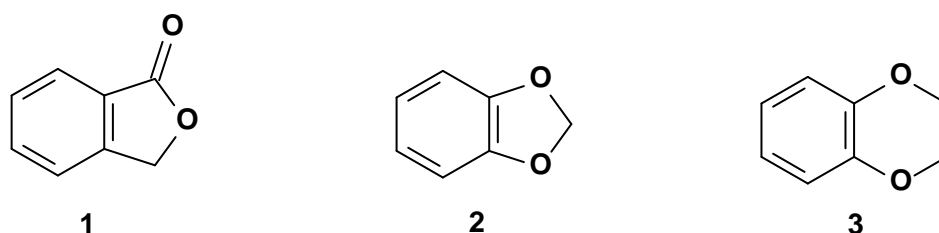


Figure 1.1. The chemical structures of phthalide (1), sesamol (2) and benzodioxane (3).

In the present study sesamol (2) and benzodioxane (3), a sesamol derived compound, will be used as scaffolds for the design of MAO inhibitors. The structures of sesamol and benzodioxane closely resemble that of phthalide, which suggests that these moieties may be useful for the design of new MAO inhibitors. This study may be viewed as an exploratory study to discover new scaffolds for MAO inhibition. In the present study derivatives of sesamol and benzodioxane will be synthesised and evaluated as potential MAO-A and MAO-B inhibitors. Since substitution at C5 of the phthalide ring with a benzyloxy side chain yielded particularly potent MAO-inhibitors (Strydom *et al.*, 2013), the envisioned sesamol (4) and benzodioxane (5) derivatives will also contain the benzyloxy substituent at the C5 and C6 positions, respectively, to yield 4a and 5a. These sesamol and benzodioxane derivatives fit the simplified pharmacophore model for MAO-B inhibition. The pharmacophore model for

MAO-B inhibition consists of two features, a hydrophilic feature and a lipophilic motif at the opposite end of the inhibitor. The lipophilic feature is frequently satisfied by an aromatic group containing a halogen substituent (such as the benzyloxy moiety), while both hydrogen bond acceptors and donors map to the hydrophilic feature. The sesamol and benzodioxane rings are thus expected to map to the hydrophilic feature of the pharmacophore model. The pharmacophore model is shown in figure 1.2. with **4a** and **5a** mapped.

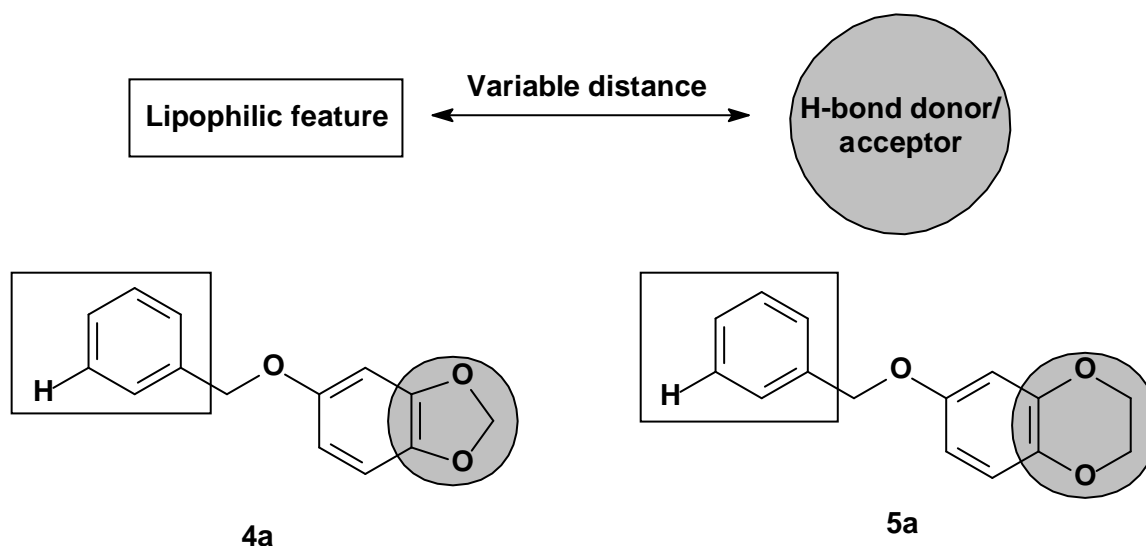
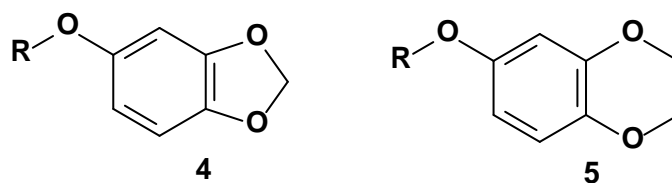


Figure 1.2. A proposed pharmacophore model for MAO-B inhibition with **4a** and **5a** mapped.

The current study will also synthesise derivatives containing the phenylethoxy (**4d** and **5d**) and phenylpropoxy (**4e** and **5e**) moieties on C5 and C6 of sesamol and benzodioxane. In addition, the phenoxyethoxy moiety (**4f** and **5f**) on C5 and C6 of sesamol and benzodioxane will also be considered. To further explore chemical space, selected derivatives will also be substituted in the *meta* positions of the benzyloxy ring with chlorine (**4b** and **5b**) and bromine (**4c** and **5c**). Furthermore the phenoxyethoxy containing derivatives, compounds (**4f** and **5f**), will be substituted in the *para* position of the phenyl ring with chlorine (**4g** and **5g**) and bromine (**4h** and **5h**). In total 16 sesamol and benzodioxane derivatives will be synthesised. The primary goal of the study is to evaluate the synthesised compounds as inhibitors of MAO-A and MAO-B.

Table 1.1. The sesamol (**4a–h**) and benzodioxane (**5a–h**) analogues that will be synthesised.



R	
a	
b	
c	
d	
e	
f	
g	
h	

1.3. Hypothesis of this study

Based on the report that substituted phthalides are highly potent MAO-B inhibitors, it is postulated that sesamol and benzodioxane derivatives, with the appropriate substitution, may also act as potent MAO-B inhibitors. It is further postulated that the benzyloxy side chain substituted at C5 and C6 of sesamol and benzodioxane, respectively, may be particularly suitable for the design of potent MAO-B inhibitors. This assumption is based on the observation that substitution of the benzyloxy moiety on C5 of phthalide results in highly potent MAO-B inhibition. It is also postulated that halogen (Cl and Br) substituents on the phenyl ring of the benzyloxy moiety will significantly enhance the inhibition potency of the sesamol and benzodioxane derivatives. Sesamol and benzodioxane may thus be promising scaffolds for the design of potent MAO-B inhibitors.

This study further explores the effect that the phenylethoxy, phenylpropoxy and phenoxyethoxy moieties on C5 and C6 of sesamol and benzodioxane, respectively, have on MAO inhibition potency. The inhibition potencies of these homologues will subsequently be compared to those of the sesamol and benzodioxane derivatives substituted with the benzyloxy side chain on C5 and C6, respectively. The effect of halogen substitution on the benzyloxy and phenoxyethoxy side chains will also be evaluated. Also for comparison, the MAO-A inhibitory properties of the sesamol and benzodioxane derivatives will be examined.

1.4. Objectives of this study

- Eight sesamol analogues will be synthesised using commercially available 5-hydroxysesamol and the appropriate alkylbromides as starting materials.
- Eight benzodioxane analogues will be synthesised using 6-hydroxybenzodioxane and the appropriate alkylbromides as starting materials. 6-Hydroxybenzodioxane is not commercially available and will be synthesised by reacting 2,3-dihydro-1,4-benzodioxine-6-carbaldehyde with *meta*-chloroperoxybenzoic acid (mCPBA) in dichloromethane.
- The sesamol and benzodioxane analogues will be evaluated as inhibitors of human MAO-A and MAO-B. The recombinant human MAO enzymes are commercially available and the inhibition potencies will be expressed as IC₅₀ values.
- For the most potent inhibitors among the sesamol and benzodioxane derivatives, the reversibility of MAO-A and MAO-B inhibition will be determined. For this purpose, the recovery of the enzymatic activity after dialysis of enzyme-inhibitor complexes will be evaluated.
- Lineweaver-Burk plots will be constructed for selected sesamol and benzodioxane derivatives to determine whether the mode of inhibition is competitive or non-competitive.

CHAPTER 2

Literature Overview

2.1. Parkinson's Disease

2.1.1. General background

Parkinson's disease, as it is commonly known, was first detailed in a monograph entitled "An Essay on the Shaking Palsy" by James Parkinson in 1817. In this essay, James Parkinson described the core clinical features with which Parkinson's disease is associated (Dauer & Przedborski, 2003). Although James Parkinson was the first to propose the unrecognised disease described in his monograph, it was Jean Martin Charcot, the father of neurology, who proposed that the disease should be referred to as Parkinson's disease (Lees *et al.*, 2009).

Parkinson's disease is a common incurable progressive bradykinetic disorder, which is characterised by tremor at rest, rigidity, bradykinesia, postural instability and freezing. The tremor associated with Parkinson's disease usually occurs at rest and decreases with voluntary movement, thus not impairing daily activities (Dauer & Przedborski, 2003). Motor symptoms, which include bradykinesia, hypokinesia and akinesia may be subtle and can easily be overlooked or wrongly attributed to other common causes such as old age (Lees *et al.*, 2009). These symptoms can be present for several years before a diagnosis have been made because they manifest as a variety of symptoms such as paucity of normal facial expression, decreased voice volume, drooling, decreased size and speed of handwriting and decreased stride length during walking (Dauer & Przedborski, 2003). Early loss of smell or hyposmia and disturbed sleep are also common symptoms that are easily overlooked (Lees *et al.*, 2009).

In the early stages of disease development, patients tend to complain more about the fear of falls, fainting, urinary incontinence, disturbed swallowing, amnesia and delirium. In the late stages of Parkinson's disease, the patients have an expressionless face, their speech is monotonous and slurred and their posture is flexed with a pill rolling tremor in one or both hands. As the disease progresses, the patient may need assistance to complete daily tasks such as dressing, bathing, feeding, and getting out of chairs or bed. Usually, younger patients (<40 years of age) presents with tremor which is more severe in the legs, whereas older patients (>70 years of age) presents with tremor of other dexterities such as the chin, jaw, lips and tongue (Lees *et al.*, 2009). Patients who suffer from Parkinson's disease may

experience cognitive changes such as passiveness and lack of initiative. Depression is common and a risk of dementia exists (Dauer & Przedborski, 2003).

2.1.2. Etiology

The most common risk factor for developing Parkinson's disease is age, although 10% of people presenting with the disease is younger than 45 years of age (Lees *et al.*, 2009). Parkinson's disease is a progressive disease with a mean age onset of 55, and with an incidence that increases markedly with age (Dauer & Przedborski, 2003). The incidence for patients between 50 and 59 years of age is 17.4 in 100 000 person years, while it is 93.1 in 100 000 person years for patients between the age of 70 and 79 (Lees *et al.*, 2009). Parkinson's disease is mainly a sporadic condition, thus without any genetic linkage, although some rare cases are linked to defects in a variety of genes (Przedborski, 2005). The cause of sporadic Parkinson's disease is unknown (Dauer & Przedborski, 2003). Parkinson's disease is not related to race or creed and a wide variety of causes have been studied, including environmental, pathological and genetic causes (Lees *et al.*, 2009).

The risk of developing Parkinson's disease is twice as high in non-smokers as in smokers, with a 25% higher risk in men, and postmenopausal women who are not using hormone replacement therapy, who ingest low daily quantities of caffeine. This may be due to the fact that both nicotine and caffeine increase the release of dopamine in the striatum in the brain, while MAO, an enzyme that can increase oxidative stress and therefore speed up neurodegeneration, is inhibited in the brains of patients that smoke. Thus, the patient's occupation, smoking, caffeine intake and drug habits should be noted prior to diagnosis or therapy (Lees *et al.*, 2009).

Previous head injuries, encephalitis, hypertension, cerebrovascular disease, middle-age obesity with lack of exercise, rural living environment and well-water ingestion may be some environmental causes that can lead to the development of Parkinson's disease (Lees *et al.*, 2009). Furthermore, chronic or limited exposure to some environmental dopaminergic neurotoxins can initiate neurodegenerative events that are similar, but not identical to that of Parkinson's disease. These dopaminergic neurotoxins include 1-methyl-4-phenyl-1,2,3,6-tetrahydropyridine (MPTP), cyanide, carbon disulphide, toluene, and several herbicides (such as paraquat) and insecticides (such as rotenone) (Dauer & Przedborski, 2003).

Another possible cause of Parkinson's disease may be the formation of an endogenous toxin, such as reactive oxygen species, which are generated from the normal metabolism of

dopamine. The formation of these endogenous toxins may be linked to distortions of normal metabolic pathways, which can lead to neurodegeneration (Dauer & Przedborski, 2003). Specific medications can induce reversible Parkinsonism, and therefore the use of these medications should be limited especially in patients with a genetic predisposition to Parkinson's disease. These medications include dopamine antagonists (prochlorperazine, metoclopramide, and chlorpromazine) and calcium-channel blockers (flunarizine, cinnarizine, sodium valproate). Some herbal remedies can also cause Parkinsonism (Lees *et al.*, 2009). Although, the main cause of Parkinson's disease is still not known, genetic and pathological input may provide clues.

2.1.3. Neurochemical and neuropathological features of Parkinson's disease

Two prominent pathological hallmarks exist in Parkinson's disease, namely the loss of nigrostriatal dopaminergic neurons and the presence of Lewy bodies. For the diagnosis of Parkinson's disease to be definite, both of these hallmarks need to be present in patients (Dauer & Przedborski, 2003).

Parkinson's disease patients exhibit low levels of brain dopamine, which results mainly from the degeneration of the nigrostriatal dopaminergic pathway. This pathway consists of dopaminergic neurons whose cell bodies are located in the SNpc and the projecting axons and nerve terminals of these neurons are found in the striatum (Przedborski, 2005). The neuronal cell loss is concentrated in the ventrolateral and caudal portions of the SNpc, which differ from normal aging. Furthermore, the striatal dopaminergic neurons seem to be the primary target of the degenerative process and may result from a "dying back" process (Dauer & Przedborski, 2003).

Intraneuronal inclusions called Lewy bodies can be found in the remaining affected nigral dopaminergic neurons. These bodies are spherical eosinophilic cytoplasmic aggregates composed of a variety of proteins, such as α -synuclein, parkin, ubiquitin and neurofilaments (Przedborski, 2005). Some of these proteins form part of the pathogenic process leading up to Parkinson's disease. The neuropathology of Parkinson's disease is not restricted to the nigrostriatal pathway, since histological abnormalities can be found in other dopaminergic as well as non-dopaminergic cell groups (Przedborski, 2005).

2.1.4. Pathogenesis and genetics of Parkinson's disease

2.1.4.1. Pathogenesis

The pathological mechanism of neuronal death in Parkinson's disease is thought to start with an otherwise healthy dopaminergic neuron being exposed to an etiological factor. This initial event causes a cascade of deleterious factors, such as free radicals, mitochondrial dysfunction, excitotoxicity, neuron inflammation and apoptosis, to interact with each other to ultimately cause the death of the neuron (Przedborski, 2005). Three types of cellular dysfunction are important in the pathogenesis of Parkinson's disease, namely (1) misfolding and aggregation of proteins, (2) mitochondrial dysfunction and oxidative stress and (3) programmed cell death or apoptosis (Dauer & Przedborski, 2003).

Misfolding and aggregation of certain proteins could be neurotoxic through a variety of mechanisms. These aggregates can directly damage neurons by either deforming the cell or interfering with intracellular clearance processes through the ubiquitin proteasome system. They may also sequester proteins that are important for cell survival (Dauer & Przedborski, 2003).

For mitochondrial function, high levels of oxygen is needed which give rise to the production of powerful oxidants as byproducts. These oxidants can form other molecules that cause cellular damage by reacting with nucleic acids, proteins and lipids. These reactive species may target the electron transport chain itself, leading to mitochondrial damage and further production of reactive oxygen species. The presence of reactive oxygen species increases the amount of misfolded proteins, which in turn increases the demand on the ubiquitin proteasome system to remove them. Dopaminergic neurons may be targeted directly, as the metabolism of dopamine produces reactive oxygen species. Furthermore, mitochondria-related energy failure disrupts dopamine storage, thus increasing the free cytosolic concentration of dopamine which may lead to dopamine-mediated reactions which can harm cellular structures (Dauer & Przedborski, 2003).

Programmed cell death is a homeostatic mechanism. When programmed cell death (apoptosis) occurs, intracellular signaling pathways are activated to initiate cell death. Dysregulation of this pathway especially in the brain may contribute to neurodegeneration in Parkinson's disease (Dauer & Przedborski, 2003).

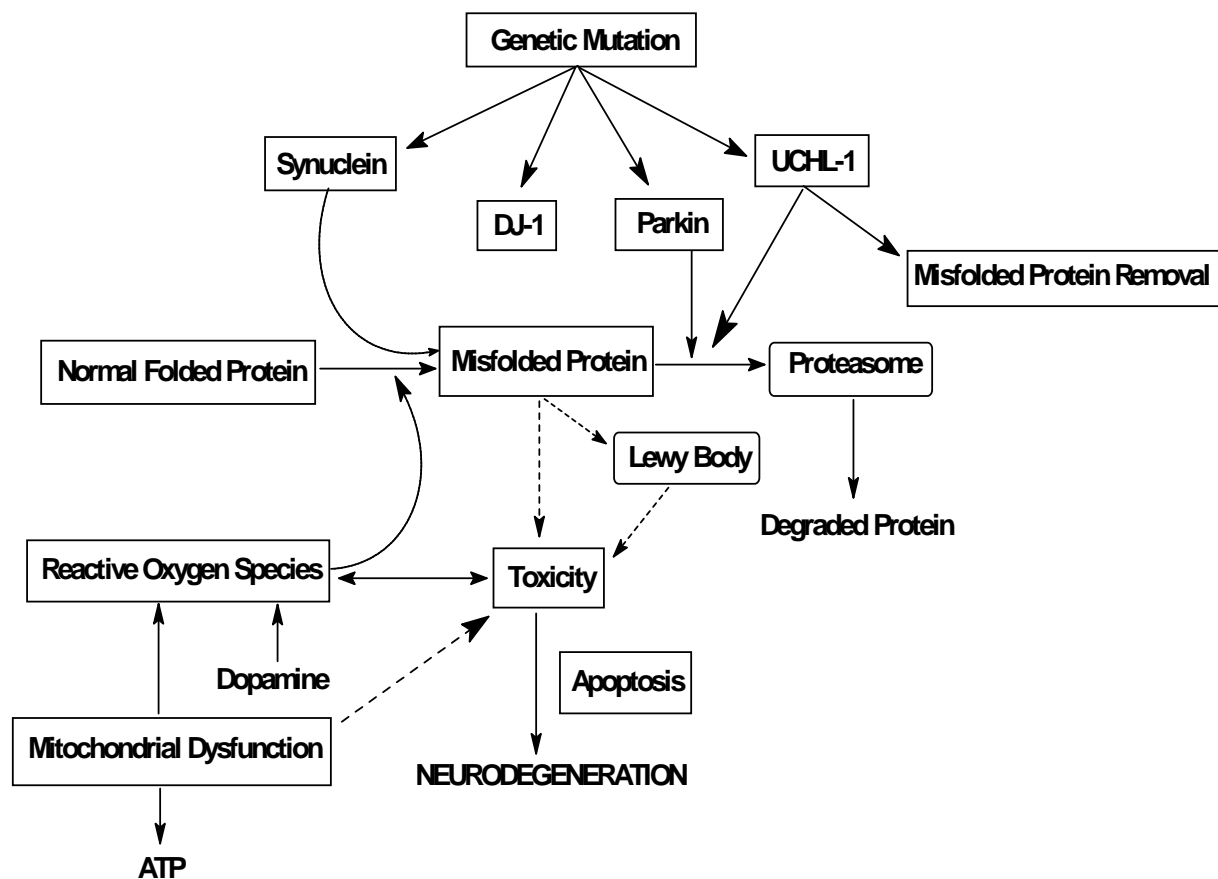


Figure 2.1. The various pathological and genetic mechanisms leading up to neurodegeneration in Parkinson's disease.

2.1.4.2. Genetics

According to genetic studies, mutations in seven genes have been linked to L-dopa-responsive Parkinsonism. Six of these pathogenic mutations are found in leucine rich repeat kinase 2 (LRRK-2) and the most common of these is the Gly2019Ser mutation. The risk for developing Parkinson's disease when younger than 60 years of age with the Gly2019Ser mutation is 28%, but the risk increases rapidly to 74% when the patient is 79 years of age. Patients with this mutation presents with a slightly more benign course of Parkinson's disease with a lower risk of developing dementia. Autopsy on patients with a LRRK-2 mutation, revealed that they have tangle pathology and non-specific neuronal loss (Lees *et al.*, 2009).

Mutations of α -synuclein (a protein found in Lewy bodies) cause a syndrome indistinguishable from Parkinson's disease, but these cases are much rarer than the LRRK-2 Gly2019Ser mutation. The ubiquitin proteasome system is responsible for the removal of dysfunctional proteins and mitochondria (Lees *et al.*, 2009). The propensity of α -synuclein to misfold and form amyloid fibrils and nonfibrillary oligomers (protofibrils) may be responsible

for its neurotoxicity (Dauer & Przedborski, 2003). Wild-type and mutant α -synuclein are degraded by the lysosomal enzymes present in the ubiquitin proteasome system, and both bind to the autophagy chaperone. After binding to the chaperone, wild-type α -synuclein is rapidly taken up and degraded by the autophagic vacuoles. However, mutant α -synuclein binds with much greater avidity to the autophagy chaperone and remains tightly attached to the chaperone. Mutant α -synuclein is thus never successfully taken up or degraded (Przedborski, 2005). It is thought that mutant α -synuclein permeate synaptic vesicles allowing dopamine to leak into the cytoplasm and increasing the oxidative stress inside the cell (Dauer & Przedborski, 2003).

Early onset Parkinsonism (<40 years of age) can also be caused by loss-of-function mutations in parkin, DJ-1, PINK1 and ATP13A2 genes. Of these mutations, parkin mutations are common while mutations of the other three genes are rare. Parkin mutations lead to nigral cell loss, restricted brain-stem neuronal loss and the absence of Lewy bodies or neurofibrillary degeneration (Lees *et al.*, 2009). The protein products of DJ-1 and PINK1 are located in the mitochondria. Mutations in these genes cause degeneration through either faulty mitochondrial localisation or the loss of activity of these proteins renders cells susceptible to mitochondrial poisons (Przedborski, 2005).

Glucocerebrosidase is another gene which is associated with Parkinson's disease. Heterozygous loss of function of this gene increases the risk for developing Parkinson's disease fivefold (Lees *et al.*, 2009). Ubiquitin C-terminal hydrolase-L1 (UCH-L1), an enzyme which plays a role in recycling ubiquitin ligated to misfolded proteins after degradation by the proteasome, also has several reported mutations. Some of these mutations appear to be protective against the development of Parkinson's disease, such as the Ser18Tyr polymorphism. The dominant mutation, Ile93Met, decreases the enzyme's activity in the ubiquitin proteasome system, which can lead to the aggregation of proteins and oxidative stress and finally the development of Parkinson's disease (Dauer & Przedborski, 2003).

These Parkinson's disease genes seem to operate through a common molecular pathway, the ubiquitin proteasome system (Dauer & Przedborski, 2003). Autopsy done on patients with these mutations showed that many of the mutations described above cause changes that are indistinguishable with those found in patients with Parkinson's disease (Lees *et al.*, 2009).

2.1.5. Treatment of Parkinson's disease

As mentioned above, Parkinson's disease is an incurable progressive disease (Lees *et al.*, 2009) with current treatment options that focus more on the replacement of dopamine to significantly improve the quality of life of patients suffering from the disease, while none of the current therapies slow or prevent the development of the disease (Yacoubian & Standaert, 2009).

2.1.5.1. Symptomatic treatment of Parkinson's disease

Symptomatic treatment of Parkinson's includes a variety of different pharmacological classes of drugs. *L*-dopa is the precursor of dopamine and may alleviate most of the major symptoms of Parkinson's disease (Dauer & Przedborski, 2003). Although long-term treatment of Parkinson's disease with *L*-dopa leads to adverse effects, generally involuntary movements termed dyskinesia (Dauer & Przedborski, 2003), this should always be the initial treatment option whatever the age of the patient. Metabolic transformation of *L*-dopa occurs at both the peripheral and central levels, limiting its use as monotherapy. For this reason *L*-dopa is usually given in combination with either a peripheral dopa decarboxylase inhibitor, such as benserazide or carbidopa or catechol-O-methyl transferase inhibitors such as entacapone and tolcapone, for the control of *L*-dopa induced dyskinesias (Gnerre *et al.*, 2000).

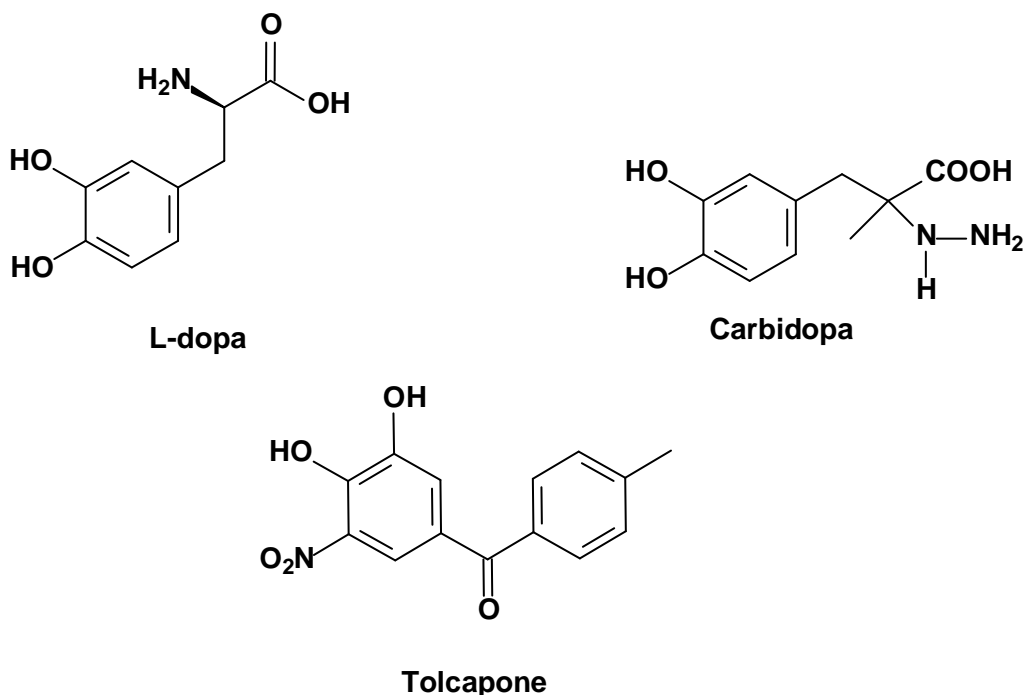
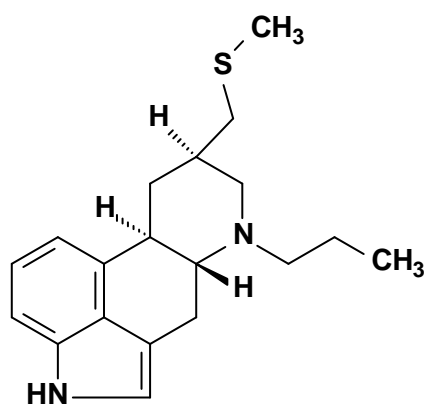


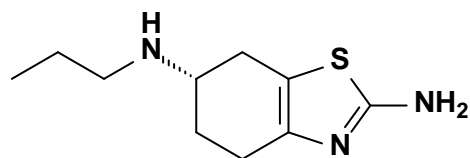
Figure 2.2. Drugs frequently used in an *L*-dopa regime for the symptomatic treatment of Parkinson's disease.

Dopamine agonists all act on dopamine D2-like receptors, however most mechanisms of action of these drugs are not fully understood and may be related to their different affinities for other dopaminergic receptor subtypes, such as the D1- and D3-like receptors. Stimulation on the postsynaptic D2 receptor leads to the anti-parkinsonian activity of these drugs, while presynaptic stimulation may have neuroprotective properties. Most patients will require the addition of *L*-dopa to their dopamine agonist regime as the disease progresses. The use of dopamine agonists as adjunctive therapy allows for the concomitant use of lower doses of *L*-dopa. Dopamine agonists are divided into ergoline (with an ergot-like structure) and nonergoline agonists. The ergoline agonists include bromocriptine, cabergoline, lisuride and pergolide, while the nonergoline agonists include apomorphine, pramipexole, ropinirole and piribedil (Lees, 2005). Although different opinions exist about the initial treatment options for Parkinson's disease, these drugs are a popular first-line treatment option in patients under 55 years of age (Lees *et al.*, 2009).

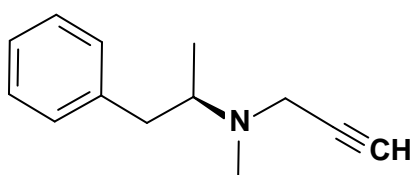
The selective MAO-B inhibitors, for which dopamine is the preferred substrate, increases the brain concentrations of both endogenous dopamine and dopamine derived from *L*-dopa administration. Thus, MAO-B inhibitors can be used as monotherapy or as adjunctive therapy in patients with *L*-dopa induced dyskinesia (Lees, 2005). Selegiline (deprenyl) is an irreversible MAO-B inhibitor which delays the initiation of dopaminergic treatment and has a disease-modifying effect in Parkinson's disease (LeWitt & Taylor, 2008). Rasagiline is another highly selective irreversible MAO-B inhibitor which is well tolerated, largely because, unlike selegiline, it is not metabolised to amphetamine derivatives (Lees, 2005). The mechanism of action of rasagiline is similar to other MAO-B inhibitors, with the exception that it enhances dopamine release, inhibits dopamine catabolism and antagonises certain cellular processes that lead to apoptosis and neurodegeneration (LeWitt & Taylor, 2008).



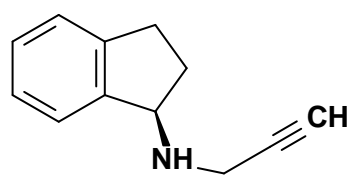
Pergolide



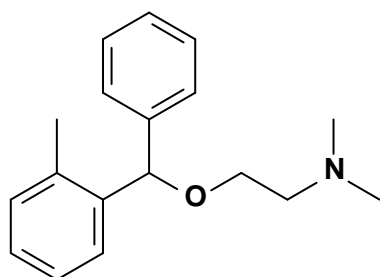
Pramipexole



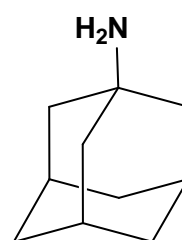
Selegiline



Rasagiline



Orphenadrine



Amantadine

Figure 2.3. Chemical structures of drugs frequently used in the symptomatic treatment of Parkinson's disease.

Anticholinergic or antimuscarinic drugs are used for the symptomatic treatment of patients with Parkinson's disease. All of these drugs are specific for muscarinic receptors and act by restoring equilibrium between striatal dopamine and acetylcholine activity. They can be used as monotherapy to offer mild symptomatic relief or in combination with other agents. The most commonly used anticholinergic drugs used in Parkinson's disease are trihexyphenidyl, bentspiron, orphenadrine and procyclidine (Lees, 2005).

Another well tolerated drug is amantadine and can be used as initial treatment of Parkinson's disease (Lees *et al*, 2009). The mechanism of action includes the enhancement

of dopamine release, blocking of dopamine reuptake, and inhibition of N-methyl-D-aspartate (NMDA) glutamate receptors. Amantadine also possesses mild antimuscarinic activity. Amantadine can be used as monotherapy for symptomatic treatment or as an add-on therapy in patients already receiving *L*-dopa or anticholinergic drugs (Lees, 2005).

The complexity of the above mentioned treatment options and adverse effects of these drugs emphasise the importance of the development of neuroprotective strategies which could be applied early in Parkinson's disease in order to prevent or delay progression and complications of the disease (Yacoubian & Standaert, 2009).

2.1.5.2. Drugs for neuroprotection

Several pathological mechanisms are present in the development and progression of Parkinson's disease. These mechanisms act synergistically through complex interactions to promote neurodegeneration (Yacoubian & Standaert, 2009).

Table 2.1. Strategies for neuroprotection in Parkinson's disease.

Pathological mechanism	Target for neuroprotection	Examples of possible agents
<ul style="list-style-type: none"> • Oxidative stress • Mitochondrial dysfunction 	<ul style="list-style-type: none"> • Inhibitors of dopamine metabolism • Electron transport enhancers • Antioxidants • Glutathione promoters 	<ul style="list-style-type: none"> • MAO inhibitors and dopamine receptor agonists • Coenzyme Q10 and selenium • Vitamin E and uric acid
<ul style="list-style-type: none"> • Protein aggregation and misfolding 	<ul style="list-style-type: none"> • Inhibitors of α-synuclein aggregation • Reducing α-synuclein levels • Enhancers of parkin function • Enhancers of UCH-L1 function • Enhancers of proteosomal or lysosomal pathways 	
<ul style="list-style-type: none"> • Neuroninflammation 	<ul style="list-style-type: none"> • Anti-inflammatory agents 	<ul style="list-style-type: none"> • Non-steroidal anti-inflammatory agents • Statins and minocycline
<ul style="list-style-type: none"> • Excitotoxicity • Apoptosis • Loss of trophic factors 	<ul style="list-style-type: none"> • NMDA receptor antagonists • Calcium channel antagonists • Anti-apoptotic agents • Neurotrophic factors 	<ul style="list-style-type: none"> • Riluzole and amantadine • Isradipine • Glial-derived neurotrophic factor (GDNF) • Neurturin

Accumulation of reactive free radicals produced by either dopamine metabolism, mitochondrial dysfunction, increased iron levels or failure of endogenous protective mechanisms, results in oxidative stress. These reactive species can interact with cellular processes causing damage and thereby disrupting the cell's normal function. In Parkinson's disease, oxidative damage appears to be present in conjunction with the overproduction of reactive species and impairment of cellular protective mechanisms. Oxidative stress can be combatted through different strategies. MAO inhibitors limits dopamine metabolism through MAO, while Coenzyme Q10 enhance mitochondrial electron transport. Antioxidants such as vitamin E and selenium quench free radicals and therefore promote endogenous buffer mechanisms (Yacoubian & Standaert, 2009).

α -Synuclein is the major component of Lewy bodies and seems to be the primary aggregating protein in Parkinson's disease. The pathological mechanism by which α -synuclein causes neuronal damage is not understood since the toxic molecular form of the protein has not yet been discovered. In some genetic forms of Parkinson's disease, other proteins have been linked to the pathogenesis of the disease, i.e. parkin and UCH-L1. Thus, strategies to prevent protein aggregation improve clearance of misfolded proteins or promote proteosomal or lysosomal degradation pathways may be critical in preventing development or progression of Parkinson's disease (Yacoubian & Standaert, 2009).

Microglia activation in conjunction with elevated pro-inflammatory cytokines and the complement system, may contribute to neurodegeneration in Parkinson's disease. Since neuroninflammation has been recognised as a contributing mechanism in the pathogenesis of Parkinson's disease, strategies including anti-inflammatory agents are crucial for prevention hereof. The anti-inflammatory agents in use include non-steroidal anti-inflammatory agents, statin drugs as well as minocycline (Yacoubian & Standaert, 2009).

Another pathogenic mechanism implicated in Parkinson's disease is excitotoxicity. Glutamate drives the excitotoxic process by the innervation of dopaminergic neurons containing high levels of NMDA receptors. Activation of these receptors by glutamate increases the intracellular calcium levels leading to cell death. NMDA receptor antagonists and calcium channel antagonists may protect against the cell death and neuron loss in Parkinson's disease. Programmed cell death or apoptosis is also implicated in the neuronal loss in Parkinson's disease, thus anti-apoptotic agents may prevent this. Several neutrophic factors are reduced in Parkinson's disease, contributing to cell death. Treatment with growth

factors, such as GDNF and neurturin, may provide a neuroprotective effect in patients with Parkinson's disease (Yacoubian & Standeart, 2009).

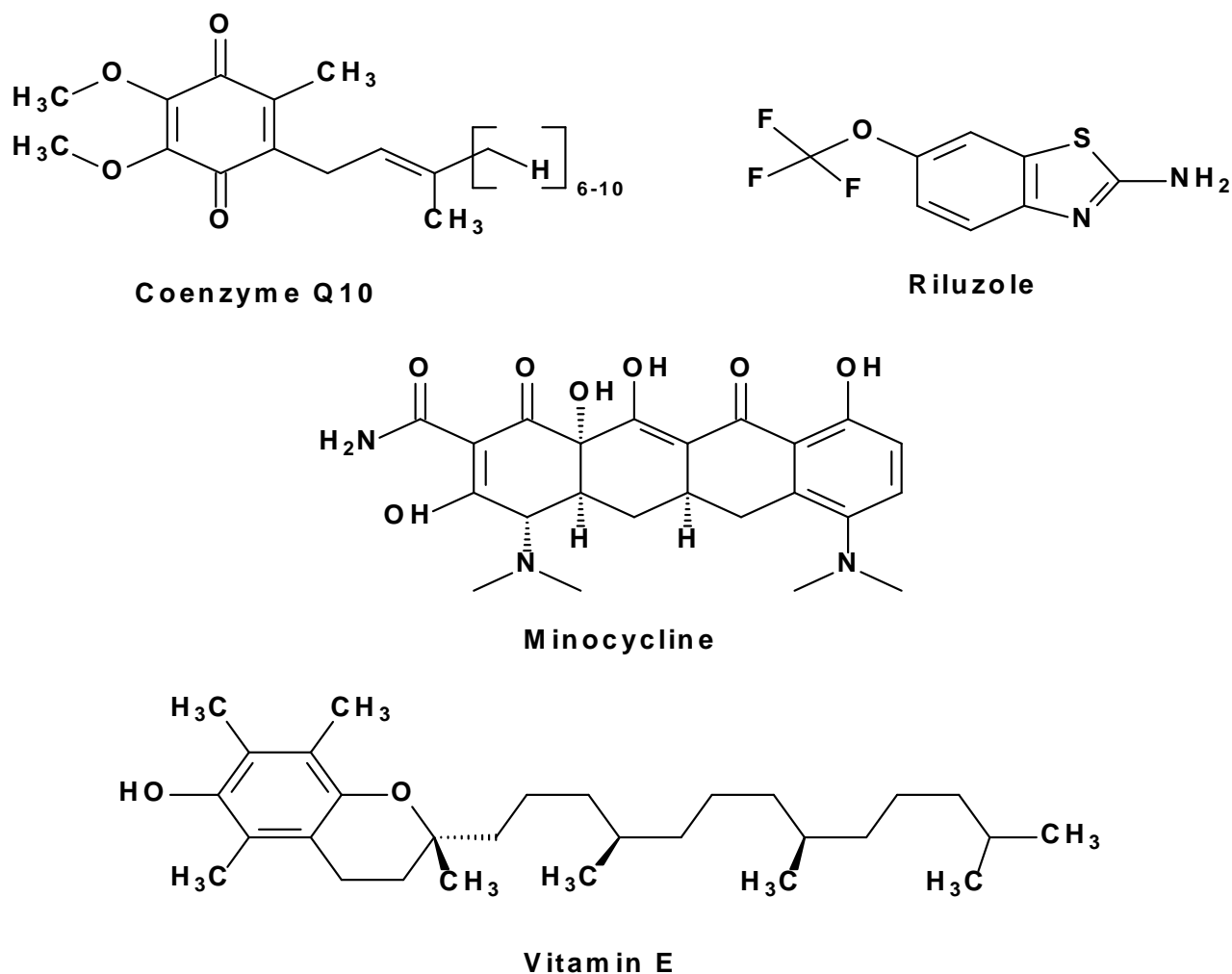


Figure 2.4. Chemical structures of agents for potential neuroprotective therapeutic use in Parkinson's disease.

2.2. Animal models of Parkinson's disease

2.2.1. 1-methyl-4-phenyl-1,2,3,6-tetrahydropyridine

MPTP toxicity was first discovered when several drug users from Northern California developed an acute state of akinesia after intravenous administration of a street preparation of 1-methyl-4-phenyl-4-propionpiperidine (MPPP) in the early 1980's. MPTP was inadvertently produced when MPPP were synthesised (Bové *et al.*, 2005).

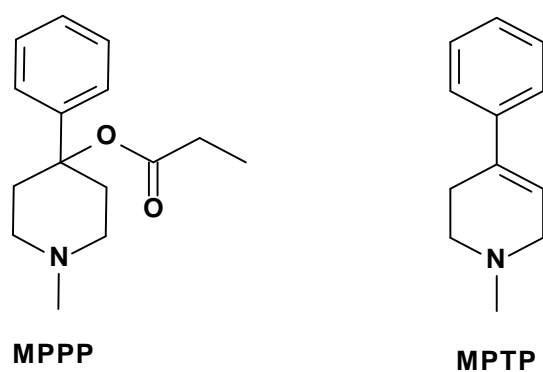


Figure 2.5. The chemical structures of MPPP and MPTP.

Since its discovery, MPTP has been used to model Parkinson's disease in a variety of mammalian species (Bové *et al.*, 2005). MPTP exerts similar effects as seen in Parkinson's disease patients in several species including primates, cats and rodents. Among rodents, only specific strains of mice are susceptible to MPTP-induced toxicity for reasons which remain unclear (Smeyne & Jackson-Lewis, 2004). Several neuroprotective therapies (i.e. GDNF) as well as the elucidation of the pathological mechanism of Parkinson's disease have been achieved through this model. The clinical picture of MPTP intoxication produces all of the cardinal features of Parkinson's disease, including tremor, rigidity, postural instability and bradykinesia (Blum *et al.*, 2001). Some patients exhibit cognitive impairments consistent with some of the cognitive alterations seen in Parkinson's disease patients. MPTP intoxication can be countered through administration of a *L*-dopa/carbidopa regimen, even though long-term treatment of *L*-dopa causes hyperkinetic motor complications. These complications remain a major impediment to the proper management of Parkinson's disease. Through the MPTP model the molecular basis of Parkinson's disease can be investigated as well as some therapeutic strategies to control it (Bové *et al.*, 2005).

Pathologically, MPTP causes damage to the nigrostriatal dopaminergic pathway identical to that seen in Parkinson's disease with greater loss of dopaminergic neurons in the SNpc than the ventral tegmental area. So far Lewy bodies have not been observed in MPTP-induced Parkinsonism. Whether this is due to the molecular mechanism of dopaminergic neuronal death or the rate by which this occurs is still unclear. Furthermore, acute MPTP exposure can lead to a self-sustained cascade of cellular and molecular events with long-lasting deleterious effects (Bové *et al.*, 2005).

In the body MPTP is first metabolised by a MAO-B-catalysed ring α -carbon 2-electron oxidation to yield 1-methyl-4-phenyl-2,3-dihydropyridium (MPDP⁺), which then undergoes another 2-electron oxidation to generate the 1-methyl-4-phenylpyridium metabolite (MPP⁺) (Ogunrombi *et al.*, 2007).

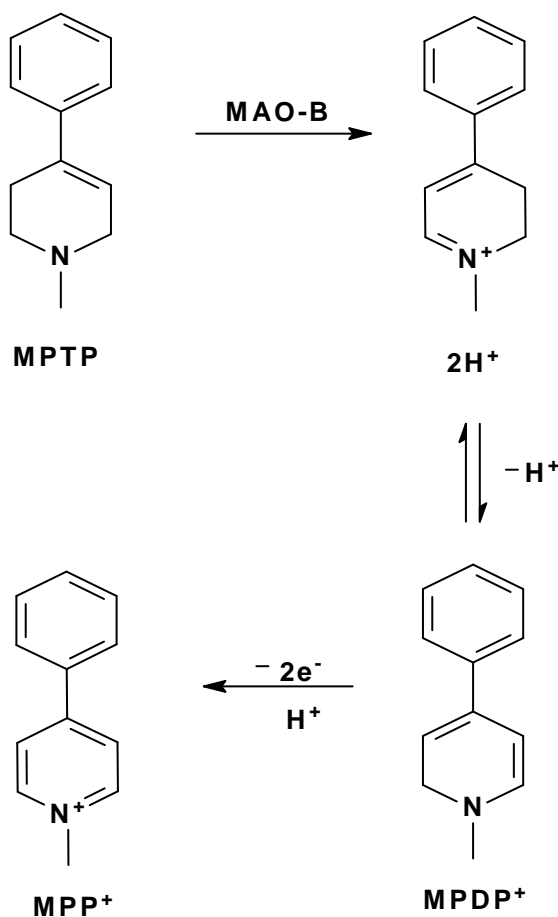


Figure 2.6. The MAO-B catalysed oxidation of MPTP to MPDP⁺ and the pyridinium metabolite, MPP⁺.

MPP⁺ cannot be transported through the blood-brain barrier and this acts as a first line of defense against the toxin. The MPTP which is not converted in the periphery rapidly enters the brain and consequently glial cells. Glia contains MAO-B and thus converts MPTP to MPP⁺, which leads to up-regulation of cytokines and in turn inducible nitric oxide synthase (iNOS). iNOS generates large amounts of nitric oxide (NO) which can freely pass through membranes for possible attack on neurons. MPP⁺ is transported out of glial cells into the extracellular space where it is taken up into dopaminergic cell by the dopamine transporter (DAT). In the dopaminergic neuron MPP⁺ can cause several damaging effects including inhibition of cellular respiration through interference with complex I of the electron transport chain or the release of excessive amounts of dopamine into the cytoplasm (Smeyne & Jackson-Lewis, 2004).

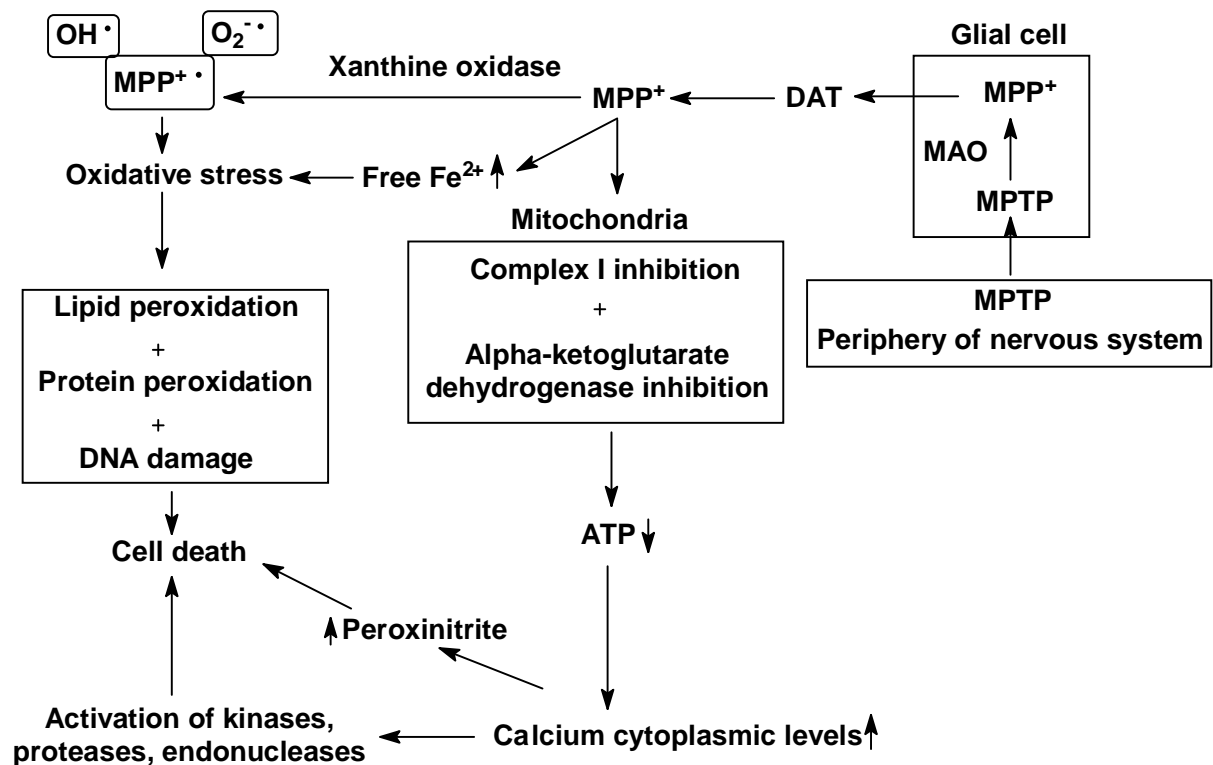


Figure 2.7. Schematic representation of the detailed pathological mechanism of MPTP

To prevent MPTP toxicity, several strategies have been proposed. Both humans and animals intoxicated with MPTP respond therapeutically well to an *L*-dopa/carbidopa regimen. Although the above mentioned regimen causes *L*-dopa induced dyskinesia, administration of a D3-dopamine partial agonist improves this side-effect (Bové *et al.*, 2005). The antibiotic minocycline can block iNOS induction and thus protect against NO neuronal damage, while coenzyme Q10 supplementation may slow the progression of Parkinson's disease and thus damage caused by MPP⁺ (Smeyne & Jackson-Lewis, 2005).

2.2.2. 6-Hydroxydopamine (6-OHDA)

6-OHDA is the most commonly used model to determine nigral degeneration *in vitro* and *in vivo* (Blum *et al.*, 2001). Generally it is classified as a catecholaminergic neurotoxin and is structurally similar to noradrenaline as well as dopamine. Essentially it is used in small animals, such as rodents, but has also been administered to nonhuman primates as well as dogs for the investigation of the cardiovascular system (Bové *et al.*, 2005). After it was isolated, its ability to destroy nerve cell endings of sympathetic neurons came to light (Blum *et al.*, 2001).

Although 6-OHDA is unable to cross the blood-brain barrier after systemic injection (Blum *et al.*, 2001), it has high affinity for several catecholaminergic plasma membrane transporters, such as DAT and norepinephrine transporters. Consequently, 6-OHDA can enter dopamine and norepinephrine neurons and damage catecholaminergic pathways in the periphery or centrally. Thus, to create specifically a Parkinson's disease model, attention should be given to the route of administration of 6-OHDA (Bové *et al.*, 2005).

For experimental models of Parkinson's disease, 6-OHDA has to be injected directly into the brain (Bové *et al.*, 2005). Preferentially, 6-OHDA is injected into the striatum, the SNpc or the ascending medial forebrain bundle for destruction of nigral dopaminergic neurons and depletion of striatal dopamine. This route of administration reproduces the physiopathological features of Parkinson's disease (Blum *et al.*, 2001). After intraventricular or intracisternal administration of 6-OHDA, a bilateral catecholaminergic lesion is observed within a few hours after administration, which may lead to death of the animal injected. Thus the unilateral intracerebral injection is most often used. After unilateral injection, dopaminergic neurons start to die within the first 24 hours, while the extracellular dopamine levels remain close to normal (Bové *et al.*, 2005). Unilateral 6-OHDA induced SNpc degeneration produces an asymmetric and quantifiable model of Parkinson's disease. This model can thus be used to control the extent of the lesion as well as determine the potential benefits of different anti-parkinsonian therapies (Blum *et al.*, 2001).

6-OHDA may be classified as an endogenous neurotoxin based on the fact that nigral dopaminergic neurons contain significant levels of dopamine, hydrogen peroxide and free iron which may lead to 6-OHDA formation through a non-enzymatic reaction between these elements. Other factors may also contribute to this endogenous formation of 6-OHDA. These include nitrite ions which can interact with dopamine to generate 6-OHDA and 6-nitrodopamine. Manganese also stimulates dopamine auto-oxidation and thus the formation of 6-OHDA (Blum *et al.*, 2001). The pathological mechanism by which 6-OHDA destroys catecholaminergic neurons includes the combined effect of reactive oxygen species and quinones. In an aerobic alkaline milieu, 6-OHDA readily oxidises to yield hydrogen peroxide and para-quinone (Bové *et al.*, 2005).

To prevent oxidative stress induced by 6-OHDA toxicity, antioxidants can be used, while selegiline inhibits the oxidation of 6-OHDA through MAO. Since iron may contribute to the pathology caused by 6-OHDA, iron chelating agents may be useful as protective strategies (Blum *et al.*, 2001).

2.2.3. Rotenone

Rotenone is the most potent member of a family of natural cytotoxic compounds that can be extracted from several parts of *Leguminosa* plant species. Rotenone is commonly used as an insecticide and piscicide. It has a short half-life since it is readily broken down with sunlight exposure and in water and soil. Thus, rotenone is not expected to be a groundwater pollutant with the likelihood of causing Parkinson's disease since the environmental exposure to rotenone is very low. The most common mechanism of rotenone exposure is through ingestion. Rotenone is highly lipophilic and can gain access to different organs including the brain. Its brain distribution is heterogeneous with accumulation in mitochondria. Rotenone inhibits reduced nicotinamide adenine dinucleotide-ubiquinone reductase activity through binding to a specific subunit of complex I of the electron transport chain. Furthermore, it inhibits microtubule formation from tubulin thus contributing to dopaminergic neurodegeneration. Although rotenone causes a clinical picture similar to Parkinson's disease, its effect is inconsistent and unpredictable making it unlikely that studies can successfully be carried out using this model (Bové *et al.*, 2005).

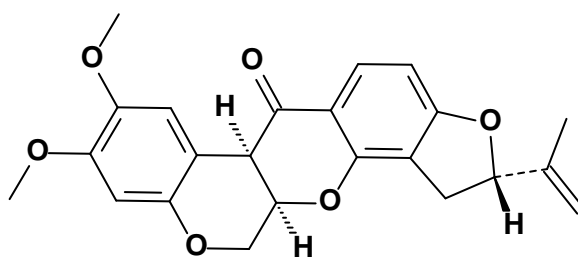


Figure 2.10. The chemical structure of the insecticide rotenone.

2.2.4. Paraquat

Another prototypic toxin which induces toxicity through oxidative stress is the potent herbicide paraquat or N,N'-dimethyl-4,4'-bipyridinium. Its toxicity is mediated through a redox cycling reaction with cellular diaphorase (such as nitric oxide synthase) leading to the formation of reactive oxygen species. Paraquat exposure usually occurs by ingestion or dermal exposure. Paraquat poorly crosses the blood-brain barrier, but recent studies have suggested that an increased risk exist to develop Parkinson's disease due to paraquat

exposure. This is due to the fact that paraquat exhibits structural similarities with MPTP's toxic metabolite MPP⁺. After exposure, paraquat can cause nigral cell loss and α -synuclein pathology, contributing to its potential use as a Parkinson's disease model. The fungicide, manganese ethylenebisdithiocarbamate (Maneb), may be used with paraquat, since the combination may produce greater effects on the dopaminergic system than paraquat or Maneb alone (Bové *et al.*, 2005).

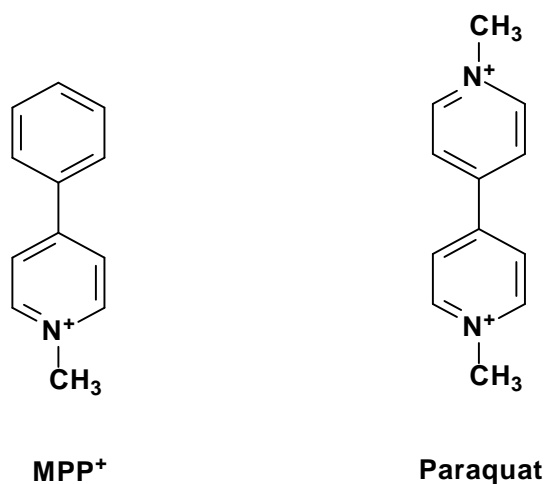


Figure 2.11. The chemical structures of the MPTP metabolite MPP⁺, and paraquat to demonstrate the structural similarities between these compounds.

2.3. Monoamine oxidase

2.3.1. General background and tissue distribution

Mary Hare-Bernheim first described monoamine oxidase as a catalytic enzyme of tyramine deamination in 1928. She named this catalytic enzyme tyramine oxidase. Hugh Blaschko later found that this tyramine oxidase corresponded with other enzymes known to metabolise primary, secondary and tertiary amines, known as noradrenaline oxidase and aliphatic amine oxidase. He thus proposed that these three enzymes are the same (Youdim & Bakhle, 2006).

MAO exists not as a single enzyme, but as two isoforms, i.e. monoamine oxidase type A (MAO-A) and monoamine oxidase type B (MAO-B) (Youdim & Bakhle, 2006). These two isoforms are ~70% identical, and are encoded by separate genes (Edmondson *et al.*, 2009). These two isoenzymes have different pH optima and sensitivity to heat inactivation (Youdim & Bakhle, 2006). Because MAO is a membrane bound enzyme, the mitochondrial microenvironment is an important factor to consider for enzyme activity, although the catalytic properties and inhibitor specificity are not influenced by microenvironmental

differences (Novaroli *et al.*, 2005). Originally MAO-A was distinguished from MAO-B using acetylenic inhibitors (clorgyline and selegiline) and determining their sensitivities to these inhibitors (Youdim *et al.*, 2006).

The first MAO inhibitor to be used therapeutically was iproniazid. Iproniazid was used as an antidepressant as well as a psychotropic drug. Although iproniazid and other MAO inhibitors developed hereafter showed distinctive therapeutic importance, their use was limited because of side effects (Youdim & Bakhle, 2006). Iproniazid caused liver toxicity related to its hydrazine structure, while non-hydrazine MAO inhibitors such as tranylcypromine and pargyline, led to an important and well known side effect, the 'cheese reaction' (Youdim *et al.*, 2006).

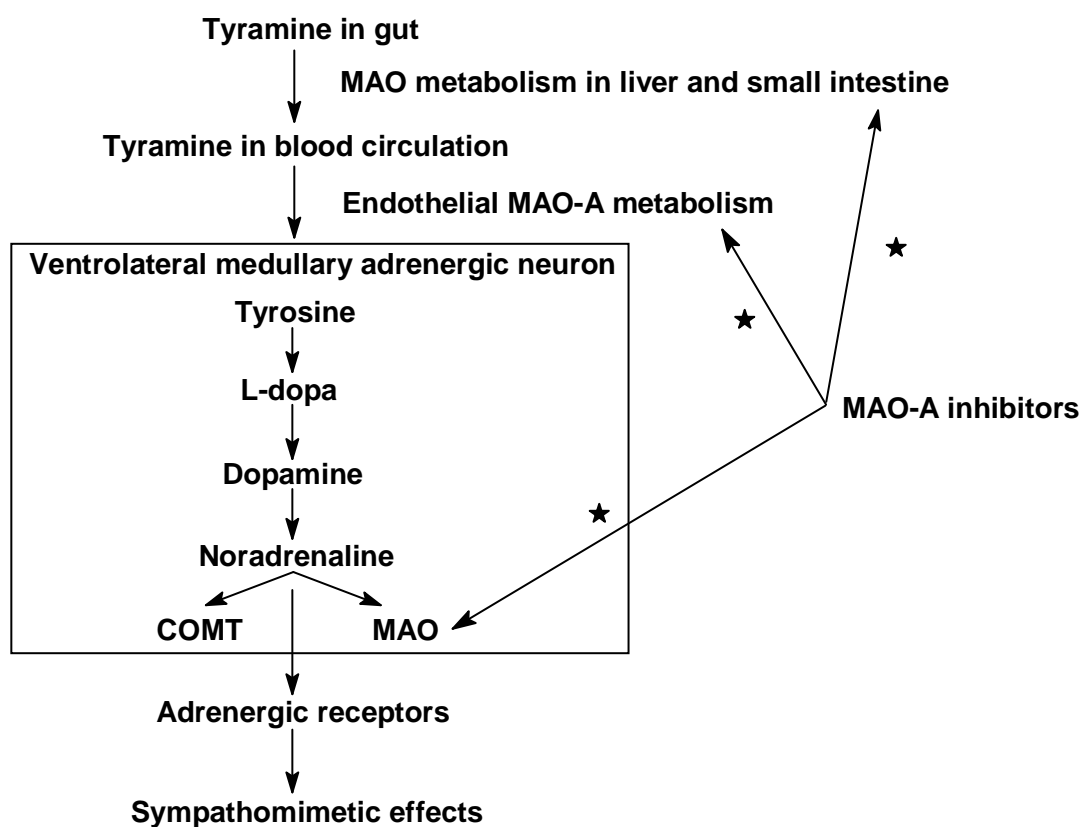


Figure 2.12. The mechanism leading up to the potentially fatal 'cheese reaction'.

MAO is primarily responsible for the oxidation and regulation of neurotransmitter levels in various tissues, but also catalyses the oxidation of xenobiotic amines such as dietary tyramine (Inoue *et al.*, 1999). Tyramine and other indirectly acting sympathomimetic amines present in a variety of food (cheese, beer, wine), taken in combination with a MAO inhibitor lead to the cheese reaction. Normally, tyramine and these other sympathomimetic amines

are extensively metabolised by MAO in the gut wall and liver so that the surviving tyramine that reaches the systemic circulation does not lead to a remarkable release of noradrenaline that cause sympathomimetic effects. In the presence of a MAO inhibitor, this system becomes inactivated and tyramine and other sympathomimetic amines are not metabolised. The intact tyramine and amines reach the systemic circulation leading to a significant release of noradrenaline from peripheral adrenergic neurons. This in turn leads to a severe hypertensive response that may be fatal (Youdim & Bakhle, 2006). Tyramine metabolism rates increase linearly with increasing concentrations of MAO-A or MAO-B (Holt *et al.*, 1997).

The MAOs are located on the outer mitochondrial membrane and are flavo-proteins with flavin adenine dinucleotide as cofactor (Youdim & Bakhle, 2006). The MAOs are present in most mammalian tissues, but the proportions to which these two isoenzymes are present differ from tissue to tissue (Youdim *et al.*, 2006). Of the total MAO activity occurring in the human liver, 80% is due to MAO-B (Inoue *et al.*, 1999). MAO-A appears before MAO-B during fetal development, with the levels of MAO-B rapidly increasing in the brain, more specifically the basal ganglia, after birth (Youdim *et al.*, 2006).

2.3.2. Mechanism of action of MAO

The reaction mechanism of MAO involves the oxidative deamination of neurotransmitters and dietary amines to yield the corresponding aldehyde and free amine. The aldehyde is rapidly converted to a carboxylic acid via aldehyde dehydrogenase (ADH), whilst the hydrogen peroxide generated through the FAD-FADH₂ cycle requires inactivation through glutathione peroxidase (Youdim & Bakhle, 2006). In the catalytic reaction, O₂ is used as the electron acceptor (Edmondson *et al.*, 2009). In this reaction, the identity of the generated aldehyde depends upon the identity of the substrate used, while the use of oxygen and the formation of hydrogen peroxide remain independent of the used substrate (Holt *et al.*, 1997). The byproducts that form during this reaction may fulfill certain functions in the brain, i.e. the aldehyde may be involved in regulation of sleep. However, at higher concentrations these products can accumulate and exert toxic effects. This may be important in Parkinson's disease, where ADH in the substantia nigra is reduced, which allows a build-up of neurotoxic aldehydes derived from dopamine by MAO (Youdim *et al.*, 2006).

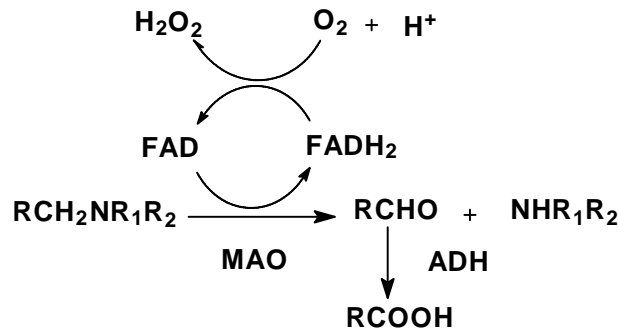


Figure 2.13. The simplistic oxidative deamination reaction catalysed by MAO (Youdim & Bakhle, 2006).

MAO catalysis occurs with cleaving of the amine C_α-H bond and the transfer of two electrons to the flavin that generates an imine and flavin hydroquinone respectively. The amine substrate needs to be in the deprotonated form to enter the substrate binding site for interaction with the flavin (Edmondson *et al.*, 2007). After the deprotonated amine moiety has bonded to the enzyme, it is oxidised to the protonated imine with the covalent 8 α -S-cysteinyl FAD cofactor being reduced to its hydroquinone form. For completion, the reduced FAD cofactor reacts with O₂, generating oxidised flavin and H₂O₂ while the protonated imine is released from the enzyme and undergoes noncatalysed hydrolysis to generate NH₄⁺ and the corresponding aldehyde (Edmondson *et al.*, 2009). Furthermore, one mole of dopaldehyde and H₂O₂ are produced for each one mole dopamine oxidised by MAO. If the generated dopaldehyde and H₂O₂ is not rapidly converted to inactive compounds by centrally located ADH and glutathione peroxidase, these products may exert neurotoxic effects (Van den Berg *et al.*, 2007).

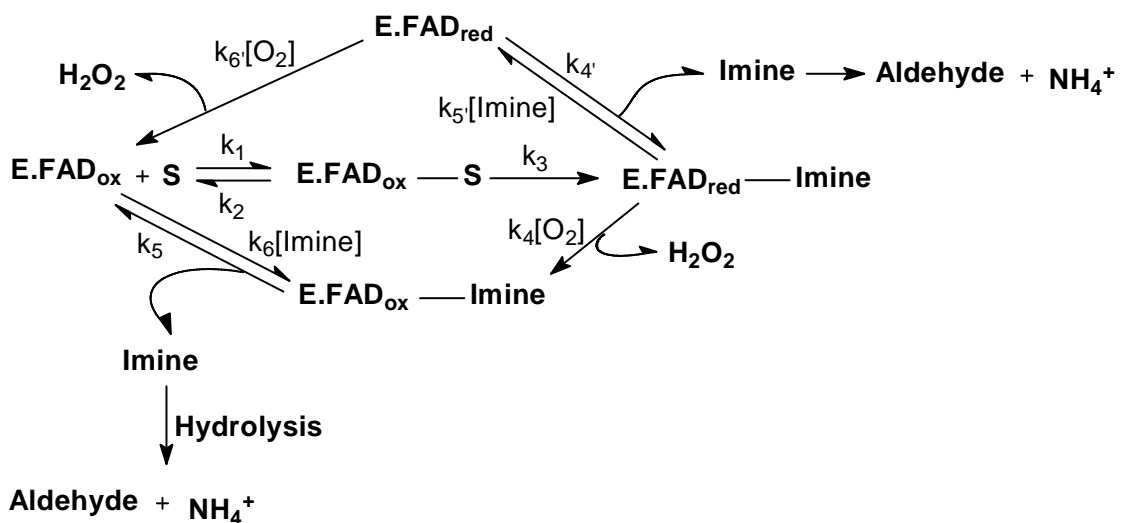


Figure 2.14. A schematic representation of the catalytic reaction pathway followed by MAO-A and MAO-B.

It is important to note that in order to have interaction with the flavin, the deprotonated form of the amine needs to bind to the MAO enzyme. Two mechanisms have been proposed for this electron transfer occurring in MAO catalysis, namely the polar nucleophilic mechanism and the single electron transfer (SET) mechanism.

The polar nucleophilic mechanism proposed by Miller and Edmondson for human MAO-catalysis, is also exhibited by rat MAO-A as well as mutants of both human and rat MAO-A. The polar nucleophilic mechanism is proposed to occur via nucleophilic attack at the oxidised flavin 4a position by the amine. Proton abstraction from the α -carbon of the amine is proposed to occur by the N5 atom of the flavin which becomes nucleophilic. Formation of the iminium product results from the elimination of the reduced flavin. Deprotonated amines do not appear to exhibit the required nucleophilicity, and thus the isoalloxazine ring of the flavin needs to exist in a bent conformation relatively to the planarity in the oxidised state of the enzyme. This allows the carbon at position 4a to be electrophilic and the N5 to be more nucleophilic (Edmondson *et al.*, 2009).

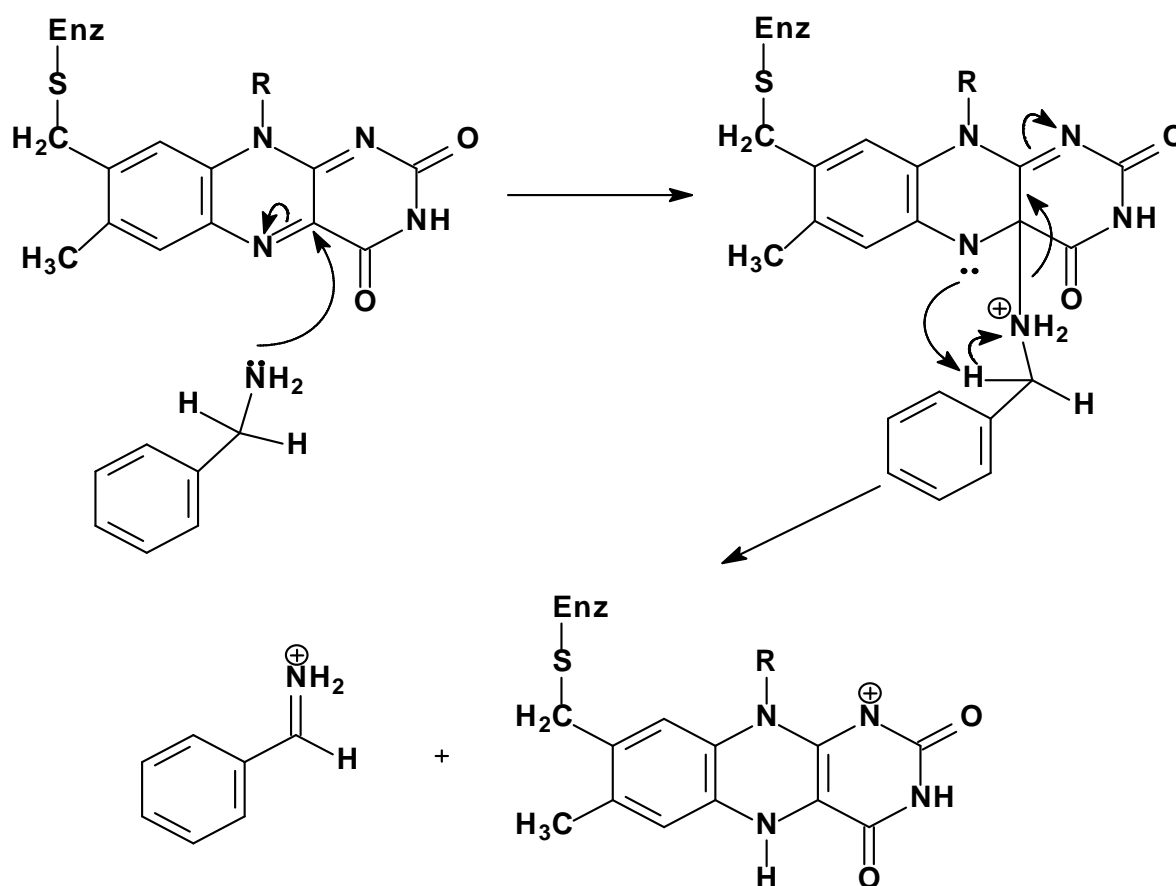


Figure 2.15. The polar nucleophilic mechanism of MAO catalysis.

According to the SET mechanism one electron is transferred from the nitrogen lone pair to the oxidised flavin to generate an aminyl radical cation. After loss of a proton a second electron is transferred to the flavin to give an iminium species. The SET mechanism is based on the rationale that one-electron oxidation of the substrate amine nitrogen will result in labilisation of the α -CH bond allowing abstraction (Edmondson *et al.*, 2007). A very strong base is needed for abstraction that will not likely be fulfilled by a basic amino acid side chain. Thus the amine is first oxidised to the amine cation radical form resulting in α -CH group acidification to lower the pK_a values of these protons for abstraction. Controversies involving the viability of this mechanism exist. In stopped-flow experiments, no flavin radical intermediates are detected spectrally, the rate of enzyme reduction is not influenced by magnetic field and the oxidation-reduction potential of the FAD cofactor is too low to act as an effective oxidant. Furthermore, the structures of MAO-A and MAO-B indicate that no basic amino acid residues could serve as active site bases in the catalysis (Edmondson *et al.*, 2009). Thus, the SET mechanism is kinetically and thermodynamically improbable.

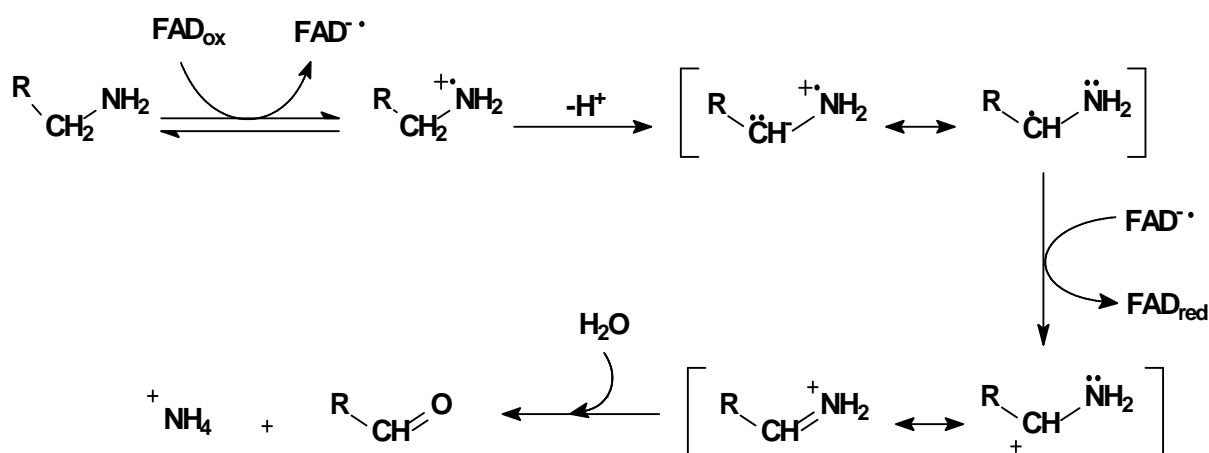


Figure 2.16. The SET mechanism of MAO catalysis.

2.3.3. Biological function of MAO-A

MAO-A is the predominant isoform in the periphery (Youdim & Bakhle, 2006), and oxidises dietary amines and prevents their entry into the systemic circulation (Youdim *et al.*, 2006). Thus the inhibition of MAO-A will lead to an increased amount of dietary amines, especially tyramine, that enter the systemic circulation and in turn the adrenergic neurons to stimulate the release of noradrenaline. This effect is known as the 'cheese reaction' and occurs mostly after the administration of irreversible MAO-A inhibitors. Reversible inhibitors can be displaced by tyramine, which will then be metabolised normally by MAO-A. This reaction is the major cause of the restricted therapeutic use of MAO-A inhibitors (Youdim & Bakhle, 2006).

In the brain, intraneuronal MAO may serve a variety of functions such as protecting the neurons from exogenous amines, terminating neurotransmitter effects and regulating intracellular amine stores (Youdim *et al.*, 2006). MAO-A metabolises noradrenaline and 5-hydroxytryptamine (5-HT; serotonin) (Youdim & Bakhle, 2006) and plays an important role in the deamination of dopamine in synaptosomes from the hypothalamus and striatum (Youdim *et al.*, 2006).

Depression is associated with a decrease in noradrenaline and 5-HT, which are both substrates for MAO-A (Youdim & Bakhle, 2006). MAO-A inhibitors are mostly used therapeutically as antidepressants since MAO-A inhibition in the central nervous system increases dopamine, noradrenaline and 5-HT brain levels (Youdim *et al.*, 2006).

The concurrent administration of MAO-A inhibitors with uptake inhibitors such as the tricyclic antidepressants or the serotonin-selective reuptake inhibitors can cause a serious adverse reaction known as the 'serotonin syndrome' (Youdim & Bakhle, 2006). MAO-A inhibitors potentiate the actions of these drugs by inhibiting the MAO-A-catalysed metabolism of 5-HT. This leads to a serious hyperpyrexia mediated by excessive 5-HT concentrations in the central nervous system (Gilman *et al.*, 1980).

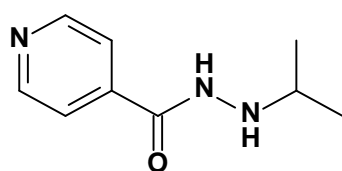
2.3.4. The potential role of MAO-A in Parkinson's disease

There has previously been established that dopamine is metabolised by both MAO-A and MAO-B and that MAO-A is present in the striatum (Youdim *et al.*, 2006). This presents the possible therapeutic application of MAO-A inhibitors in the treatment of Parkinson's disease. Moclobemide, a reversible MAO-A inhibitor, has a mild symptomatic benefit in the treatment of Parkinson's disease, especially in the improvement of motor functions (Youdim *et al.*, 2006). Selective inhibition of MAO-A will not significantly increase dopamine brain levels compared to when both isoenzymes are inhibited (Youdim & Bakhle, 2006), but selective inhibition will affect the release of dopamine. Moclobemide does not provoke the 'cheese reaction', is well tolerated in patients receiving combination therapy of *L*-dopa and peripheral decarboxylase inhibitors, and was first assessed as an antidepressant (Youdim *et al.*, 2006).

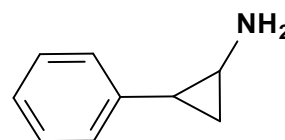
The application of moclobemide as an antidepressant is also useful in patients with Parkinson's disease. 40–60% of patients with Parkinson's disease exhibit signs of depression which results from not only the decrease in striatal dopamine, but also from the reductions in noradrenaline and 5-HT in other brain regions (Youdim *et al.*, 2006).

2.3.5. Inhibitors of MAO-A

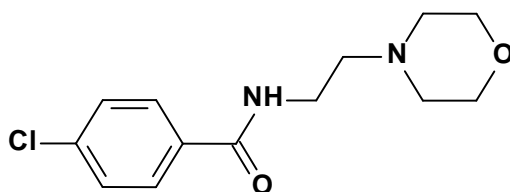
Iproniazid was the first drug to exhibit inhibitory actions towards MAO. It was initially developed to treat tuberculosis, but was later applied in the treatment of depression (Youdim & Bakhle, 2006). Other hydrazine derived MAO inhibitors were developed, such as phenelzine, but these drugs were withdrawn due to serious side effects. These side effects were overcome by the development of non-hydrazine inhibitors, i.e. tranylcypromine and pargyline (Youdim *et al.*, 2006). These non-hydrazine inhibitors, although not causing side-effects associated with the hydrazine inhibitors, exhibited another serious adverse reaction, the 'cheese reaction'. As already mentioned, drugs such as moclobemide, which are reversible MAO-A inhibitors do not cause the cheese reaction due to the fact that they can be displaced by dietary amines. The amines may thus be normally metabolised by MAO (Youdim & Bakhle, 2006).



Iproniazid



Tranylcypromine



Moclobemide

Figure 2.17. The chemical structures of several MAO-A inhibitors.

Non-selective irreversible inhibitors (clorgyline, phenelzine and tranylcypromine) and reversible MAO-A inhibitors (moclobemide, brofaromine, befloxatone and toloxatone) are still clinically used in the treatment of depression in elderly patients, as well as several anxiety and depressive illnesses. Phenelzine also increases corticosterone levels associated with hypothalamic-pituitary-adrenocortical axis activity, while, as mentioned moclobemide has anti-parkinsonian activity (Youdim *et al.*, 2006).

2.3.6. The three dimensional structure of MAO-A

Recently a 3.0 Å structure of human MAO-A in complex with clorgyline has been solved, which makes it possible to attain detail about the molecular structure of the active site of MAO-A (Youdim *et al.*, 2006). From the diffraction pattern of rat MAO-A the entire C-terminal can be elucidated. Rat MAO-A crystallises as a dimer, while human MAO-A crystallises as a monomer. This contrast is due to an amino acid difference at position 151, with human MAO-A possessing a lysine instead of a glutamic acid residue at this position (Youdim *et al.*, 2006).

In rat MAO-A, the carboxy (C)-terminal region is a transmembrane α -helix that anchors the enzyme to the mitochondrial outer membrane, leaving the rest of the protein exposed in the cytoplasm. Entry of either a substrate or inhibitor into the hydrophobic active site cavity (~450 Å) occurs near the intersection of the enzyme with the surface of the mitochondrial membrane. The human MAO-A active site is a single hydrophobic cavity of ~550 Å³. One of the main differences between rat and human MAO-A is the conformation of the cavity-shaping loop formed by residues 210–216, with the rat MAO-A loop being the same as the homologous loop in human MAO-B (Youdim *et al.*, 2006). Rat and human MAO-A consists of single substrate binding cavities with protein loops at the entrances of their cavities. The substrate binding site in MAO-A is quite hydrophobic with the *re* face of the covalent FAD being one of the faces of the substrate binding site opposite to the entrance. Two nearly parallel tyrosine residues, Tyr407 and Tyr444, respectively, forms an “aromatic cage” in front of the flavin (Edmondson *et al.*, 2007).

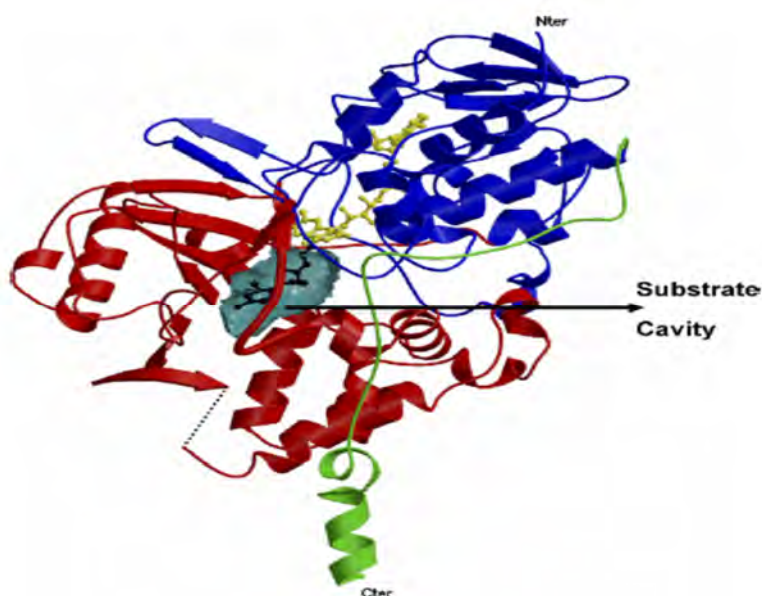


Figure 2.18. A ribbon diagram representing the structure of human MAO-A (Edmondson *et al.*, 2007).

Differences in the active sites of rat MAO-A and human MAO-A affects the conformation of inhibitors when bound to the enzyme. The irreversible inhibitor clorgyline, when bound to rat MAO-A, is extended, while it is in a more folded conformation when bound to human MAO-A. Thus extrapolating results obtained with MAO-A in one species to another cannot be done because of species differences in the structures of MAO-A (Youdim *et al.*, 2006).

2.3.7. Biological function of MAO-B

MAO-B is the isoenzyme with greater activity in the basal ganglia (Youdim & Bakhle, 2006). Originally, the two isoenzymes were distinguished by their sensitivities to the acetylenic inhibitors as well as their substrate specificities. MAO-B is inhibited by low concentrations of the acetylenic inhibitor selegiline and catalyses the oxidation of benzylamine and 2-phenylethylamine, in conjunction with other neurotransmitters and amines. These include noradrenaline, adrenaline, tryptamine and tyramine. Generally MAO-B serves a protective function, especially MAO-B present in the microvessels of the blood-brain barrier (Youdim *et al.*, 2006).

The expression and distribution of MAO may be affected by certain genomic traits. MAO-A and MAO-B proteins are 70% identical, but differ in that MAO-B expression is regulated by a mitogen-activated protein kinase pathway. Certain personality traits (sensation seeking, impulsiveness, extraversion and substance abuse) may be associated with low MAO-B activity in platelets (Youdim *et al.*, 2006).

2.3.8. The role of MAO-B in Parkinson's disease

The metabolism of amines by MAO generates several neurotoxic byproducts, such as neurotoxic aldehydes and hydrogen peroxide. In normal physiology, these metabolites are rapidly converted and excreted, but in the case of Parkinson's disease a deficiency of the enzymes that catalyses this conversion is present. This allows the metabolites to accumulate and contribute to neurodegeneration (Youdim & Bakhle, 2006). Since MAO-B is the main isoform of MAO present in the basal ganglia (Youdim *et al.*, 2006), it can be assumed that MAO-B is responsible for most of the amine metabolism in this region and thus contribute more to the development of Parkinson's disease.

Ageing is a contributing factor to the changing levels of MAO in the human brain (Youdim *et al.*, 2006), with increasing levels of MAO-B while MAO-A levels remain constant (Novaroli *et al.*, 2006). Increased MAO-B activity in the human brain is due to glial cell proliferation, which occurs not only during aging, but is also seen in patients with Parkinson's disease

(Youdim *et al.*, 2006). Oxidative stress is thus increased through glial cell proliferation, a process which may accelerate neuronal loss (Novaroli *et al.*, 2006). Dopamine levels will decrease in the presence of increased MAO-B and thus the levels of the metabolic products of dopamine, namely dopanil and H₂O₂, will increase. The former may be implicated in α -synuclein aggregation while the latter promote apoptosis. Both metabolites thus contribute to the pathogenesis of Parkinson's disease (Edmondson *et al.*, 2009).

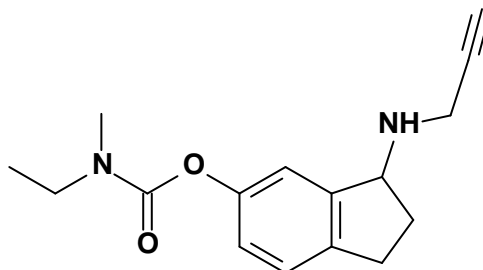
2.3.9. Inhibitors of MAO-B

Selegiline is an irreversible selective MAO-B inhibitor which inhibits the oxidative deamination of all neurotransmitter amines except noradrenaline and 5-HT at low doses (Youdim & Bakhle, 2006). As an irreversible selective MAO-B inhibitor, return of enzyme activity following selegiline administration requires *de novo* synthesis of the MAO-B protein (Vlok *et al.*, 2006). The use of selegiline in depression is inconclusive unless it is administered in concentrations high enough to lose its selectivity for MAO-B and inhibit MAO-A. Selegiline can also enhance recovery after cerebral infarction by decreasing the hydrogen peroxide generated by MAO during ischaemia-reperfusion. Selegiline is used therapeutically in the treatment of Parkinson's disease either as an adjuvant to *L*-dopa or as monotherapy (Youdim *et al.*, 2006). Through the inhibition of the MAO-B-catalysed oxidation of dopamine in the central nervous system, the already depleted dopamine supply of the Parkinson's disease patient is conserved, thus delaying the need for *L*-dopa therapy (Vlok *et al.*, 2006). One of its metabolites, *l*-amphetamine releases dopamine and may contribute to the anti-parkinsonian activity, but can cause sympathomimetic effects which is a disadvantage. Furthermore, it is known that selegiline slow disease progression during the first year of treatment, but this protective effect is lost at higher concentrations (Youdim *et al.*, 2006). The neuroprotective effect of selegiline may be due to the blocking of apoptotic cell death as well as a decrease in the formation of hydrogen peroxide in dopamine metabolism (Vlok *et al.*, 2006).

Rasagiline, a potent selective MAO-B inhibitor has no sympathomimetic effects and presents with greater neuroprotective activity than selegiline (Youdim & Bakhle., 2006). Its neuroprotective activity is related to its propargyl moiety which may be responsible for anti-apoptotic activity (Youdim *et al.*, 2006).

Combined treatment with a MAO inhibitor plus one of the approved cholinesterase inhibitors may be beneficial in Parkinson's disease therapy. One molecule exists that combines these two enzyme inhibitory functions, namely ladostigil (Youdim *et al.*, 2006). Ladostigil is an

inhibitor of both butyryl- and acetylcholinesterases, with a structure related to that of rasagiline. After chronic treatment, it inhibits MAO activity irreversibly and non-selectively. Ladostigil exhibits neuroprotective activity with anti-apoptotic activity identical to that of rasagiline (Youdim & Bakhle, 2006).



Ladostigil

Figure 2.19. The chemical structure of the selective irreversible MAO-B inhibitor, ladostigil.

The MAO-B inhibitors discussed above are all selective irreversible inhibitors, who do not exhibit the serious adverse effect, the 'cheese reaction'. This is due to the fact that little MAO-B is present in the intestine, thus available tyramine is effectively metabolised by intestinal MAO-A (Youdim *et al.*, 2006).

Reversible inhibitors of MAO-B include lazabemide, isatin, (E)-8-(3-chlorostyryl)caffeine, 1,4-diphenylbutene, trans-trans-farnesol and safinamide (Youdim *et al.*, 2006). (E)-8-(3-chlorostyryl)caffeine is an A_{2A} adenosine receptor antagonist as well as a selective MAO-B inhibitor (Youdim *et al.*, 2006). The mode of inhibition of (E)-8-(3-chlorostyryl)caffeine is competitive (Vlok *et al.*, 2006; Strydom *et al.*, 2010). Similar to the inhibition of MAO-B, (E)-8-(3-chlorostyryl)caffeine is also a reversible competitive inhibitor of MAO-A (Strydom *et al.*, 2010). Trans,trans-farnesol is a potent reversible specific MAO-B inhibitor and is a component of tobacco smoke. It has been reported that lazabemide aid smoking cessation and abstinence thereafter, and can also delay progression of disabilities associated with Parkinson's disease and thus have a neuroprotective effect (Youdim *et al.*, 2006). Therapeutically, reversible inhibitors may be more desirable since enzyme activity can be regained after withdrawal of the inhibitor, which is not the case with irreversible inhibitors where the enzyme protein needs to be synthesised *de novo* before activity can be regained (Van den Berg *et al.*, 2007).

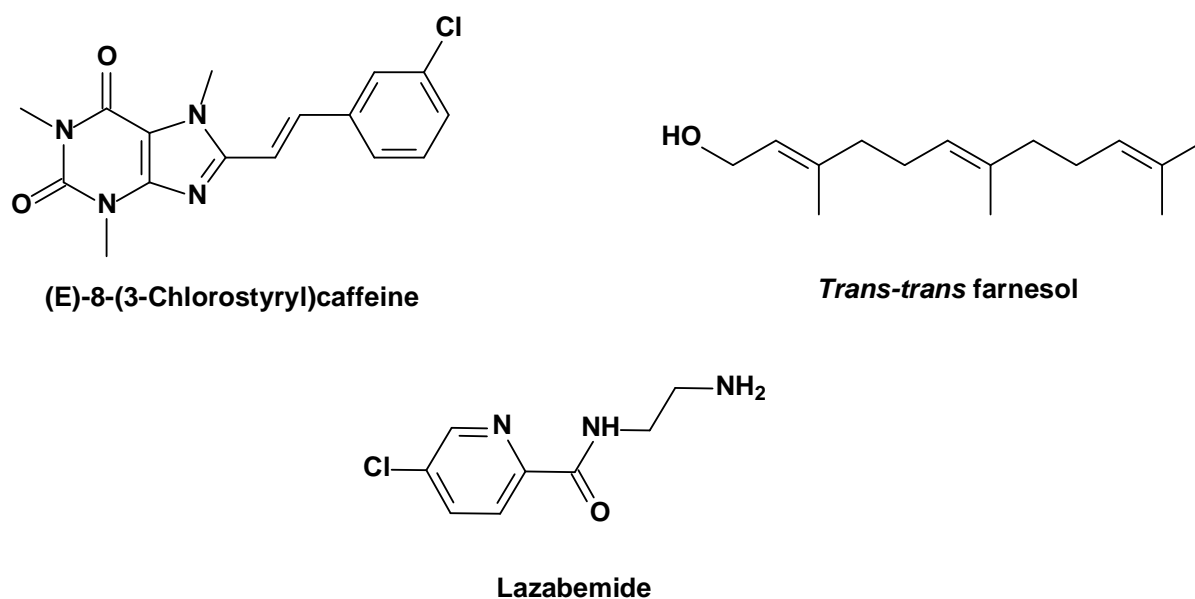


Figure 2.20. Chemical structures of several reversible MAO-B inhibitors.

2.3.10. Three dimensional structure of MAO-B

Human MAO-B crystallises as a dimer (Edmondson *et al.*, 2007) with the C-terminal region not showing well defined electron density with diffraction. This may be because the C-terminal region of human MAO-B consists of transmembrane α -helices that anchor the enzyme to the mitochondria leaving the rest of the protein exposed to the cytoplasm. Substrate entry into the active site of MAO-B occurs near the intersection of the enzyme with the mitochondrial outer membrane (Youdim *et al.*, 2006), and a substrate must negotiate a protein loop at the entrance of the active site before reaching the “entrance cavity”. The entrance cavity leads to the “substrate cavity” which contains the flavin coenzyme (Edmondson *et al.*, 2007). The side chain of Ile199 separates the two cavities and serves as a “gate” between them. The side chain of Ile199 can exist in either an open or closed conformation depending on the substrate or bound inhibitor (Edmondson *et al.*, 2007). The substrate cavity is hydrophobic and is occupied by the FAD coenzyme which binds covalently to the enzyme (Youdim *et al.*, 2006) via an 8α -thioether linkage to Cys397 (Edmondson *et al.*, 2007). The energetically unfavorable *cis*-conformation of the peptide bond between Cys397 and Tyr398 allows the phenolic ring of Tyr398 to align in the proper orientation in the active site. The flavin ring exists in a twisted nonplanar conformation, making the N5 and C4a atoms more sp^3 -like in conformation. In conjunction with the other flavin-dependent amine oxidases, an ordered water molecule forms a hydrogen bond to the N5 of the flavin and the ϵ -amino group of Lys296. Other ordered captive water molecules fill the vacant space in the inhibitor binding cavity. Therefore, future MAO-B inhibitors should

have hydrophilic substituents that would displace this water molecules resulting in greater affinity and specificity (Binda *et al.*, 2003).

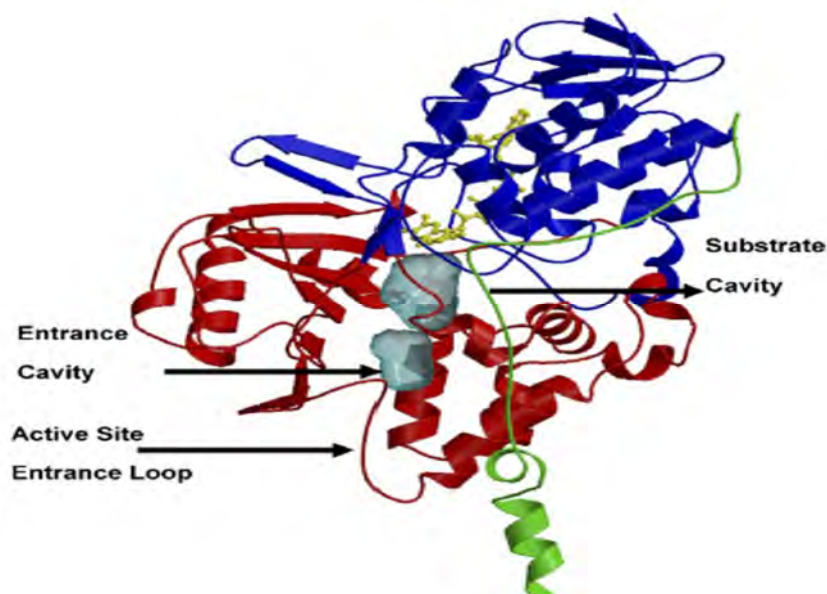


Figure 2.21. Ribbon diagram representing the structure of human MAO-B in monomeric form (Edmondson *et al.*, 2007).

MAO inhibitors that bind covalently to MAO-B, bind to the N5 position of the flavin moiety. The inhibitors are positioned between two tyrosine residues (Tyr398 and Tyr435) perpendicular to the *re* face of the flavin ring. An 'aromatic sandwich' structure is thus formed by the phenolic side chains of Tyr398 and Tyr435, and the bound inhibitor. Substrates and inhibitors must pass between the two tyrosine phenolic rings to reach the flavin ring and potentially exhibit a pharmacological effect (Youdim *et al.*, 2006).

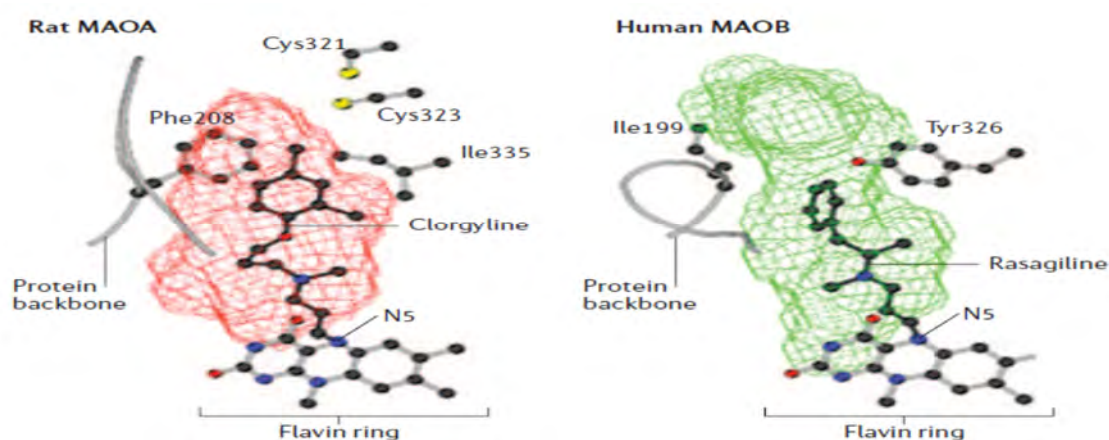


Figure 2.22. Comparison of the active site cavities of rat MAO-A and human MAO-B with the selective inhibitors clorgyline and rasagiline, respectively, bound (Youdim *et al.*, 2006).

Human MAO-B can bind compounds of different sizes, which demonstrates the plasticity of the MAO-B active site cavity. For an inhibitor to gain access to the substrate cavity, it must first pass through an entrance cavity as seen with small inhibitors. In contrast, large inhibitors exhibit a dual binding mode that involves traversing both the entrance and substrate cavities (Van den Berg *et al.*, 2007). As described above, the conformation of Ile199 determine whether the cavity can host small inhibitors (such as isatin or tranylcypramine), or cavity-filling ligands (such as trans,trans-farnesol, safinamide and 1,4-diphenyl-2-butene) (Edmondson *et al.*, 2009). Trans,trans-farnesol, for example, spans both the entrance and substrate cavities only after the side chain of Ile199 rotates into the open conformation. In contrast, the small inhibitor, isatin, binds only to the substrate cavity of MAO-B, and the side chain of Ile199 is thus in the closed position (Van den Berg *et al.*, 2007). Other MAO-B inhibitors induce a midspan type of binding mode because they are large enough to push Ile199 into the open conformation resulting in a more bipartic cavity character. These inhibitors include rasagiline, N-(2-aminoethyl)-p-chlorobenzamide and selegiline (Edmondson *et al.*, 2009).

2.3.11. In vitro measurements of MAO activity

Originally, MAO-A was purified using placental mitochondria as source while MAO-B was derived from bovine liver mitochondria. These preparations were used in several studies requiring purified preparations of the enzymes. Various difficulties arose from using these sources, until *Saccharomyces cerevisiae* was used as the host expression system and thus the first successful heterologous expression of human MAO activity was reported. This system was not a viable source since levels of MAO expression were too low. *Pichia pastoris* is the only source which provides heterologous MAO expression in quantities large enough for further research on the enzymes (Edmondson *et al.*, 2007). MAO-B present in platelets exhibit the same amino acid sequence found in human brain MAO-B, thus human platelets can also be used to indirectly assess MAO-B activity in the central nervous system (Novaroli *et al.*, 2005).

The acidic metabolites formed through the metabolism of 5-HT (5-hydroxyindole acetic acid) or dopamine (dihydroxyphenylacetic acid) are commonly used to measure MAO activity *in vivo* or *in vitro* (Youdim & Bakhle, 2006).

To determine MAO activity *in vitro* most investigators, however, use a specific MAO-A and MAO-B substrate or employ selective MAO inhibitors. For example, to measure MAO-B activity, the selective MAO-A inhibitor, clorgyline, may be added to preparations containing

both enzymes. In this instance a mixed MAO-A/B substrate may be used (Inoue *et al.*, 1999). To measure MAO-A activity, the selective MAO-B inhibitor, selegiline, may be added to preparations containing both enzymes. In this instance a mixed MAO-A/B substrate may also be used.

Holt *et al.* (1997) described a spectrophotometric assay which is suitable for continuous measurement of MAO amine metabolism as well as metabolism by semicarbazide-sensitive amine oxidase (SSAO). This method monitors the formation of hydrogen peroxide during the MAO-catalysed reactions. Holt *et al.* (1997) adapted the commonly used peroxidase-linked method by using 4-aminoantipyrine as the proton donor in the peroxidase reaction. 4-Aminoantipyrine is firstly oxidised by hydrogen peroxide in a peroxidase-coupled reaction, and the oxidised product subsequently condenses with 4-hydroxy-3-methoxybenzoic acid (vanillic acid) that to produce a red quinoneimine dye which absorb light at a wavelength maxima of 498 nm. The H_2O_2 formed during amine metabolism is directly proportional to the measured absorbance in the assay. This rapid quantitative spectrophotometric assay utilises 96-well microtiter plates or cuvettes which is suitable for the continuous or discontinuous measurement of amine metabolism by several enzymes in crude tissue homogenates (Holt *et al.*, 1997).

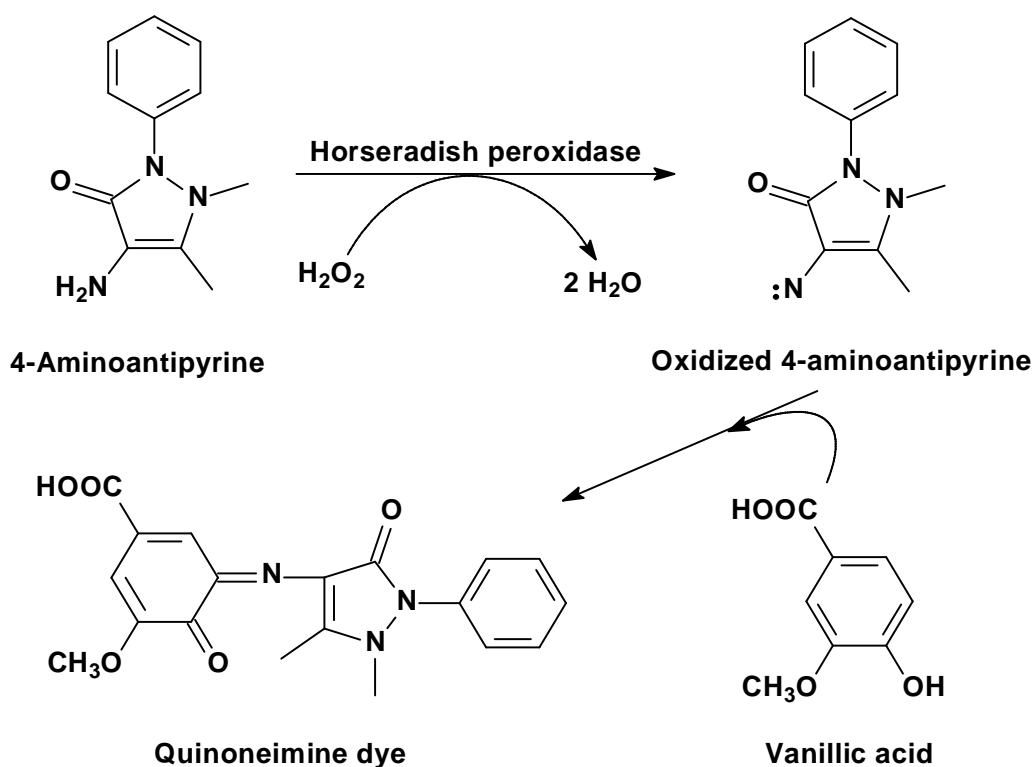


Figure 2.23. The peroxidase-linked continuous assay for amine oxidase enzymes.

Another method to assay MAO activity is to measure, spectrophotometrically, the extent by which MAO oxidises 1-methyl-4-(1-methylpyrrol-2-yl)-1,2,3,6-tetrahydropyridine (MMTP) to form the corresponding dihydropyridinium metabolite (MMDP⁺) (Vlok *et al.*, 2006). MMDP⁺ absorbs light maximally at a wavelength of 420 nm, where the substrate does not absorb light. Because of the favorable chromophoric characteristics as well as the *in vitro* chemical stability of MMDP⁺, this assay has frequently been used to determine MAO activity (Van den Berg *et al.*, 2007).

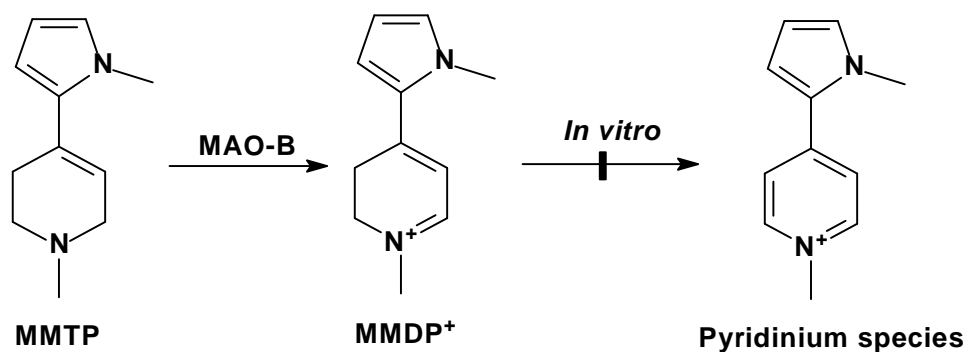


Figure 2.24. The MAO-B catalysed oxidation of MMTP to the corresponding dihydropyridinium product.

Vlok *et al.* (2006) determined the extent of benzylamine oxidation by MAO-B using a high-performance liquid chromatography ultraviolet assay. MAO-B oxidises benzylamine to yield benzaldehyde, which is subsequently measured by HPLC analysis. Benzylamine is the most thoroughly characterised substrate of MAO-B and is widely used in inhibition and mechanistic studies. When purified MAO-B enzyme is used as source, background interference is limited and thus the concentration of the resulting α -carbon oxidation product, in this case benzaldehyde, may be measured spectrophotometrically at a wavelength of 250 nm. When mitochondrial preparations of MAO-B are used, background interference prohibits the spectrophotometric measurement of benzylamine. In this case HPLC analysis is more appropriate.

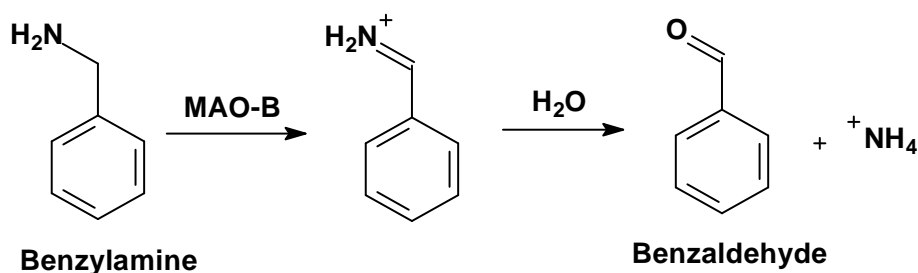


Figure 2.25. The MAO-B catalysed oxidation of benzylamine.

Another useful method for determining MAO-A and MAO-B activities utilises kynuramine as MAO substrate. This assay depends on the direct spectrofluorometric measurement of 4-hydroxyquinoline, the ultimate MAO oxidation product of kynuramine. An advantage of this method is that it can be applied to crude tissue extracts and appears to be the method of choice for following the localisation and purification of MAO. Kynuramine is a MAO-A/B mixed substrate, and is oxidised by the MAO enzymes to yield the fluorescent metabolite, 4-hydroxyquinoline. Concentration measurements of 4-hydroxyquinoline may be conveniently carried out by fluorescence spectrophotometry (excitation wavelength of 310; emission wavelength of 400 nm) (Weissbach *et al.*, 1960).

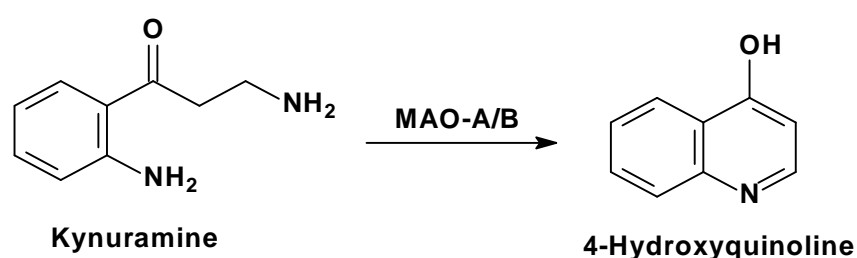


Figure 2.26. The MAO-A/B catalysed oxidation of kynuramine to the fluorescent metabolite, 4-hydroxyquinoline.

2.4. Copper-containing amine oxidases

2.4.1. General background and classification

The enzymatic classification of amine oxidases are traditionally divided into two main groups, which is based on the chemical nature of the attached cofactor, namely FAD or topa-quinone (TPQ). The TPQ-containing enzymes are collectively designated as SSAO. These two classes of enzymes differ in their cofactors, subcellular distribution, substrates, inhibitors and also their biological function (Jalkanen & Salmi, 2001).

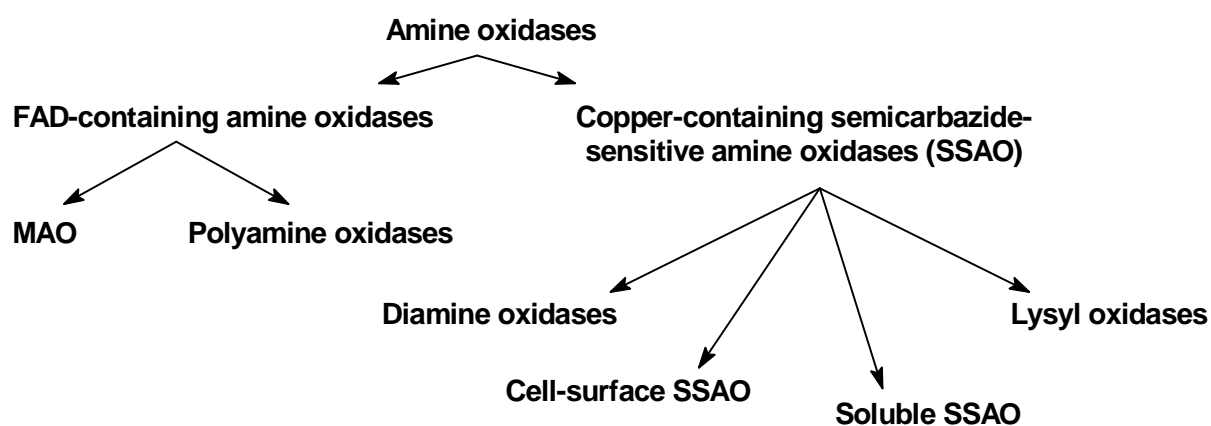


Figure 2.27. A schematic illustration of the different classes of amine oxidases.

2.4.2. Substrates and known inhibitors of copper-containing amine oxidases

The different subclasses of SSAOs each prefer their own substrate. For example, diamine oxidase prefers diamines such as putrescine and cadaverine as its substrates, while the soluble and cell surface SSAOs prefer different substrates. Different species exhibit a wide variation in the preferred substrates, thus caution should be exerted when generalising results. Most SSAOs use benzylamine as substrate, with methylamine and allylamine also being acceptable substrates in humans (Jalkanen & Salmi, 2001). Substrates such as N-methylbenzylamine, which is a secondary amine, are not SSAO substrates. The reason for this exclusion remains unknown, but it has been proposed that SSAOs have evolved in such a manner that it deliberately statically exclude secondary amines as not to interact with the N-alkyl reductively aminated cofactor (Lee *et al.*, 2002).

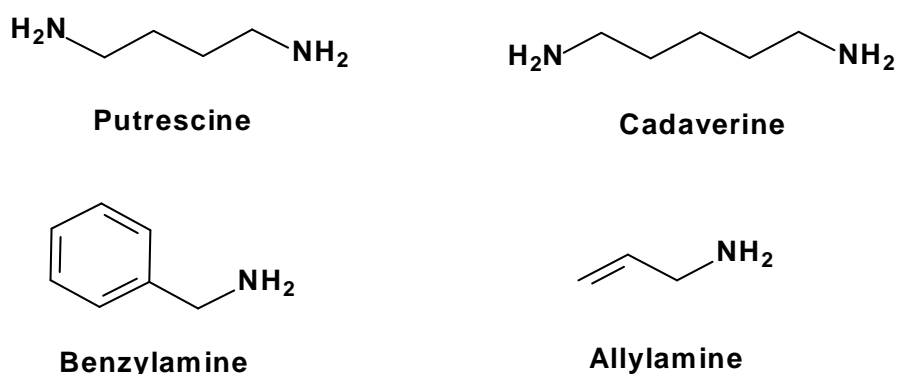


Figure 2.28. The chemical structures of several substrates of copper-containing amine oxidases.

Historically SSAOs have been defined by their inhibition with carbonyl-reactive compounds such as semicarbazide, although several other inhibitors have been described since. In contrast to semicarbazide, hydroxylamine is a more potent and selective SSAO inhibitor. Other inhibitors include propargylamine, aminoguanidine, carbidopa and procarbazine, although these inhibitors are not selective towards SSAO. Some clinically used drugs may also inhibit SSAOs, such as isoniazid, hydralazine and mexiletine. Recently more selective SSAO inhibitors have been developed, namely B24 or 3,5-ethoxy-4-aminomethylpyridine and MDL72274 (Jalkanen & Salmi, 2001). Mechanism-based irreversible inactivators are another class of SSAO inhibitors that result in long-acting inhibition *in vivo* and offer secondary selectivity. Overall the approach for the development of new inhibitors is to target the imine shift mechanism of SSAOs. Since FAD-containing enzymes do not utilise an imine shift mechanism, only the copper-containing amine oxidases will be affected by such inhibitors. This will result in potentially extremely specific inhibitors (Lee *et al.*, 2002).

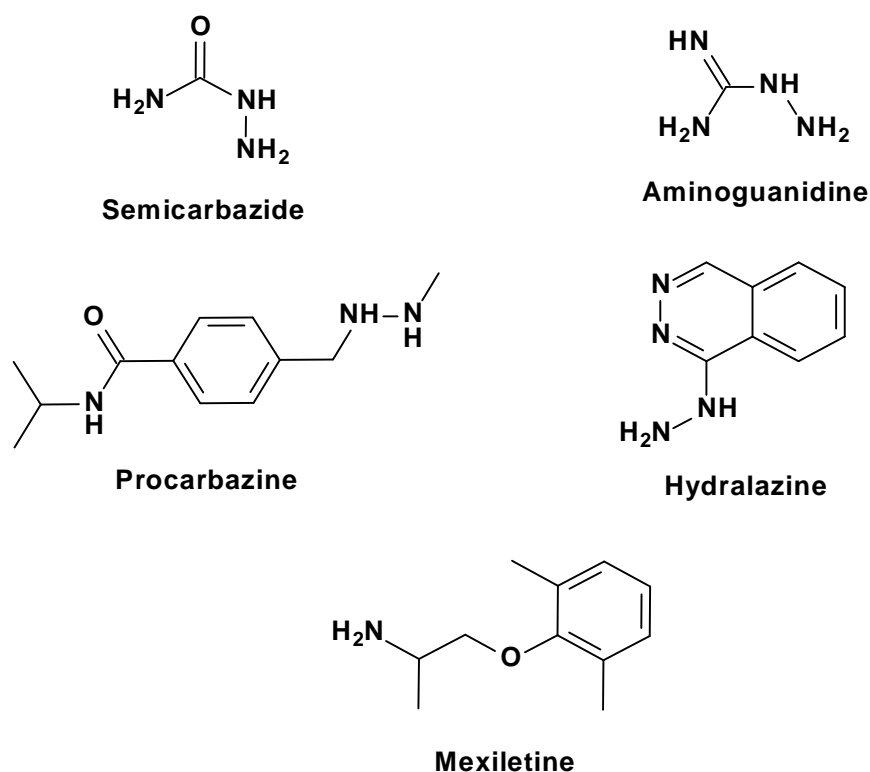


Figure 2.29. The chemical structures of several SSAO inhibitors.

2.4.3. Biological function and mechanism of action of SSAOs

The quinone-dependent copper amine oxidases mediate a pyridoxal phosphate transamination mechanism for the oxidative deamination of primary amines to the corresponding aldehydes (Jalkanen & Salmi, 2001). This reaction is illustrated in the figure below.

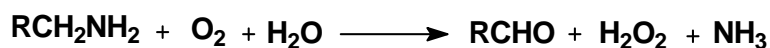


Figure 2.30. Simplified reaction of the oxidative deamination of primary amines to yield the resulting aldehydes via SSAOs.

The reaction displayed above consists of two half-reactions: (1) reduction of SSAO by the substrate while the corresponding aldehyde is released, and (2) oxidation of SSAO with the release of H_2O_2 and ammonia/ammonium ($\text{NH}_4^+/\text{NH}_3$). The reductive half-reaction involves the sequential formation of multiple transition stages (Jalkanen & Salmi, 2001), while the oxidation via the substrate is initiated by Schiff base formation between the primary amine and the TPQ cofactor. From here the “substrate Schiff base” tautomerises to yield a “product Schiff base” resulting in the aldehyde product through hydrolysis. The reduced cofactor generated by this hydrolysis, is oxidatively recycled to the original quinone with the release of H_2O_2 (Lee *et al.*, 2002).

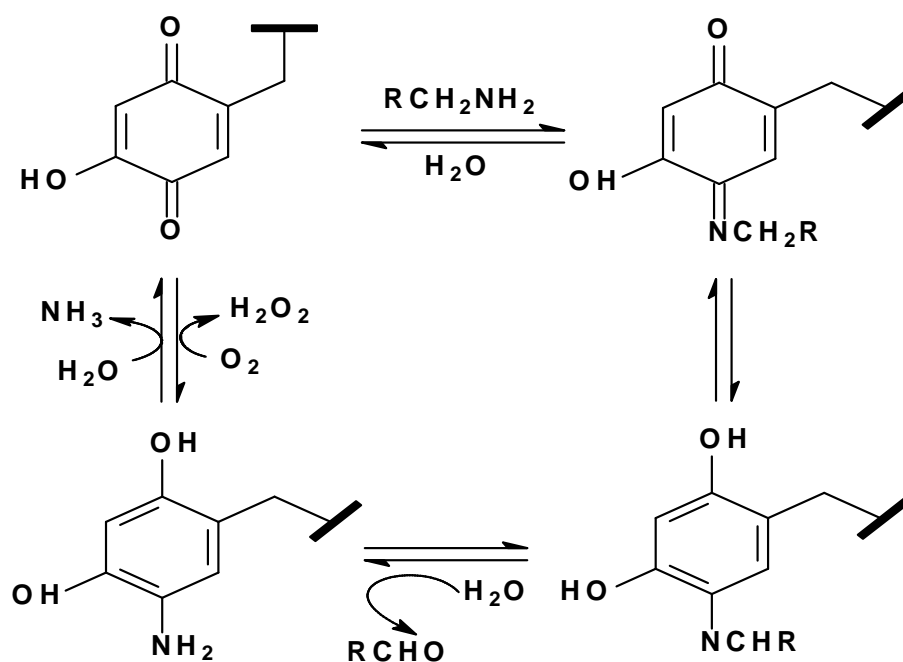


Figure 2.31. The mechanism of action of SSAO, demonstrating the Schiff base formation.

Human SSAO can use a variety of xenobiotic amines as substrates which are usually converted to more toxic products than the parent compound. Some of these toxic products may be of physiological significance. Acrolein is derived from allylamine, which may account for atherosclerotic lesions, while methylamine generates formaldehyde and the deamination of amino-acetone yields methylglyoxal. All products formed through SSAO-catalysed catabolism are biologically active, as seen with H_2O_2 . H_2O_2 generated by the mechanism displayed in figure 2.30, may act as a signal-transducing molecule, in addition to regulating the function of transcription factors and expression of various genes. Furthermore, H_2O_2 regulates the proliferation and adhesion of endothelial and smooth muscle cells in the vascular wall. Generally, SSAOs biological function in mammals focusses on the metabolism of exogenous and endogenous amines. Soluble SSAOs is present in high levels in specific diseases (diabetes and liver disorders), contributing to the pathology of these diseases. Recently different functions of SSAOs have been proposed, namely regulation of glucose metabolism in adipose cells and regulation of leukocyte trafficking in endothelial cells. In mature adipocytes high levels of SSAO are present which co-localises with GLUT4 vesicles responsible for glucose uptake. In the presence of SSAO substrates an increase in glucose transport occurs, making the biological significance more evident (Jalkanen & Salmi, 2001).

2.4.4. The three-dimensional structure of the copper-containing amine oxidases

The activity of SSAOs can be determined by measuring enzymatic amine oxidase activity in cells, tissues and bodily fluids. Several SSAOs from a variety of species have recently been cloned. One of the SSAOs to be cloned was from bovine liver. Most SSAOs are dimers with two copper atoms per dimer, resulting in molecular masses of 140-180 kDa. The TPQ cofactor associated with SSAO is generated from an intrinsic tyrosine in SSAO utilising a bound copper ion and molecular oxygen. SSAOs are a multimember family with three independent groups identified in humans, which all cluster in the long arm of chromosome 17 of the human genome. Enzymes isolated from the same species exhibit a high degree of identity among the amino acids, while intra- and extracellular enzymes within one species differ more in sequence. However, most SSAOs display the same conserved signature motif at the active site. A tyrosine is always responsible for the generation of TPQ cofactor with three conserved histidines coordinating the copper atoms. In all alignments of the enzyme, a His-X-His motif is present at approximately 50 residues from the cofactor towards the C-terminal. Another histidine is located 20–30 residues towards the N-terminus from TPQ. A conserved Asp residue plays an important role in the reductive half-reaction by acting as a catalytic base and resides approximately 100 residues towards the N-terminal from TPQ (Jalkanen & Salmi, 2001).

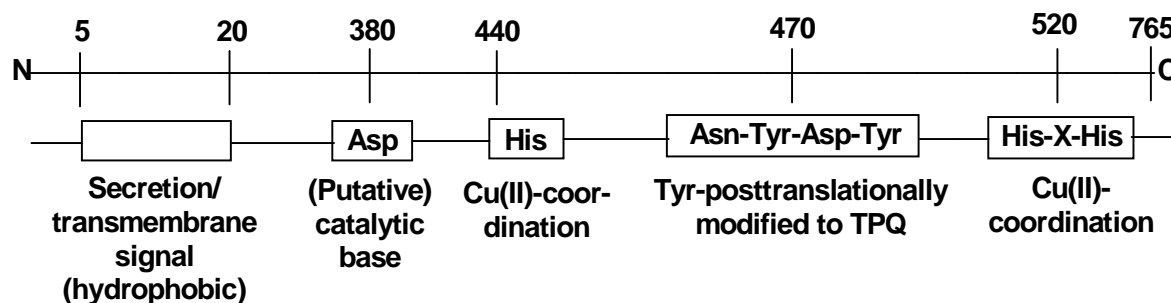


Figure 2.32. The most important structural motifs of SSAOs.

2.5. Conclusion

In this chapter, Parkinson's disease was discussed as a common neurodegenerative disorder with an unknown pathological mechanism of neurodegeneration. The symptomatic treatment options for Parkinson's disease were briefly discussed, as well as some neuroprotective strategies to delay the progress of the disease. Further, the enzymes proposed to contribute to the pathogenesis of Parkinson's disease, the MAOs, were discussed in detail. Background information was given on the biological mechanisms, proposed pathological roles in Parkinson's disease, and the three dimensional structures of these enzymes to give insight to the therapeutic potential of drugs that inhibit these

enzymes. Known inhibitors of MAO were briefly discussed, although the aim of this study is to synthesise new MAO inhibitors, specifically MAO-B inhibitors, with reversible action and a better adverse effect profile. The methods of *in vitro* measurements of monoamine oxidase were briefly discussed to provide insight into the enzymology section of the study. The chapter also provides background information on the copper-containing amine oxidases and current animal models used to mimic Parkinson's disease with the intention of determining the optimal treatment options and future targets for drug development. The inhibitors that will be designed and synthesised in this study may contribute to the knowledge of current anti-parkinsonian drugs and may be useful in the future design and development of drugs for the therapy of Parkinson's disease.

CHAPTER 3

Preparation of synthetic targets

3.1. Introduction

In the search for novel MAO inhibitors, phthalide (**1**) has emerged as a promising scaffold. In previous studies, substituted phthalides have been shown to act as highly potent competitive inhibitors of MAO-A and MAO-B (Strydom *et al.*, 2013). It was further shown that substitution on the C5 of the phthalide ring with a benzyloxy side chain generates particularly potent MAO inhibitors. In the current study, sesamol and benzodioxane derivatives will be synthesised and investigated as potential inhibitors of MAO-A or MAO-B. Based on their structural similarities with phthalide, sesamol (**2**) and benzodioxane (**3**) may also be useful scaffolds for the design of MAO inhibitors. Since the benzyloxy side chain was found to enhance the MAO inhibitory potencies of phthalide, the benzyloxy side chain will similarly be attached to the C5 or C6 positions on the phenyl ring of sesamol and benzodioxane, respectively. It is proposed that, as with phthalide, the substitution on C5 or C6 of sesamol and benzodioxane will yield potent inhibitors of MAO-A or MAO-B. The analogues that will be prepared in this study are illustrated in table 3.1. As shown in the table, sesamol derivatives (**4**) and benzodioxane derivatives (**5**) containing the benzyloxy side chain on C5 (**4a**) or C6 (**5a**), respectively, will be synthesised. Compounds that contain *meta* substituents (chlorine (**4b** and **5b**), bromine (**4c** and **5c**)) on the benzyloxy phenyl ring will also be synthesised. To explore chemical space, derivatives will be synthesised which differ in the length of the attached side chain. In this respect, sesamol and benzodioxane derivatives containing the phenylethoxy (**4d** and **5d**) and phenylpropoxy (**4e** and **5e**) substituents on C5 or C6, respectively, will be synthesised. Furthermore sesamol and benzodioxane will be substituted with the phenoxyethoxy (**4f** and **5f**) side chain. Derivatives containing *para* substituents (chlorine (**4g** and **5g**)) and bromine (**4h** and **5h**)) will also be included in this study.

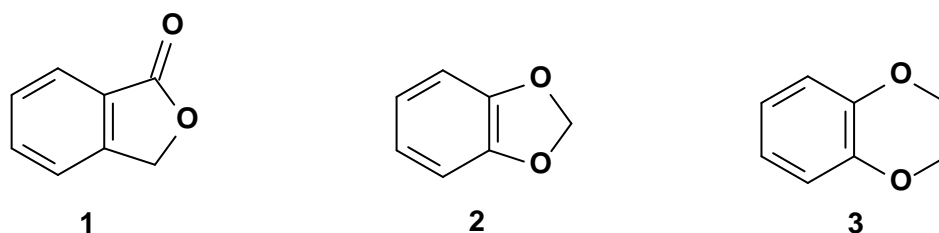
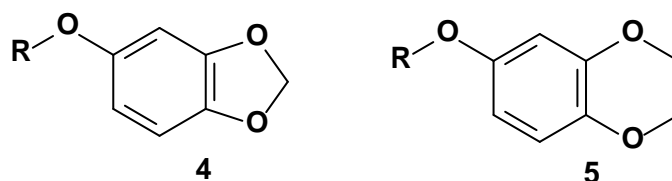


Figure 3.1. The chemical structures of phthalide (**1**), sesamol (**2**) and benzodioxane (**3**).

Table 3.1. The chemical structures of the sesamol and benzodioxane derivatives that will be synthesised in this study.



R			
a		b	
c		d	
e		f	
g		h	

Considering the structural features of the compounds that will be synthesised, the following structure-activity relationships (SARs) may be determined:

- The effect that halogen (chlorine and bromine) substitution on the *meta* position of the benzyloxy phenyl ring may have on the MAO-A and MAO-B inhibition potencies of the sesamol and benzodioxane derivatives **4a** and **5a** (**4b**, **4c** vs. **4a**, and **5b**, **5c** vs. **4a**).
- The effect that differing lengths of the attached C5 and C6 side chains may have on the MAO-A and MAO-B inhibition potencies of the sesamol and benzodioxane derivatives **4a** and **5a** (**4d**, **4e** vs. **4a**, and **5d**, **5e** vs. **4a**).
- The effect that the phenoxyethoxy side chain may have on the MAO-A and MAO-B inhibition potencies of the selected sesamol and benzodioxane derivatives (**4f** vs. **4a**, and **5f** vs. **4a**).

- The effect that halogen (chlorine and bromine) substitution on the *para* position of the phenoxyethoxy phenyl ring may have on the MAO-A and MAO-B inhibition potencies of the sesamol and benzodioxane derivatives **4f** and **5f** (**4g**, **4h** vs. **4f**, and **5g**, **5h** vs. **4f**).
- The MAO inhibition potencies of the sesamol derivative inhibitors (**4a–h**) will be compared to the inhibition potencies of the benzodioxane derivative inhibitors (**5a–h**).
- It will be determined whether the sesamol and bezodiozane analogues examined in this study exhibit selective inhibition of either MAO-A and MAO-B.

However, the main goal of this study is to discover novel highly potent inhibitors of human MAO-A and MAO-B.

3.2. Synthesis of target compounds

3.2.1. Literature method

In this study, the following two synthetic procedures will be followed:

- The synthesis of sesamol analogues have previously been reported by Bezerra-Netto *et al.* (2006). Employing the reported procedure, 5-hydroxysesamol (**6**) in a solution of freshly distilled DMF will be reacted with an appropriate alkyl bromide in the presence of potassium carbonate (K_2CO_3). Thin layer chromatography (TLC) will be used to determine the consumption of **6** as an indication of the completion of the reaction. Upon completion, the reaction mixture will be poured into water. The resulting precipitate will be collected by filtration, air dried and recrystallised from methanol to yield the C5-substituted sesamol derivatives (**4a–h**).

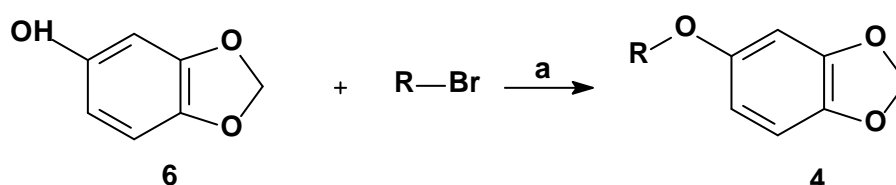


Figure 3.2. The general synthetic route for the synthesis of C5-substituted sesamol derivatives (**4**). Key: (a) DMF, K_2CO_3 .

- 6-Hydroxy-1,4-benzodioxane (**7**) will serve as key starting material. The synthesis of 6-hydroxy-1,4-benzodioxane was previously reported (Broka *et al.* 2005). Employing this procedure, to a solution of 1,4-benzodioxan-6-carboxaldehyde in dichloromethane (CH_2Cl_2) *meta*-chloroperoxybenzoic acid (mCPBA) will be added.

After work-up, the target 6-hydroxy-1,4-benzodioxane (**7**) will be obtained. For the preparation of the C6-substituted benzodioxane (**5a–h**) derivatives, 6-hydroxy-1,4-benzodioxane will be reacted with an appropriate alkyl bromide in the presence of K_2CO_3 as described above for the synthesis of the sesamol derivatives (**4a–h**).

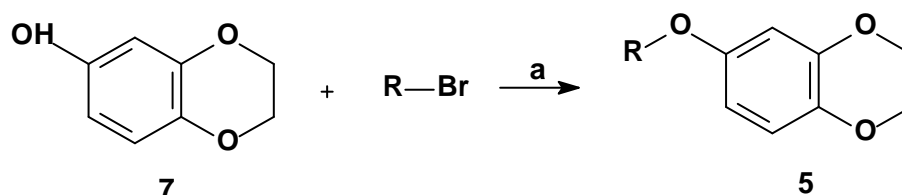


Figure 3.3. The general synthetic route for the synthesis of C6-substituted benzodioxane derivatives (**5**). Key: (a) DMF, K_2CO_3 .

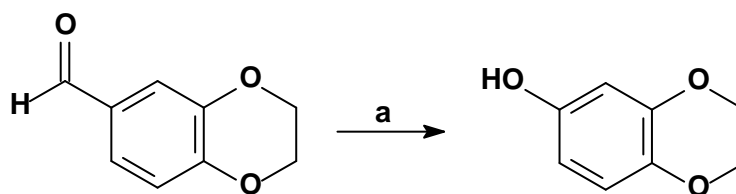


Figure 3.4. The general synthetic route for the synthesis of 6-hydroxy-1,4-benzodioxane (**7**). Key: (a) CH_2Cl_2 , mCPBA.

3.2.2. Materials and instrumentation

Materials

All starting materials and solvents were obtained from Sigma-Aldrich, and were used without further purification.

Thin layer chromatography

TLC was used to determine whether the reactions proceeded to completeness. Silica gel TLC sheets were used with a mobile phase consisting of ethyl acetate (10%) and petroleum ether (90%). The thin layer sheets were observed under an UV-lamp at a wavelength of 254 nm.

Melting points

The melting points of all the synthesised compounds were determined using a Buchi M-545 melting point apparatus and are uncorrected.

Mass spectra

High resolution mass spectra (HRMS) were recorded with a Bruker micrOTOF-Q II mass spectrometer in atmospheric-pressure chemical ionization (APCI) mode.

Nuclear magnetic resonance (NMR)

Proton (^1H) and carbon (^{13}C) NMR spectra were recorded on a Bruker Avance III 600 spectrometer at a frequency of 600 MHz for ^1H NMR spectra and 150 MHz for ^{13}C NMR spectra.

High pressure liquid chromatography

HPLC was used to determine the purities of the synthesised compounds. The HPLC analyses were conducted with an Agilent 1100 HPLC system equipped with a quaternary pump and a diode array detector. HPLC grade acetonitrile (Merck) and Milli-Q water (Millipore) was used for the chromatography. A Venusil XBP C18 column (4.60 × 150 mm, 5 μm) was used for separation and the mobile phase consisted initially of 30% acetonitrile and 70% Milli-Q water at a flow rate of 1 ml/min. At the start of each HPLC run a solvent gradient program was initiated by linearly increasing the composition of the acetonitrile in the mobile phase to 85% acetonitrile over a period of 5 min. Each HPLC run lasted 15 min and a time period of 5 min was allowed for equilibration between runs. A volume of 20 μl of solutions of the test compounds in acetonitrile (1 mM) was injected into the HPLC system and the eluent was monitored at wavelengths of 210, 254 and 300 nm.

3.2.3. Detailed synthetic procedures

3.2.3.1. Procedure for the synthesis of C5-substituted sesamol derivatives (4)

The following is an account of the procedure followed to synthesise the various C5-substituted sesamol derivatives (**4a–h**):

The synthesis of sesamol analogues have previously been reported by Bezerra-Netto *et al.* (2006). Employing the reported procedure, 5-hydroxysesamol (**6**, 3 mmol) was dissolved in DMF (5 ml) and anhydrous K_2CO_3 (9 mmol) was subsequently added. The mixture was stirred at room temperature for 30 min. An appropriate alkyl bromide (3 mmol) was subsequently added to the reaction and the mixture was stirred at room temperature for 20 h. After TLC analysis established the total consumption of **6**, the mixture was poured into water (150 ml) and the resulting precipitate was collected by filtration. The precipitate was air dried and dissolved in boiling methanol (~17 ml). The resulting solution was hot filtered

and allowed to crystallise first at room temperature and subsequently at 2–8 °C and –20 °C. The formed crystals were collected by filtration and air dried.

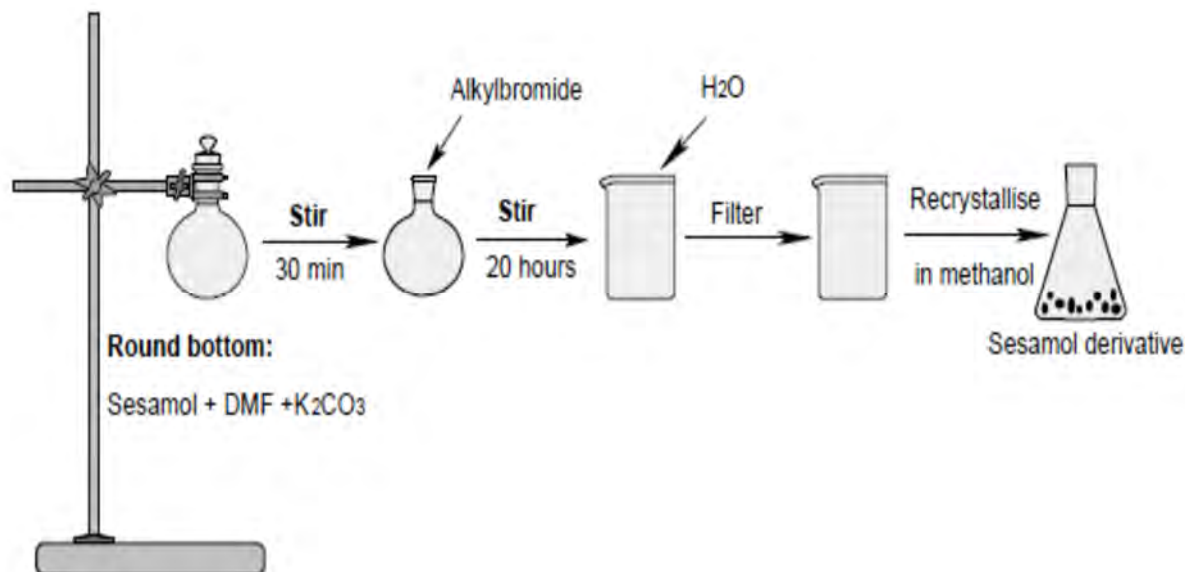


Figure 3.5. Experimental setup for the synthesis of C5-substituted sesamol derivatives (**4a–h**).

3.2.3.2. Procedure for the synthesis of 6-hydroxy-1,4-benzodioxane (7)

The following is an overview for the method used to synthesise 6-hydroxy-1,4-benzodioxane (**7**) that was required as a reactant in the synthesis of the C6-substituted benzodioxane derivatives (**5**):

The synthesis of 6-hydroxybenzodioxane has been previously reported (Broka *et al.*, 2005). Employing this procedure, 1,4-benzodioxan-6-carboxaldehyde (6 mmol) in a solution of dichloromethane (CH₂Cl₂, 16 ml) was treated with mCPBA (7.2 mmol) and heated to 50 °C. After 16 h, saturated sodium bicarbonate (NaHCO₃, 50 ml) was added to the mixture. The mixture was extracted using CH₂Cl₂ (50 ml) and concentrated *in vacuo*. The residue was subsequently dissolved in methanol (16 ml), and NaOH (6.5 mmol) was added to the solution. The resulting mixture was stirred for 2 h, and then treated with concentrated hydrochloric acid (HCl, 6.5 ml). The mixture was extracted to ethyl acetate (3 x 50 ml). The combined organic fractions were washed with saturated NaHCO₃ (50 ml) and brine (50 ml), concentrated *in vacuo* and taken up in CH₂Cl₂ (50 ml). To remove the precipitate, the solution was filtered. The resulting filtrate was stirred with saturated NaHCO₃ (50 ml) for 1 h. The CH₂Cl₂ phase was separated, dried over magnesium sulphate (MgSO₄, 3 g), filtered and concentrated *in vacuo* to yield 6-hydroxy-1,4-benzodioxane (**7**).

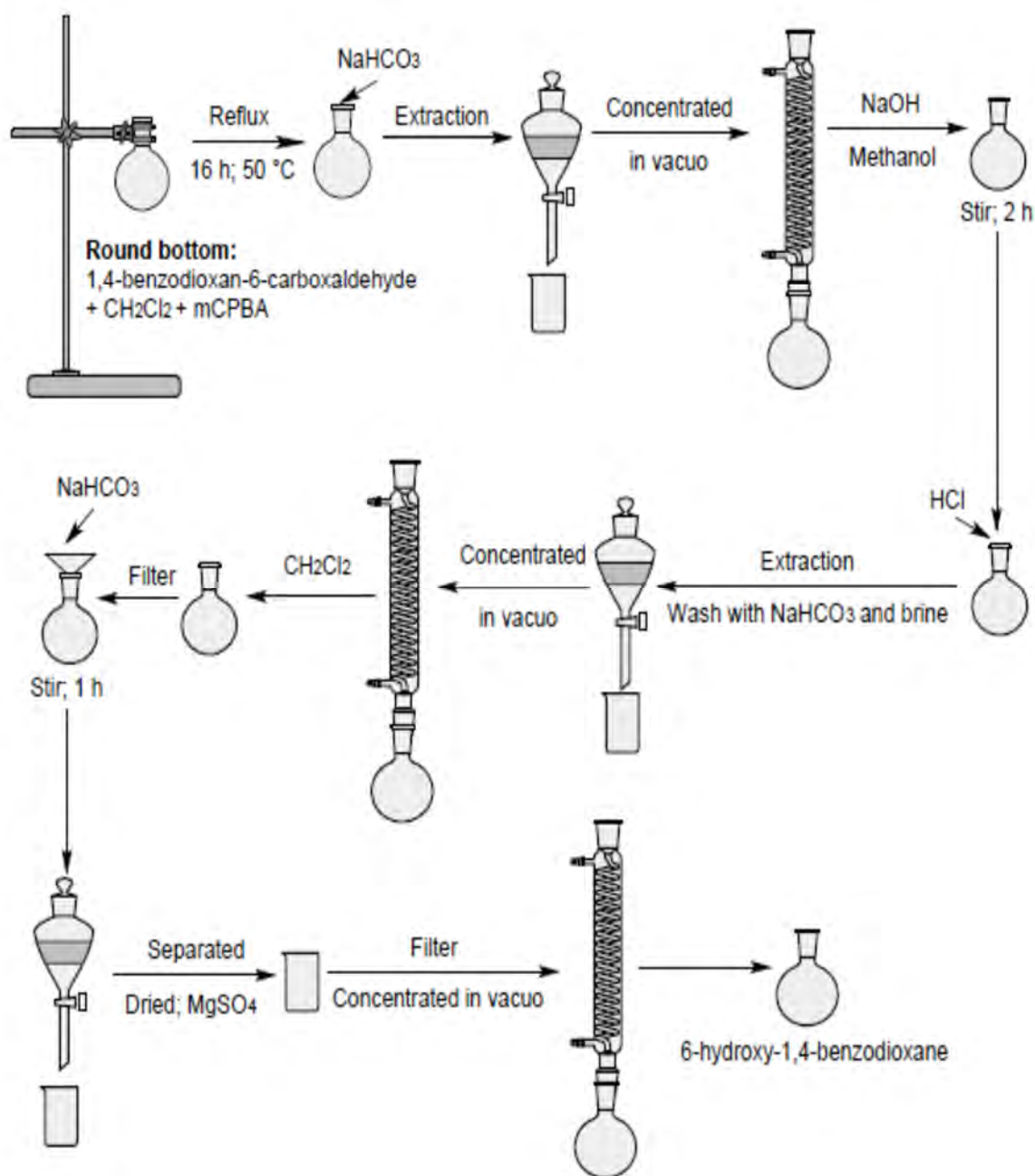


Figure 3.6. Experimental setup for the synthesis of 6-hydroxy-1,4-benzodioxane (7).

3.2.3.3. Procedure for the synthesis of C6-substituted benzodioxane derivatives (5)

The following is the procedure employed to synthesise the various C6-substituted benzodioxane derivatives (5a–h):

6-Hydroxy-1,4-benzodioxane (7, 2 mmol) was dissolved in DMF (3.33 ml) and K₂CO₃ (6 mmol) was subsequently added. The mixture was stirred at room temperature for 30 min. An appropriate alkyl bromide (2 mmol) was added to the reaction and the mixture was stirred at room temperature for a further 20 h. After TLC analysis established the total consumption

of **7**, the mixture was poured into water (150 ml) and the resulting precipitate was collected by filtration. The precipitate was air dried and dissolved in boiling methanol (~17 ml). The resulting solution was hot filtered and allowed to crystallise first at room temperature and then subsequently at 2–8 °C and –20 °C. The formed crystals were collected by filtration and air dried. For those compounds which were oils (**5a–5e**), after the reaction mixture was poured into water (150 mL), the product was extracted to ethyl acetate (1 × 50 mL). The organic fraction was dried over anhydrous magnesium sulphate (3 g) en concentrated in vacuo. Purification of the residue was done by silica gel column chromatography (40 mm × 75 mm) using petroleum ether/ ethyl acetate (7:3) as mobile phase. For this purpose the VersaFlash flash chromatography purification system was employed (Supelco).

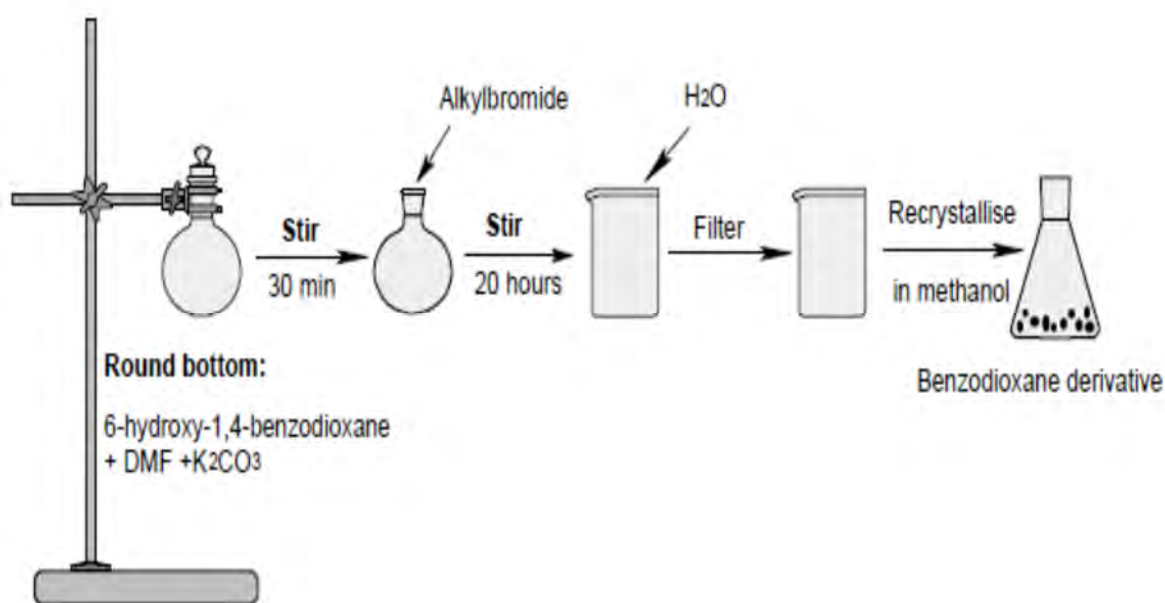


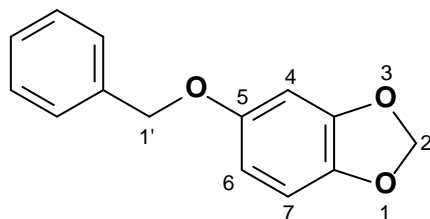
Figure 3.7. Experimental setup for the synthesis of C6-substituted benzodioxane derivatives (**5a–h**).

3.3. Physical characterisation of the synthesised compounds

3.3.1. NMR-spectra

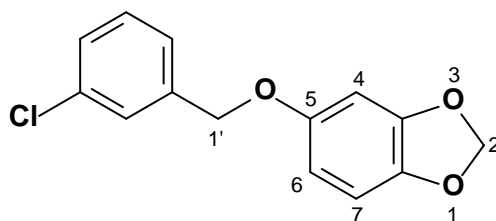
The NMR-spectra of the synthesised compounds are given in the appendix. Below, the ¹H and ¹³C NMR-spectra are correlated with the synthesised target compound structures. The appropriate signals were observed for the compounds.

4a: 5-(Benzyloxy)-2H-1,3-benzodioxole



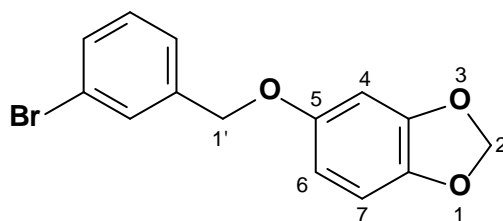
The title compound was prepared in a yield of 36.1%: mp 48.8 °C. ^1H NMR (Bruker Avance III 600, CDCl_3) δ 4.98 (s, 2H), 5.90 (s, 2H), 6.40 (dd, 1H, $J = 2.63, 8.66$ Hz); 6.56 (d, 1H, $J = 2.26$ Hz), 6.69 (d, 1H, $J = 8.28$ Hz), 7.30–7.33 (m, 1H), 7.36–7.42 (m, 4H); ^{13}C NMR (Bruker Avance III 600, CDCl_3) δ 70.9, 98.4, 101.1, 106.0, 107.9, 127.4, 127.9, 128.5, 137.0, 141.8, 148.2, 154.2; APCI-HRMS m/z : calcd for $\text{C}_{14}\text{H}_{13}\text{O}_3$ (MH^+), 228.0859, found 229.0849; Purity (HPLC): 99.0%.

<u>^1H NMR:</u>	<u>^{13}C NMR:</u>
<ul style="list-style-type: none">• The CH_2 protons at C1' correspond to the singlet at 4.98 ppm (The signal integrates for 2 protons).• The CH_2 protons at C2 correspond to the singlet at 5.90 ppm (The signal integrates for 2 protons).• Based on the coupling constants, the doublet of doublets at 6.40 ppm represents the proton at C6, the doublet at 6.56 ppm represents the proton at C4 and the doublet at 6.69 ppm represents the proton at C7.• Aromatic protons on the phenyl ring of the side chain corresponds to the multiplets at 7.30–7.33 (This signal integrates for 1 proton), and 7.36–7.42 (This signal integrates for 4 protons).	<ul style="list-style-type: none">• The aliphatic carbons at C2 and C1' are represented by the signals at 70.9 and 101.1 ppm.• The aromatic carbons are represented by the signals at 98.4, 106.0, 107.9, 127.4, 127.9, 128.5, 137.0, 141.8, 148.2 and 154.2 ppm.
<u>^{13}C DEPT 90 °, ^{13}C DEPT 135 °:</u>	
<ul style="list-style-type: none">• The aliphatic CH_2 carbons at C2 and C1' correspond to the signals at 70.9 and 101.1 ppm.• The aromatic CH carbons correspond to the signals at 98.4, 106.0, 107.9, 127.4, 127.9 and 128.5 ppm.	

4b: 5-[(3-Chlorophenyl)methoxy]-2H-1,3-benzodioxole

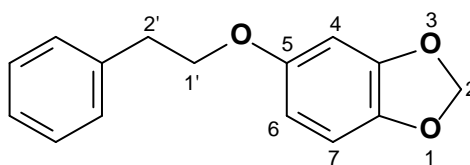
The title compound was prepared in a yield of 62.9%: mp 51.4 °C (methanol). ^1H NMR (Bruker Avance III 600, CDCl_3) δ 4.94 (s, 2H), 5.90 (s, 2H), 6.36 (dd, 1H, $J = 2.63, 8.66$ Hz), 6.53 (d, 1H, $J = 2.64$ Hz), 6.70 (d, 1H, $J = 8.28$ Hz), 7.26–7.30 (m, 3H), 7.40 (s, 1H); ^{13}C NMR (Bruker Avance III 600, CDCl_3) δ 70.1, 98.4, 101.2, 106.0, 107.9, 125.3, 127.4, 128.0, 129.8, 134.5, 139.1, 142.0, 148.3, 153.9; APCI-HRMS m/z : calcd for $\text{C}_{14}\text{H}_{12}\text{ClO}_3$ (MH^+), 263.0469, found 263.0466; Purity (HPLC): 100%.

^1H NMR:	^{13}C NMR:
<ul style="list-style-type: none"> The CH_2 protons at C1' are represented by the singlet at 4.94 ppm (The signal integrates for 2 protons). The CH_2 protons at C2 are represented by the singlet at 5.90 ppm (The signal integrates for 2 protons). Based on the coupling constants, the doublet of doublets at 6.36 ppm represents the proton at C6, the doublet at 6.53 ppm represents the proton at C4 and the doublet at 6.70 ppm corresponds to the proton at C7. The aromatic protons on the phenyl ring of the side chain are represented by the multiplet at 7.26–7.30 ppm (These signals integrate for 3 protons) and the singlet at 7.40 ppm (The signal integrates for 1 proton). 	<ul style="list-style-type: none"> The aliphatic carbons at C2 and C1' are represented by the signals at 70.1 ppm and 101.2 ppm. The aromatic carbons are represented by the signals at 98.4, 106.0, 107.9, 125.3, 127.4, 128.0, 129.8, 134.5, 139.1, 142.0, 148.3 and 153.9 ppm.
^{13}C DEPT 90 °, ^{13}C DEPT 135 °:	
<ul style="list-style-type: none"> The aliphatic CH_2 carbons at C2 and C1' correspond to the signals at 70.1 and 101.2 ppm. The aromatic CH carbons correspond to the signals at 98.4, 106.0, 107.9, 125.3, 127.4, 128.0 and 129.8 ppm. 	

4c: 5-[(3-Bromophenyl)methoxy]-2H-1,3-benzodioxole

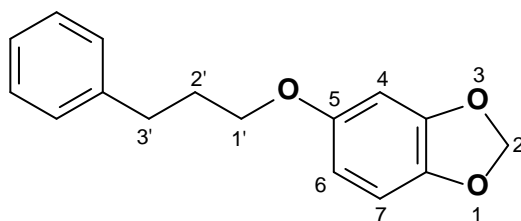
The title compound was prepared in a yield of 69.5%: mp 69.2 °C (methanol). ¹H NMR (Bruker Avance III 600, CDCl₃) δ 4.96 (s, 2H), 5.93 (s, 2H), 6.39 (dd, 1H, J = 2.26, 8.28 Hz), 6.56 (d, 1H, J = 2.64 Hz), 6.71 (d, 1H, J = 8.28 Hz), 7.27 (d, 1H, J = 7.91 Hz), 7.34 (d, 1H, J = 7.91 Hz), 7.46 (d, 1H, J = 7.91 Hz), 7.59 (s, 1H); ¹³C NMR (Bruker Avance III 600, CDCl₃) δ 70.0, 98.4, 101.2, 106.0, 107.9, 122.6, 125.8, 130.1, 130.3, 131.0, 139.4, 142.0, 148.3, 153.9; APCI-HRMS *m/z*: calcd for C₁₄H₁₂BrO₃ (MH⁺), 306.9964, found 306.9960; Purity (HPLC): 98.8%.

<u>¹H NMR:</u>	<u>¹³C NMR:</u>
<ul style="list-style-type: none">• The CH₂ protons at C1' are represented by the singlet at 4.96 ppm (The signal integrates for 2 protons).• The CH₂ protons at C2 are represented by the singlet at 5.93 ppm (The signal integrates for 2 protons).• Based on the coupling constants, the doublet of doublets at 6.39 ppm represents the proton at C6, the doublet at 6.56 ppm represents the proton at C4 and the doublet at 6.71 ppm corresponds to the proton at C7.• The aromatic protons on the phenyl ring of the side chain are represented by the doublet at 7.27 ppm (The signal integrates for 1 proton), the doublet at 7.34 ppm (The signal integrates for 1 proton), the doublet at 7.46 ppm (The signal integrates for 1 proton) and the singlet at 7.59 ppm (The signal integrates for 1 proton).	<ul style="list-style-type: none">• The aliphatic carbons at C2 and C1' are represented by the signals at 70.0 ppm and 101.2 ppm.• The aromatic carbons are represented by the signals at 98.4, 106.0, 107.9, 122.6, 125.8, 130.3, 131.0, 139.4, 142.0, 148.3 and 153.9 ppm.
<u>¹³C DEPT 90 °, ¹³C DEPT 135 °:</u>	
<ul style="list-style-type: none">• The aliphatic CH₂ carbons at C2 and C1' are represented by the signals at 70.0 ppm and 101.2 ppm.• The aromatic CH carbons are represented by the signals at 98.4, 106.0, 107.9, 125.8, 130.1, 130.3 and 131.0 ppm.	

4d: 5-(2-Phenylethoxy)-2H-1,3-benzodioxole

The title compound was prepared in a yield of 6.3%: mp 66.6 – 67.9 °C (methanol). ¹H NMR (Bruker Avance III 600, CDCl₃) δ 2.98 (t, 2H, J = 7.15 Hz), 4.01 (t, 2H, J = 7.15 Hz), 5.81 (s, 2H), 6.23 (dd, 1H, J = 2.64, 8.28 Hz), 6.41 (d, 1H, J = 2.64 Hz), 6.61 (d, 1H, J = 8.28), 7.14–7.17 (m, 1H), 7.18–7.25 (m, 2H), 7.22 – 7.25 (m, 2H); ¹³C NMR (Bruker Avance III 600, CDCl₃) δ 35.8, 69.6, 98.1, 101.1, 105.7, 107.9, 126.4, 128.4, 129.0, 138.2, 141.6, 148.2, 154.3; APCI-HRMS *m/z*: calcd for C₁₅H₁₅O₃ (MH⁺), 243.1016, found 243.1015; Purity (HPLC): 99.2%.

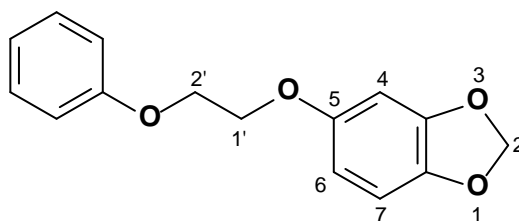
<u>¹H NMR:</u>	<u>¹³C NMR:</u>
<ul style="list-style-type: none"> • The CH₂ protons at C1' and C2' are represented by the triplets at 2.98 ppm (The signal integrates for 2 protons) and 4.01 ppm (The signal integrates for 2 protons), respectively. • The CH₂ protons at C1 are represented by the singlet at 5.81 ppm (The signal integrates for 2 protons). • Based on the coupling constants, the doublet of doublets at 6.23 ppm represents the proton at C6, the doublet at 6.41 ppm represents the proton at C4 and the doublet at 6.61 ppm corresponds to the proton at C7. • The aromatic protons on the phenyl ring of the side chain are represented by the multiplets at 7.14–7.17 ppm (These signals integrate for 1 proton), 7.18–7.25 ppm (These signals integrate for 2 protons) and 7.22–7.25 ppm (These signals integrate for 2 protons). 	<ul style="list-style-type: none"> • The aliphatic carbons at C2, C1' and C2' are represented by the signals at 35.8, 69.6 and 101.1 ppm. • The aromatic carbons are represented by the signals at 98.1, 105.7, 107.9, 126.4, 128.4, 129.0, 138.2, 141.6, 148.2 and 154.3 ppm.
<u>¹³C DEPT 90 °. ¹³C DEPT 135 °:</u>	
<ul style="list-style-type: none"> • The aliphatic CH₂ carbons at C2, C1' and C2' are represented by the signals at 35.8, 69.6 and 101.1 ppm • The aromatic CH carbons are represented by the signals at 98.1, 105.7, 107.9, 126.4, 128.4 and 129.0 ppm. 	

4e: 5-(3-Phenylpropoxy)-2H-1,3-benzodioxole

The title compound was prepared in a yield of 47.9%: mp 56.6–62.0 °C (methanol). ^1H NMR (Bruker Avance III 600, CDCl_3) δ 2.08 (qn, 2H, $J = 7.53$ Hz), 2.79 (t, 2H, $J = 7.53$ Hz), 3.88 (t, 2H, $J = 6.40$ Hz), 5.90 (s, 2H), 6.31 (dd, 1H, $J = 2.26, 8.28$ Hz), 6.49 (d, 1H, $J = 2.26$ Hz), 6.69 (d, 1H, $J = 8.28$ Hz), 7.18–7.21 (m, 3H), 7.28–7.30 (m, 2H); ^{13}C NMR (Bruker Avance III 600, CDCl_3) δ 30.8, 32.1, 67.8, 98.0, 101.0, 105.7, 107.9, 125.9, 128.4, 128.5, 141.5, 148.2, 154.5; APCI-HRMS m/z : calcd for $\text{C}_{16}\text{H}_{17}\text{O}_3$ (MH^+), 257.1172, found 257.1163; Purity (HPLC): 100%.

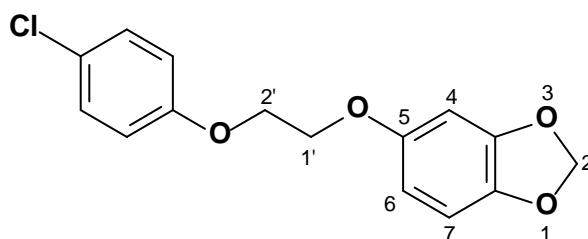
^1H NMR:	^{13}C NMR:
<ul style="list-style-type: none"> The CH_2 protons at C1' and C3' are represented by the triplets at 2.79 ppm (The signal integrates for 2 protons) and 3.88 ppm (The signal integrates for 2 protons). The CH_2 protons at C2' correspond to the quintet at 2.08 ppm (The signal integrates for 2 protons). The CH_2 protons at C2 are represented by the singlet at 5.90 ppm (The signal integrates for 2 protons). Based on the coupling constants, the doublet of doublets at 6.31 ppm represents the proton at C6, the doublet at 6.49 ppm represents the proton at C4 and the doublet at 6.69 ppm corresponds to the proton at C7. The aromatic protons on the side chain phenyl ring are represented by the multiplets at 7.18–7.21 ppm (The signal integrates for 3 protons) and 7.28–7.30 ppm (The signal integrates for 2 protons). 	<ul style="list-style-type: none"> The aliphatic carbons at C2, C1', C2' and C3' are represented by the signals at 30.8, 32.1, 67.8 and 101.0 ppm. The aromatic carbons are represented by the signals at 98.0, 105.7, 107.9, 125.9, 128.4, 128.5, 141.5, 148.2, and 154.5 ppm.
^{13}C DEPT 90 °, ^{13}C DEPT 135 °:	
<ul style="list-style-type: none"> The aliphatic CH_2 carbons correspond to the signals at 30.8, 32.1, 67.8 and 101.0 ppm. The aromatic CH carbons correspond to the signals at 98.0, 105.7, 107.9, 125.9, 128.4 and 128.5 ppm. 	

4f: 5-(2-Phenoxyethoxy)-2H-1,3-benzodioxole



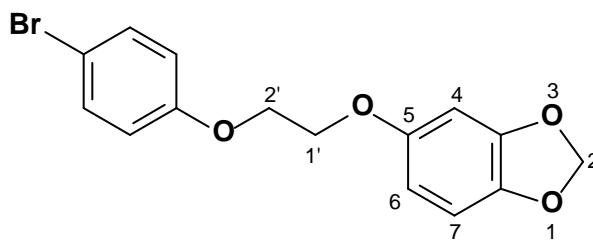
The title compound was prepared in a yield of 0.7%: mp 100.6–101.2 °C (methanol). ^1H NMR (Bruker Avance III 600, CDCl_3) δ 4.23–4.24 (m, 2H), 4.27–4.28 (m, 2H), 5.91 (s, 2H), 6.37 (dd, 1H, $J = 2.64, 8.66$ Hz), 6.54 (d, 1H, $J = 2.64$ Hz), 6.69 (d, 1H, $J = 8.28$ Hz), 6.94–6.97 (m, 3H), 7.27–7.30 (m, 2H); ^{13}C NMR (Bruker Avance III 600, CDCl_3) δ 66.4, 67.5, 98.4, 101.1, 105.9, 107.9, 114.6, 121.1, 129.5, 141.9, 148.2, 154.1, 158.6; APCI-HRMS m/z : calcd for $\text{C}_{15}\text{H}_{15}\text{O}_4$ (MH^+), 259.0965, found 259.0953; Purity (HPLC): 96.8%.

<u>^1H NMR:</u>	<u>^{13}C NMR:</u>
<ul style="list-style-type: none"> • The CH_2 protons at C1' and C2' are represented by the multiplets at 4.23–4.24 ppm (The signal integrates for 2 protons) and 4.27–4.28 ppm (The signal integrates for 2 protons). • The CH_2 protons at C2 are represented by the singlet at 5.91 ppm (The signal integrates for 2 protons). • Based on the coupling constants, the doublet of doublets at 6.37 ppm represents the proton at C6, the doublet at 6.54 ppm represents the proton at C4 and the doublet at 6.69 ppm corresponds to the proton at C7. • The aromatic protons on the phenyl ring of the side chain are represented by the multiplets at 6.94–6.97 ppm (The signal integrates for 3 protons) and 7.27–7.30 ppm (The signal integrates for 2 protons), respectively. 	<ul style="list-style-type: none"> • The aliphatic carbons at C2, C1' and C2' are represented by the signals at 66.4, 67.5 and 101.1 ppm. • The aromatic carbons are represented by the signals at 98.4, 105.9, 107.9, 114.6, 121.1, 129.5, 141.9, 148.2, 154.1 and 158.6 ppm.
<u>^{13}C DEPT 90 °, ^{13}C DEPT 135 °:</u>	
<ul style="list-style-type: none"> • The aliphatic CH_2 carbons at C2, C1', and C2' correspond to the signals at 66.4, 67.5 and 101.1 ppm. • The aromatic CH carbons correspond to the signals at 98.4, 105.9, 107.9, 114.6, 121.1 and 129.5 ppm. 	

4g: 5-[2-(4-Chlorophenoxy)ethoxy]-2H-1,3-benzodioxole

The title compound was prepared in a yield of 11.3%: mp 105.7–107.4 °C (methanol). ^1H NMR (Bruker Avance III 600, CDCl_3) δ 4.20–4.24 (m, 4H), 5.90 (s, 2H), 6.36 (dd, 1H, $J = 2.64, 8.28$ Hz), 6.52 (d, 1H, $J = 2.26$ Hz), 6.69 (d, 1H, $J = 8.66$ Hz), 6.86 (d, 2H, $J = 9.04$ Hz), 7.23 (d, 2H, $J = 9.04$ Hz); ^{13}C NMR (Bruker Avance III 600, CDCl_3) δ 66.8, 67.4, 98.4, 101.2, 105.9, 107.9, 115.9, 125.9, 129.3, 142.0, 148.3, 154.0, 157.2, APCI-HRMS m/z : calcd for $\text{C}_{15}\text{H}_{14}\text{ClO}_4$ (MH^+), 293.0575, found 293.0565; Purity (HPLC): 100%.

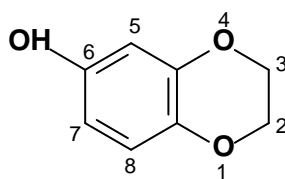
^1H NMR:	^{13}C NMR:
<ul style="list-style-type: none"> The CH_2 protons at C1' and C2' are represented by the multiplet at 4.20–4.24 ppm (The signal integrates for 4 protons). The CH_2 protons at C2 are represented by the singlet at 5.90 ppm (The signal integrates for 2 protons). Based on the coupling constants, the doublet of doublets at 6.36 ppm represents the proton at C6, the doublet at 6.52 ppm represents the proton at C4 and the doublet at 6.69 ppm corresponds to the proton at C7. The aromatic protons on the phenyl ring of the side chain are represented by the two doublets at 6.86 ppm (The signal integrates for 2 protons) and 7.23 ppm (The signal integrates for 2 protons). 	<ul style="list-style-type: none"> The aliphatic carbons at C2, C1' and C2' are represented by the signals at 66.8, 67.4 and 101.2 ppm. The aromatic carbons are represented by the signals at 98.4, 105.9, 107.9, 115.9, 125.9, 129.3, 142.0, 148.3, 154.0 and 157.2 ppm.
^{13}C DEPT 90 °, ^{13}C DEPT 135 °:	
<ul style="list-style-type: none"> The aliphatic CH_2 carbons at C2, C1', and C2' correspond to the signals at 66.8, 67.4 and 101.2 ppm. The aromatic CH carbons correspond to the signals at 98.4, 105.9, 107.9, 115.9 and 129.3 ppm. 	

4h: 5-[2-(4-Bromophenoxy)ethoxy]-2H-1,3-benzodioxole

The title compound was prepared in a yield of 21.7%: mp 111.3–114.0 °C (methanol). ^1H NMR (Bruker Avance III 600, CDCl_3) δ 4.20–4.24 (m, 4H), 5.90 (s, 2H), 6.35 (dd, 1H, $J = 2.64, 8.28$ Hz), 6.52 (d, 1H, 2.26 Hz), 6.70 (d, 1H, $J = 8.66$ Hz), 6.81 (d, 2H, $J = 9.04$ Hz), 7.37 (d, 2H, $J = 9.04$ Hz); ^{13}C NMR (Bruker Avance III 600, CDCl_3) δ 66.8, 67.4, 98.4, 101.2, 105.9, 107.9, 113.3, 116.5, 132.3, 142.0, 148.3, 154.0, 157.7; APCI-HRMS m/z : calcd for $\text{C}_{15}\text{H}_{14}\text{BrO}_4$ (MH^+), 337.0070, found 337.0072; Purity (HPLC): 95.3%.

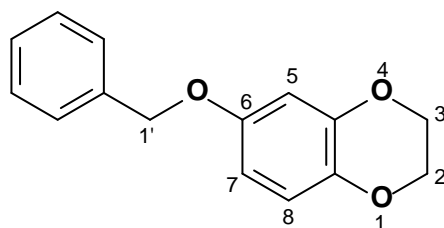
^1H NMR:	^{13}C NMR:
<ul style="list-style-type: none"> The CH_2 protons at C1' and C2' are represented by the multiplet at 4.20–4.24 ppm (The signal integrates for 4 protons). The CH_2 protons at C2 are represented by the singlet at 5.90 ppm (The signal integrates for 2 protons). Based on the coupling constants, the doublet of doublets at 6.35 ppm represents the proton at C6, the doublet at 6.52 ppm represents the proton at C6 and the doublet at 6.70 ppm corresponds to the proton at C4. The aromatic protons on the phenyl ring of the side chain are represented by the two doublets at 6.81 ppm (The signal integrates for 2 protons) and 7.37 ppm (The signal integrates for 2 protons). 	<ul style="list-style-type: none"> The aliphatic carbons at C2, C1' and C2' are represented by the signals at 66.8, 67.4 and 101.2 ppm. The aromatic carbons are represented by the signals at 98.4, 105.9, 107.9, 113.3, 116.5, 132.3, 142.0, 148.3, 154.0 and 157.7 ppm.
^{13}C DEPT 90 °, ^{13}C DEPT 135 °:	
<ul style="list-style-type: none"> The aliphatic CH_2 carbons at C2, C1', and C2' correspond to the signals at 66.8, 67.4 and 101.2 ppm. The aromatic CH carbons correspond to the signals at 98.4, 105.9, 107.9, 116.5 and 132.3 ppm. 	

7: 6-Hydroxy-1,4-benzodioxane



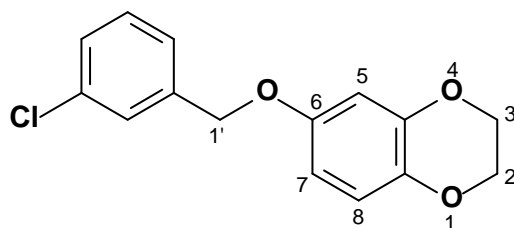
The title compound was prepared in a yield of 161.3% (oil): ^1H NMR (Bruker Avance III 600, CDCl_3) δ 4.17–4.18 (m, 2H), 4.20–4.22 (m, 2H), 5.31 (s, 1H), 6.32 (dd, 1H, $J = 3.00, 8.66$ Hz), 6.37 (d, 1H, $J = 2.64$ Hz), 6.69 (d, 1H, $J = 8.66$ Hz); ^{13}C NMR (Bruker Avance III 600, CDCl_3) δ 64.1, 64.5, 104.3, 108.3, 117.5, 137.5, 143.7, 149.9, APCI-HRMS m/z : calcd for $\text{C}_8\text{H}_9\text{O}_3$ (MH^+), 153.0546, found 153.0552; Purity (HPLC): 98.9%.

<u>^1H NMR:</u>	<u>^{13}C NMR:</u>
<ul style="list-style-type: none">• The CH_2 protons at C2 and C3 correspond to the multiplets at 4.17–4.18 ppm (The signal integrates for 2 protons) and 4.20–4.22 ppm (The signal integrates for 2 protons).• The hydroxyl group at C6 is represented by the singlet at 5.31 ppm (The signal integrates for 1 proton).• Based on the coupling constants, the doublet of doublets at 6.32 ppm represents the proton at C7, the doublet at 6.37 ppm represents the proton at C5 and the doublet at 6.69 ppm corresponds to the proton at C8.	<ul style="list-style-type: none">• The aliphatic carbons at C2 and C3 are represented by the signals at 64.1 and 64.5 ppm.• The aromatic carbons are represented by the signals at 104.3, 108.3, 117.5, 137.5, 143.7 and 149.9 ppm.
<u>^{13}C DEPT 90 °, ^{13}C DEPT 135 °:</u>	
<ul style="list-style-type: none">• The aliphatic CH_2 carbons at C2 and C3 are represented by the signals at 64.1 and 64.5 ppm.• The aromatic CH carbons are represented by the signals at 104.3, 108.3 and 117.5 ppm.	

5a: 6-(Benzyloxy)-2,3-dihydro-1,4-benzodioxine

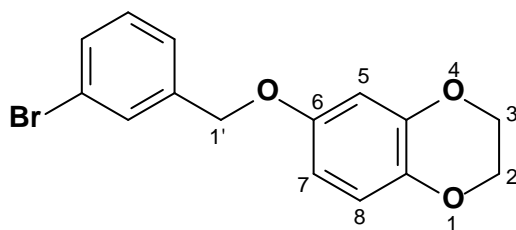
The title compound was prepared in a yield of 35.9% (oil). ^1H NMR (Bruker Avance III 600, CDCl_3) δ 4.18–4.20 (m, 2H), 4.22–4.23 (m, 2H), 4.97 (s, 2H), 6.48 (dd, 1H, $J = 3.01, 9.04$ Hz), 6.52 (d, 1H, $J = 3.01$ Hz), 6.76 (d, 1H, $J = 9.04$ Hz), 7.29–7.32 (m, 1H), 7.36–7.38 (m, 2H), 7.40–7.41 (m, 2H); ^{13}C NMR (Bruker Avance III 600, CDCl_3) δ 64.1, 64.5, 70.5, 103.8, 108.2, 117.4, 127.4, 128.0, 128.5, 137.1, 137.8, 143.7, 153.4; APCI-HRMS m/z : calcd for $\text{C}_{15}\text{H}_{15}\text{O}_3$ (MH^+), 243.1016, found 243.1028; Purity (HPLC): 94.3%.

^1H NMR:	^{13}C NMR:
<ul style="list-style-type: none"> The CH_2 protons at C2 and C3 correspond to the multiplets at 4.18–4.20 ppm (The signal integrates for 2 protons) and 4.22–4.23 ppm (The signal integrates for 2 protons). The CH_2 protons at C1' represents the singlet at 4.97 ppm (The signal integrates for 2 protons). Based on the coupling constants, the doublet of doublets at 6.48 ppm represents the proton at C7, the doublet at 6.52 ppm represents the proton at C5 and the doublet at 6.76 ppm corresponds to the proton at C8. The aromatic protons are represented by the multiplets at 7.29–7.32 ppm (The signal integrates for 1 proton), 7.36–7.38 ppm (The signal integrates for 2 protons) and the 7.40–7.41 ppm (The signal integrates for 2 protons). 	<ul style="list-style-type: none"> The aliphatic carbons at C2, C3 and C1' are represented by the signals at 64.1, 64.5 and 70.5 ppm. The aromatic carbons are represented by the signals at 103.8, 108.2, 117.4, 127.4, 128.0, 128.5, 137.1, 137.8, 143.7 and 153.4 ppm.
^{13}C DEPT 90 °, ^{13}C DEPT 135 °:	
<ul style="list-style-type: none"> The aliphatic CH_2 carbons at C2, C3 and C1' are represented by the signals at 64.1, 64.5 and 70.5 ppm. The aromatic CH carbons are represented by the signals at 103.8, 108.2, 117.4, 127.4, 128.0 and 128.5 ppm. 	

5b: 6-[(3-Chlorophenyl)methoxy]-2,3-dihydro-1,4-benzodioxine

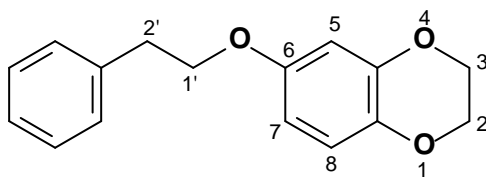
The title compound was prepared in a yield of 64.9% (oil): $^1\text{H NMR}$ (Bruker Avance III 600, CDCl_3) δ 4.18–4.19 (m, 2H), 4.21–4.23 (m, 2H), 4.93 (s, 2H), 6.45 (dd, 1H, $J = 3.01, 9.04$ Hz), 6.49 (d, 1H, $J = 2.64$ Hz), 6.77 (d, 1H, $J = 8.66$ Hz), 7.26–7.30 (m, 3H), 7.40 (s, 1H); $^{13}\text{C NMR}$ (Bruker Avance III 600, CDCl_3) δ 64.1, 64.5, 69.7, 103.8, 108.1, 117.4, 125.3, 127.3, 128.0, 129.8, 134.4, 138.0, 139.2, 143.8, 153.0, APCI-HRMS m/z . calcd for $\text{C}_{15}\text{H}_{14}\text{ClO}_3$ (MH^+), 277.0626, found 277.0638; Purity (HPLC): 91.2%.

$^1\text{H NMR}$:	$^{13}\text{C NMR}$:
<ul style="list-style-type: none"> The CH_2 protons at C2 and C3 correspond to the multiplets at 4.18–4.19 ppm (The signal integrates for 2 protons) and 4.21–4.23 ppm (The signal integrates for 2 protons). The CH_2 protons at C1' represents the singlet at 4.93 ppm (The signal integrates for 2 protons). Based on the coupling constants, the doublet of doublets at 6.45 ppm represents the proton at C7, the doublet at 6.49 ppm represents the proton at C5 and the doublet at 6.77 ppm corresponds to the proton at C8. The aromatic protons are represented by the multiplet at 7.26–7.30 ppm (The signal integrates for 3 protons) and the singlet at 7.40 ppm (The signal integrates for 1 proton). 	<ul style="list-style-type: none"> The aliphatic carbons at C2, C3 and C1' are represented by the signals at 64.1, 64.5 and 69.7 ppm. The aromatic carbons are represented by the signals at 103.8, 108.1, 117.4, 125.3, 127.3, 128.0, 129.8, 134.4, 138.0, 139.2, 143.8 and 153.0 ppm.
$^{13}\text{C DEPT } 90^\circ$, $^{13}\text{C DEPT } 135^\circ$:	
<ul style="list-style-type: none"> The aliphatic CH_2 carbons at C2, C3 and C1' are represented by the signals at 64.1, 64.5 and 69.7 ppm. The aromatic CH carbons are represented by the signals at 103.8, 108.1, 117.4, 125.3, 127.3, 128.0 and 129.8 ppm. 	

5c: 6-[(3-Bromophenyl)methoxy]-2,3-dihydro-1,4-benzodioxine

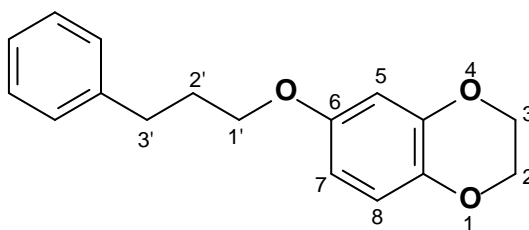
The title compound was prepared in a yield of 51.5% (oil): ^1H NMR (Bruker Avance III 600, CDCl_3) δ 4.18–4.19 (m, 2H), 4.21–4.23 (m, 2H), 4.93 (s, 2H), 6.46 (dd, 1H, $J = 2.64$, 8.66 Hz), 6.48 (d, 1H, $J = 2.64$ Hz), 6.75 (d, 1H, $J = 8.66$ Hz), 7.22 (t, 1H, $J = 7.91$ Hz), 7.30 (d, 1H, $J = 8.28$ Hz), 7.42 (d, 1H, $J = 8.28$ Hz), 7.56 (s, 1H); ^{13}C NMR (Bruker Avance III 600, CDCl_3) δ 64.1, 64.5, 69.6, 103.9, 108.1, 117.4, 122.6, 125.8, 130.1, 130.3, 130.9, 138.0, 139.5, 143.8, 153.0, APCI-HRMS m/z : calcd for $\text{C}_{15}\text{H}_{14}\text{BrO}_3$ (MH^+), 321.0121, found 321.0122; Purity (HPLC): 84.3%.

<u>^1H NMR:</u>	<u>^{13}C NMR:</u>
<ul style="list-style-type: none"> The CH_2 protons at C2 and C3 correspond to the multiplets at 4.18–4.19 ppm (The signal integrates for 2 protons) and 4.21–4.23 ppm (The signal integrates for 2 protons). The CH_2 protons at C1' represents the singlet at 4.93 ppm (The signal integrates for 2 protons). Based on the coupling constants, the doublet of doublets at 6.46 ppm represents the proton at C7, the doublet at 6.48 ppm represents the proton at C5 and the doublet at 6.75 ppm corresponds to the proton at C8. The aromatic protons are represented by the triplet at 7.22 ppm (The signal integrates for 1 proton), the doublet at 7.30 ppm (The signal integrates for 1 proton), the doublet at 7.42 ppm (The signal integrates for 1 proton) and the singlet at 7.56 ppm (The signal integrates for 1 proton). 	<ul style="list-style-type: none"> The aliphatic carbons at C2, C3 and C1' are represented by the signals at 64.1, 64.5 and 69.6 ppm. The aromatic carbons are represented by the signals at 103.9, 108.1, 117.4, 122.6, 125.8, 130.1, 130.3, 130.9, 138.0, 139.5, 143.8 and 153.0 ppm.
<u>^{13}C DEPT 90 °, ^{13}C DEPT 135 °:</u>	
<ul style="list-style-type: none"> The aliphatic CH_2 carbons are represented by the signals at 64.1, 64.5 and 69.6 ppm. The aromatic CH carbons are represented by the signals at 103.9, 108.1, 117.4, 125.8, 130.1, 130.3 and 130.9 ppm. 	

5d: 6-(2-Phenylethoxy)-2,3-dihydro-1,4-benzodioxine

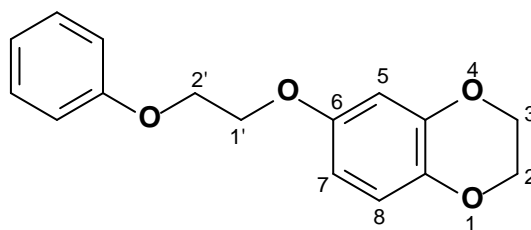
The title compound was prepared in a yield of 49.6% (oil): ^1H NMR (Bruker Avance III 600, CDCl_3) δ 3.07 (t, 2H, $J = 7.15$ Hz), 4.10 (t, 2H, $J = 7.15$ Hz), 4.19–4.20 (m, 2H), 4.22–4.24 (m, 2H), 6.43 (dd, 1H, $J = 3.01, 9.04$ Hz), 6.46 (d, 1H, $J = 3.01$ Hz), 6.76 (d, 1H, $J = 9.04$ Hz), 7.23–7.25 (m, 1H), 7.27–7.28 (m, 2H), 7.31–7.33 (m, 2H); ^{13}C NMR (Bruker Avance III 600, CDCl_3) δ 35.7, 64.1, 64.5, 69.2, 103.5, 107.9, 117.3, 126.4, 128.4, 128.9, 137.6, 138.3, 143.7, 153.4; APCI-HRMS m/z : calcd for $\text{C}_{16}\text{H}_{17}\text{O}_3$ (MH^+), 257.1172, found 257.1172; Purity (HPLC): 91.0%.

<u>^1H NMR:</u>	<u>^{13}C NMR:</u>
<ul style="list-style-type: none"> • The CH_2 protons at C1' and C2' represents the triplets at 3.07 ppm (The signal integrates for 2 protons) and 4.10 ppm (The signal integrates for 2 protons), respectively. • The CH_2 protons at C2 and C3 correspond to the multiplets at 4.19–4.20 ppm (The signal integrates for 2 protons) and 4.22–4.24 ppm (The signal integrates for 2 protons). • Based on the coupling constants, the doublet of doublets at 6.43 ppm represents the proton at C7, the doublet at 6.46 ppm represents the proton at C5 and the doublet at 6.76 ppm corresponds to the proton at C8. • The aromatic protons are represented by the multiplets at 7.23–7.25 ppm (The signal integrates for 1 proton), 7.27–7.28 ppm (The signal integrates for 2 protons) and 7.31–7.33 ppm (The signal integrates for 2 protons). 	<ul style="list-style-type: none"> • The aliphatic carbons at C2, C3, C1' and C2' are represented by the signals at 35.7, 64.1, 64.5 and 69.2 ppm. • The aromatic carbons are represented by the signals at 103.5, 107.9, 117.3, 126.4, 128.4, 128.9, 137.6, 138.3, 143.7 and 153.4 ppm.
<u>^{13}C DEPT 135 $^\circ$:</u>	
<ul style="list-style-type: none"> • The aliphatic CH_2 carbons at C2, C3, C1' and C2' are represented by the signals at 35.7, 64.1, 64.5 and 69.2 ppm. • The aromatic CH carbons are represented by the signals at 103.5, 107.9, 117.3, 126.4, 128.4 and 128.9 ppm 	

5e: 6-(3-Phenylpropoxy)-2,3-dihydro-1,4-benzodioxine

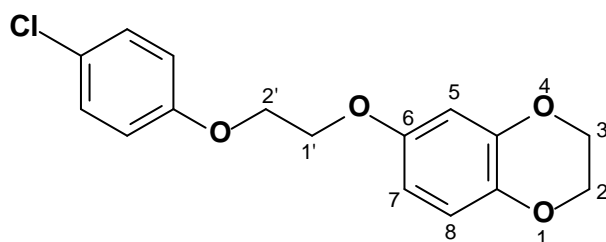
The title compound was prepared in a yield of 69.9% (oil): ^1H NMR (Bruker Avance III 600, CDCl_3) δ 2.06 (qn, 2H, $J = 7.91$ Hz), 2.78 (t, 2H, $J = 7.91$ Hz), 3.87 (t, 2H, $J = 6.02$ Hz), 4.18–4.20 (m, 2H), 4.22–4.23 (m, 2H), 6.41 (dd, 1H, $J = 3.01, 8.66$ Hz), 6.44 (d, 1H, $J = 2.64$ Hz), 6.76 (d, 1H, $J = 8.66$ Hz), 7.17–7.20 (m, 3H), 7.28 (t, 2H, $J = 7.53$ Hz); ^{13}C NMR (Bruker Avance III 600, CDCl_3) δ 30.8, 32.1, 64.1, 64.6, 67.4, 103.4, 107.9, 117.3, 125.9, 128.4, 128.5, 137.5, 141.5, 143.7, 153.6; APCI-HRMS m/z : calcd for $\text{C}_{17}\text{H}_{19}\text{O}_3$ (MH^+), 271.1329, found 271.1341; Purity (HPLC): 90.2%.

<u>^1H NMR:</u>	<u>^{13}C NMR:</u>
<ul style="list-style-type: none"> • The CH_2 protons at C2' correspond to the quintet at 2.06 ppm (The signal integrates for 2 protons). • The CH_2 protons at C1' and C3' represents the triplets at 2.78 ppm (The signal integrates for 2 protons) and 3.87 ppm (The signal integrates for 2 protons), respectively. • The CH_2 protons at C2 and C3 correspond to the multiplets at 4.18–4.20 ppm (The signal integrates for 2 protons) and 4.22–4.23 ppm (The signal integrates for 2 protons). • Based on the coupling constants, the doublet of doublets at 6.41 ppm represents the proton at C7, the doublet at 6.44 ppm represents the proton at C5 and the doublet at 6.76 ppm corresponds to the proton at C8. • The aromatic protons are represented by the multiplet at 7.17–7.20 ppm (The signal integrates for 3 protons) and the triplet at 7.28 ppm (The signal integrates for 2 protons). 	<ul style="list-style-type: none"> • The aliphatic carbons at C2, C3, C1', C2' and C3' are represented by the signals at 30.8, 32.1, 64.1, 64.6 and 67.4 ppm. • The aromatic carbons correspond to the signals at 103.4, 107.9, 117.3, 125.9, 128.4, 128.5, 137.5, 141.5, 143.7 and 153.6 ppm.
<u>^{13}C DEPT 90°, ^{13}C DEPT 135 °:</u>	
<ul style="list-style-type: none"> • The aliphatic CH_2 carbons are represented by the signals at 30.8, 32.1, 64.1, 64.6 and 67.4 ppm. • The aromatic CH carbons correspond to the signals at 103.4, 107.9, 117.3, 125.9, 128.4 and 128.5 ppm. 	

5f: 6-(2-Phenoxyethoxy)-2,3-dihydro-1,4-benzodioxine

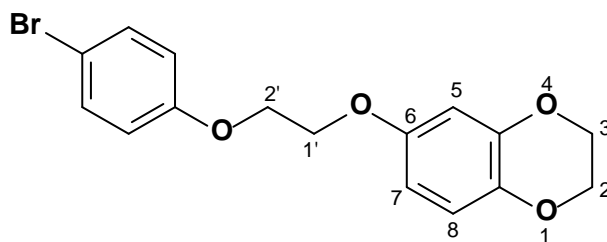
The title compound was prepared in a yield of 19.1%: mp 103.1–105.7 °C (methanol). ^1H NMR (Bruker Avance III 600, CDCl_3) δ 4.19–4.20 (m, 2H), 4.22–4.24 (m, 4H), 4.26–4.28 (m, 2H), 6.47 (dd, 1H, $J = 3.01, 8.66$ Hz), 6.51 (d, 1H, 3.01 Hz), 6.77 (d, 1H, 8.66 Hz), 6.93–6.97 (m, 3H), 7.28 (t, 2H, $J = 7.15$ Hz); ^{13}C NMR (Bruker Avance III 600, CDCl_3) δ 64.1, 64.5, 66.4, 67.1, 103.8, 108.1, 114.6, 117.4, 121.0, 129.4, 137.9, 143.7, 153.2, 158.6; APCI-HRMS m/z : calcd for $\text{C}_{16}\text{H}_{17}\text{O}_4$ (MH^+), 273.1121, found 273.1136; Purity (HPLC): 99.7%.

^1H NMR:	^{13}C NMR:
<ul style="list-style-type: none">• The CH_2 protons at C1' and C2' represents the multiplets at 4.19–4.20 ppm (The signal integrates for 2 protons) and 4.26–4.28 ppm (The signal integrates for 2 protons), respectively.• The CH_2 protons at C2 and C3 correspond to the multiplet 4.22–4.24 ppm (The signal integrates for 4 protons).• Based on the coupling constants, the doublet of doublets at 6.47 ppm represents the proton at C7, the doublet at 6.51 ppm represents the proton at C5 and the doublet at 6.77 ppm corresponds to the proton at C8.• The aromatic protons are represented by the multiplet at 6.93–6.97 ppm (The signal integrates for 3 protons) and the triplet at 7.28 ppm (The signal integrates for 2 protons).	<ul style="list-style-type: none">• The aliphatic carbons at C2, C3, C1' and C2' are represented by the signals at 64.1, 64.5, 66.4 and 67.1 ppm.• The aromatic carbons are represented by the signals at 103.8, 108.1, 114.6, 117.4, 121.0, 129.4, 137.9, 143.7, 153.2 and 158.6 ppm.

5g: 6-[2-(4-Chlorophenoxy)ethoxy]-2,3-dihydro-1,4-benzodioxine

The title compound was prepared in a yield of 32.4%: mp 126.6–127.9 °C (methanol). ^1H NMR (Bruker Avance III 600, CDCl_3) δ 4.18–4.23 (m, 8H), 6.45 (dd, 1H, $J = 2.64, 8.66$ Hz), 6.48 (d, 1H, $J = 2.64$ Hz), 6.76 (d, 1H, 8.66 Hz), 6.86 (d, 2H, $J = 9.04$ Hz), 7.22 (d, 2H, $J = 9.04$ Hz); ^{13}C NMR (Bruker Avance III 600, CDCl_3) δ 64.1, 64.5, 66.8, 67.0, 103.8, 108.0, 115.9, 117.4, 125.9, 129.3, 138.0, 143.8, 153.1, 157.2; APCI-HRMS m/z : calcd for $\text{C}_{16}\text{H}_{16}\text{ClO}_4$ (MH^+), 307.0732, found 307.0744; Purity (HPLC): 99.8%.

^1H NMR:	^{13}C NMR:
<ul style="list-style-type: none">• The CH_2 protons at C2, C3, C1' and C2' represents the multiplet at 4.18–4.23 ppm (The signal integrates for 8 protons).• Based on the coupling constants, the doublet of doublets at 6.45 ppm represents the proton at C7, the doublet at 6.48 ppm represents the proton at C5 and the doublet at 6.76 ppm corresponds to the proton at C8.• The aromatic protons are represented by the doublets at 6.86 ppm (The signal integrates for 2 protons) and 7.22 ppm (The signal integrates for 2 protons).	<ul style="list-style-type: none">• The aliphatic carbons at C2, C3, C1' and C2' are represented by the signals at 64.1, 64.5, 66.8 and 67.0 ppm.• The aromatic carbons are represented by the signals at 103.8, 108.0, 115.9, 117.4, 125.9, 129.3, 138.0, 143.8, 153.1 and 157.2 ppm.

5h: 6-[2-(4-Bromophenoxy)ethoxy]-2,3-dihydro-1,4-benzodioxine

The title compound was prepared in a yield of 13.8%: mp 131.0–133.3 °C (methanol). ^1H NMR (Bruker Avance III 600, CDCl_3) δ 4.18–4.23 (m, 8H), 6.44 (dd, 1H, $J = 3.01, 8.66$ Hz), 6.48 (d, 1H, $J = 3.01$ Hz), 6.77 (d, 1H, $J = 8.66$ Hz), 6.81 (d, 2H, $J = 9.04$ Hz), 7.36 (d, 2H, $J = 9.04$ Hz); ^{13}C NMR (Bruker Avance III 600, CDCl_3) δ 64.1, 64.6, 66.8, 67.0, 103.8, 108.1, 113.2, 116.5, 117.4, 132.2, 138.0, 143.8, 153.1, 157.7, APCI-HRMS m/z : calcd for $\text{C}_{16}\text{H}_{16}\text{BrO}_4$ (MH^+), 351.0226, found 351.0220; Purity (HPLC): 98.2%.

^1H NMR:	^{13}C NMR:
<ul style="list-style-type: none">• The CH_2 protons at C2, C3, C1' and C2' represents the multiplet at 4.18–4.23 ppm (The signal integrates for 8 protons).• Based on the coupling constants, the doublet of doublets at 6.44 ppm represents the proton at C7, the doublet at 6.48 ppm represents the proton at C5 and the doublet at 6.77 ppm corresponds to the proton at C8.• The aromatic protons are represented by the doublets at 6.81 ppm (The signal integrates for 2 protons) and 7.36 ppm (The signal integrates for 2 protons).	<ul style="list-style-type: none">• The aliphatic carbons at C2, C3, C1' and C2' are represented by the signals at 64.1, 64.6, 66.8 and 67.0 ppm.• The aromatic carbons are represented by the signals at 103.8, 108.1, 113.2, 116.5, 117.4, 132.2, 138.0, 143.8, 153.1 and 157.7 ppm.
^{13}C DEPT 135 °:	
<ul style="list-style-type: none">• The aliphatic CH_2 carbons at C2, C3, C1' and C2' are represented by the signals at 64.1, 64.6, 66.8 and 67.0 ppm.• The aromatic CH carbons are represented by the signals at 103.8, 108.1, 116.5, 117.4 and 132.2 ppm.	

3.3.2 Interpretation of mass spectra

The sesamol derivatives (**4a–h**) and benzodioxane derivatives (**5a–h**) that were synthesised in this study were also characterised by mass spectrometry. The calculated and experimentally determined high resolution masses are noted in table 3.2. The small differences between the calculated and experimentally determined masses are indicative that the structures of these compounds correspond to those given in table 3.1. $\text{ppm} = \left(\frac{\text{Found} - \text{Calcd.}}{\text{Calcd.}} \right) \times 1000000$. A ppm smaller than 5 is considered to be good agreement.

Table 3.2. The calculated and experimentally determined high resolution masses of the various synthesised sesamol derivatives (**4a–h**). All masses are given as MH^+ .

Compound	Calculated mass	Experimental mass	Formula	ppm
4a	229.0859	229.0849	$\text{C}_{14}\text{H}_{13}\text{O}_3$	-6.98
4b	263.0469	263.0466	$\text{C}_{14}\text{H}_{12}\text{ClO}_3$	-3.42
4c	306.9964	306.9960	$\text{C}_{14}\text{H}_{12}\text{BrO}_3$	-3.26
4d	243.1016	243.1015	$\text{C}_{15}\text{H}_{15}\text{O}_3$	-2.47
4e	257.1172	257.1163	$\text{C}_{16}\text{H}_{17}\text{O}_3$	-5.83
4f	259.0965	259.0953	$\text{C}_{15}\text{H}_{15}\text{O}_4$	-6.56
4g	293.0575	293.0565	$\text{C}_{15}\text{H}_{14}\text{ClO}_4$	-5.46
4h	337.0070	337.0072	$\text{C}_{15}\text{H}_{14}\text{BrO}_4$	-0.89

Table 3.3. The calculated and experimentally determined high resolution masses of the various synthesised benzodioxane derivatives (**5a–h**). All masses are given as MH^+ .

Compound	Calculated mass	Experimental mass	Formula	ppm
7	153.0546	153.0552	$\text{C}_8\text{H}_9\text{O}_3$	0
5a	243.1016	243.1028	$\text{C}_{15}\text{H}_{15}\text{O}_3$	2.88
5b	277.0626	277.0638	$\text{C}_{15}\text{H}_{14}\text{ClO}_3$	2.53
5c	321.0121	321.0122	$\text{C}_{15}\text{H}_{14}\text{BrO}_3$	-1.25
5d	257.1172	257.1172	$\text{C}_{16}\text{H}_{17}\text{O}_3$	-2.33
5e	271.1329	271.1341	$\text{C}_{17}\text{H}_{19}\text{O}_3$	2.58
5f	273.1121	273.1136	$\text{C}_{16}\text{H}_{17}\text{O}_4$	3.30
5g	307.0732	307.0744	$\text{C}_{16}\text{H}_{16}\text{ClO}_4$	2.28
5h	351.0226	351.0220	$\text{C}_{16}\text{H}_{16}\text{BrO}_4$	-3.13

3.3.3. Interpretation of the HPLC analyses

HPLC analyses were carried out on all the synthesised compounds to estimate their purities. Conditions were selected based on the expected chromatographic properties of the sesamol derivatives (**4a–h**) and benzodioxane derivatives (**5a–h**). It is expected that the synthesised compounds will elute under strong eluting conditions (up to 85% acetonitrile) and will be detectable at low wavelengths (210, 254 and 300 nm). The chromatograms obtained are given in the addendum. As can be seen in the chromatograms, a single peak for each compound analysed is observed, which may indicate a high degree of purity of each compound. Where additional peaks were observed, the purities were calculated based on the integrated areas of the analyte and impurity peaks. ($\% \text{ purity} = \frac{\text{Integrated area of the analyte}}{\text{Integrated area of analyte} + \text{Integrated area of impurity}}$). For this purpose the chromatograms recorded at 254 nm were used. The purities range from 84–100%, most of which may be deemed acceptable for biological evaluation.

Table 3.4. HPLC analysis results of the synthesised sesamol derivatives (**4a–h**).

Compound	Retention time (min)	Area (mAUxs)	Height (mAU)	Purity (%)
4a	8.227	1.66505 ^{x4}	1921.06653	99.0
4b	8.868	1.61470 ^{x4}	1944.48450	100.0
4c	9.155	1.79579 ^{x4}	1949.73889	98.8
4d	8.527	1.49372 ^{x4}	1936.32422	99.2
4e	9.416	1.64856 ^{x4}	1918.52051	100.0
4f	7.846	1.26545 ^{x4}	1950.76917	96.8
4g	8.583	1.41762 ^{x4}	1956.09863	100.0
4h	8.685	1.17312 ^{x4}	1950.56433	95.3

Table 3.5. HPLC analysis results of the synthesised benzodioxane derivatives (**5a–h**).

Compound	Retention time (min)	Area (mAUxs)	Height (mAU)	Purity (%)
7	4.154	1.12654 ^{x4}	1887.54517	98.9
5a	7.940	1.45421 ^{x4}	1939.79333	94.3
5b	8.883	1.64206 ^{x4}	1905.00110	91.2
5c	9.118	1.79294 ^{x4}	1945.87903	84.3

5d	8.433	1.55686 ^{x4}	1896.81897	91.0
5e	10.045	1.22882 ^{x4}	1908.56860	90.2
5f	7.804	1.39267 ^{x4}	1942.59241	99.7
5g	8.536	1.57203 ^{x4}	1944.93054	99.8
5h	8.804	1.43582 ^{x4}	1941.80798	98.2

3.4. Conclusion

Eight sesamol analogues were successfully synthesised from commercially available 5-hydroxysesamol and the appropriate substituted alkyl bromide reagents. Eight benzodioxane analogues were also successfully synthesised using 6-hydroxy-1,4-benzodioxane and the appropriate alkyl bromides. In total sixteen compounds were thus synthesised. The prototype compounds **4a** and **5a**, contained a benzyloxy side chain on C5 or C6 positions on the phenyl ring of the sesamol and benzodioxane moieties, respectively. The benzyloxy side chain phenyl rings were further substituted on the *meta* position with chlorine and bromine (**4b–c** and **5b–c**). Compounds were also synthesised which possessed the phenylethoxy (**4d** and **5d**) and phenylpropoxy (**4e** and **5e**) substituents on C5 or C6, respectively. Furthermore sesamol and benzodioxane derivatives with the phenoxyethoxy side chain (**4f** and **5f**) were also successfully synthesised. Derivatives containing the phenoxyethoxy moiety (**4f** and **5f**) were substituted with *para* substituents (chlorine, bromine) to yield compounds **4g** and **5g** (chlorine) as well as **4h** and **5h** (bromine). The structures of all of the synthesised compounds were characterised and confirmed with NMR and MS analyses. There were good correlation between the ¹H NMR and ¹³C NMR spectra and the proposed structures of the compounds, as well as their experimentally determined masses and the calculated masses. The purities of the compounds were estimated by HPLC analysis. The melting points of the compounds were also noted and are cited in section 3.3.1. Thus, it can therefore be concluded that the structures of the synthesised compounds correspond to the proposed structures of the sesamol and benzodioxane derivatives, and that the most compounds are of an acceptable degree of purity for further biological evaluation.

CHAPTER 4

Enzymology

4.1. Introduction

The sesamol (**4a–h**) and benzodioxane (**5a–h**) derivatives synthesised in this study will be investigated as inhibitors of human MAO-A and MAO-B in this chapter. Several methods for measuring MAO activity *in vitro* have been reported as discussed in chapter 2. In this study fluorescence spectrophotometry was used to determine the IC₅₀ values for the inhibition of the MAOs by the synthesised inhibitors. This protocol uses kynuramine as substrate. Kynuramine is oxidised by MAO-A and MAO-B to ultimately yield 4-hydroxyquinoline, a metabolite which fluoresces ($\lambda_{\text{ex}} = 310 \text{ nm}$; $\lambda_{\text{em}} = 400 \text{ nm}$) in alkaline media (Strydom *et al.*, 2010). Using fluorescence spectrophotometry, the formation of 4-hydroxyquinoline can be readily measured in the presence of the test inhibitors since the sesamol (**4a–h**) and benzodioxane (**5a–h**) derivatives do not fluoresce under the assay conditions employed. From the MAO activity measurements in the presence of the test inhibitors, sigmoidal dose-response curves were constructed and the inhibition potencies, the corresponding IC₅₀ values, were calculated.

4.2. MAO activity measurements

4.2.1. General background

The activities of MAO-A and MAO-B in this study were measured by employing the MAO-A/B mixed substrate, kynuramine, as enzyme substrate. These measurements were based on the observation that certain substrates of the MAOs can be oxidised by these enzymes to yield fluorescent products. For example, kynuramine is oxidised by both MAO-A and MAO-B to 4-hydroxyquinoline, a fluorescent compound (Figure 4.1). In the first step of this reaction, MAO oxidatively deaminates kynuramine to yield an aldehyde. The generated aldehyde can either condense to yield 4-hydroxyquinoline or generate an acid or lactam (2,4-dihydroxyquinoline) by undergoing further oxidation. *In vitro*, the non-enzymatic condensation of the aldehyde occurs faster than the further oxidation to the acid or lactam. Thus 4-hydroxyquinoline is generated by the action of the MAOs on kynuramine *in vitro*. Since 4-hydroxyquinoline fluoresces in alkaline media, it may be conveniently measured with a fluorescence spectrophotometer (Weissbach *et al.*, 1960). This method has been developed into a rapid and reliable assay for MAO activity, which will be used in this study to determine whether the synthesised sesamol (**4a–h**) and benzodioxane (**5a–h**) derivatives exhibit MAO-A and MAO-B inhibition activities.

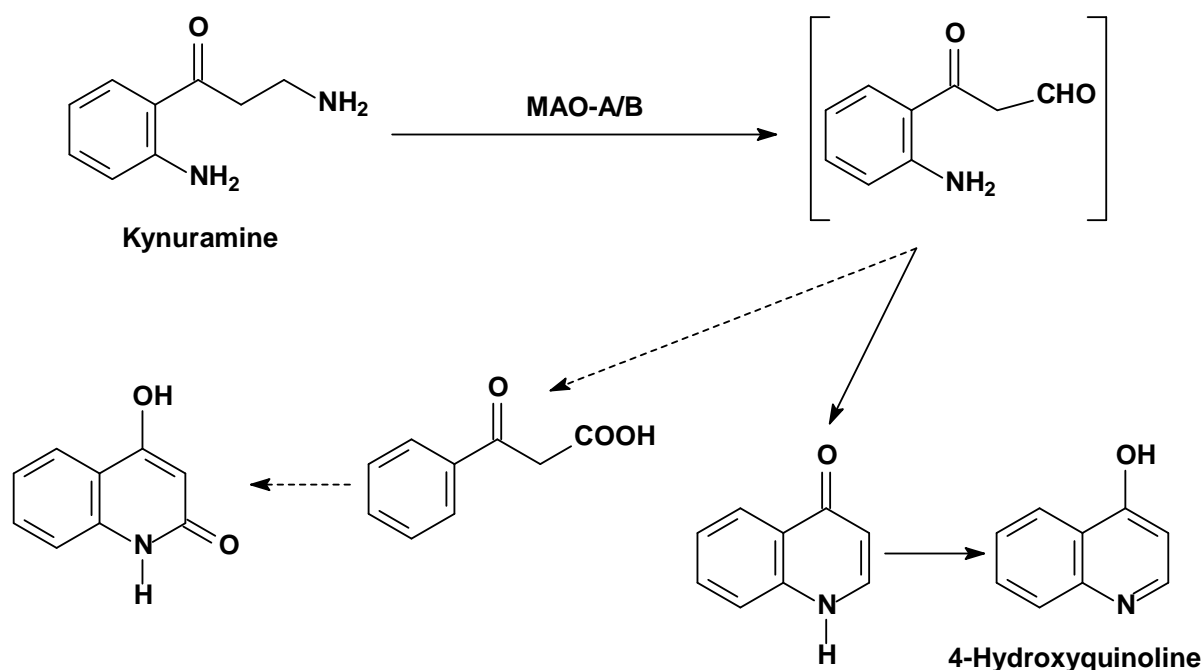


Figure 4.1. The oxidation of kynuramine by MAO-A and MAO-B to yield 4-hydroxyquinoline.

4.2.2. Materials and instrumentation

A Varian Cary Eclipse fluorescence spectrophotometer was employed for the fluorometric measurements. Kynuramine.2HBr, 4-hydroxyquinoline, (*R*)-deprenyl as well as insect cell microsomes containing recombinant human MAO-A and MAO-B (5 mg/ml) were obtained from Sigma-Aldrich. The Graphpad Prism 5 software package was used to construct sigmoidal dose-response curves and to determine the IC_{50} values of the inhibitors. The following were obtained from Merck: polypropylene 96-well microtiter plates, potassium phosphate (K_2HPO_4/KH_2PO_4), KCl, sucrose, NaOH and DMSO. Milli-Q deionised water (Millipore) was used to prepare all buffers.

Slide-A-Lyzer dialysis cassettes with a molecular weight cut-off of 10 000 and a sample volume capacity of 0.5–3 ml were obtained from Thermo Scientific.

4.2.3. Experimental method for IC_{50} determination

In this study, IC_{50} values were determined for the sesamol (**4a–h**) and benzodioxane (**5a–h**) derivatives. The IC_{50} values are a measure of the MAO-A and MAO-B inhibition potencies of the test compounds. To determine IC_{50} values, sigmoidal dose-response curves were constructed and the IC_{50} values were calculated using the Prism software package. The most potent inhibitor of MAO-A and MAO-B may be identified as the compound having the lowest IC_{50} value.

4.2.3.1. Method

Recombinant human MAO-A (5 mg/ml) and human MAO-B (5 mg/ml) were obtained from Sigma-Aldrich, pre-aliquoted, and stored at $-70\text{ }^{\circ}\text{C}$ for the determination of IC_{50} values. All enzymatic reactions were carried out in white polypropylene 96-well microtiter plates. The enzymatic reactions contained the following:

- 92 μl potassium phosphate ($\text{K}_2\text{HPO}_4/\text{KH}_2\text{PO}_4$) buffer (100 mM, pH 7.4, made isotonic with KCl 20.2 mM).
- 50 μl kynuramine to yield a final concentration of 50 μM for the studies with both MAO-A and MAO-B.
- 8 μl of the various test inhibitors to yield final concentrations of 0–100 μM . Stock solutions of the inhibitors were prepared in DMSO.

These reactions were incubated for 30 min at $37\text{ }^{\circ}\text{C}$ after which 50 μl of the enzyme was added. The final concentrations of MAO-A and MAO-B in the reactions were 0.0075 mg protein/ml and 0.015 mg protein/ml, respectively. After a further 20 min of incubation, the reactions were terminated by the addition of 80 μl NaOH (2 N). Concentration measurements of 4-hydroxyquinoline in the microtiter plates were subsequently carried out fluorometrically by measuring the fluorescence at an excitation wavelength of 310 nm and an emission wavelength of 400 nm. The spectrophotometer's PMT voltage was set to medium with an excitation slit width of 5 nm and emission slit width of 10 nm, respectively.

A linear calibration curve was used to make quantitative estimations of 4-hydroxyquinoline in the enzymatic reactions. For this purpose, known amounts (0.047–1.50 μM) of 4-hydroxyquinoline were dissolved to a final volume of 200 μl in $\text{K}_2\text{HPO}_4/\text{KH}_2\text{PO}_4$ buffer (100 mM, pH 7.4, made isotonic with KCl 20.2 mM). 80 μl NaOH was subsequently added to each calibration standard. To confirm that the test inhibitors do not fluoresce or quench the fluorescence of 4-hydroxyquinoline, control samples were included in the assay. These control samples (200 μl) contained 1.50 μM of 4-hydroxyquinoline and 100 μM of the test inhibitor. 80 μl NaOH was added to each control sample. The fluorescence of the calibration standards used in this assay should bracket the fluorescence values recorded in the inhibition studies. The calibration curve should display linearity of 0.999 to be deemed acceptable.

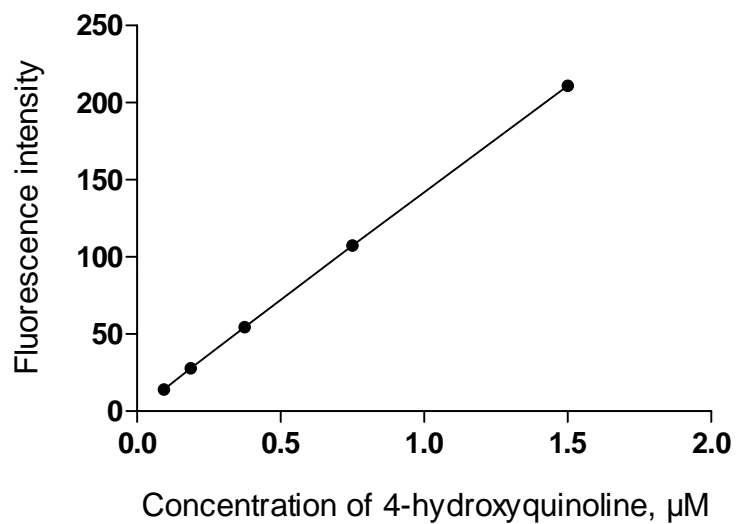


Figure 4.2. An example of a calibration curve routinely constructed in this study. The graph is that of the fluorescence of 4-hydroxyquinoline versus the concentration (μM) of authentic 4-hydroxyquinoline.

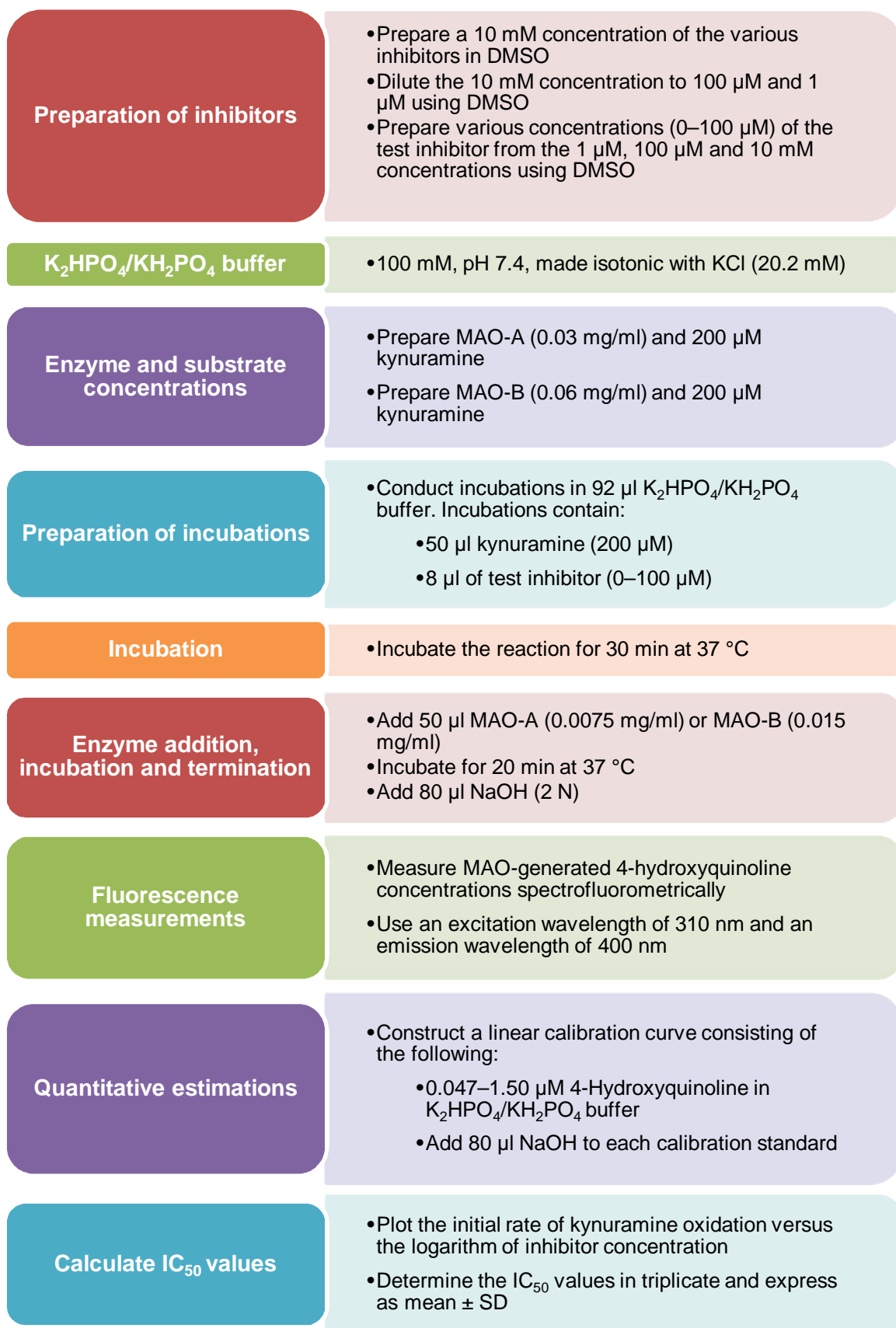
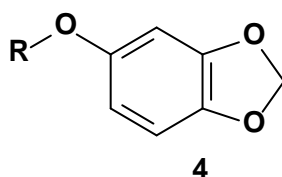


Figure 4.3. Flow diagram summarising the experimental method for IC₅₀ determination.

4.2.3.2. Results

Table 4.1. IC₅₀ values of the synthesised sesamol derivatives (**4a–h**) for the inhibition of human MAO-A and MAO-B.



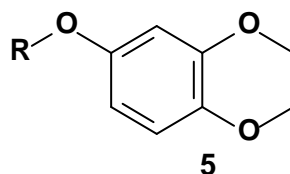
Compound		IC ₅₀ MAO-A (μM) [*]	IC ₅₀ MAO-B (μM) [*]	SI ^a
4a	C ₆ H ₅ CH ₂ –	No inhibition ^b	0.513 ± 0.041	> 195
4b	3-ClC ₆ H ₄ CH ₂ –	51.8 ± 4.52	0.248 ± 0.046	209
4c	3-BrC ₆ H ₄ CH ₂ –	38.4 ± 6.05	0.164 ± 0.034	234
4d	C ₆ H ₅ (CH ₂) ₂ –	87.7 ± 4.41	3.31 ± 0.213	26
4e	C ₆ H ₅ (CH ₂) ₃ –	77.1 ± 3.73	7.29 ± 0.140	11
4f	C ₆ H ₅ O(CH ₂) ₂ –	No inhibition ^b	1.14 ± 0.080	> 88
4g	4-ClC ₆ H ₄ O(CH ₂) ₂ –	No inhibition ^b	1.69 ± 0.273	> 59
4h	4-BrC ₆ H ₄ O(CH ₂) ₂ –	No inhibition ^b	7.07 ± 0.714	> 14

^{*} All values are expressed as the mean ± SD of triplicate determinations.

^a Selectivity index (SI) = IC₅₀(MAO-A)/ IC₅₀(MAO-B). This value is indicative of the extent to which the inhibitor is more selective for MAO-B compared to MAO-A.

^b No inhibition observed at maximum tested concentration of 100 μM.

Table 4.2. IC₅₀ values of the synthesised benzodioxane derivatives (**5a–h**) for the inhibition of human MAO-A and MAO-B.



Compound		IC ₅₀ MAO-A (μM) [*]	IC ₅₀ MAO-B (μM) [*]	SI ^a
5a	C ₆ H ₅ CH ₂ –	36.0 ± 4.252	0.168 ± 0.027	215
5b	3-ClC ₆ H ₄ CH ₂ –	13.2 ± 0.786	0.057 ± 0.010	232

5c	3-BrC ₆ H ₄ CH ₂ -	16.9 ± 0.600	0.045 ± 0.009	375
5d	C ₆ H ₅ (CH ₂) ₂ -	27.8 ± 4.05	0.048 ± 0.012	579
5e	C ₆ H ₅ (CH ₂) ₃ -	70.4 ± 2.44	0.947 ± 0.052	74
5f	C ₆ H ₅ O(CH ₂) ₂ -	69.4 ± 3.99	0.109 ± 0.006	637
5g	4-ClC ₆ H ₄ O(CH ₂) ₂ -	No inhibition ^b	0.348 ± 0.034	> 287
5h	4-BrC ₆ H ₄ O(CH ₂) ₂ -	No inhibition ^b	0.941 ± 0.194	> 106

* All values are expressed as the mean ± SD of triplicate determinations

^a Selectivity index (SI) = IC₅₀(MAO-A)/ IC₅₀(MAO-B). This value is indicative of the extent to which the inhibitor is more selective for MAO-B compared to MAO-A.

^b No inhibition observed at maximum tested concentration of 100 µM.

The IC₅₀ values for the inhibition of human MAO-A and MAO-B by the synthesised sesamol (**4a–h**) and benzodioxane (**5a–h**) derivatives are given in tables 4.1 and 4.2. The IC₅₀ values are expressed as the mean ± SD. Potent MAO-A and MAO-B inhibitors are indicated by low IC₅₀ values. The SI indicates the selectivity of a compound for the MAO-B isoform. A number of compounds did not inhibit the MAO-A isoform, even at a maximal tested concentration of 100 µM. For these, the SI values are given as the lowest possible value, assuming that the IC₅₀ value is 100 µM. From the results the following observations and comparisons may be made:

- A number of sesamol and benzodioxane derivatives are potent inhibitors of human MAO-A and MAO-B, with IC₅₀ values in the submicromolar range. All compounds display selectivity towards the MAO-B isoform. In this regard, the SI values ranged from 11–637. Since the SI values represent the selectivity of inhibition of the MAO-B isoform, all the derivatives examined are thus MAO-B selective inhibitors.
- Compound **4c** is the most potent human MAO-A (IC₅₀ 38.4 µM) and MAO-B (0.164 µM) inhibitor among the sesamol derivatives. This compound is 234-fold more selective for MAO-B compared to the MAO-A isoform.
- Among all of the compounds evaluated, compound **5b** is the most potent human MAO-A inhibitor with an IC₅₀ value of 13.2 µM.
- Among all of the compounds evaluated, compound **5c** is the most potent human MAO-B inhibitor with an IC₅₀ value of 0.045 µM.
- The compound exhibiting the highest selectivity towards human MAO-B is **5f** being 637-fold more selective for MAO-B.

- Generally the benzodioxane derivatives are more potent inhibitors of human MAO-A and MAO-B than the sesamol derivatives. For example, among the benzodioxane derivatives, all compounds inhibited MAO-B with IC_{50} values in the submicromolar range (0.045–0.947 μM). Among the sesamol derivatives, only three compounds inhibited MAO-B with IC_{50} values in the submicromolar range (0.164–0.513 μM). The most potent MAO-B inhibitor of the series, compound **5c** ($IC_{50} = 0.045 \mu\text{M}$), was also found among the benzodioxane derivatives, while the least potent MAO-B inhibitor, compound **4e** ($IC_{50} = 7.29 \mu\text{M}$), is a sesamol derivative. Thus the benzodioxane scaffold is more suitable for the design of MAO-B inhibitors than sesamol. In this respect benzodioxane derivatives act as highly potent MAO-B selective inhibitors.

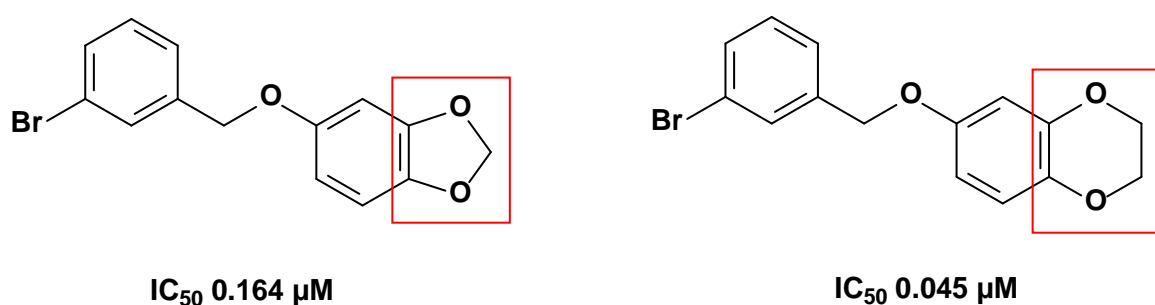


Figure 4.4. Comparison between sesamol (**4a**) and benzodioxane (**5a**) derivatives to establish the most suitable scaffold for MAO-B inhibition.

- The effect that the chain length of the side chain has on the inhibition potencies of the sesamol derivatives may be evaluated. For this purpose, the inhibition potencies of compound **4a** will be compared to those of compounds **4d** and **4e**. The results show that increasing the chain length with one methylene unit from the benzyloxy (**4a**, $IC_{50} = 0.513 \mu\text{M}$) to phenylethoxy (**4d**; $IC_{50} = 3.31 \mu\text{M}$) results in a 6-fold decrease in MAO-B inhibition potency. Increasing the chain length to yield the phenylpropoxy-substituted derivative **4e** ($IC_{50} = 7.29 \mu\text{M}$), results in a further 14-fold (compared to **4a**) decrease in MAO-B inhibition potency. This result shows that the benzyloxy moiety is more optimal for MAO-B inhibition of sesamol derivatives compared to the phenylethoxy and phenylpropoxy moieties. For MAO-A inhibition, the phenylpropoxy-substituted derivative, **4e** ($IC_{50} = 77.1 \mu\text{M}$), is a more potent inhibitor than the phenylethoxy- (**4d**; $IC_{50} = 87.7 \mu\text{M}$) and benzyloxy (**4a**; $IC_{50} = > 100 \mu\text{M}$) substituted derivatives. The benzyloxy-substituted derivative is the least potent MAO-A inhibitor with no inhibition observed at 100 μM . It may thus be concluded that the phenylpropoxy moiety is more optimal for MAO-A inhibition than the benzyloxy and phenylethoxy moieties.

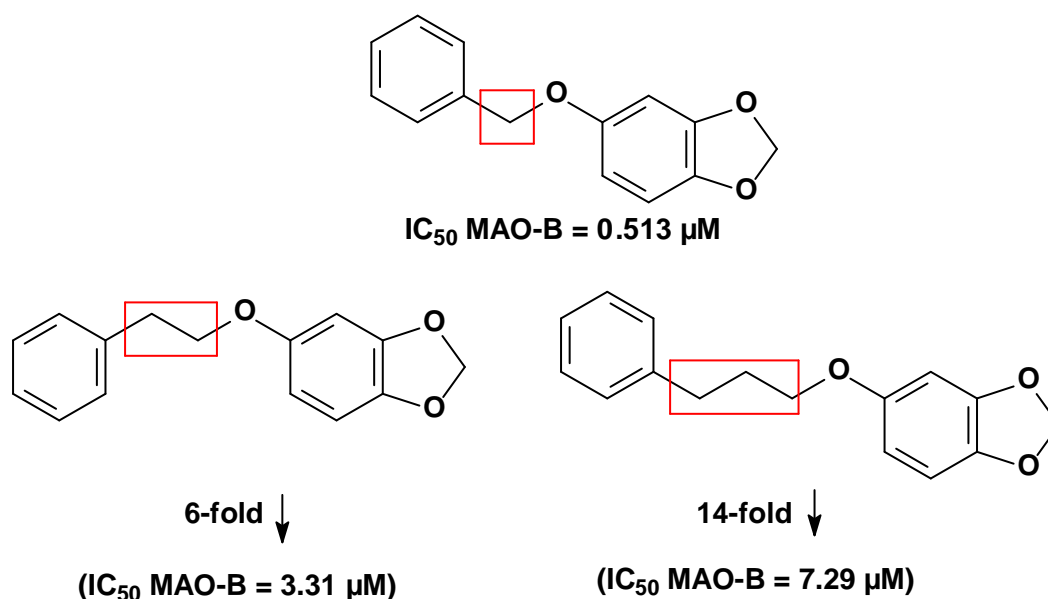


Figure 4.5. Comparison of the effect of the side chain length of sesamol derivatives (**4a** vs. **4d** and **4e**) on MAO-B inhibition potency.

- The effect that the chain length of the side chain has on the inhibition potencies of the benzodioxane derivatives may also be evaluated. For this purpose, the inhibition potencies of compound **5a** will be compared to those of compounds **5d** and **5e**. The results show that increasing the chain length with one methylene unit from the benzyloxy (**5a**, IC_{50} = 0.168 μ M) to phenylethoxy (**5d**; IC_{50} = 0.048 μ M) results in a 3.5-fold increase in MAO-B inhibition potency. Increasing the chain length to yield the phenylpropoxy-substituted derivative **5e** (IC_{50} = 0.947 μ M), results in a 6-fold (compared to **5a**) decrease in MAO-B inhibition potency. This result shows that the phenylethoxy moiety is more optimal for MAO-B inhibition by the benzodioxane derivatives compared to the benzyloxy and phenylpropoxy moieties. For MAO-A inhibition, the phenylethoxy-substituted derivative, **5d** (IC_{50} = 27.8 μ M), is a more potent inhibitor than the benzyloxy- (**5a**; IC_{50} = 36.0 μ M) and phenylpropoxy- (**5e**; IC_{50} = 70.4 μ M) substituted derivatives. It may thus be concluded that the phenylethoxy moiety is more optimal for MAO-A inhibition than the benzyloxy and phenylpropoxy moieties.

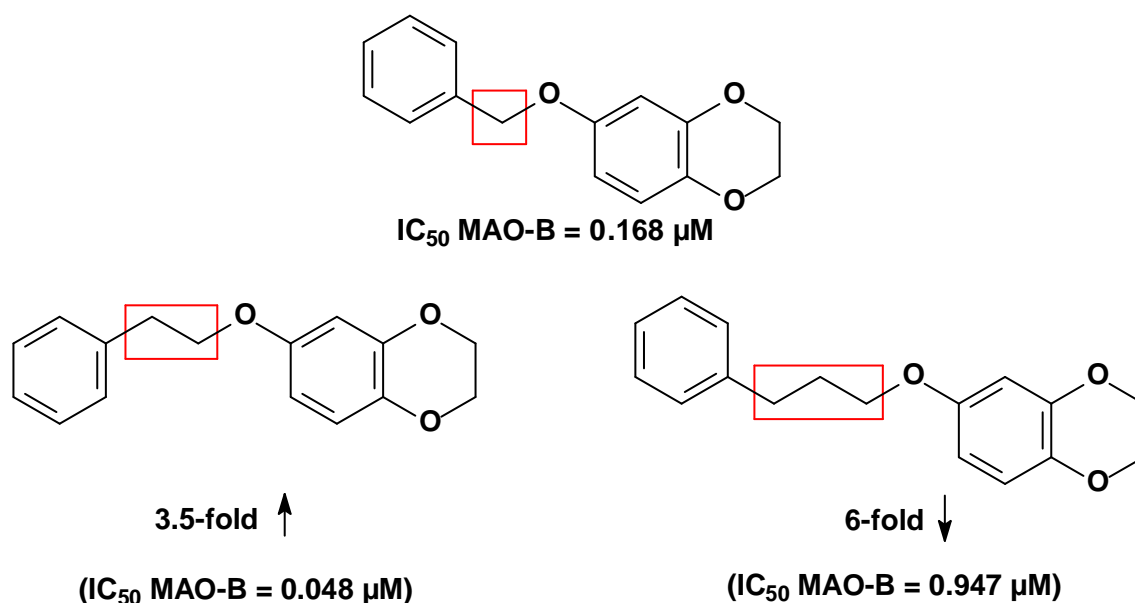


Figure 4.6. Comparison of the effect of the side chain length of benzodioxane derivatives (**5a** vs. **5d** and **5e**) on MAO-B inhibition potency.

- It is noteworthy that, for the benzodioxane derivatives, halogen (Cl, Br) substitution on the benzyloxy phenyl ring enhances MAO-B inhibition potency compared to the unsubstituted derivative **5a**. For example, the chlorine (**5b**, IC_{50} = 0.057 μ M) and bromine (**5c**, IC_{50} = 0.045 μ M) substituted derivatives are 3–4 fold more potent than the unsubstituted derivative **5a** (IC_{50} = 0.168 μ M). For the sesamol derivatives, a similar trend was observed with the chlorine and bromine substituted derivatives **4b** (IC_{50} = 0.248 μ M) and **4c** (IC_{50} = 0.164 μ M) exhibiting more potent MAO-B inhibition than the unsubstituted derivative **4a** (IC_{50} = 0.513 μ M). From these data it is also evident that bromine substitution yields more potent MAO-B inhibitors compared to chlorine substitution. For the inhibition of MAO-A by the benzodioxane derivatives, halogen substitution on the benzyloxy phenyl ring also enhances inhibition potency. For example, the chlorine (**5b**, IC_{50} = 13.2 μ M) and bromine (**5c**, IC_{50} = 16.9 μ M) substituted derivatives are 2–3 fold more potent than the unsubstituted derivative **5a** (IC_{50} = 36.0 μ M) as MAO-A inhibitors.

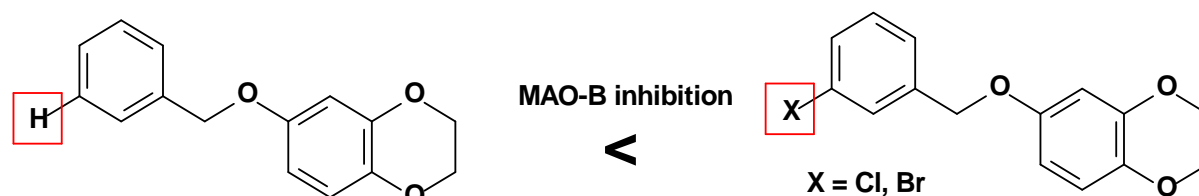


Figure 4.7. The effect that halogen substitution on the benzyloxy phenyl ring of benzodioxane derivatives has on MAO-B inhibition potency.

- The effect that the phenoxyethoxy side chain has on the MAO-A and MAO-B inhibition potencies of the sesamol and benzodioxane derivatives may be evaluated

by comparing **4f** to **4a**, and **5f** to **5a**. The results document that **4f** ($IC_{50} = 1.14 \mu\text{M}$) is a 2-fold weaker MAO-B inhibitor than **4a** ($IC_{50} = 0.513 \mu\text{M}$), which shows that for sesamol derived compounds; the benzyloxy moiety is more favorable for MAO-B inhibition than the phenoxyethoxy moiety. The results further document that **5f** ($IC_{50} = 0.109 \mu\text{M}$) is a 1.5-fold more potent MAO-B inhibitor than **5a** ($IC_{50} = 0.168 \mu\text{M}$), which shows that for benzodioxane derived compounds; the phenoxyethoxy moiety is more favorable for MAO-B inhibition than the benzyloxy moiety.

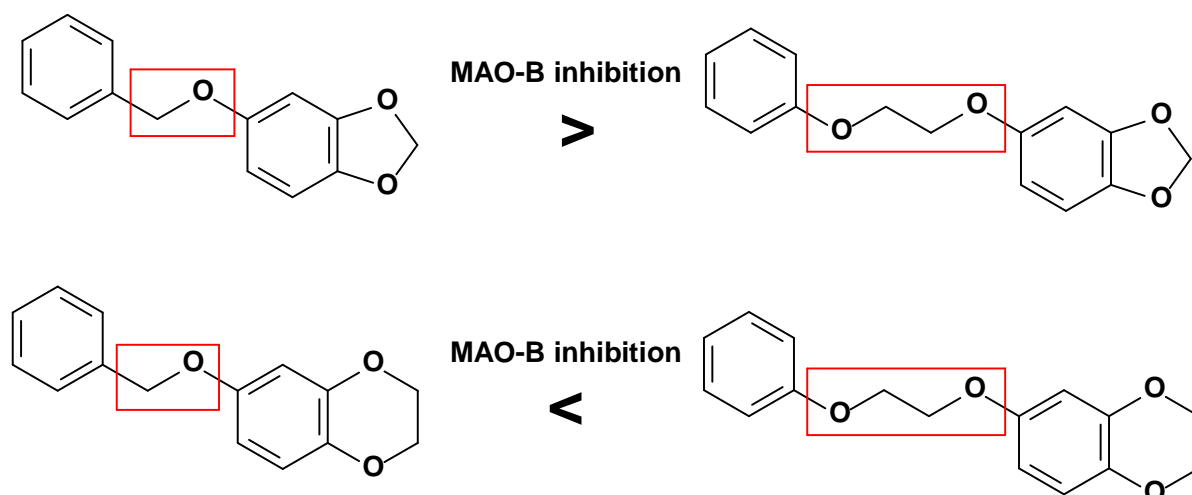


Figure 4.8. The effect of the phenoxyethoxy side chain on the MAO-B inhibitory potencies of sesamol and benzodioxane derivatives.

- The effect that halogen (chlorine and bromine) substitution on the *para* position of the phenoxyethoxy phenyl ring may have on the MAO-A and MAO-B inhibition potencies of the sesamol and benzodioxane derivatives **4f** and **5f** may be evaluated by comparing **4g** and **4h** to **4f**, and **5g** and **5h** to **5f**. It is interesting that, for the benzodioxane derivatives, halogen substitution on the phenoxyethoxy phenyl ring reduces MAO-B inhibition potency. For example, the chlorine (**5g**, $IC_{50} = 0.348 \mu\text{M}$) and bromine (**5h**, $IC_{50} = 0.941 \mu\text{M}$) substituted derivatives are 3–9-fold weaker than the unsubstituted derivative **5f** ($IC_{50} = 0.109 \mu\text{M}$). For the sesamol derivatives, a similar trend was observed with the chlorine and bromine substituted derivatives **4g** ($IC_{50} = 1.69 \mu\text{M}$) and **4h** ($IC_{50} = 7.07 \mu\text{M}$) exhibiting weaker MAO-B inhibition than the unsubstituted derivative **4f** ($IC_{50} = 1.14 \mu\text{M}$). This finding is in contrast to that observed for the benzyloxy-substituted derivatives where halogen substitution enhances MAO-B inhibition potency. Although further investigation is necessary to determine the molecular basis of this difference, it should be noted that for the phenoxyethoxy-substituted derivatives, halogen substitution is in the *para* position while for the benzyloxy-substituted derivatives halogen substitution is in the *meta*

position. This difference may account, at least in part, for the opposite trends observed.

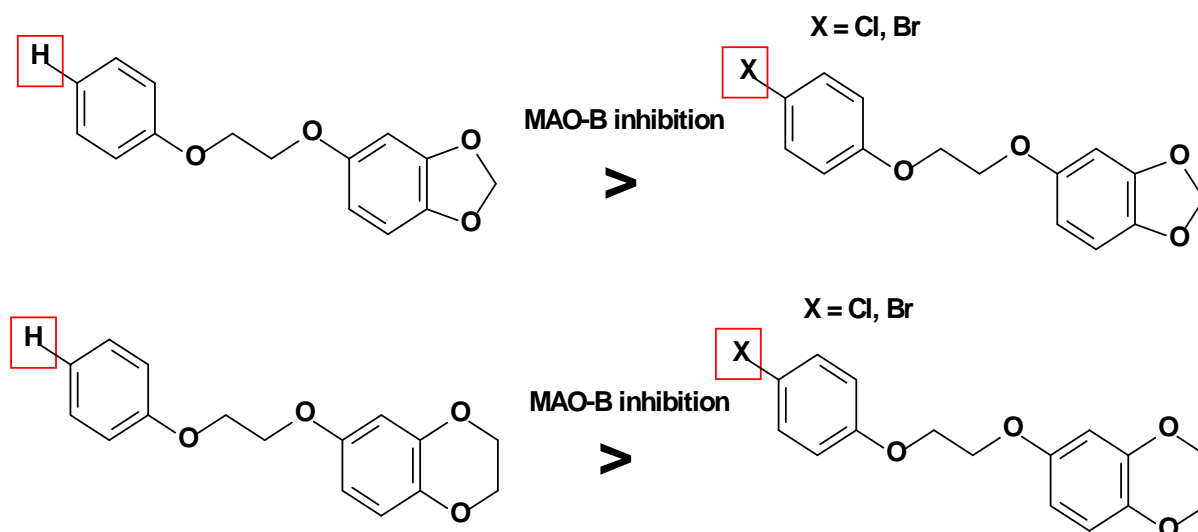


Figure 4.9. The effect that halogen substitution on the phenoxyethoxy phenyl ring of sesamol and benzodioxane derivatives has on MAO-B inhibition potency.

- The inhibition potencies of the sesamol and benzodioxane derivatives may finally be compared to those of the lead compounds for this study, 5-benzyloxyphthalide and other phthalide derivatives. 5-Benzyloxyphthalide is reported to inhibit human MAO-B with an IC_{50} value of 0.024 μM (Strydom *et al.*, 2013). The benzyloxy-substituted benzodioxane homologue **5a** ($IC_{50} = 0.168 \mu\text{M}$) is therefore a 7-fold weaker MAO-B inhibitor. Similarly, the benzyloxy-substituted sesamol homologue **4a** ($IC_{50} = 0.513 \mu\text{M}$) is a 21-fold weaker MAO-B inhibitor than 5-benzyloxyphthalide. The observation that the phthalide derivative is a more potent MAO-B inhibitor than the sesamol and benzodioxane derivatives seems to be general since the MAO-B inhibition activities of the most potent reported phthalide derivatives are an order of magnitude more potent than that of the most potent MAO-B inhibitor discovered in this study. For example, the most potent reported phthalide derivative, inhibited MAO-B with an IC_{50} value of 0.0014 μM , approximately 32-fold more potent than the most potent inhibitor of this study, compound **5c** ($IC_{50} = 0.045 \mu\text{M}$).

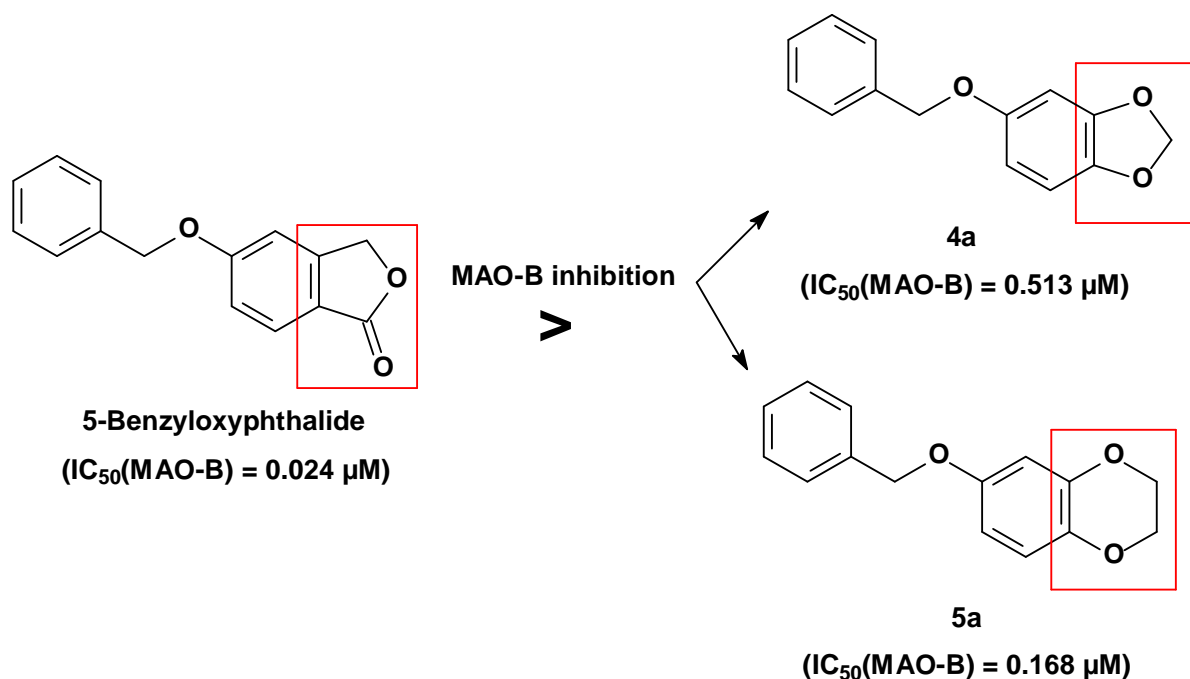


Figure 4.10. Comparison of the MAO-B inhibition potencies of 5-benzyloxyphthalide with those of **4a** and **5a**.

- A similar analysis may be carried out for the inhibition of MAO-A. 5-Benzyloxyphthalide is reported to inhibit human MAO-A with an IC_{50} value of $1.19 \mu\text{M}$ (Strydom *et al.*, 2013). The benzyloxy-substituted benzodioxane homologue **5a** ($IC_{50} = 36.0 \mu\text{M}$) is therefore a 30-fold weaker MAO-A inhibitor, and the benzyloxy-substituted sesamol homologue **4a** ($IC_{50} = > 100 \mu\text{M}$) is at least 84-fold weaker as a MAO-A inhibitor than 5-benzyloxyphthalide. Also, the most potent reported phthalide derivatives are two orders of magnitude more potent than the most potent MAO-A inhibitor discovered here. For example, the most potent reported phthalide derivative, inhibited MAO-A with an IC_{50} value of $0.096 \mu\text{M}$, approximately 138-fold more potent than the most potent inhibitor of this study, compound **5b** ($IC_{50} = 13.2 \mu\text{M}$).

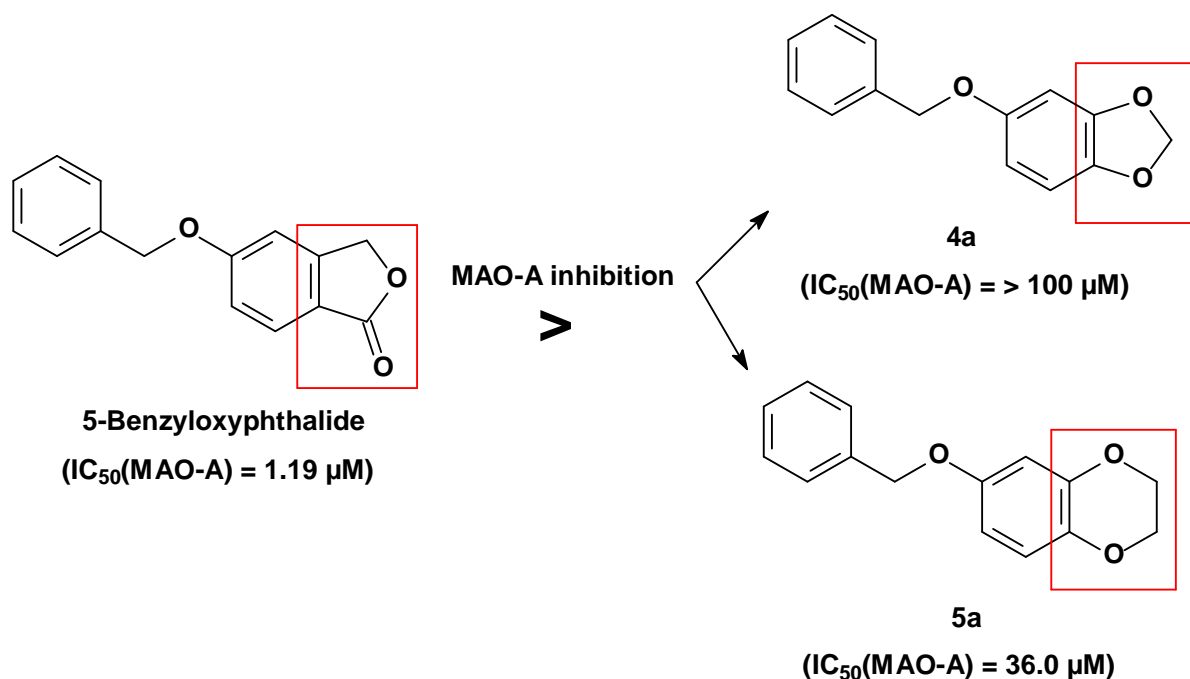


Figure 4.11. Comparison of the MAO-A inhibition potencies of 5-benzyloxyphthalide to those of the sesamol and benzodioxane derivatives.

4.2.4. Experimental method for the determination of the reversibility of inhibition

To evaluate the reversibility of inhibition, the recovery of enzyme activities after dialysis of the enzyme-inhibitor complexes was examined (Petzer *et al.*, 2012). For this purpose, MAO-B and a selected test inhibitor, compound **5c**, was pre-incubated for 15 min at 37 °C. The inhibitor concentration for this study was equal to $4 \times IC_{50}$. The reactions were subsequently placed into hydrated dialysis cassettes and dialysed for 20–25 h at 4 °C in 80 ml sucrose buffer. After dialysis, the residual MAO-B activities were measured by adding kynuramine to the dialysed mixtures. After 20 min incubation, 4-hydroxyquinoline, generated from the MAO-B-catalysed oxidation of kynuramine was quantified by fluorescence spectrophotometry. The MAO-B activities in dialysed and non-dialysed enzyme-inhibitor complexes were recorded and compared to determine whether the selected compound (**5c**) is a reversible MAO-B inhibitor.

4.2.4.1. Method

A single inhibitor, compound **5c** was selected for the reversibility studies. The reversibility of the MAO-B inhibition by **5c** was examined by dialysis. Slide-A-Lyzer dialysis cassettes (Thermo Scientific) with a molecular weight cut-off of 10 000 and a sample volume capacity of 0.5–3 ml were used for these studies. The selected inhibitor, at a concentration equal to $4 \times IC_{50}$ (0.18 μM) was pre-incubated with recombinant human MAO-B (0.03 mg protein/ml) for 15 min at 37 °C. The enzyme-inhibitor incubations were carried out in potassium phosphate

buffer (100 mM, pH 7.4, made isotonic with KCl) containing 5% sucrose. Control incubations were conducted in the absence of inhibitor and presence of the irreversible inhibitor (*R*)-deprenyl ($IC_{50}(\text{MAO-B}) = 0.079 \mu\text{M}$). DMSO (4%) was added as co-solvent to all pre-incubations, and the final volume of the incubations was 0.8 ml. The enzyme-inhibitor complexes were dialysed for 20–25 h at 4 °C in 80 ml outer buffer (100 mM potassium phosphate, pH 7.4, 5% sucrose). The sucrose buffer was replaced at 3 h and 7 h after the start of dialysis. To determine the residual MAO-B activity, the reactions were diluted two-fold with the addition of kynuramine as substrate. The final concentration of MAO-B was 0.015 mg protein/ml and the final kynuramine concentration was 50 μM . The reactions were incubated for 20 min, and terminated with the addition of 400 μl NaOH and 1000 μl deionised water. The MAO-generated 4-hydroxyquinoline concentrations were measured spectrofluorometrically at an excitation wavelength of 310 nm and an emission wavelength of 400 nm. These reactions were carried out in triplicate and the residual catalytic rates were expressed as mean \pm SD. For comparison, non-dialysed enzyme-inhibitor complexes were maintained at 4 °C for the same period and the residual MAO-B activity was measured spectrofluorometrically as described above.

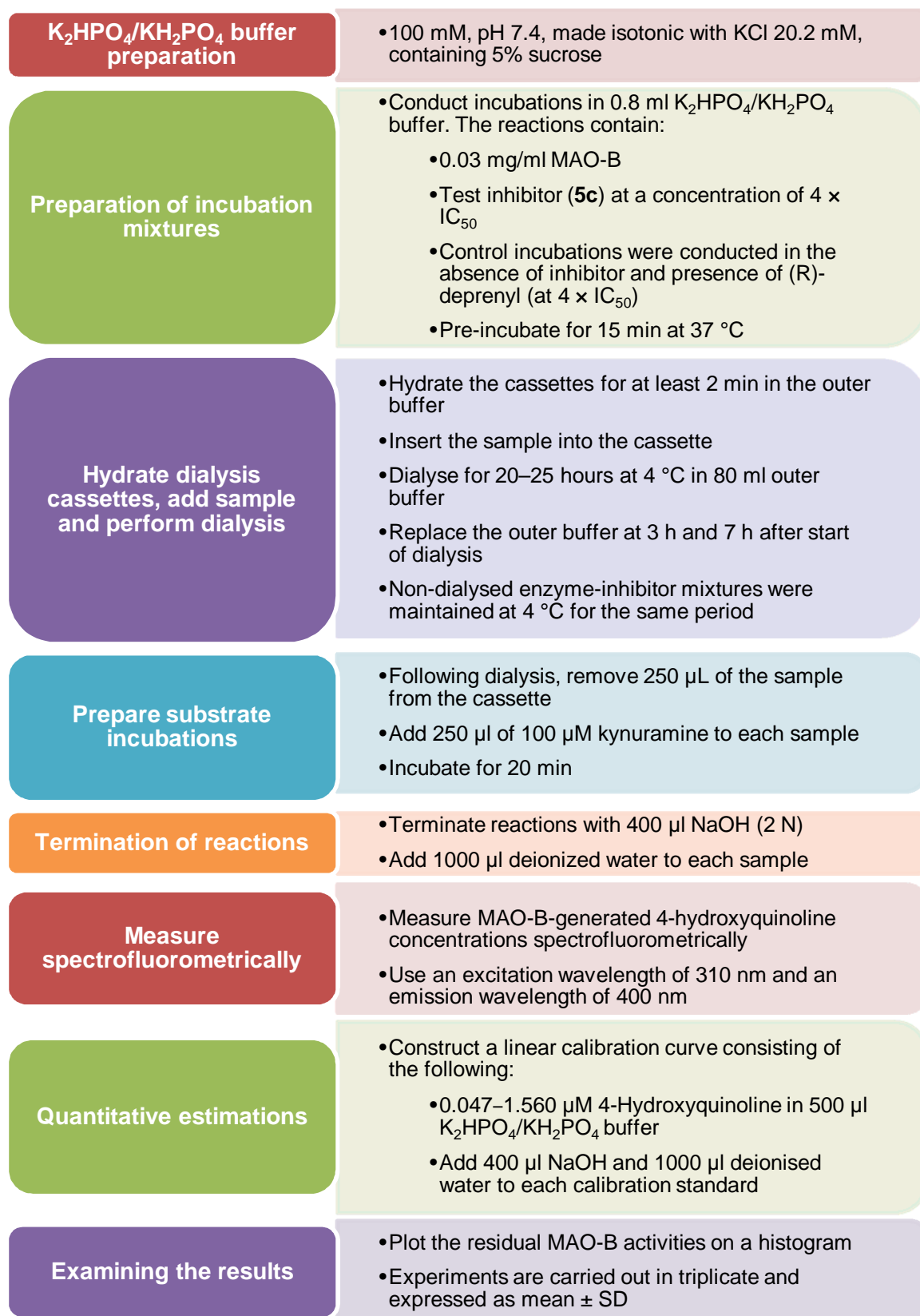


Figure 4.12. Flow diagram summarising the experimental method for the determination of the reversibility of inhibition by dialysis.

4.2.4.2. Results

As shown in figure 4.13, MAO-B inhibition by **5c** is completely reversed after 24 h of dialysis, with MAO-B catalytic activity recovering to a level of 87% of the control value (recorded in the absence of inhibitor). In contrast, the MAO-B activity of non-dialysed mixtures of MAO-B and **5c** is 21% of the control value. These data suggest that **5c** is a reversible MAO-B inhibitor. After similar treatment and dialysis of mixtures of MAO-B and the irreversible inhibitor, (R)-deprenyl, the enzyme activity is not recovered, with the residual enzyme activity at a level of only 2% of the control value. It may therefore be concluded that compound **5c**, and most likely all synthesised sesamol (**4a–h**) and benzodioxane (**5a–h**) derivatives presented in this study, are reversible inhibitors of human MAO-B.

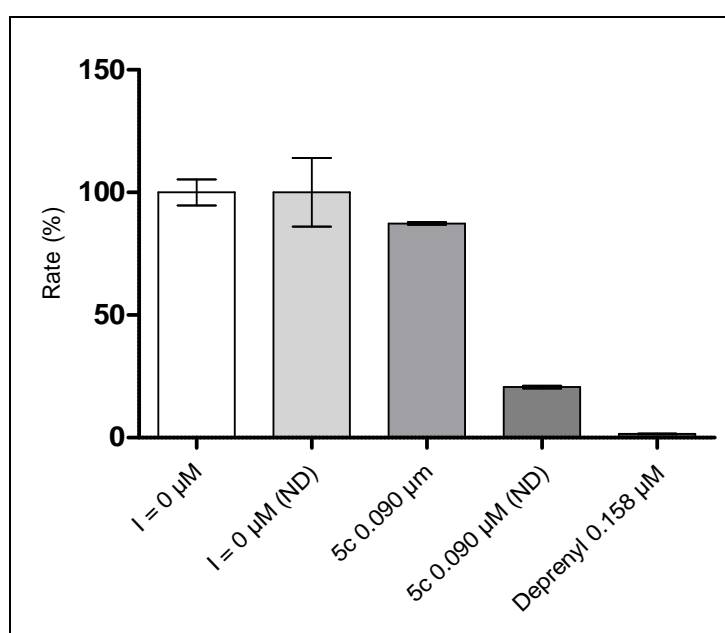


Figure 4.13. Histogram depicting the reversibility of inhibition of MAO-B by compound **5c**. MAO-B and **5c** (at $4 \times \text{IC}_{50}$) were pre-incubated for 15 min, dialysed for 24 h and the residual enzyme activity was measured (**5c**–dialysed). MAO-B was similarly pre-incubated in the absence (No inhibitor–dialysed) and presence of the irreversible inhibitor, (R)-deprenyl (Depr–dialysed), and dialysed. For comparison, the residual MAO activity of non-dialysed mixtures of MAO-B with **5c** is also shown (**5c**–non-dialysed).

4.2.5. Experimental method for construction of Lineweaver-Burk plots

Lineweaver-Burk plots can be used to determine the mode of inhibition of test inhibitors. In this study, Lineweaver-Burk plots were constructed for a selected inhibitor, compound **5c**, to determine whether the inhibitor exhibits a competitive or noncompetitive mode of inhibition.

For this purpose, the MAO-B catalytic rates were recorded at 8 different kynuramine concentrations (15–250 μM) in the absence of inhibitor, and presence of five different inhibitor concentrations ($\frac{1}{4} \times \text{IC}_{50}$, $\frac{1}{2} \times \text{IC}_{50}$, $\frac{3}{4} \times \text{IC}_{50}$, $1 \times \text{IC}_{50}$ and $1\frac{1}{4} \times \text{IC}_{50}$) of **5c**.

4.2.5.1. Method

Recombinant human MAO-B (5 mg/ml), obtained from Sigma-Aldrich, were pre-aliquoted and stored at $-70\text{ }^{\circ}\text{C}$. All enzymatic reactions were conducted in $\text{K}_2\text{HPO}_4/\text{KH}_2\text{PO}_4$ buffer (100 mM, pH 7.4, made isotonic with KCl 20.2 mM) to a final volume of 500 μl . The reactions contained:

- kynuramine as substrate (15–250 μM final concentration)
- MAO-B (0.015 mg/ml final concentration)
- **5c** at various concentrations ($\frac{1}{4} \times \text{IC}_{50}$, $\frac{1}{2} \times \text{IC}_{50}$, $\frac{3}{4} \times \text{IC}_{50}$, $1 \times \text{IC}_{50}$ and $1\frac{1}{4} \times \text{IC}_{50}$). A Lineweaver-Burk plot was also constructed in the absence of the inhibitor,
- DMSO (4%) as co-solvent

The reactions were incubated at $37\text{ }^{\circ}\text{C}$ for 20 min and terminated by the addition of 400 μl NaOH and 1000 μl deionised water. The reactions were subsequently centrifuged for 10 min at 16 000 g. The initial rates by which MAO-B catalyses the oxidation of kynuramine were determined spectrofluorometrically as described in previous sections. The MAO-B-generated 4-hydroxyquinoline was determined by measuring the fluorescence of the supernatant at an excitation wavelength of 310 nm and an emission wavelength of 400 nm, with the PMT voltage of the spectrofluorometer set to medium with an excitation and emission slit width of 5 mm each. A calibration curve was constructed with known amounts (0.047–1.560 μM) of 4-hydroxyquinoline dissolved in 500 μl $\text{K}_2\text{HPO}_4/\text{KH}_2\text{PO}_4$ buffer (100 mM, pH 7.4, made isotonic with KCl 20.2 mM). Volumes of 400 μl NaOH and 1000 μl water were added to each calibration standard. Lineweaver-Burk plots were constructed from these data sets.

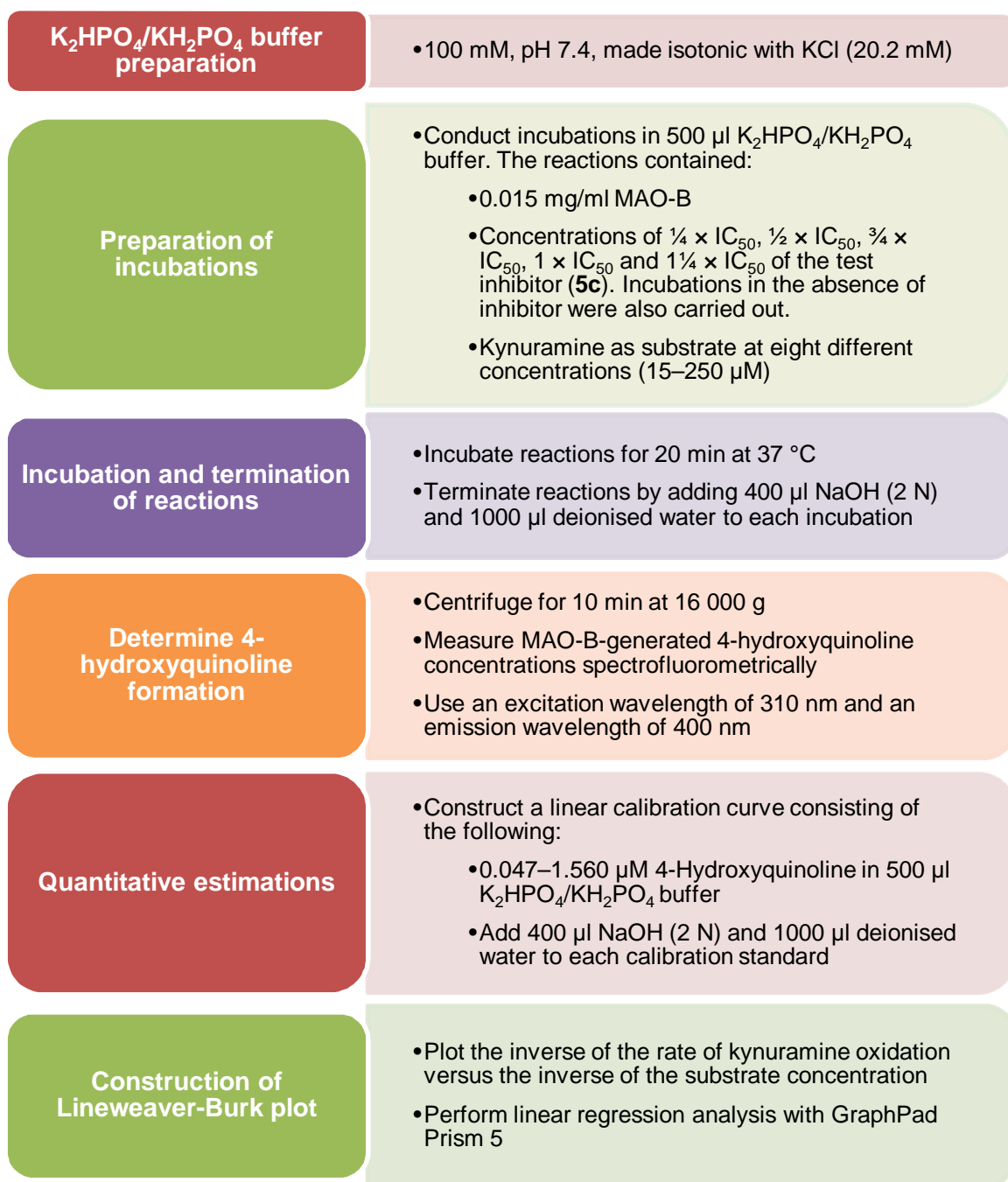


Figure 4.14. Flow diagram summarising the experimental method for constructing Lineweaver-Burk plots.

4.2.5.2. Results

Since compound **5c** exhibited the most potent inhibitory activity towards human MAO-B, it was selected as representative inhibitor for the construction of Lineweaver-Burk plots for this study. The inverse of the initial rate of kynuramine oxidation was plotted against the inverse of the substrate concentrations used. The plots were constructed in the absence of the selected inhibitor and presence of five different inhibitor concentrations.

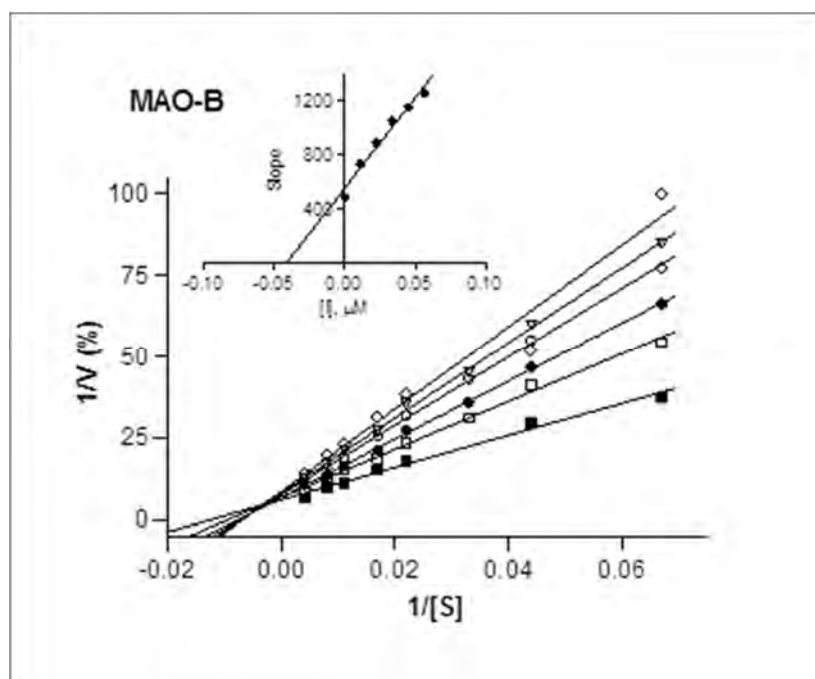


Figure 4.15. Lineweaver-Burk plots of the human MAO-B activities in the absence (filled squares) and presence of various concentrations of **5c** ($IC_{50} = 0.045 \mu\text{M}$). For these studies the concentrations of the inhibitor were $\frac{1}{4} \times IC_{50}$, $\frac{1}{2} \times IC_{50}$, $\frac{3}{4} \times IC_{50}$, $1 \times IC_{50}$ and $1\frac{1}{4} \times IC_{50}$. The inset is a graph of the slopes of the Lineweaver-Burk plots versus inhibitor concentration ($K_i = 0.0413 \mu\text{M}$).

Compound **5c** exhibited Lineweaver-Burk plots typical of competitive inhibition, which is evident from the observation that the lines are linear and intersect on the Y-axis. Therefore it may be concluded that compound **5c** acts as a competitive inhibitor of human MAO-B. From a graph of the slopes of the Lineweaver-Burk plots versus the concentrations of **5c**, the enzyme-inhibitor dissociation constant may be estimated. Using this graph, the negative of the x-axis intercept is equal to the K_i value. Compound **5c** exhibited a K_i of $0.0413 \mu\text{M}$. Similar to the IC_{50} values, the lower the K_i value the more potent the inhibitor. Based on the findings of this experiment, it may be proposed that all synthesised sesamol (**4a–h**) and benzodioxane (**5a–h**) derivatives most likely exhibit competitive inhibition of human MAO-B.

4.3. Conclusion

In this chapter the *in vitro* biological evaluation of the synthesised sesamol (**4a–h**) and benzodioxane (**5a–h**) derivatives are presented. For all compounds, the inhibition potencies were expressed as the IC_{50} values. For this purpose, recombinant human MAO-A and MAO-B were employed as enzyme sources and kynuramine served as non-selective MAO-A/B substrate. The MAO enzymes oxidise kynuramine to yield 4-hydroxyquiniline, a

fluorescent metabolite. By measuring the MAO activities in the presence of various concentrations of the test inhibitors, sigmoidal dose-response curves were constructed. Subsequently, the inhibition potencies, the corresponding IC_{50} values, were calculated from these curves. It may be concluded that the C6-substituted benzodioxane derivatives are potent and selective inhibitors of human MAO-B, with the most potent compound, **5c**, exhibiting an IC_{50} value of 0.045 μ M. This compound is furthermore a reversible inhibitor of MAO-B as determined by dialysis. Compound **5c** also is a competitive MAO-B inhibitor with a measured K_i value of 0.0413 μ M.

In general, benzodioxane derivatives are potent, selective, reversible and competitive inhibitors of human MAO-B and thus promising leads for the future development of therapy for Parkinson's disease.

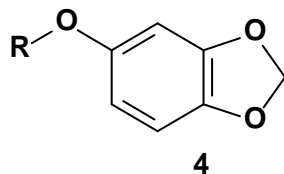
CHAPTER 5

Conclusion

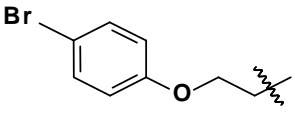
Parkinson's disease is an age-related neurodegenerative disorder with a slow onset, which progressively worsens over time. This disorder is characterised by the loss of neurons in the SNpc which results in striatal dopamine deficiency and subsequently motor symptoms and balance impairment. Current treatment options are symptomatic and do not prevent progression of the disease. *L*-dopa is the main treatment for Parkinson's disease, but with disease progression patients develop dyskinesia associated with *L*-dopa therapy. Combination treatment, such as *L*-dopa with MAO inhibitors, may delay the onset of dyskinesia. Since MAO-B is the main enzyme responsible for dopamine degradation, the inhibition of MAO-B increases endogenous dopamine in the brain. The current study aimed to discover new potent and reversible inhibitors of MAO-B, as potential therapy of Parkinson's disease.

The lead compounds for the present study are derived from phthalide, which has previously been shown to possess MAO inhibition activity, particularly towards MAO-B. Although phthalide itself proved to be a weak MAO-B inhibitor, 5-benzyloxy-substituted phthalides exhibited improved inhibition activity. Thus, the scaffolds used for the present study, sesamol (**4**) and benzodioxane (**5**), similarly were substituted with a benzyloxy moiety on C5 and C6, respectively. Appropriate alkyloxy (phenylethoxy, phenylpropoxy and phenoxyethoxy) substitutions were subsequently made at C5 and C6 of sesamol and benzodioxane in order to determine the effect of side chain lengthening on MAO-inhibitory activity. To explore chemical space selected inhibitors contained halogen (Cl and Br) substitution on the phenyl ring of the side chain in the *meta* position (benzyloxy and phenylethoxy derivatives) as well as the *para* position (phenoxyethoxy derivatives), respectively. The synthesised sesamol and benzodioxane derivatives which were evaluated as inhibitors of MAO-A and MAO-B are shown in table 5.1 and table 5.2.

Table 5.1. The synthesised sesamol (4) derivatives which were evaluated as MAO inhibitors.



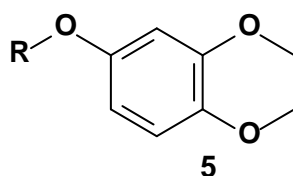
	R	IC ₅₀ MAO-A (μM) [*]	IC ₅₀ MAO-B (μM) [*]
a		No inhibition ^a	0.513
b		51.8	0.248
c		38.4	0.164
d		87.7	3.31
e		77.1	7.29
f		No inhibition ^a	1.14
g		No inhibition ^a	1.69

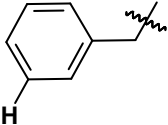
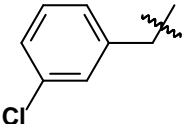
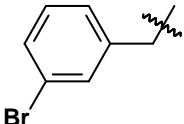
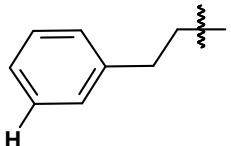
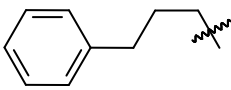
h		No inhibition ^a	7.07
---	---	----------------------------	------

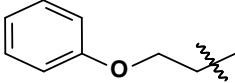
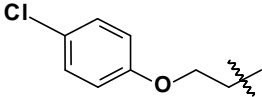
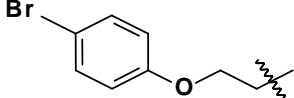
* All values are expressed as the mean of triplicate determinations.

^a No inhibition observed at maximum tested concentration of 100 μM .

Table 5.2. The synthesised benzodioxane (**5**) derivatives which were evaluated as MAO inhibitors.



	R	IC_{50} MAO-A (μM) [*]	IC_{50} MAO-B (μM) [*]
a		36.0	0.168
b		13.2	0.057
c		16.9	0.045
d		27.8	0.048
e		70.4	0.947

f		69.4	0.109
g		No inhibition ^a	0.348
h		No inhibition ^a	0.941

* All values are expressed as the mean of triplicate determinations.

^a No inhibition observed at maximum tested concentration of 100 μ M.

Sixteen sesamol (**4a–h**) and benzodioxane (**5a–h**) derivatives were successfully synthesised by reacting sesamol and 6-hydroxy-1,4-benzodioxane, respectively, with an appropriate alkyl bromide in the presence of potassium carbonate (K_2CO_3) in DMF. 6-Hydroxy-1,4-benzodioxane, in turn, was synthesised from 1,4-benzodioxan-6-carboxaldehyde. The structures and purities of the target compounds were verified by NMR, MS and HPLC analyses. It was concluded that the synthesised compounds correspond with the proposed structures and that these compounds are of an acceptable degree of purity.

Subsequently, the sesamol (**4a–h**) and benzodioxane (**5a–h**) analogues were evaluated as inhibitors of commercially available recombinant human MAO-A and MAO-B. Kynuramine was employed as a MAO-A/B mixed substrate. The MAO activity measurements were based on the oxidative deamination of kynuramine to yield the fluorescent product, 4-hydroxyquinoline. The concentrations of 4-hydroxyquinoline were measured spectrofluorometrically. By measuring MAO activities in the presence of various concentrations of the test inhibitors, sigmoidal dose-response curves were constructed and the corresponding IC_{50} values were calculated. The results indicated that both the sesamol (**4a–h**) and benzodioxane (**5a–h**) derivatives are potent MAO inhibitors with selectivity towards the MAO-B isoform. The compounds thus showed more significant inhibition activity towards MAO-B, with moderate to poor inhibition of MAO-A. The most potent inhibitor was found to be 6-(3-bromobenzyloxy)-1,4-benzodioxane (**5c**) with an IC_{50} value of 0.045 μ M towards MAO-B. In general, the benzodioxane derivatives were more potent MAO-B inhibitors than the corresponding sesamol-derived compounds. It was shown that

lengthening of the side chain at C5 decreases MAO-B inhibition activity for the sesamol derivatives but increases inhibition potency for benzodioxane derivatives, when substituted at C6. For both the sesamol and benzodioxane derivatives, halogen (Cl, Br) substitution on the benzyloxy phenyl ring enhances MAO-B inhibition potency. In contrast halogen substitution on the phenoxyethoxy phenyl ring reduces MAO-B inhibition potency for both classes of compounds. It was also established that for sesamol derived compounds, the benzyloxy moiety is more favorable for MAO-B inhibition than the phenoxyethoxy moiety. For benzodioxane derived compounds, the phenoxyethoxy moiety is more favorable for MAO-B inhibition than the benzyloxy moiety.

The reversibility of the inhibition of recombinant human MAO-B by compound **5c** was evaluated, since it exhibited the highest MAO-B inhibition activity. The results indicated that compound **5c** was a reversible inhibitor with MAO-B activity returning after removal of the inhibitor by dialysis. A set of Lineweaver-Burk plots were also constructed for compound **5c** to further determine the mode of inhibition. Since the plots were linear and the plots constructed in the presence of various inhibitor concentrations intersected on the y-axis, it is proposed that **5c** acts as a competitive inhibitor of human MAO-B. Thus, it may be assumed that the synthesised sesamol (**4a–h**) and benzodioxane (**5a–h**) derivatives act as competitive reversible inhibitors of human MAO.

This study showed that the benzodioxane scaffold with C6 benzyloxy substitution is preferred for MAO-B inhibition activity. Halogen substitution on the benzyloxy phenyl ring yields particularly potent MAO-B inhibitors. In this regard 6-benzyloxy-substituted benzodioxane is a promising scaffold for future MAO-B inhibitor design.

Based upon the discussion above, it may be concluded that the objectives of this study has been achieved and that the hypothesis has been proofed: sesamol and benzodioxane derivatives, with the appropriate benzyloxy and halogen substitution yields potent MAO-B inhibitors. Thus the sesamol and benzodioxane are promising scaffolds for the future design of selective reversible competitive MAO-B inhibitors. Such compounds may be suitable drug candidates in the future symptomatic anti-parkinsonian treatment.

Future recommendations

From the results of this study, the following recommendations are made for future studies:

1. The study showed that structural modification of sesamol and benzodioxane yield potent MAO-B inhibitors. Sesamol and benzodioxane may thus be used as scaffolds for the future design of MAO-B inhibitors. Both series may be expanded with substitution on C5 and C6 to derive additional SAR.
2. Since compound **4c** is the most potent and selective MAO-B inhibitor amongst the sesamol derivatives, this structure can be applied as lead compound for future MAO-B inhibitor design. The halogen on the benzyloxy phenyl ring may be substituted with other halogens and alkyl groups to determine which substituent results in the most potent MAO-B inhibition.
3. Since compound **5c** is the most potent MAO-B inhibitor amongst the benzodioxane derivatives, this structure can be applied as lead compound for future MAO-B inhibitor design. The halogen on the benzyloxy phenyl ring may be substituted with other halogens and alkyl groups to determine which substituent results in the most potent MAO-B inhibition.
4. The most selective MAO-B inhibitor for the study, **5f**, may serve as lead compound to improve the selectivity of future design of MAO-B inhibitors.
5. Since the halogen substituted phenoxyethoxy compounds, **4g**, **4h** and **5g**, **5h**, do not have any MAO-A inhibitory activities, these compounds may be applied for the future design of specific MAO-B inhibitors. The halogens may be substituted with for example alkyl groups to enhance the MAO-B inhibition potency.

BIBLIOGRAPHY

Bezerra-Netto, H.J.C., Lacerda, D.I., Miranda, A.L.P., Alves, H.M., Berreiro, E.J. and Fraga, C.A.M. 2006. Design and synthesis of 3,4-methylenedioxy-6-nitrophenoxyacetylhydrazone derivatives obtained from natural safrole: New lead-agents with analgesic and antipyretic properties. *Bioorganic & medicinal chemistry*. 14:7924–7935.

Binda, C., Li, M., Hubalek, F., Restelli, N., Edmondson, D.E. and Mattevi, A. 2003. Insights into the mode of inhibition of human mitochondrial monoamine oxidase B from high-resolution crystal structures. *Proceedings of the national academy of sciences of the United States of America*. 100:9750–9755.

Binda, C., Wang, J., Pisani, L., Caccia, C., Carotti, A., Salvatti, P., Edmondson, D.E. and Mattevi, A. 2003. Structures of human monoamine oxidase B complexes with selective noncovalent inhibitors: safinamide and coumarin analogs. *Journal of medicinal chemistry*. 50:5848–5852.

Blum, D., Torch, S., Lambeng, N., Nissou, M., Benabid, A., Sadoul, R. and Verna, J. 2001. Molecular pathways involved in the neurotoxicity of 6-OHDA, dopamine and MPTP: contribution to the apoptotic theory in Parkinson's disease. *Progress in neurobiology*. 65:135–172.

Bové, J., Prou, D., Perier, C. and Przedborski, S. 2005. Toxin-induced models of Parkinson's disease. *The journal of the American society for experimental neurotherapeutics*. 2:484–494.

Broka, C.A., Carter, D.S., Dillon, M.P., Hawley, R.C., Jahangir, A., Lin, C.J.J. and Parish, D.W. 2005. Diaminopyrimidines as P2X3 and P2X2/3 antagonists. US Patent 2005/0209260 A1.

Dauer, W. and Przedborski, S. 2003. Parkinson's disease: mechanisms and models. *Neuron*. 39:889–909.

Edmondson, D.E., Binda, C. and Mattevi, A. 2007. Structural insights into the mechanism of amine oxidation by monoamine oxidases A and B. *Archives of biochemistry and biophysics*. 464:269–276.

Edmondson, D.E., Binda, C., Wang, J., Upadhyay, A.K. and Mattevi, A. 2009. Molecular and mechanistic properties of membrane-bound mitochondrial monoamine oxidase, *Biochemistry*. 48:4220–4230.

Gnerre, C., Catto, M., Leonetti, F., Weber, P., Carrupt, P.A., Altomare, C., Carotti, A. and Testa, B. 2000. Inhibition of monoamine oxidases by functionalized coumarin derivatives: biological activities, QSARs, and 3D-QSARs. *Journal of medicinal chemistry*. 43:4747–4758.

Gilman, A.G., Goodman, L.S. & Gilman, A., eds. *Goodman and Gilman's The pharmacological basis of therapeutics*. 6th ed. New York: Macmillan. 1980:609–646.

Holt, A., Sharman, D.F., Baker, G.B. and Palcic, M.M. 1997. A continuous spectrophotometric assay for monoamine oxidase and related enzymes in tissue homogenates. *Analytical biochemistry*. 244:384–392.

Inoue, H., Castagnoli, K., Van der Schyf, C., Mabic, S., Igarashi, K. and Castagnoli, N., Jr. 1999. Species-dependent differences in monoamine oxidase A and B-catalyzed oxidation of various C4 substituted 1-methyl-4-phenyl-1,2,3,6-tetrahydropyridinyl derivatives. *Journal of pharmacology and experimental therapeutics*. 291:856–864.

Jalkanen, S. and Salmi, M. 2001. Cell surface monoamine oxidase: enzymes in search of a function. *The EMBO journal*. 20:3893–3901.

Lee, Y., Ling, K.Q., Lu, X., Silverman, R.B., Shepard, E.M., Dooley, D.M. and Sayre, L.M. 2002. 3-Pyrrolines are mechanism-based inactivators of the quinone-dependent amine oxidases but only substrates of the flavin-dependent amine oxidases. *Journal of the American chemical society*. 124:12135–12143.

Lees, A. 2005. Alternatives to levodopa in the initial treatment of early Parkinson's disease. *Drugs & aging*. 22:731–770.

Lees, A.J., Hardy, J. and Revesz, T. 2009. Parkinson's disease. *Lancet*. 373:2055–2066.

LeWitt, P.A. and Taylor, D.C. 2008. Protection against Parkinson's disease progression: clinical experience. *Neurotherapeutics*. 5:210–225.

Novaroli, L., Reist, M., Favre, E., Carotti, A., Catto, M. and Carrupt, P.A. 2005. Human recombinant monoamine oxidase B as reliable and efficient enzyme source for inhibitor screening. *Bioorganic & medicinal chemistry*. 13:6212–6217.

Novaroli, L., Daina, A., Favre, E., Bravo, J., Carotti, A., Leonetti, F., Catto, M., Carrupt, P.A. and Reist, M. 2006. Impact of species-dependent differences on screening, design, and development of MAO B inhibitors. *Journal of medicinal chemistry*. 49:6264–6272.

Ogunrombi, M.O., Malan, S.F., Terre'Blanche, G., Castagnoli, K., Castagnoli, N., Jr., Bergh, J.J. and Petzer, J.P. 2007. Neurotoxicity studies with the monoamine oxidase B substrate 1-methyl-3-phenyl-3-pyrroline. *Life sciences*. 81:458–467.

Petzer, A., Harvey, B.H., Wegener, G. and Petzer, J.P. 2012. Azure B, a metabolite of methylene blue, is a high-potency, reversible inhibitor of monoamine oxidase. *Toxicology and applied pharmacology*. 258(3):403–409.

Przedborski, S. 2005. Pathogenesis of nigral cell death in Parkinson's disease. *Parkinsonism and related disorders*. 11:S3–S7.

Smeyne, R.J. and Jackson-Lewis, V. 2004. The MPTP model of Parkinson's disease. *Brain research. Molecular brain research*. 134:57–66.

Strydom, B., Malan, S.F., Castagnoli, N., Jr., Bergh, J.J. and Petzer, J.P. 2010. Inhibition of monoamine oxidase B by 8-benzoyloxycaffeine analogues. *Bioorganic & medicinal chemistry*. 18:1018–1028.

Strydom, B., Bergh, J.J. and Petzer, J.P. 2013. Inhibition of monoamine oxidase by phthalide analogues. *Bioorganic & medicinal chemistry*. 23:1269–1273.

Van den Berg, D., Zoellner, K.R., Ogunrombi, M.O., Malan, S.F., Terre'Blanche, G., Castagnoli, N., Jr., Bergh, J.J. and Petzer, J.P. 2007. Inhibition of monoamine oxidase B by selected benzimidazole and caffeine analogues. *Bioorganic & medicinal chemistry*. 15:3692–3702.

Vlok, N., Malan, S.F., Castagnoli, N., Jr., Bergh, J.J. and Petzer, J.P. 2006. Inhibition of monoamine oxidase B by analogues of the adenosine A_{2A} receptor antagonist (E)-8-(3-chlorostyryl) caffeine (CSC). *Bioorganic & medicinal chemistry*. 14:3512–3521.

Weissbach, H., Smith, T.E., Daly, J.W., Witkop, B. and Udenfriend, S. 1960. A rapid spectrophotometric assay of monoamine oxidase based on the rate of disappearance of kynuramine. *The journal of biological chemistry*. 235:1160–1163.

Yacoubian, T.A. and Standaert, D.G. 2009. Targets for neuroprotection in Parkinson's disease. *Biochimica et biophysica acta*. 1792:676–687.

Youdim, M.B. and Bakhle, Y.S. 2006. Monoamine oxidase: isoforms and inhibitors in Parkinson's disease and depressive illness. *British journal of pharmacology*. 147(Suppl 1):S287–296.

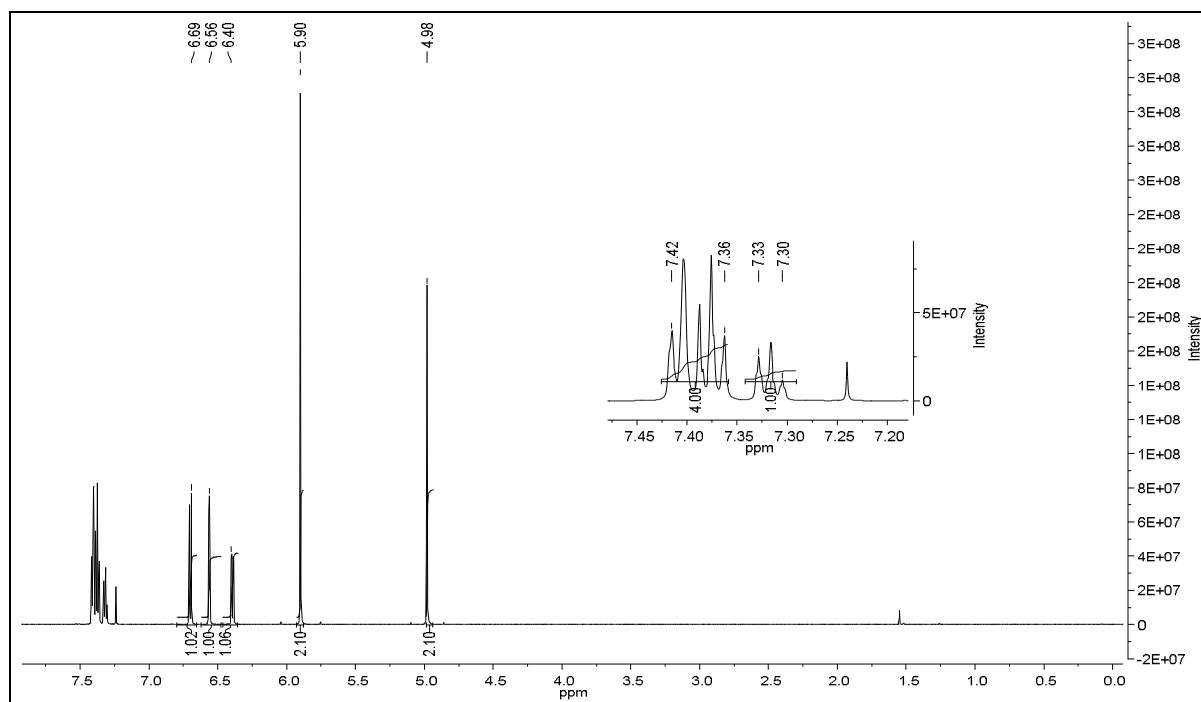
Youdim, M.B., Edmondson, D. and Tipton, K.F. 2006. The therapeutic potential of monoamine oxidase inhibitors. *Nature reviews. Neuroscience*. 7:295–309.

APPENDIX

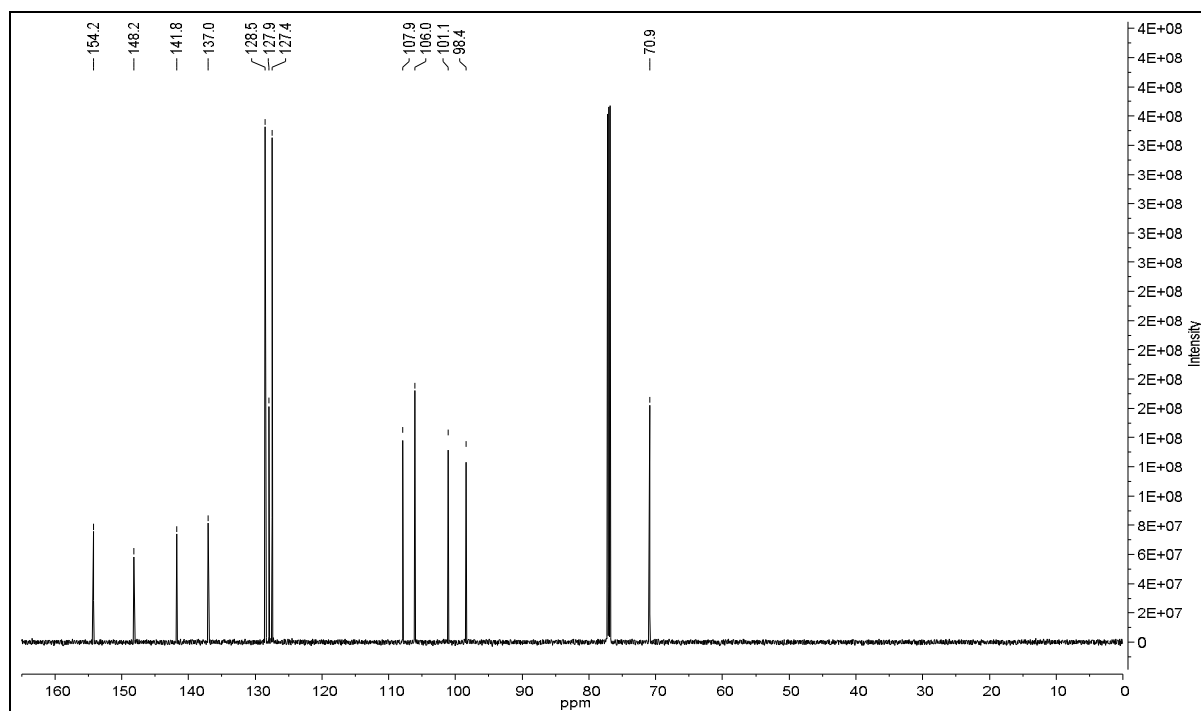
Section 1: ^1H NMR and ^{13}C NMR spectra

4a: 5-(Benzyloxy)-2H-1,3-benzodioxole

^1H

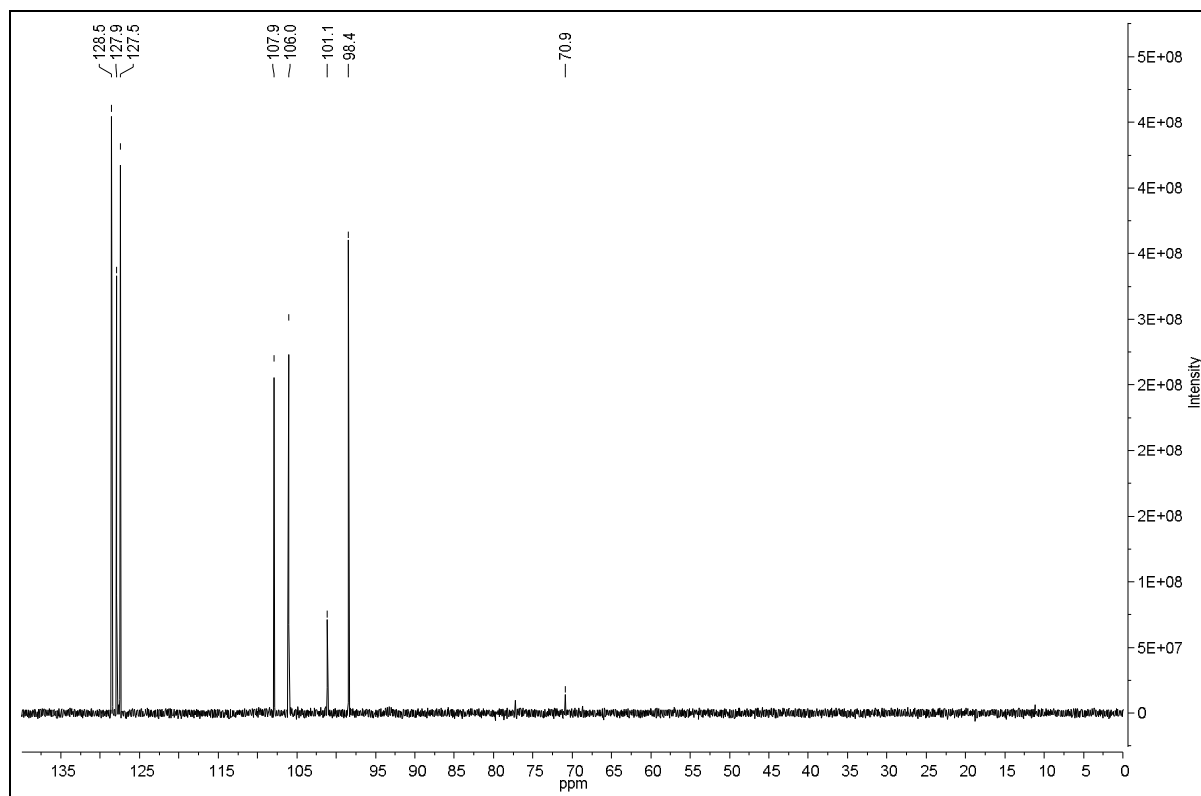


^{13}C

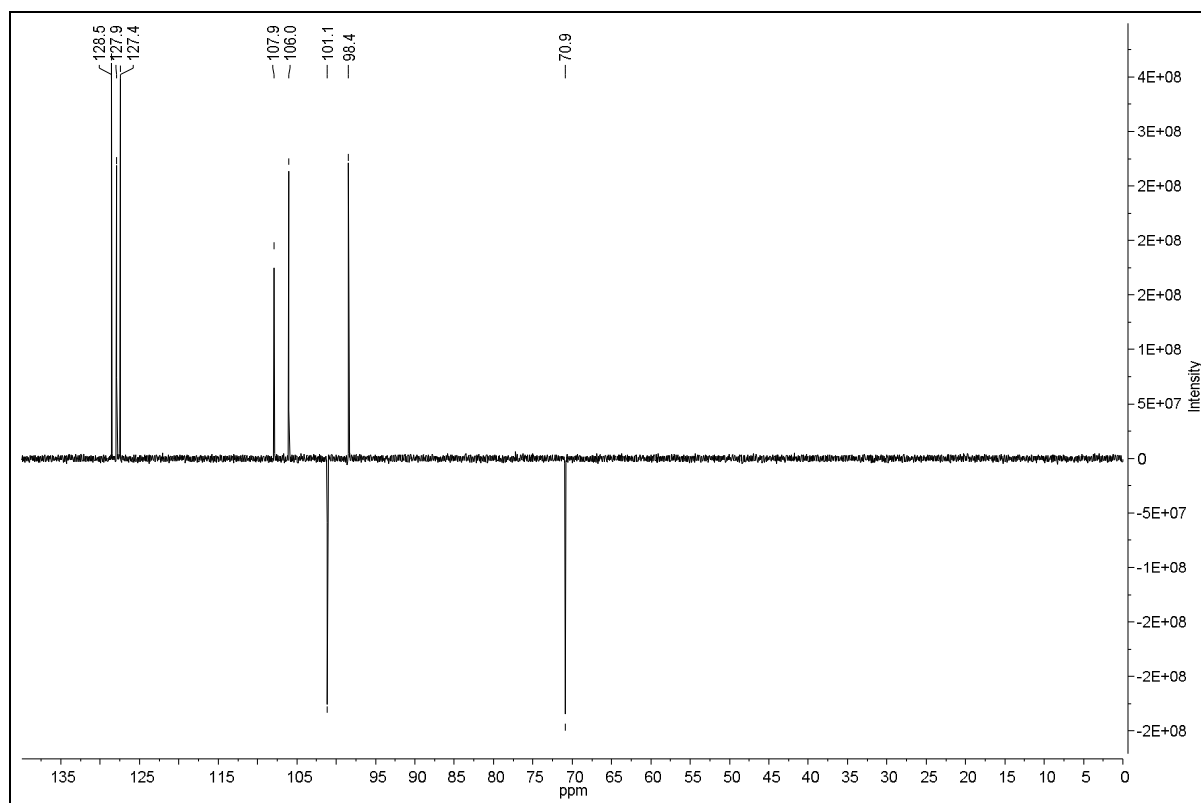


4a: 5-(Benzyloxy)-2H-1,3-benzodioxole

^{13}C NMR DEPT 90°

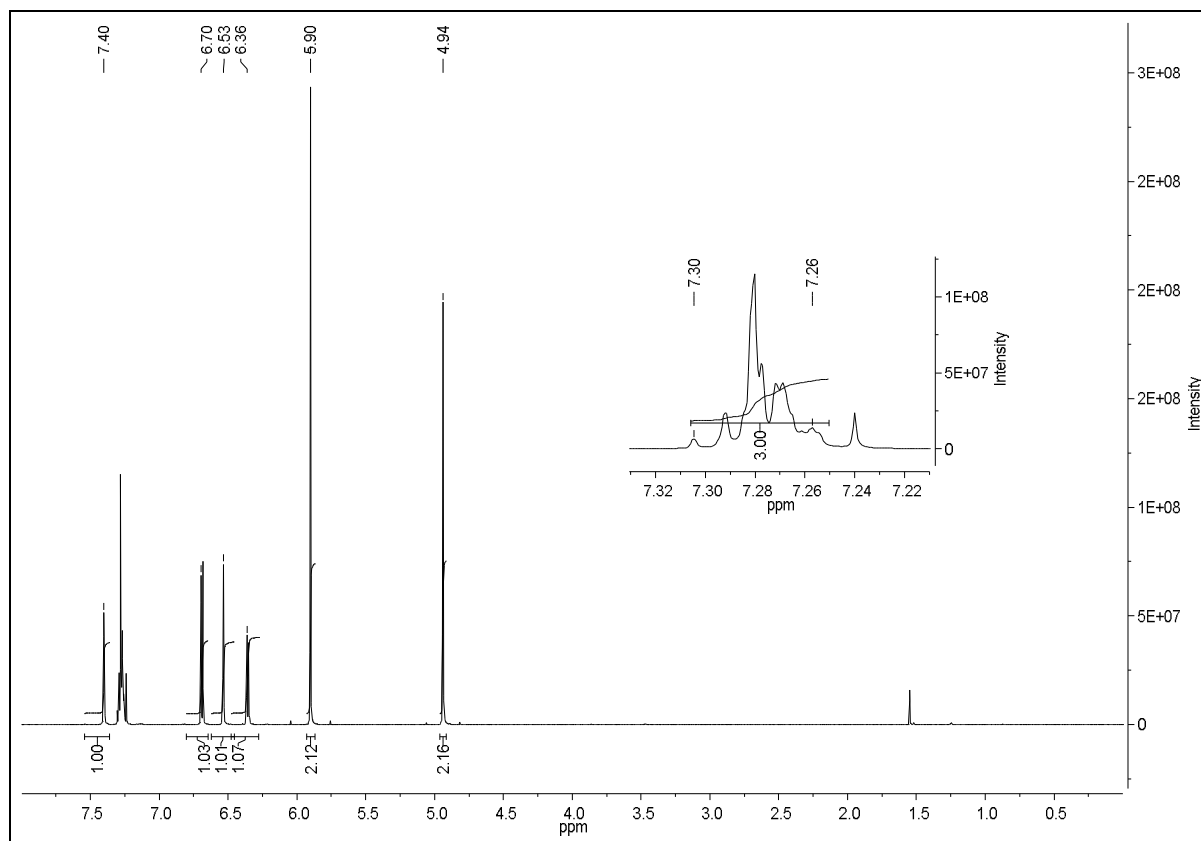


^{13}C NMR DEPT 135°

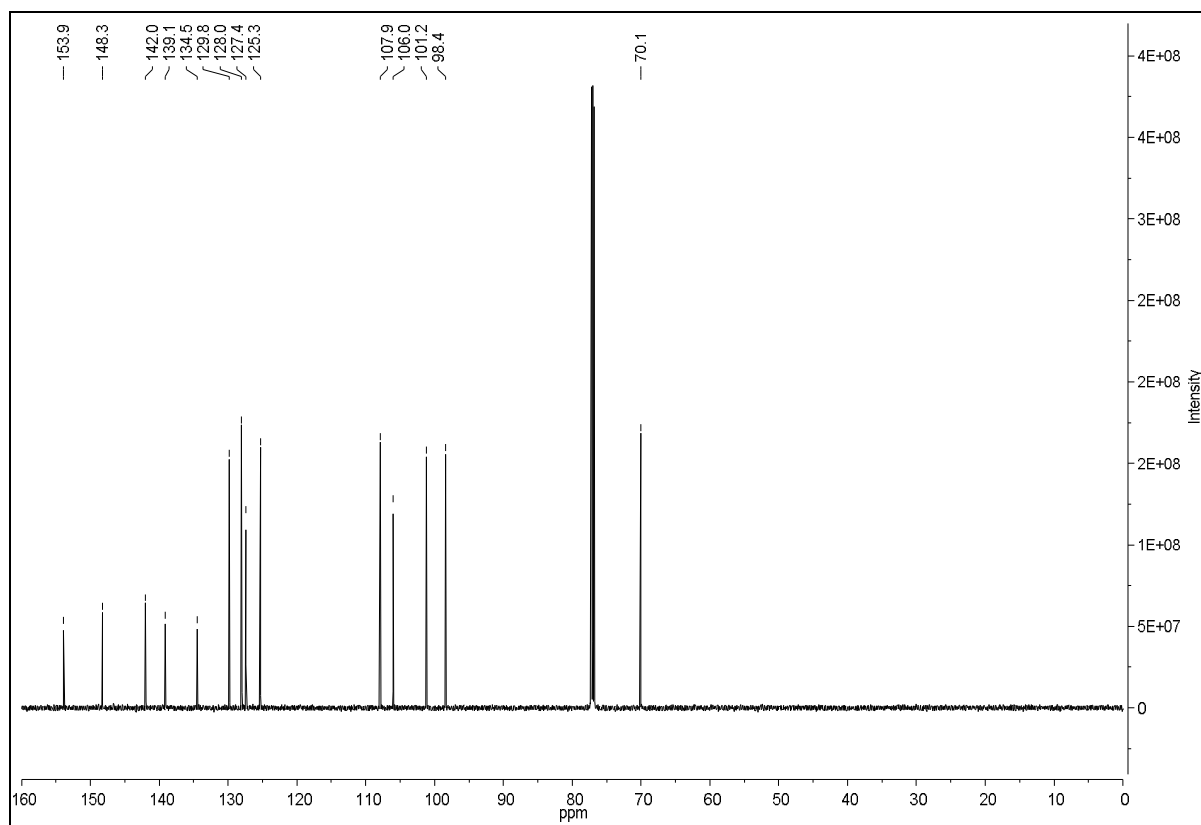


4b: 5-[(3-Chlorophenyl)methoxy]-2H-1,3-benzodioxole

¹H

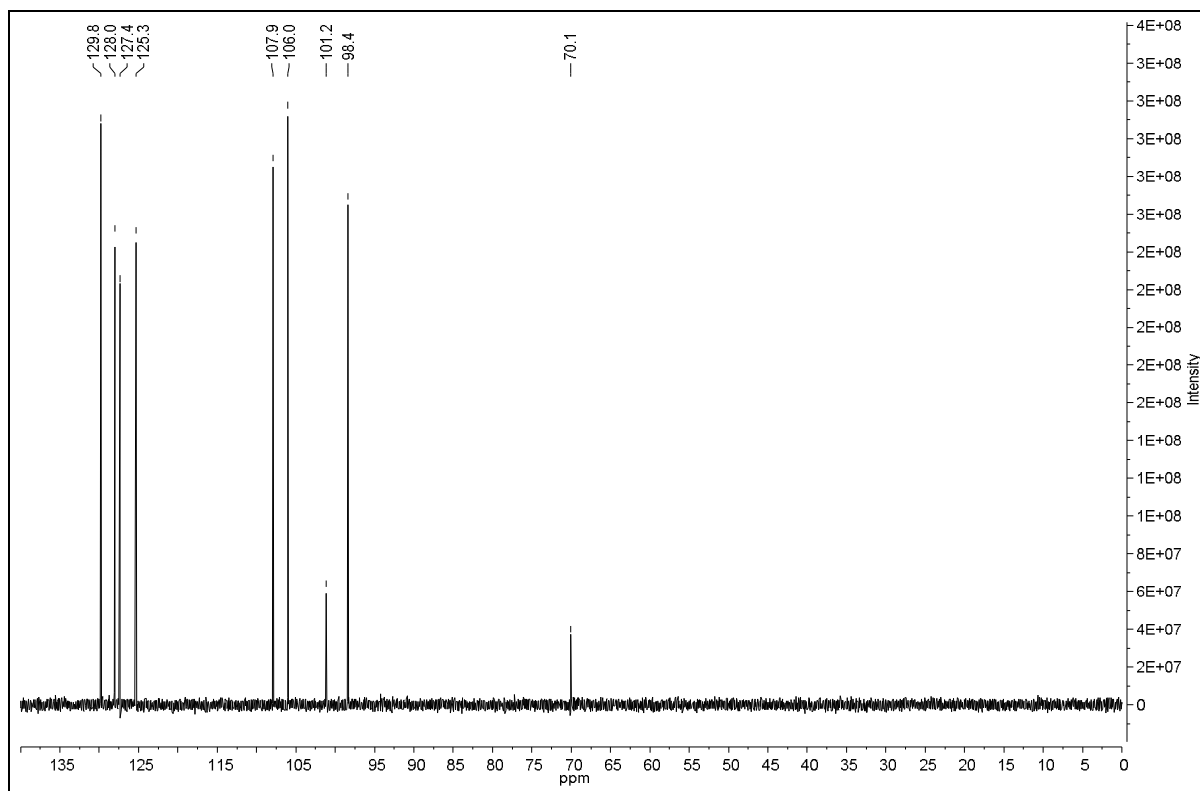


¹³C

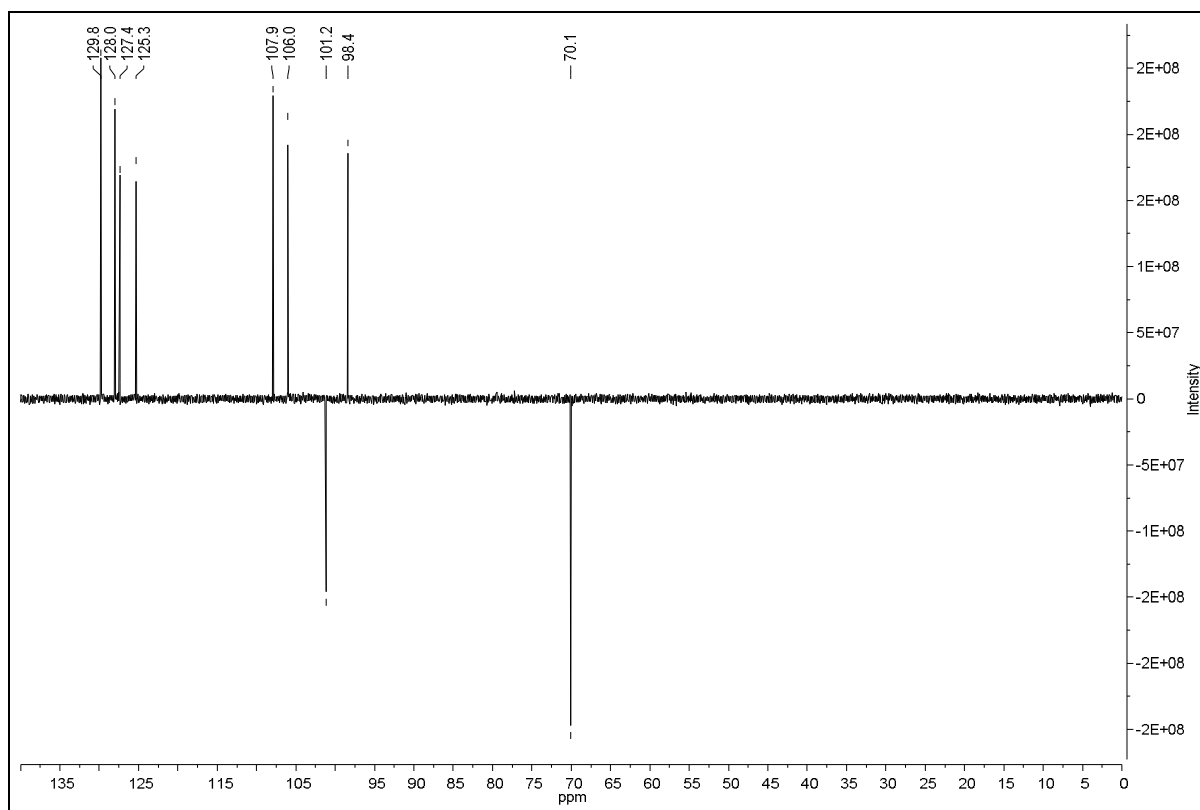


4b: 5-[(3-Chlorophenyl)methoxy]-2H-1,3-benzodioxole

^{13}C NMR DEPT 90°

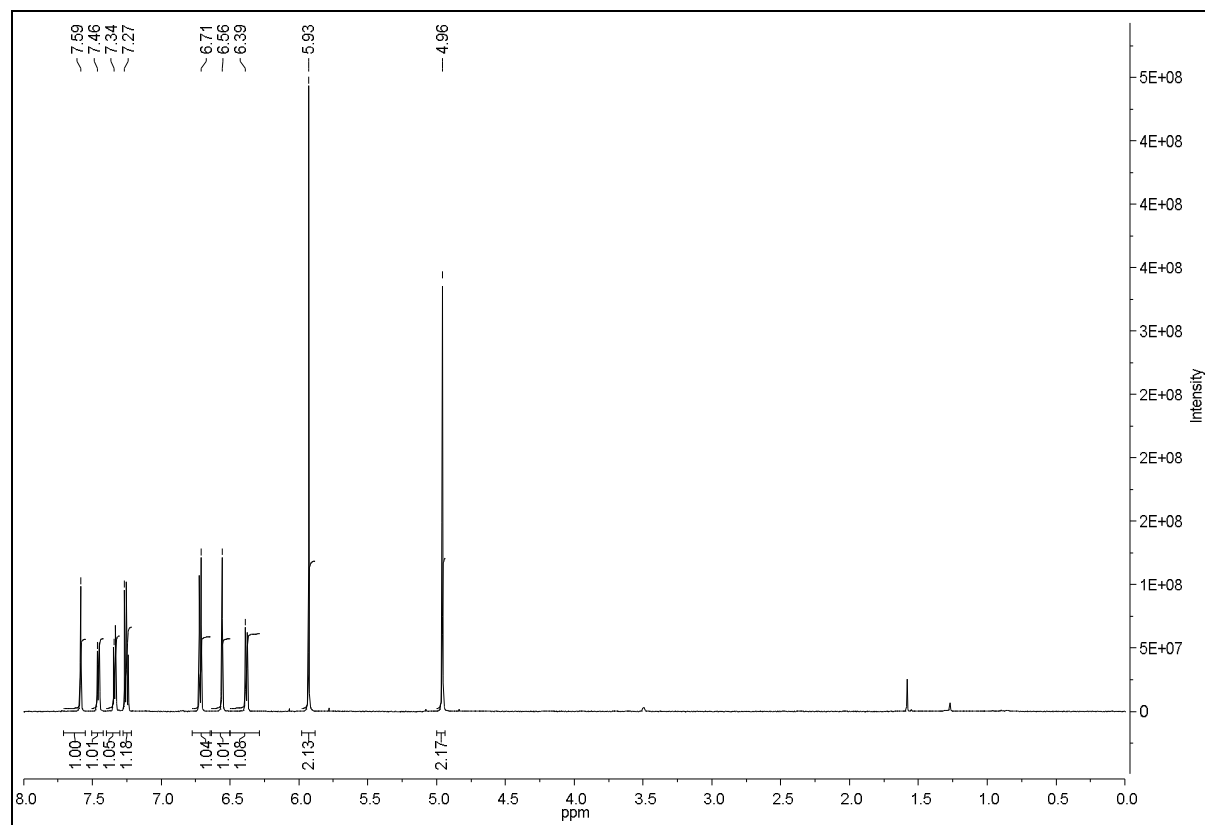


^{13}C NMR DEPT 135°

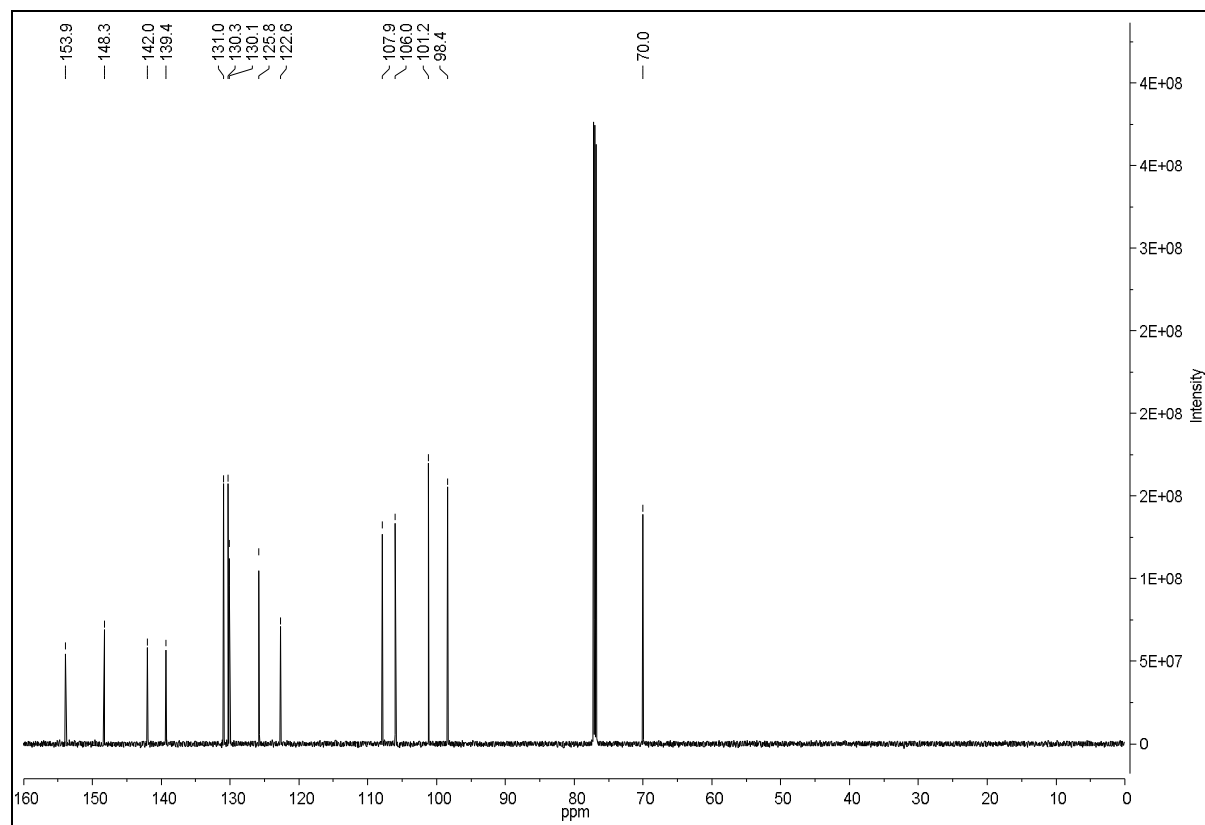


4c: 5-[(3-Bromophenyl)methoxy]-2H-1,3-benzodioxole

¹H

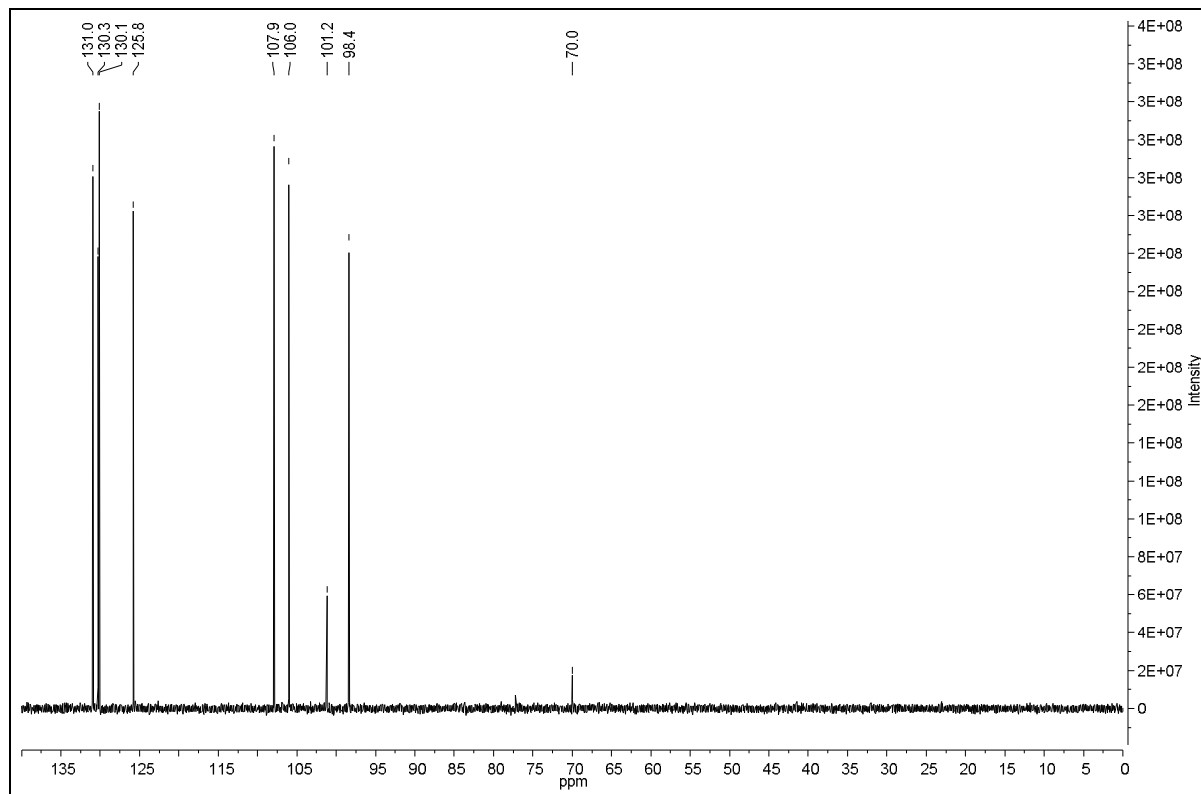


¹³C

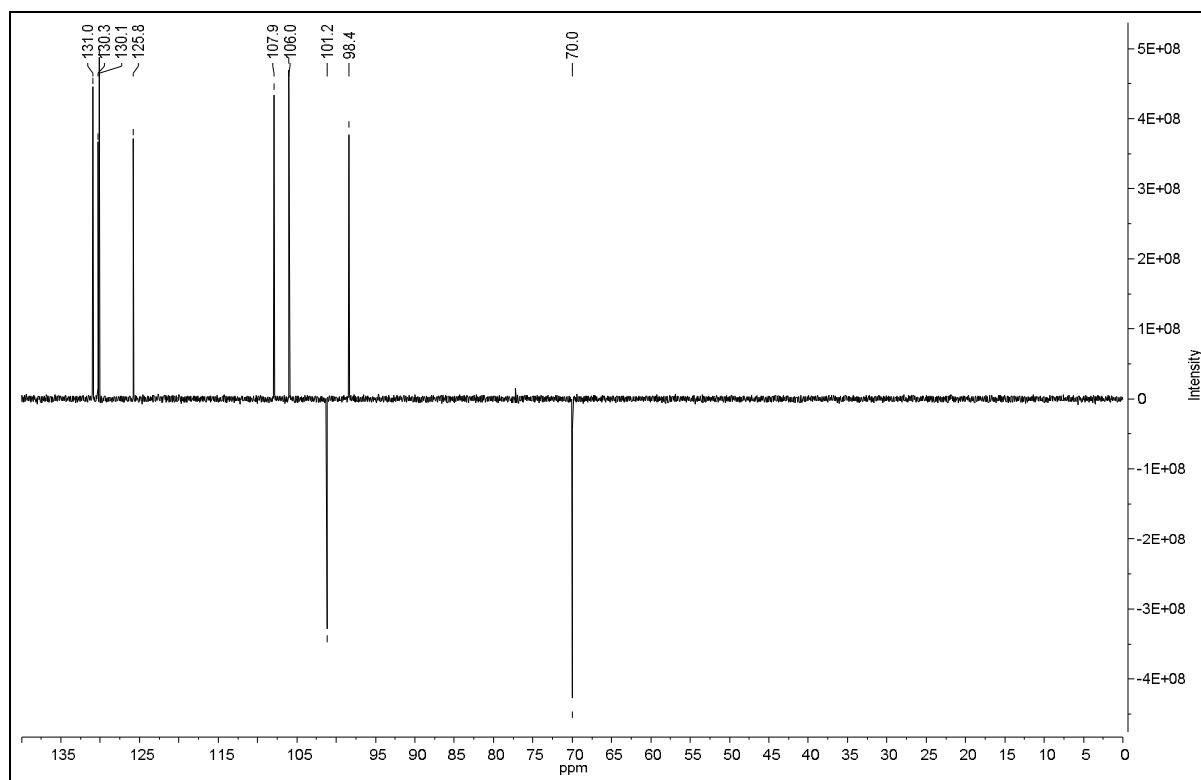


4c: 5-[(3-Bromophenyl)methoxy]-2H-1,3-benzodioxole

^{13}C NMR DEPT 90°

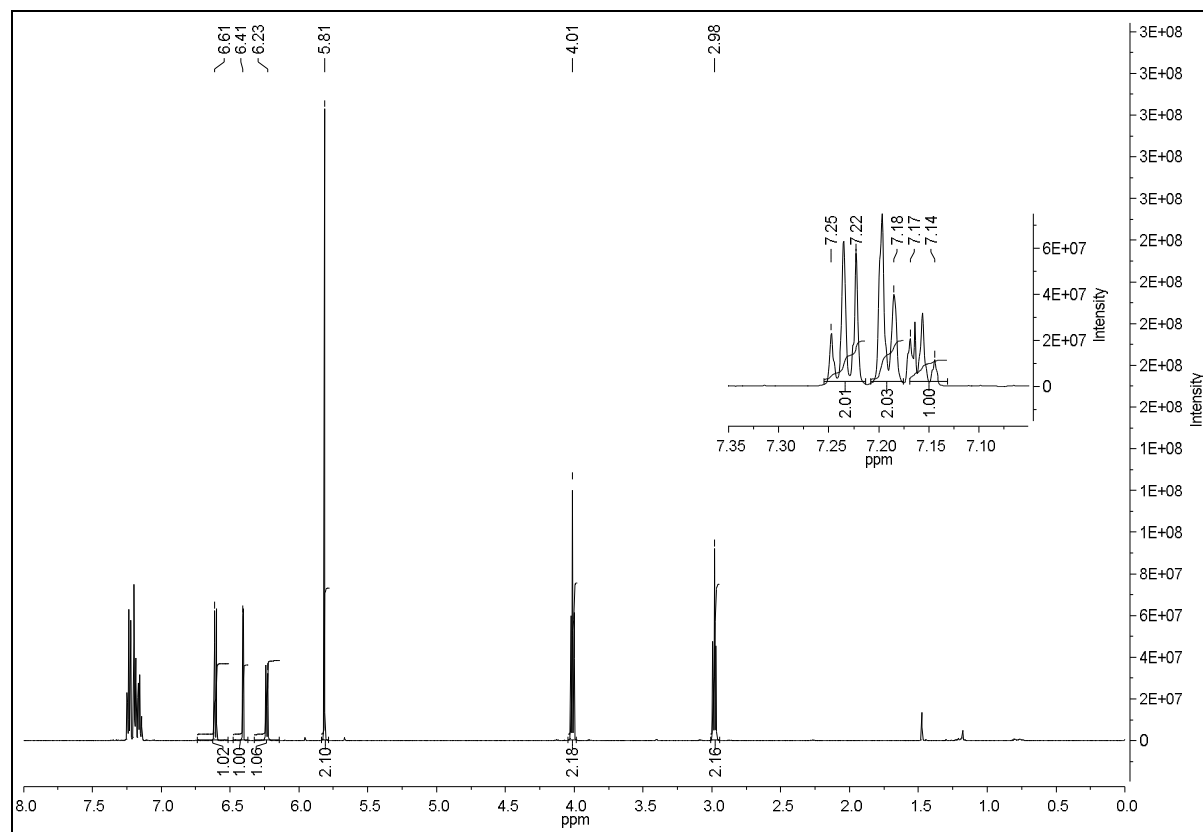


^{13}C NMR DEPT 135°

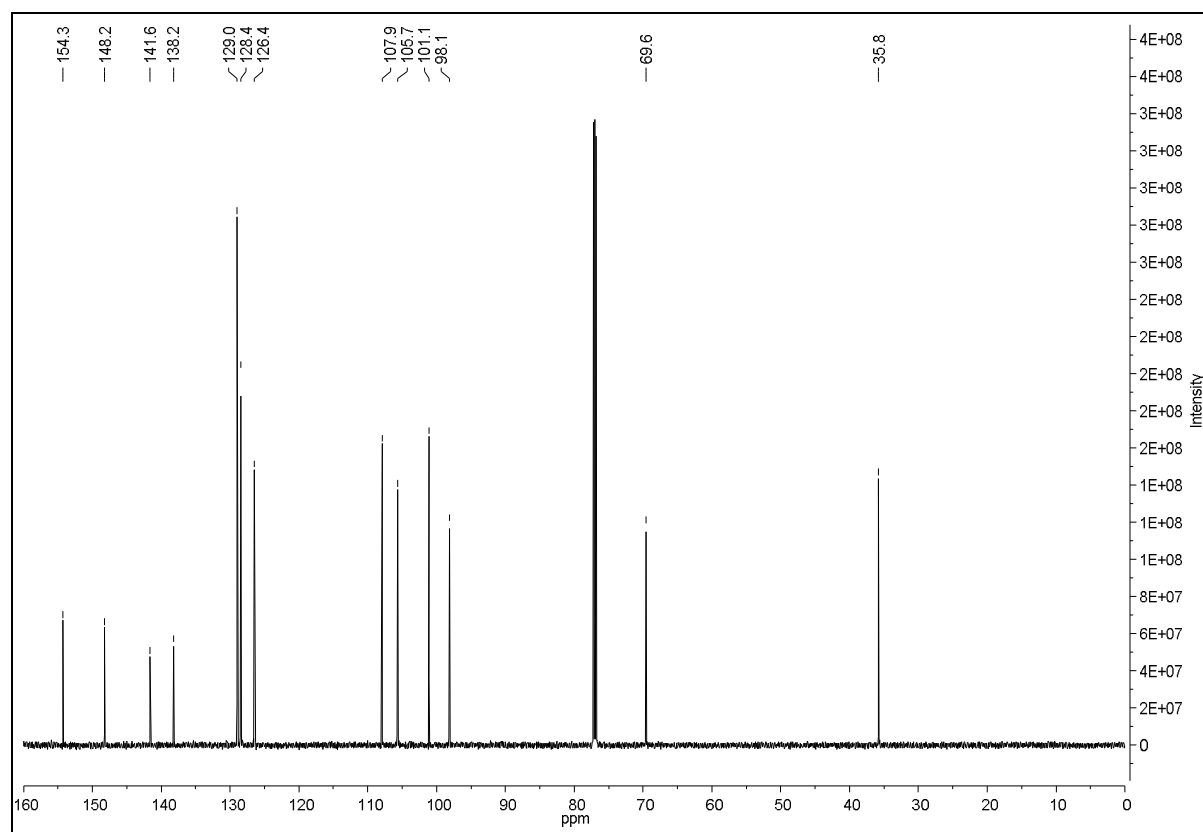


4d: 5-(2-Phenylethoxy)-2H-1,3-benzodioxole

¹H

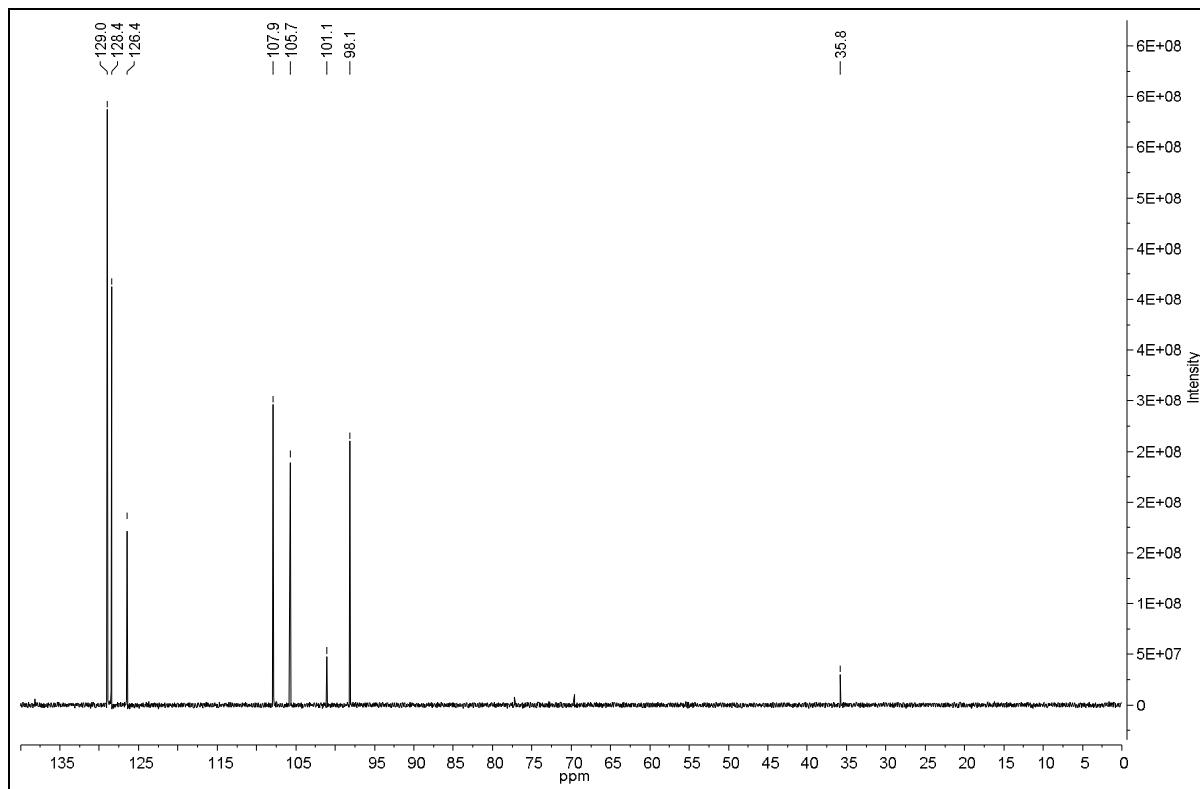


¹³C

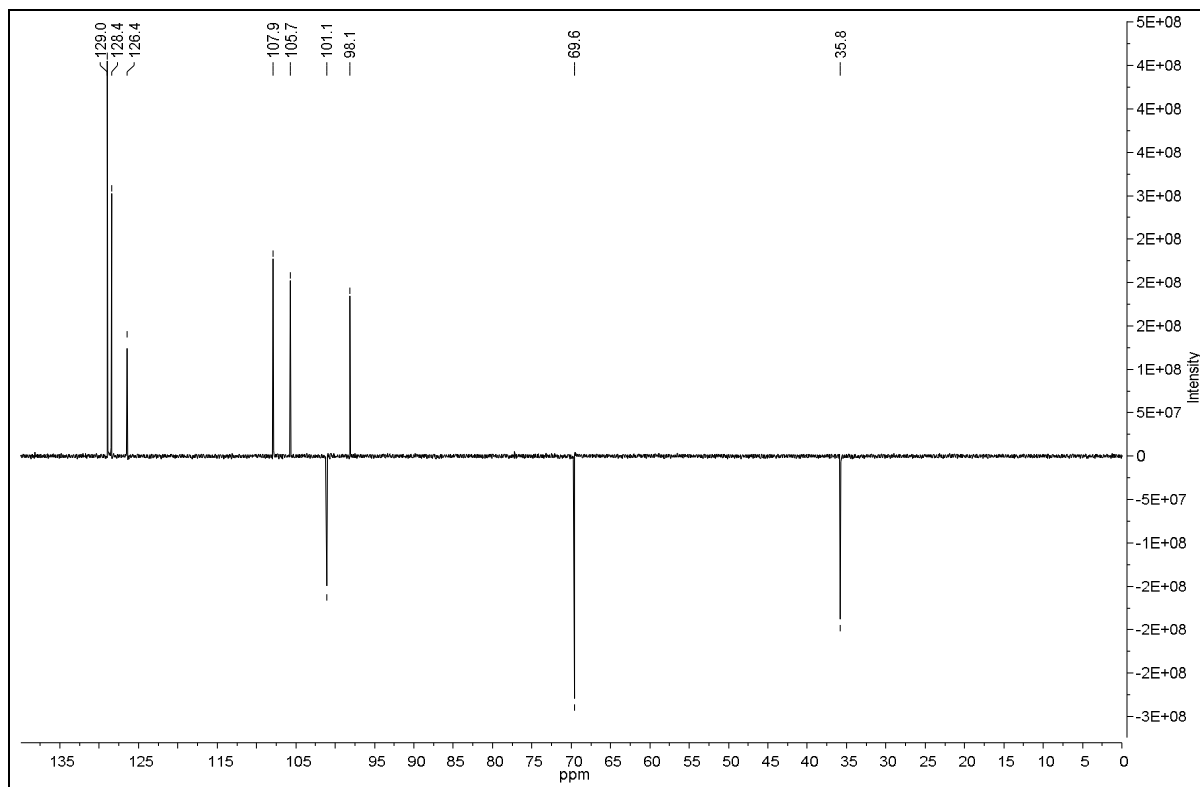


4d: 5-(2-Phenylethoxy)-2H-1,3-benzodioxole

^{13}C NMR DEPT 90°

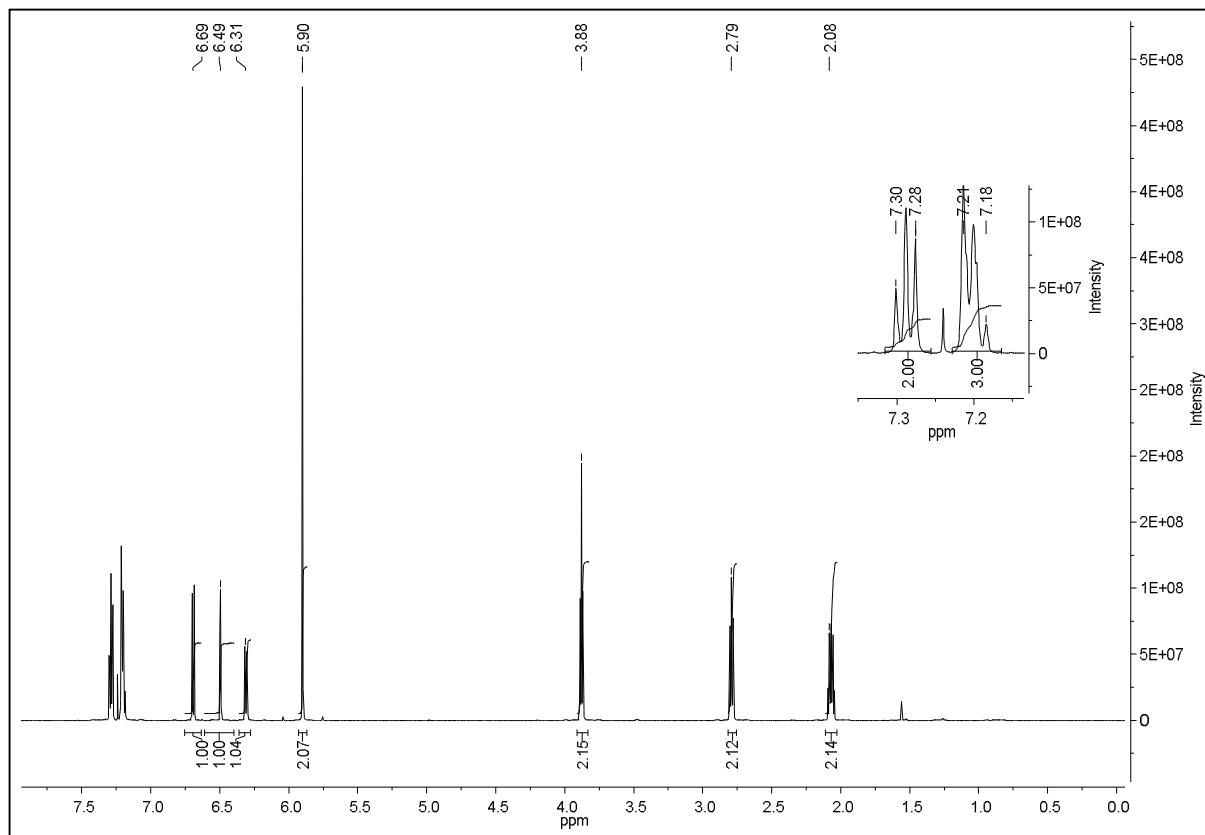


^{13}C NMR DEPT 135°

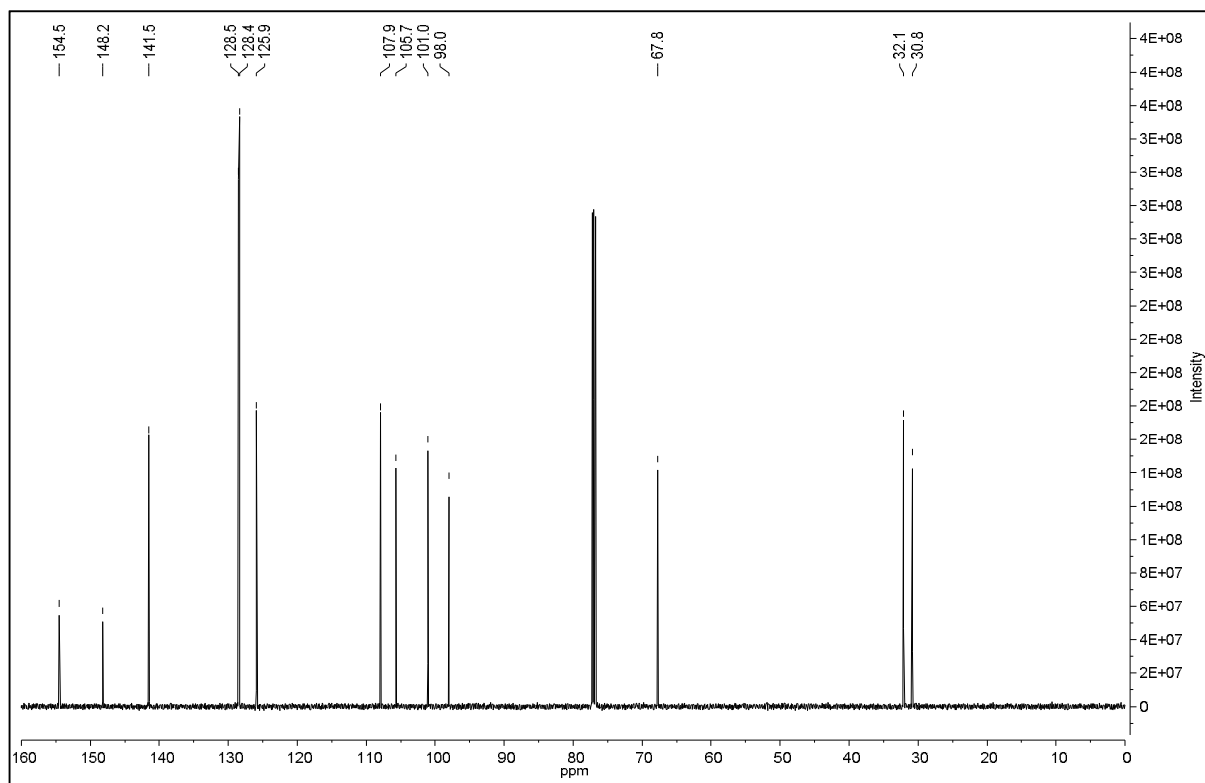


4e: 5-(3-Phenylpropoxy)-2H-1,3-benzodioxole

¹H

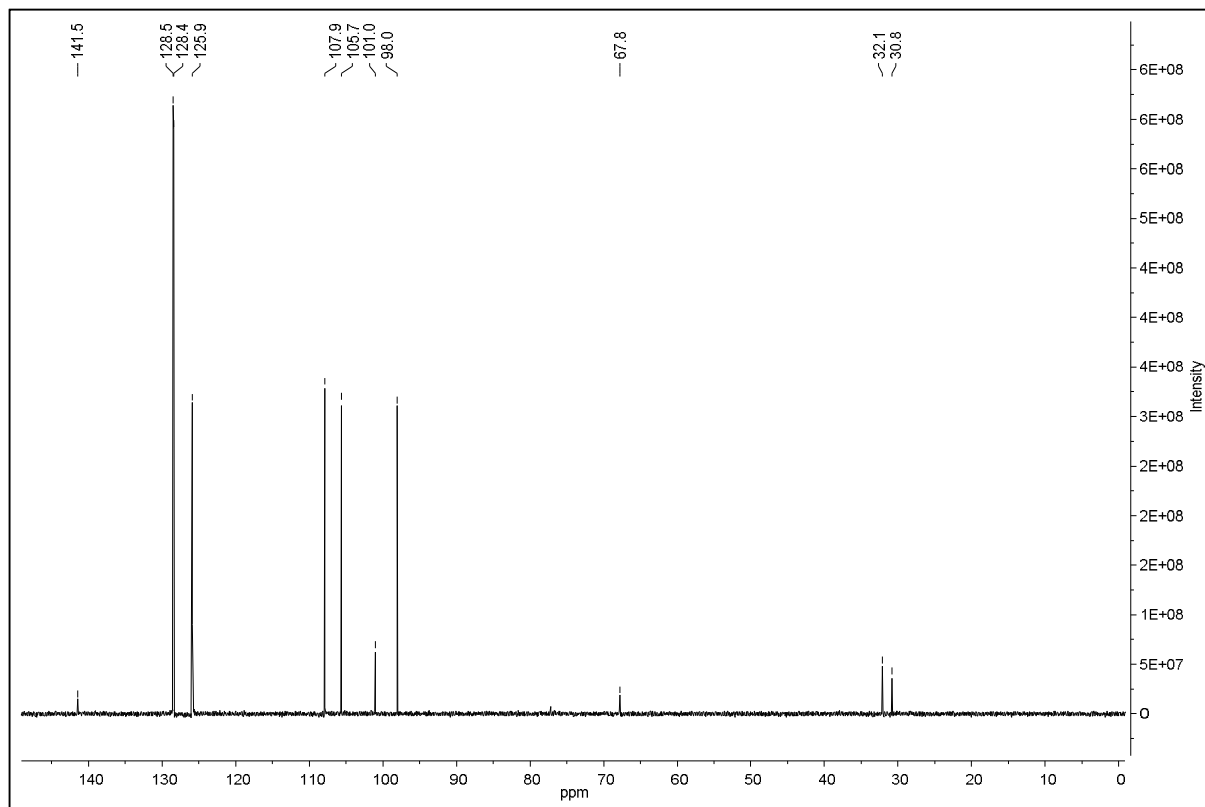


¹³C

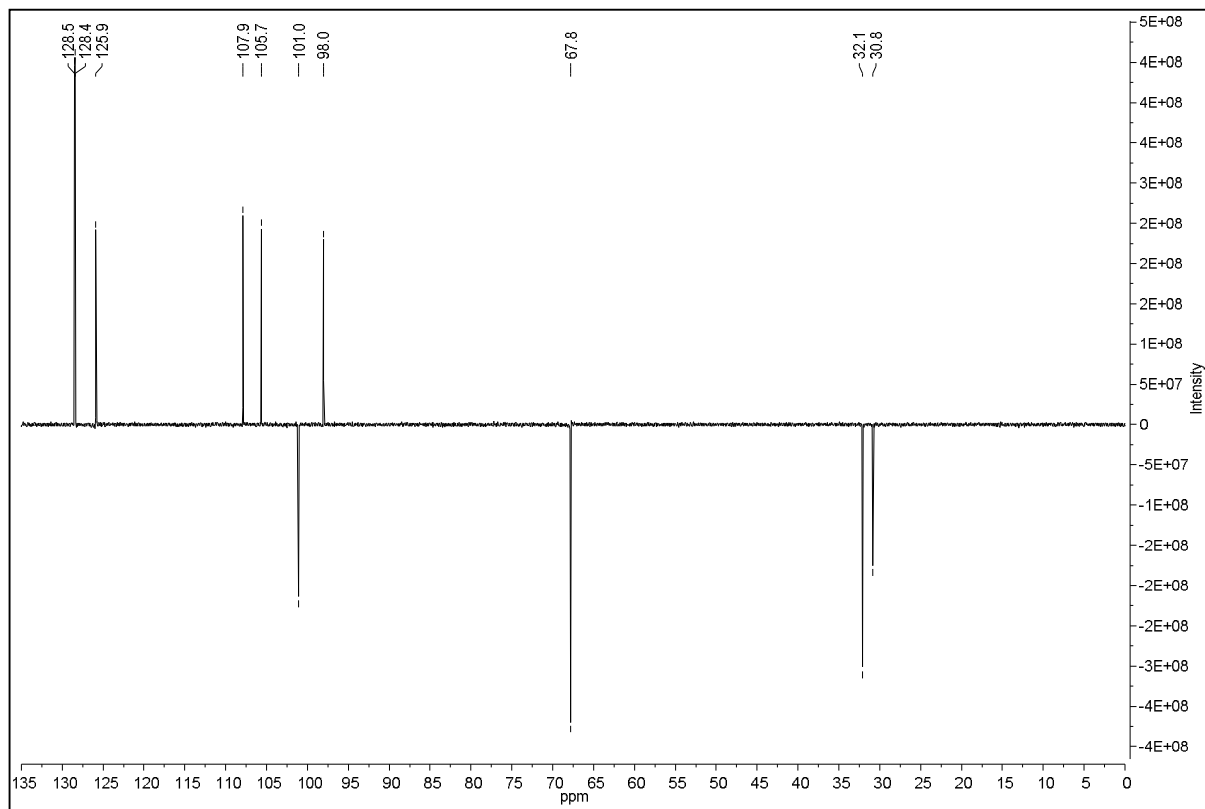


4e: 5-(3-Phenylpropoxy)-2H-1,3-benzodioxole

¹³C NMR DEPT 90°

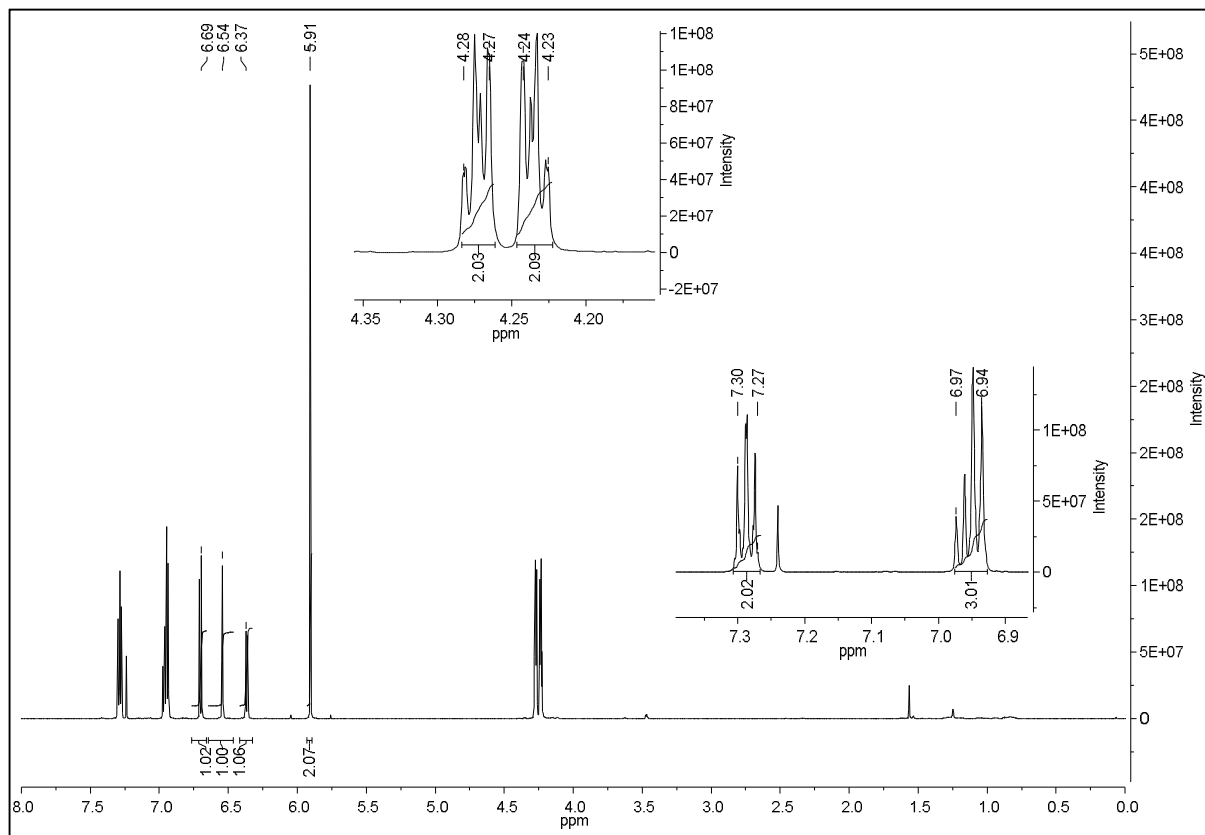


¹³C NMR DEPT 135°

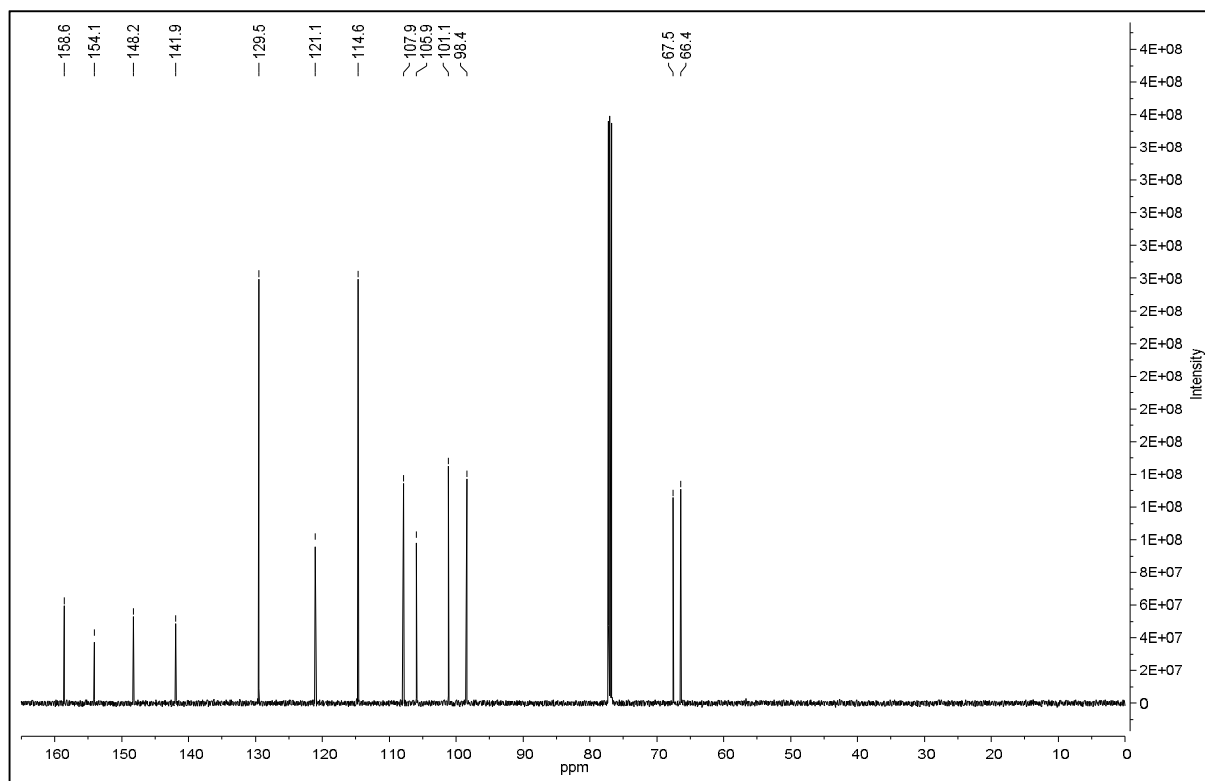


4f: 5-(2-Phenoxyethoxy)-2H-1,3-benzodioxole

¹H

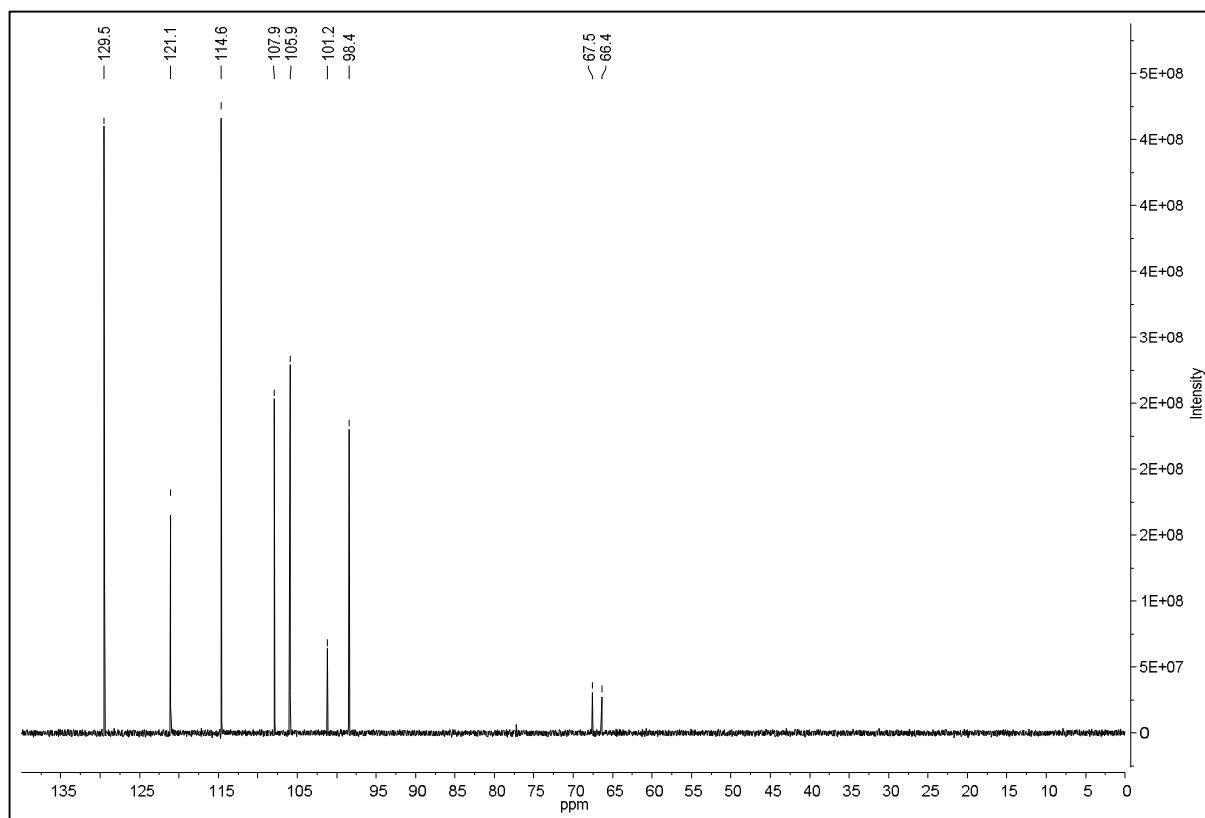


¹³C

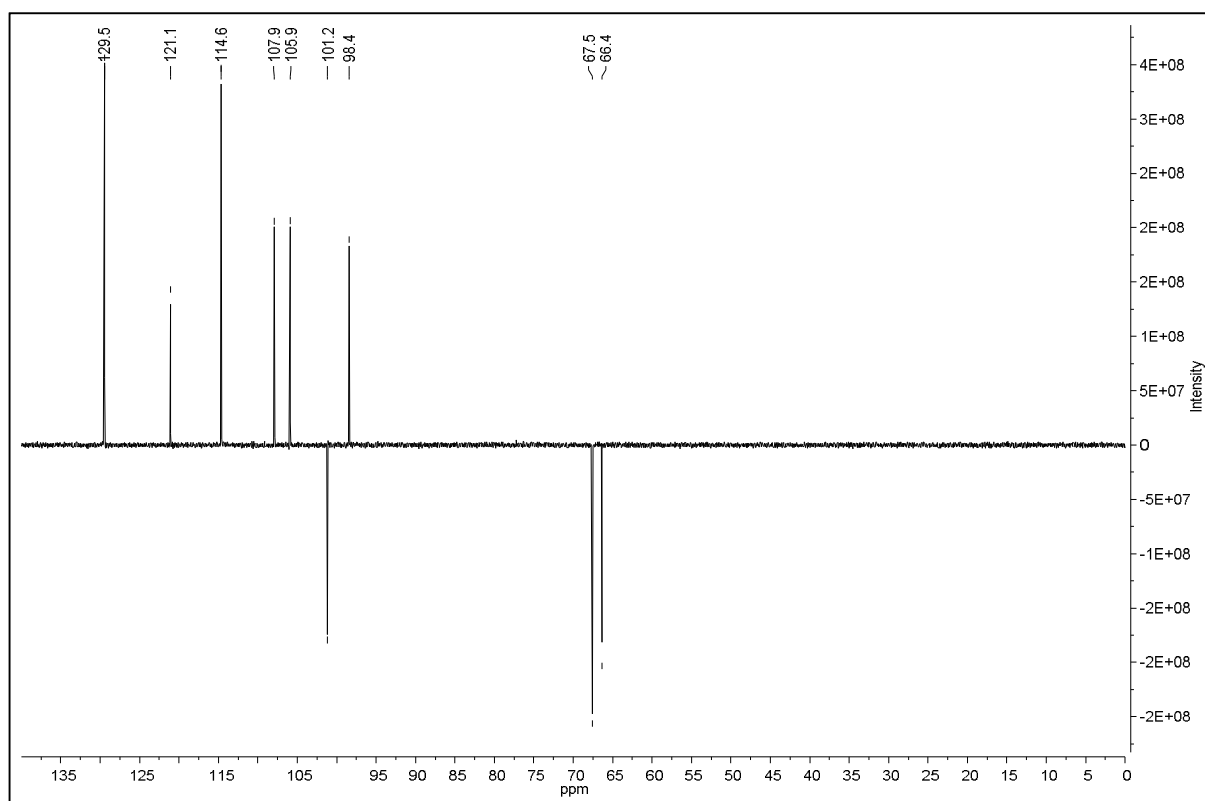


4f: 5-(2-Phenoxyethoxy)-2H-1,3-benzodioxole

^{13}C NMR DEPT 90°

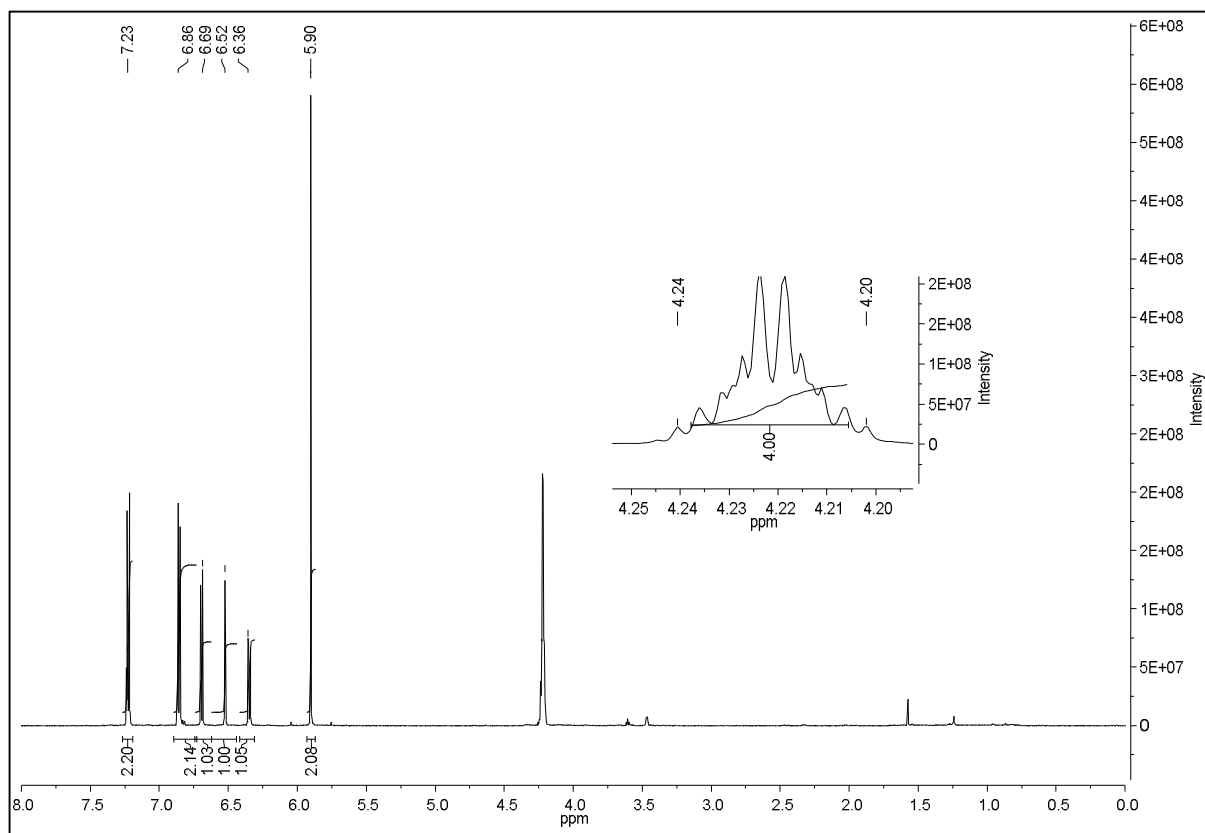


^{13}C NMR DEPT 135°

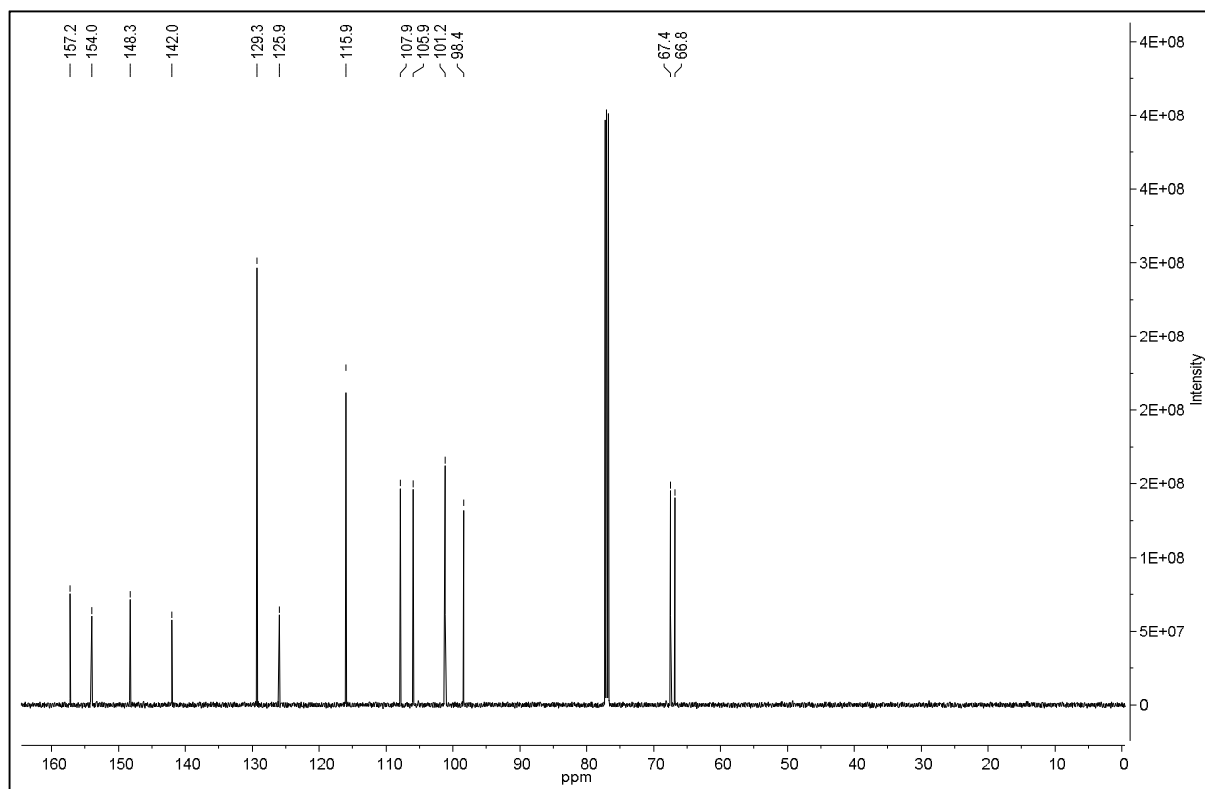


4g: 5-[2-(4-Chlorophenoxy)ethoxy]-2H-1,3-benzodioxole

¹H

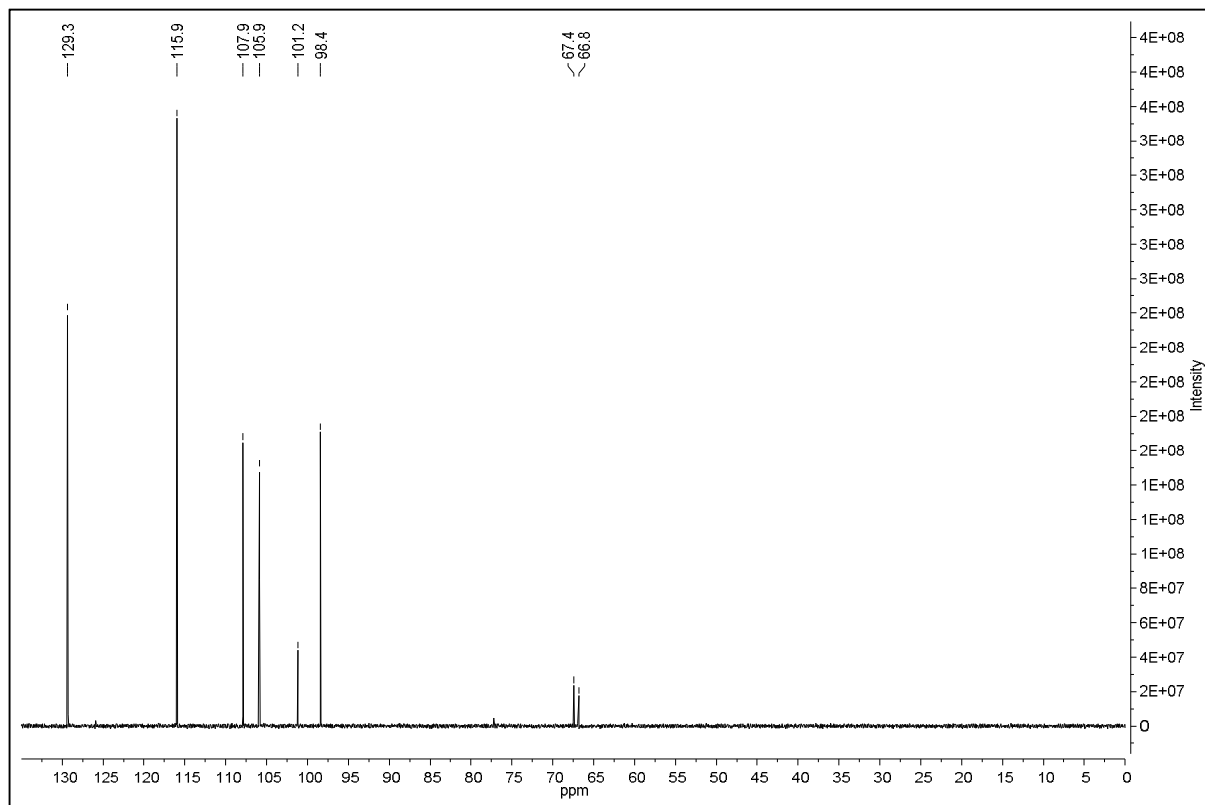


¹³C

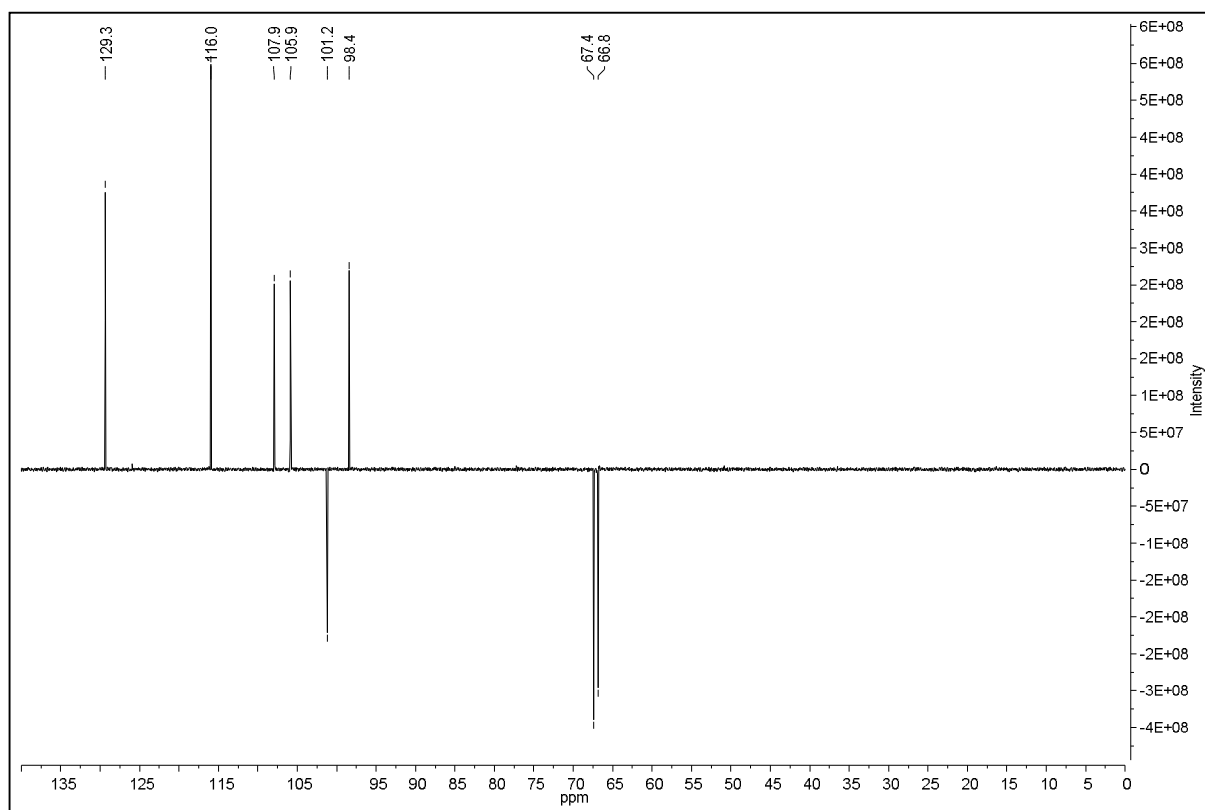


4g: 5-[2-(4-Chlorophenoxy)ethoxy]-2H-1,3-benzodioxole

^{13}C NMR DEPT 90°

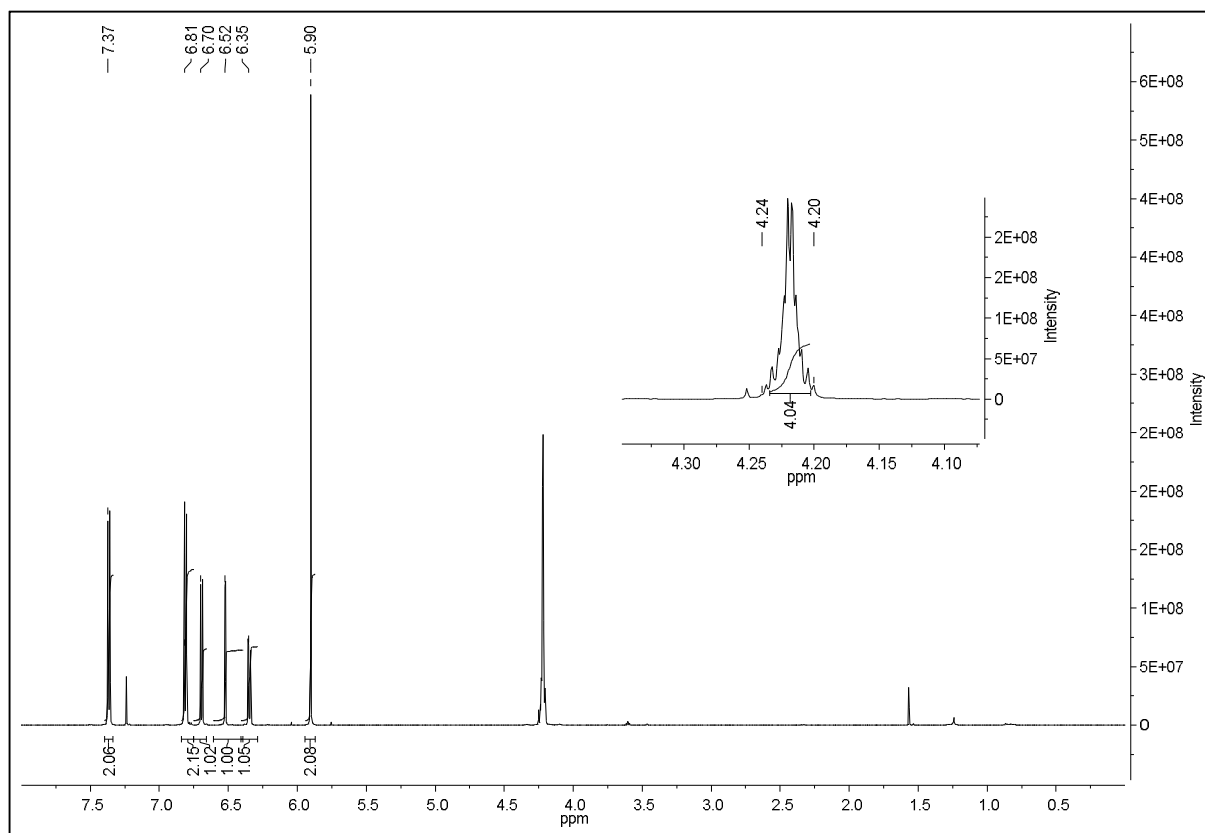


^{13}C NMR DEPT 135°

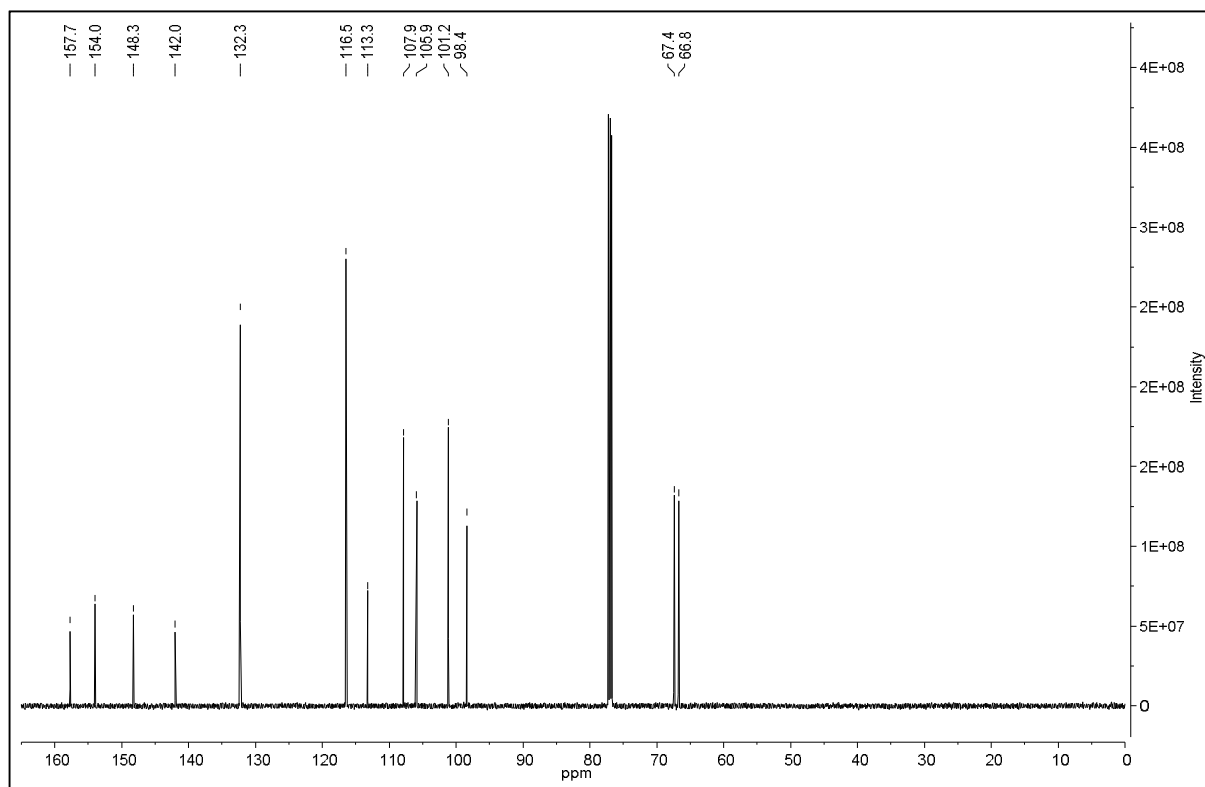


4h: 5-[2-(4-Bromophenoxy)ethoxy]-2H-1,3-benzodioxole

¹H

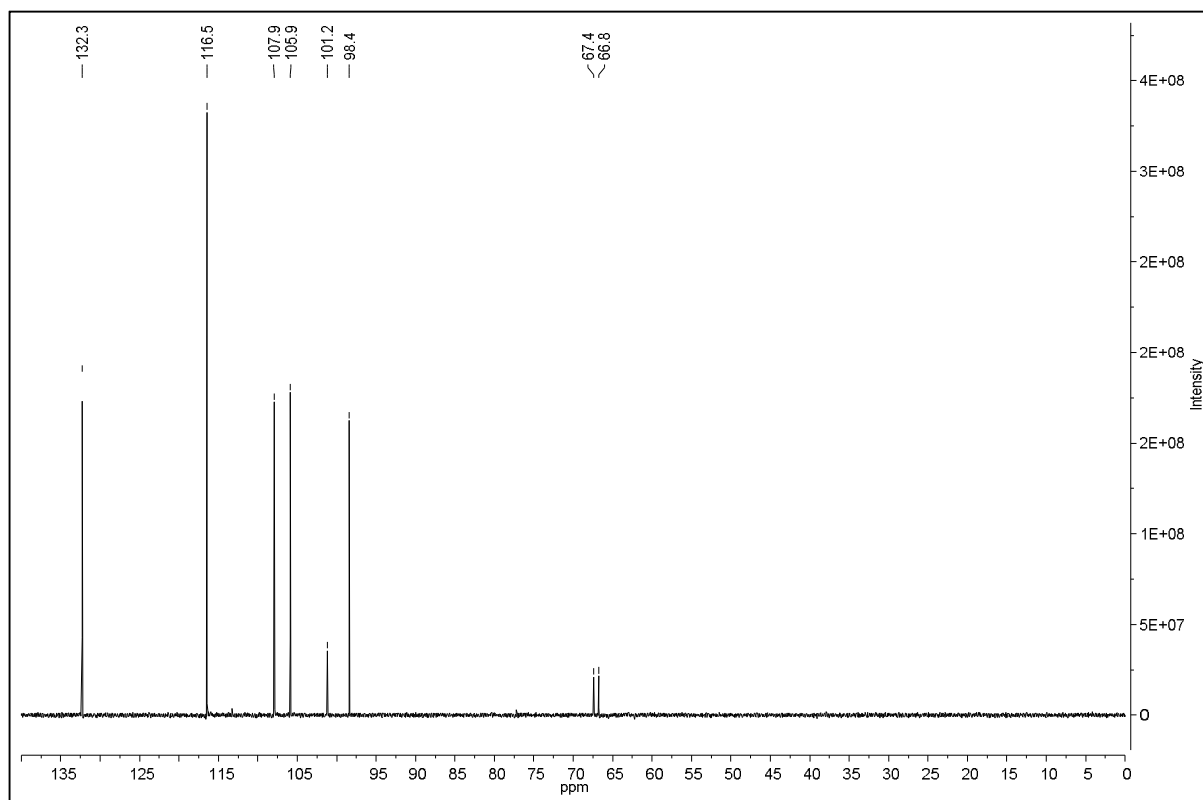


¹³C

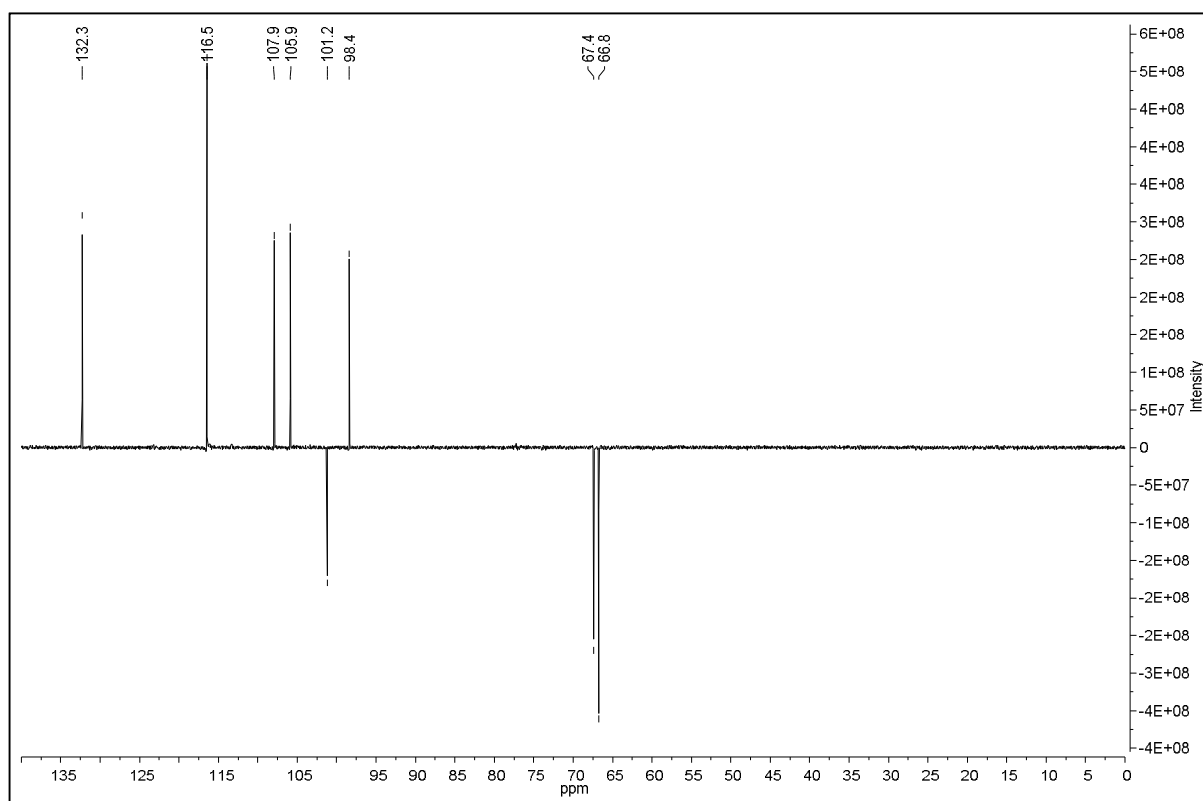


4h: 5-[2-(4-Bromophenoxy)ethoxy]-2H-1,3-benzodioxole

^{13}C NMR DEPT 90°

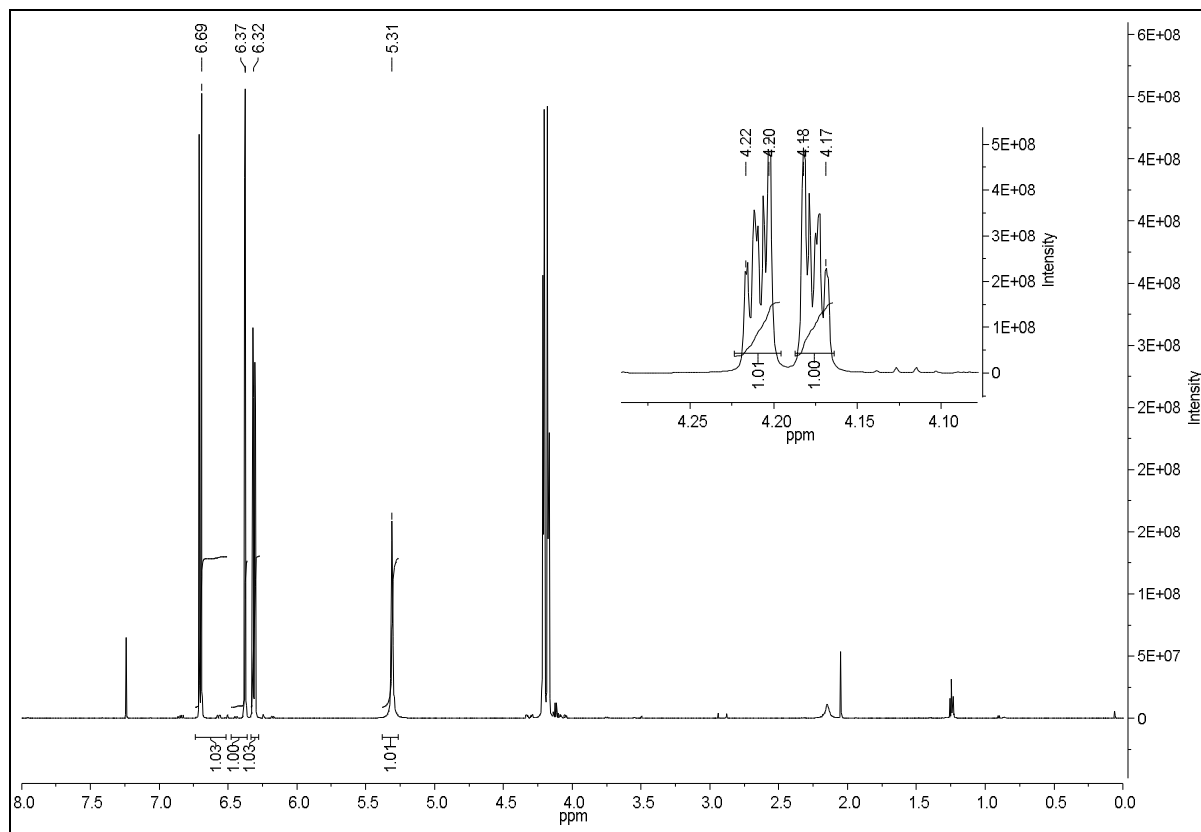


^{13}C NMR DEPT 135°

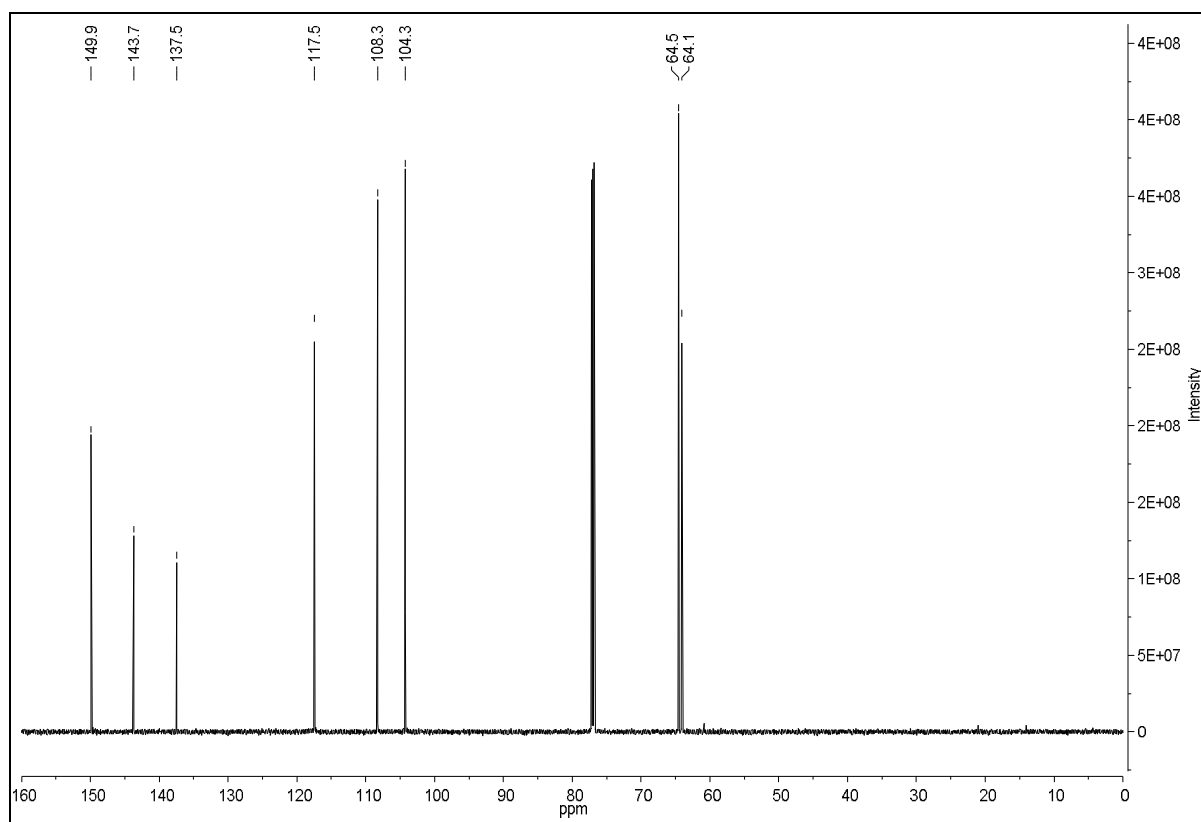


7: 6-Hydroxy-1,4-benzodioxane

^1H

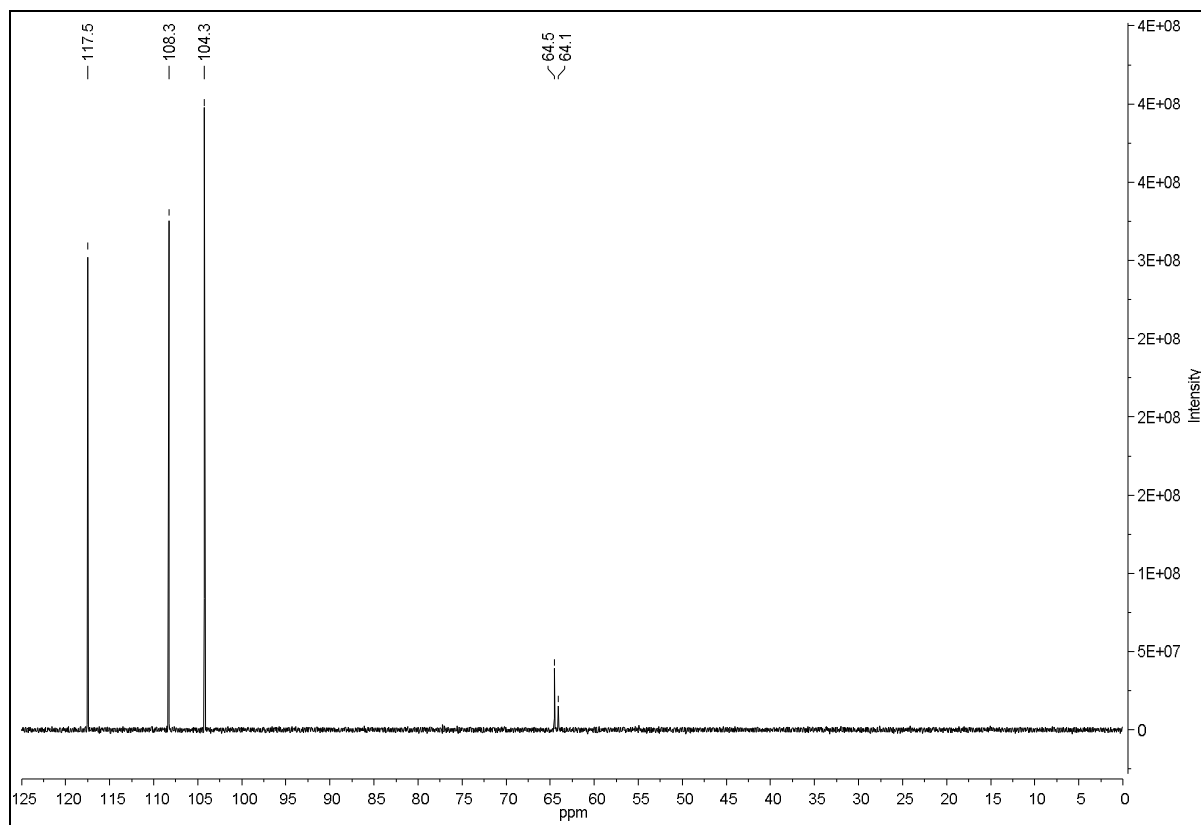


^{13}C

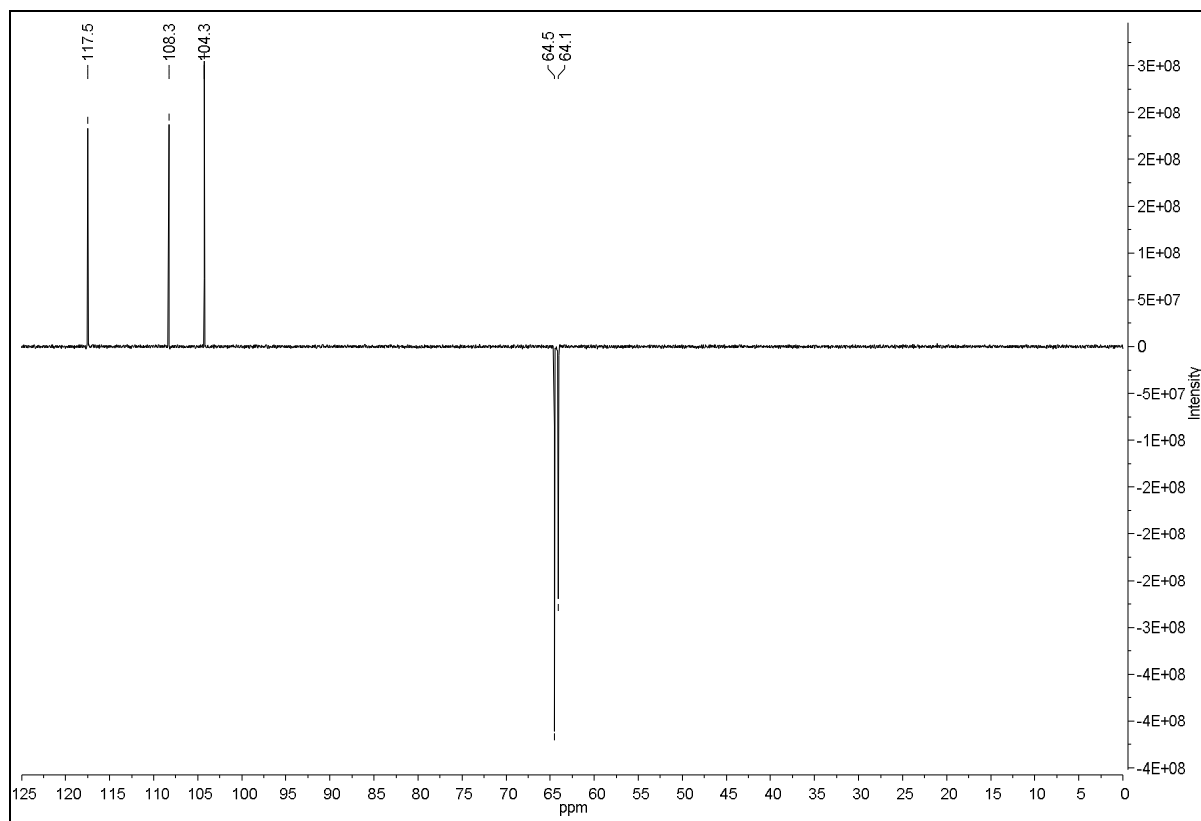


7: 6-Hydroxy-1,4-benzodioxane

^{13}C NMR DEPT 90°

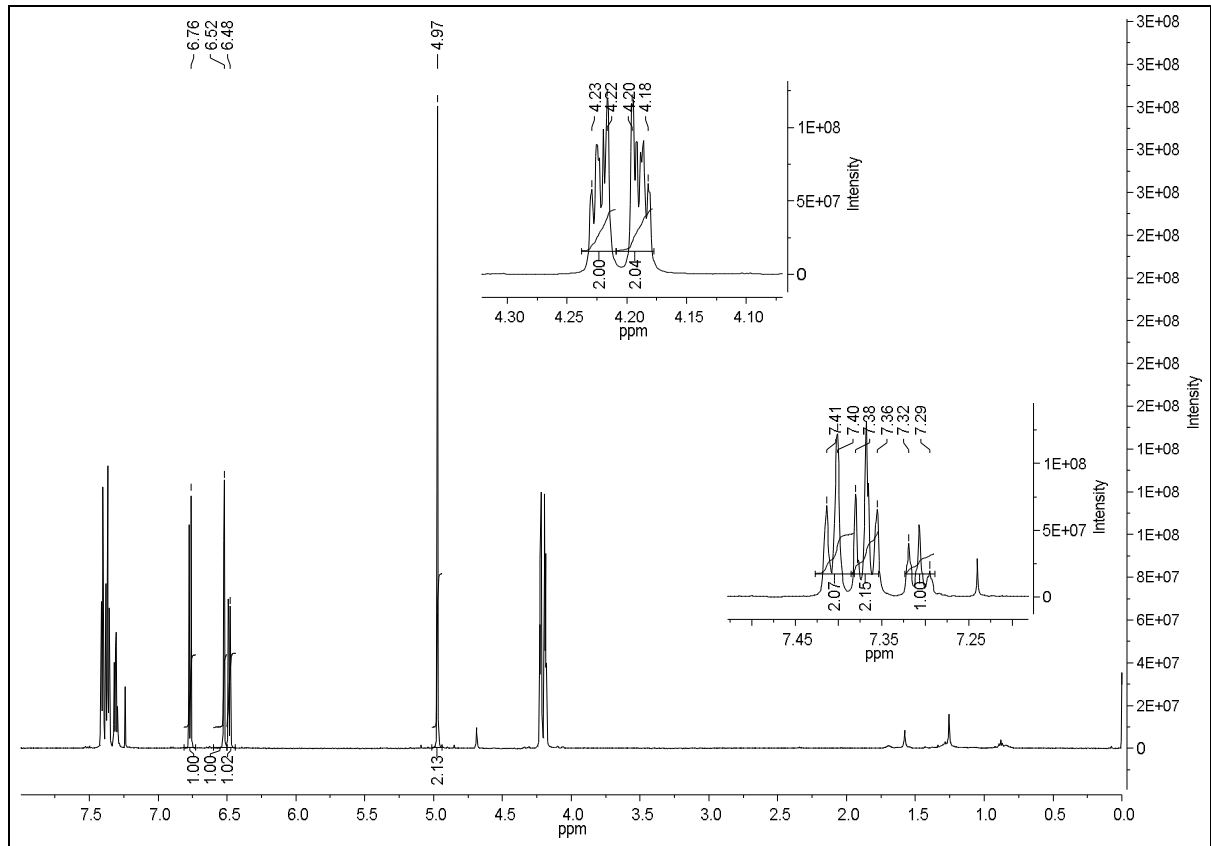


^{13}C NMR DEPT 135°

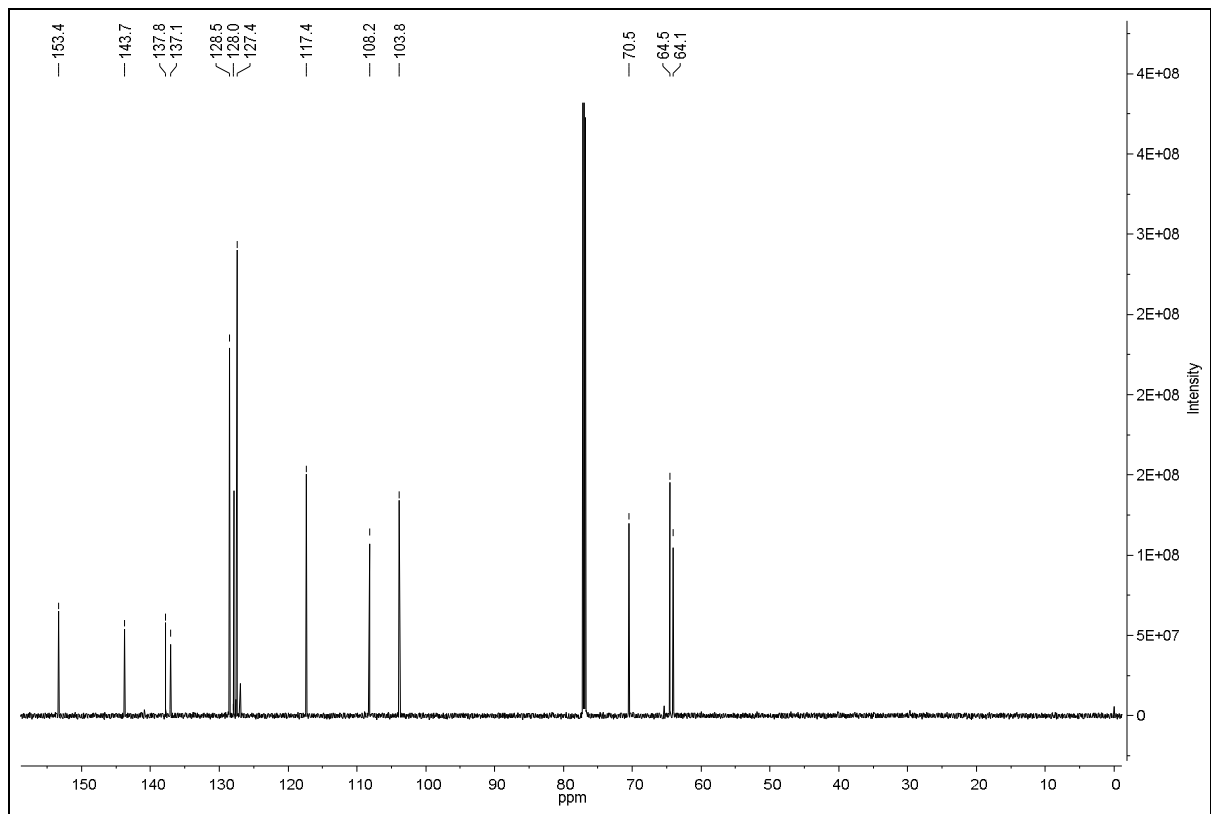


5a: 6-(Benzyloxy)-2,3-dihydro-1,4-benzodioxine

¹H

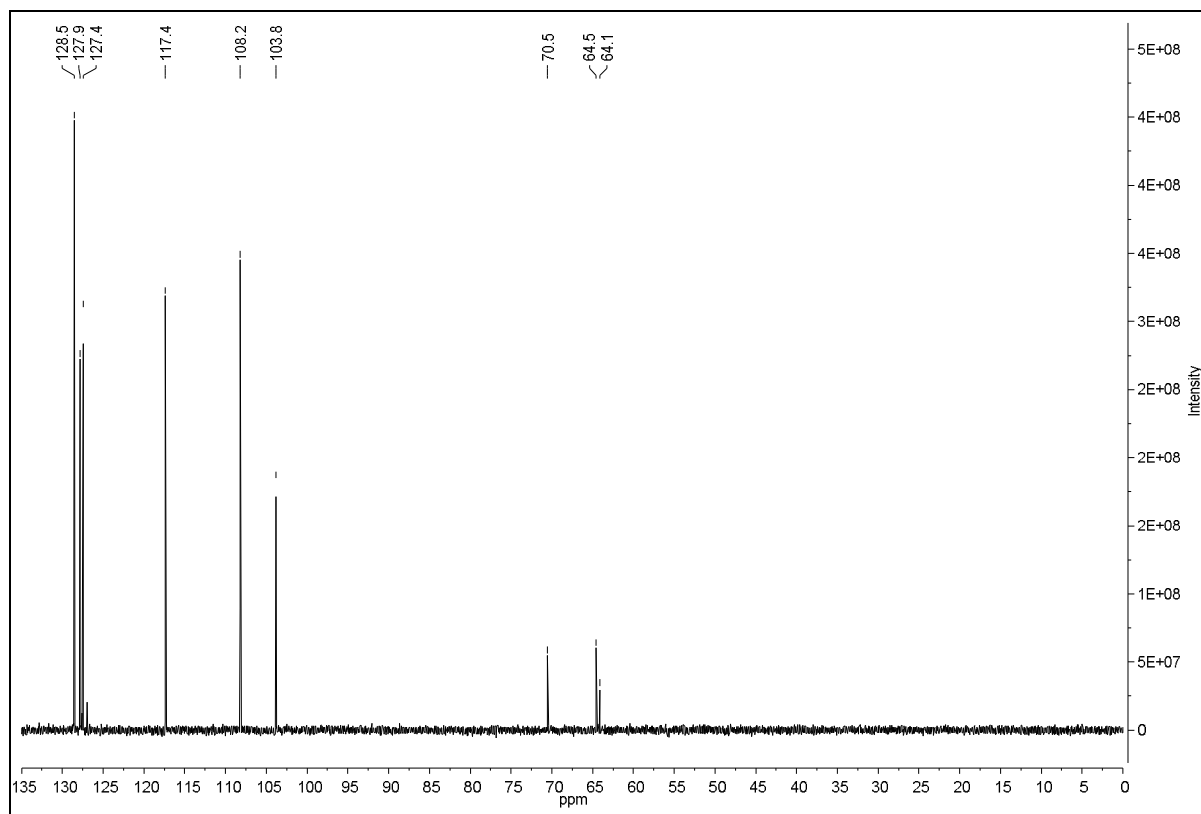


¹³C

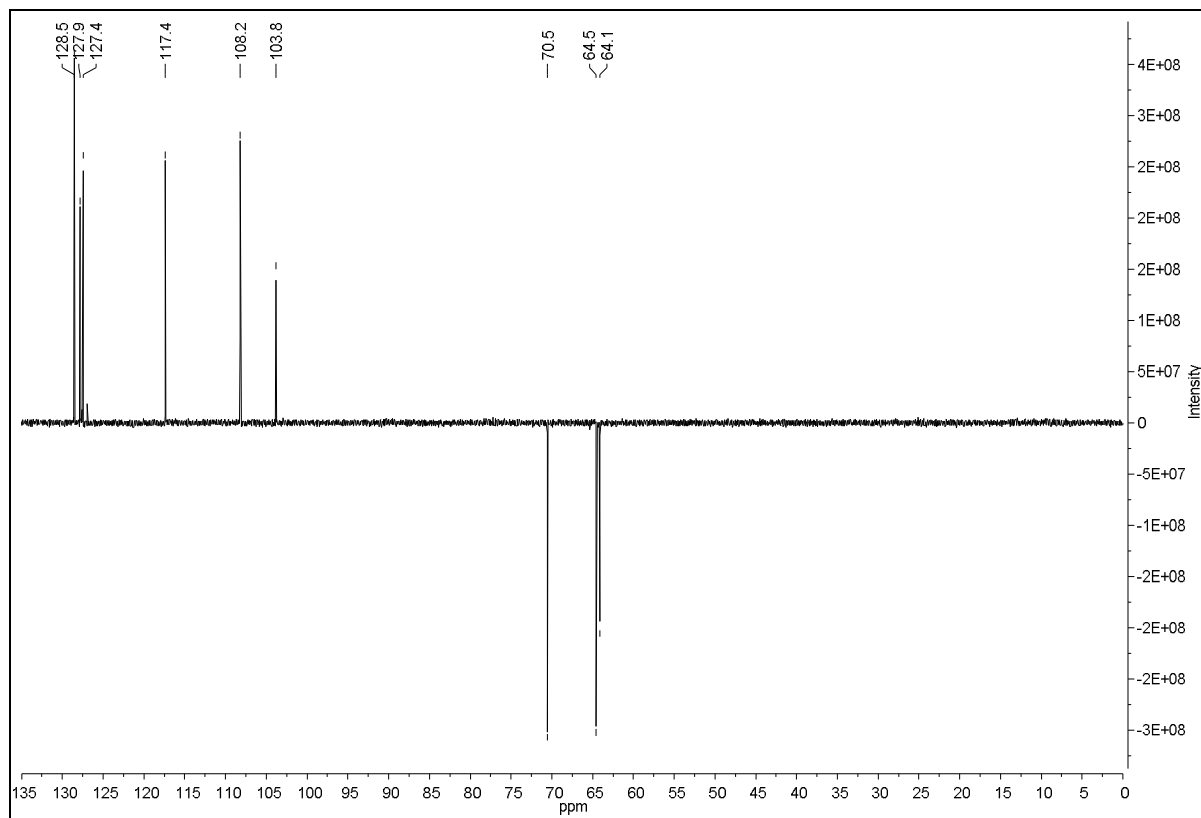


5a: 6-(Benzyloxy)-2,3-dihydro-1,4-benzodioxine

^{13}C NMR DEPT 90°

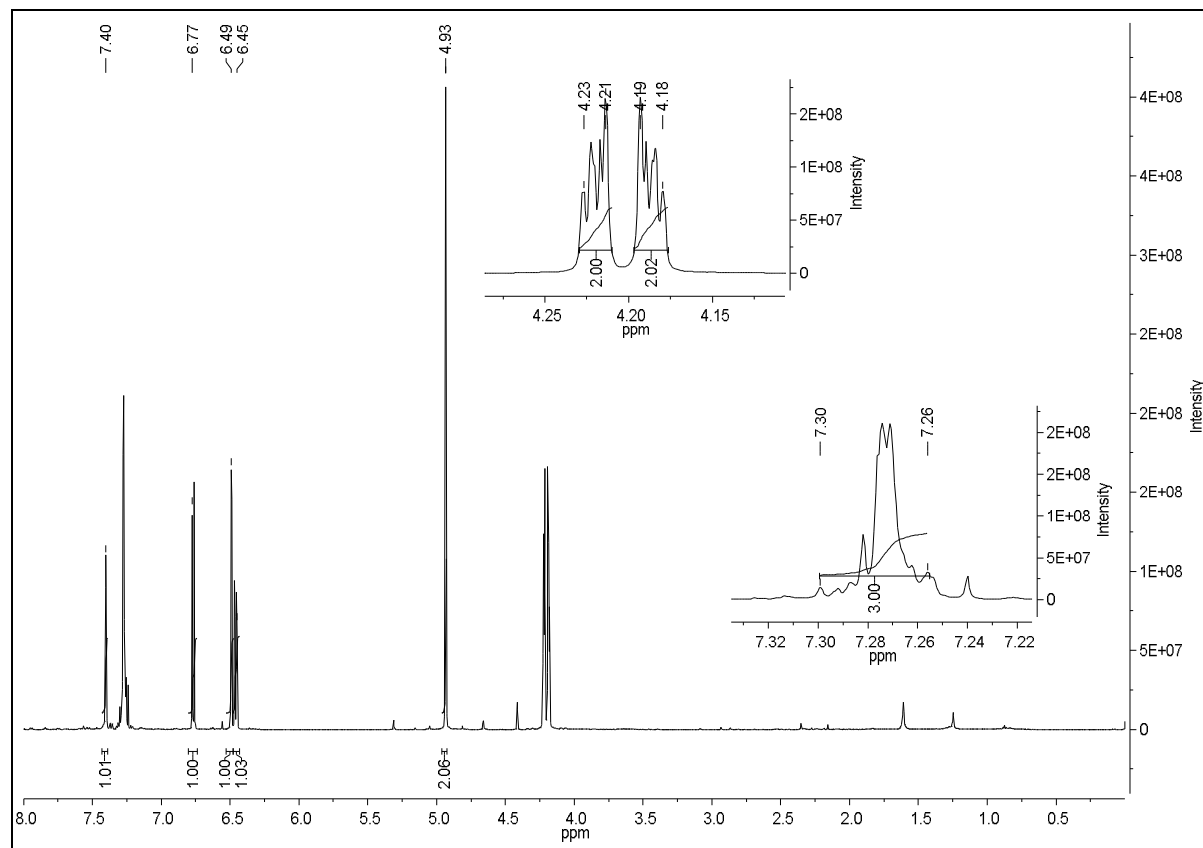


^{13}C NMR DEPT 135°

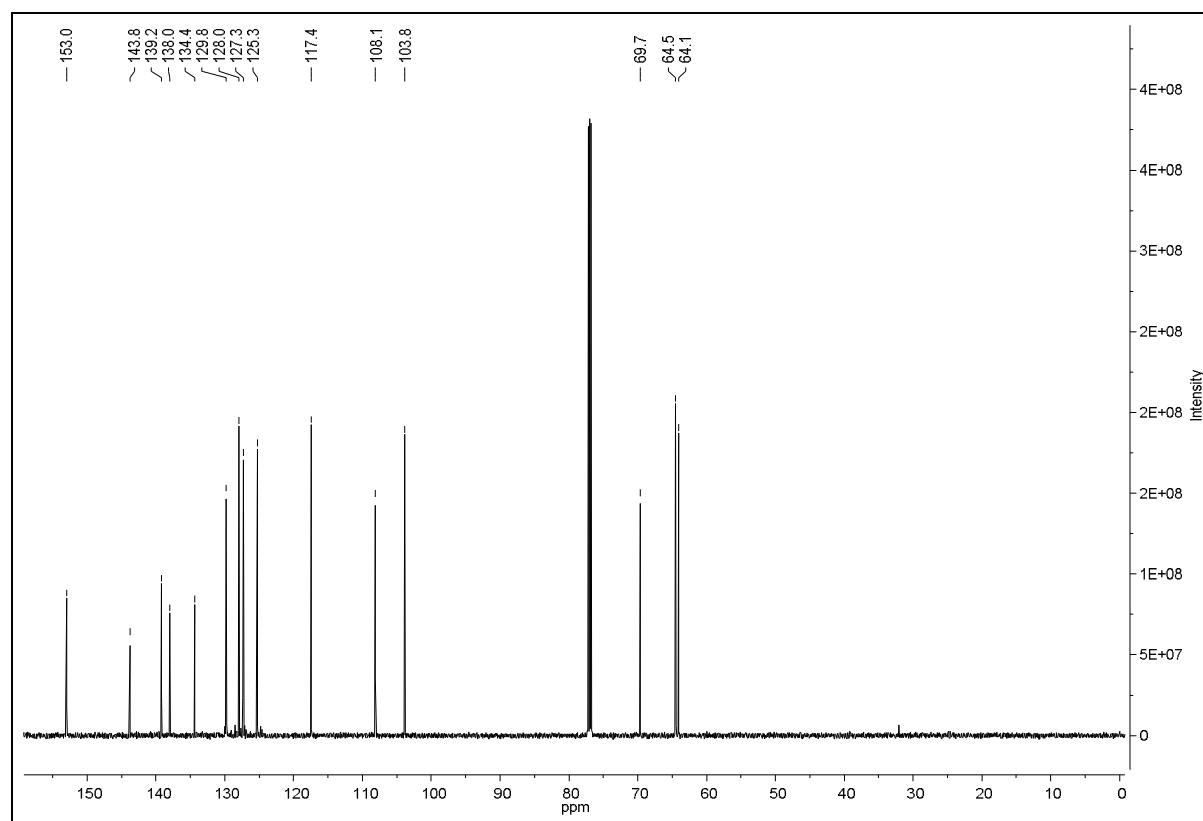


5b: 6-[(3-Chlorophenyl)methoxy]-2,3-dihydro-1,4-benzodioxine

¹H

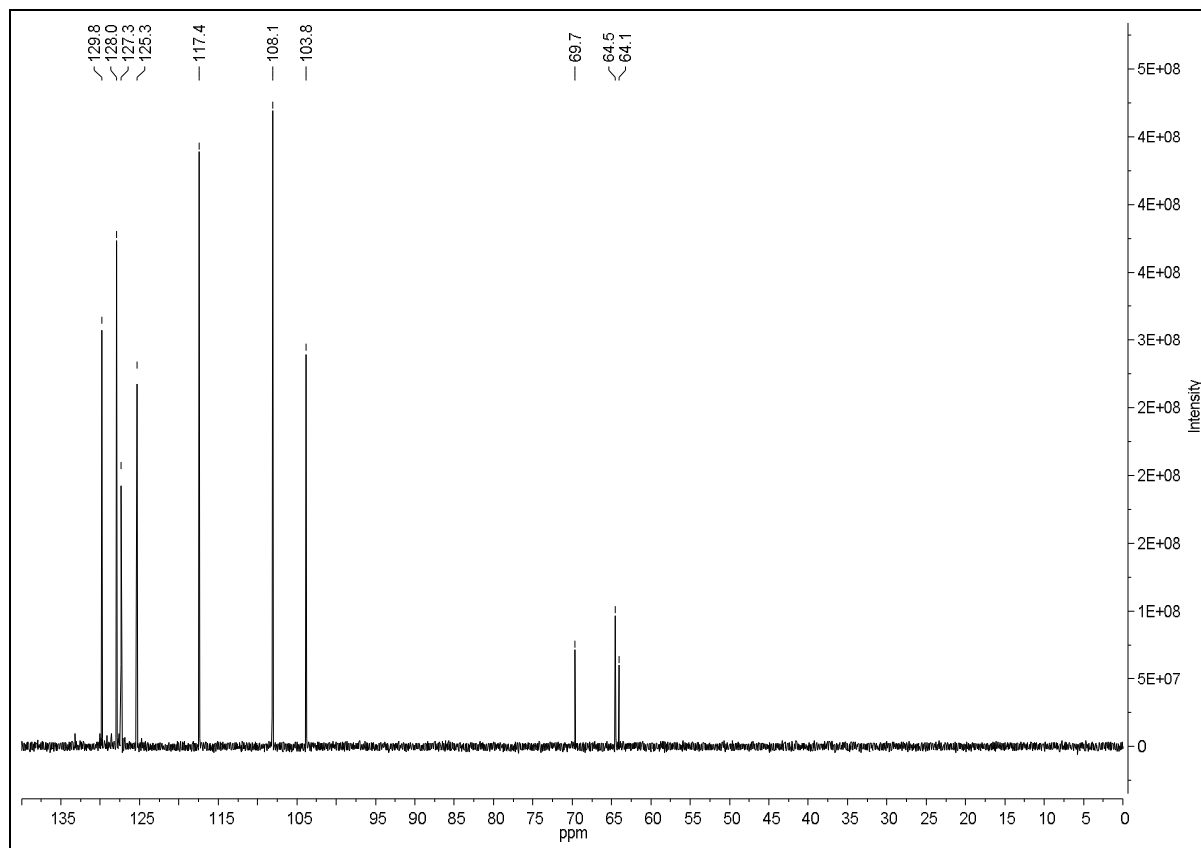


¹³C

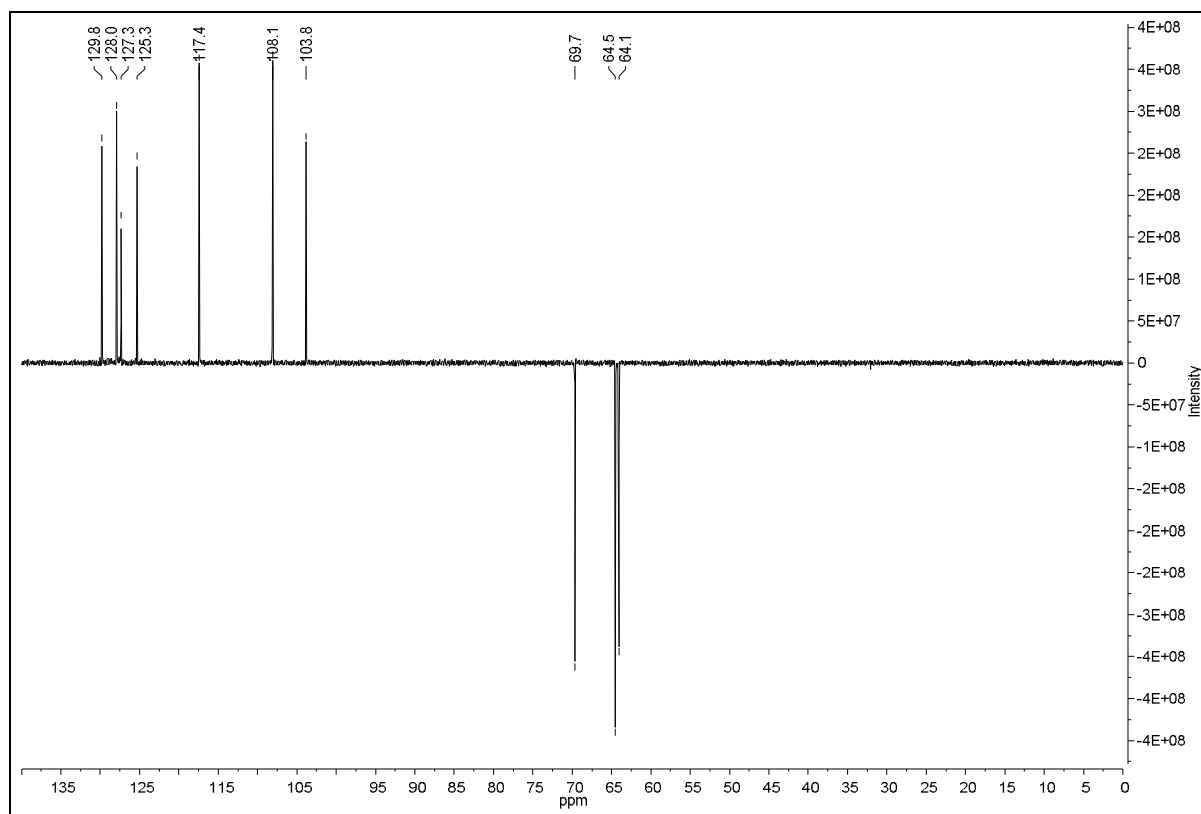


5b: 6-[(3-Chlorophenyl)methoxy]-2,3-dihydro-1,4-benzodioxine

^{13}C NMR DEPT 90°

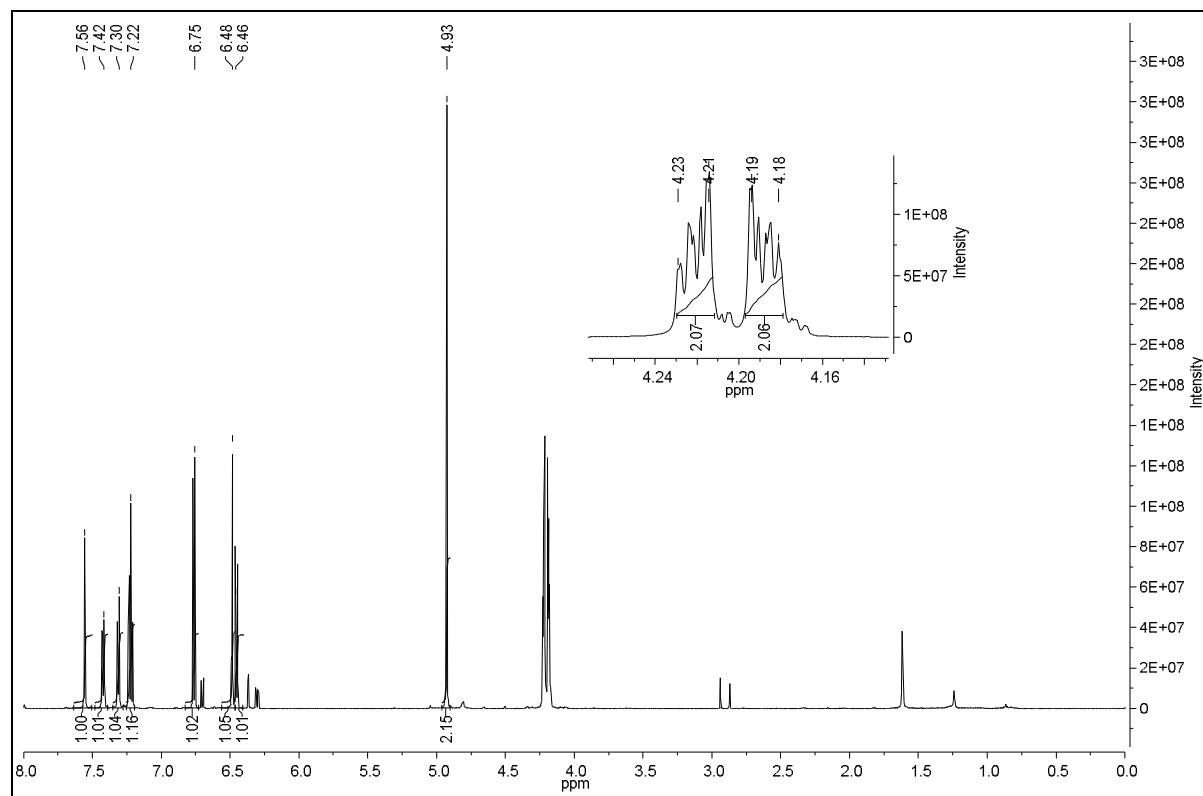


^{13}C NMR DEPT 135°

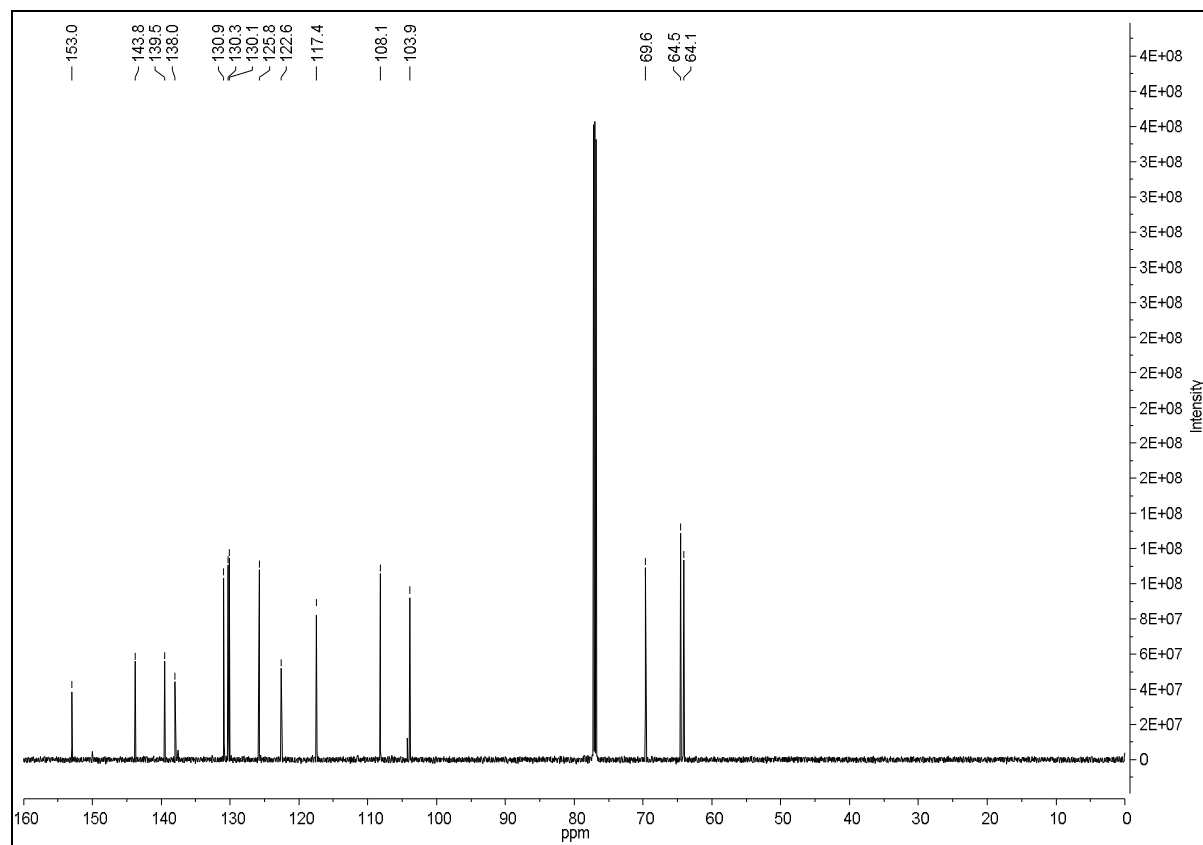


5c: 6-[(3-Bromophenyl)methoxy]-2,3-dihydro-1,4-benzodioxine

¹H

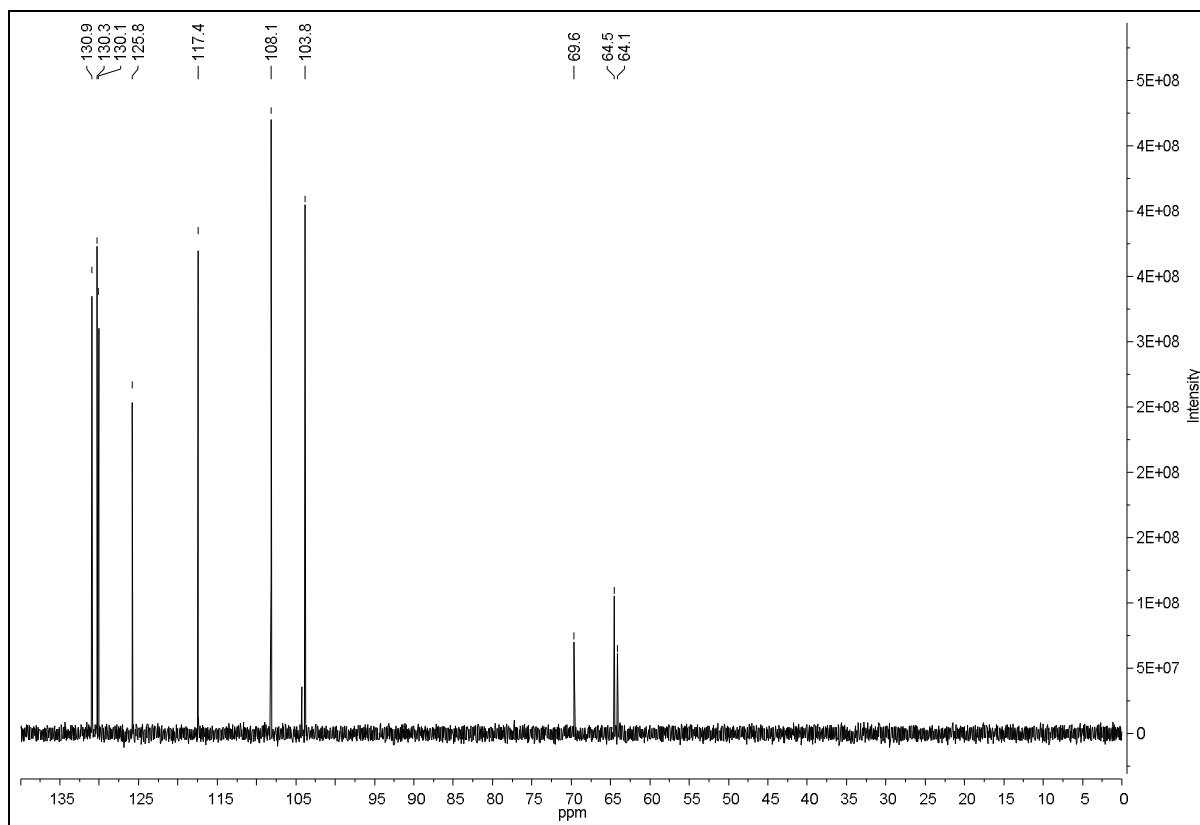


¹³C

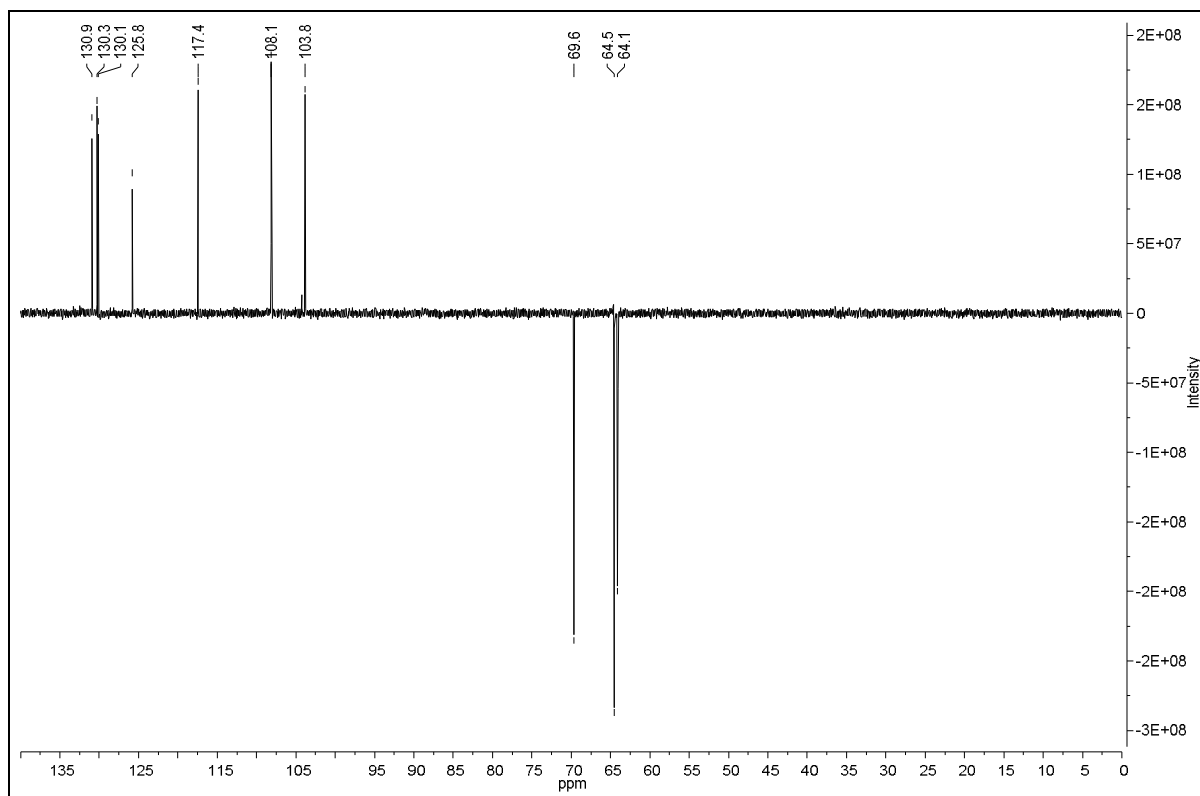


5c: 6-[(3-Bromophenyl)methoxy]-2,3-dihydro-1,4-benzodioxine

^{13}C NMR DEPT 90°

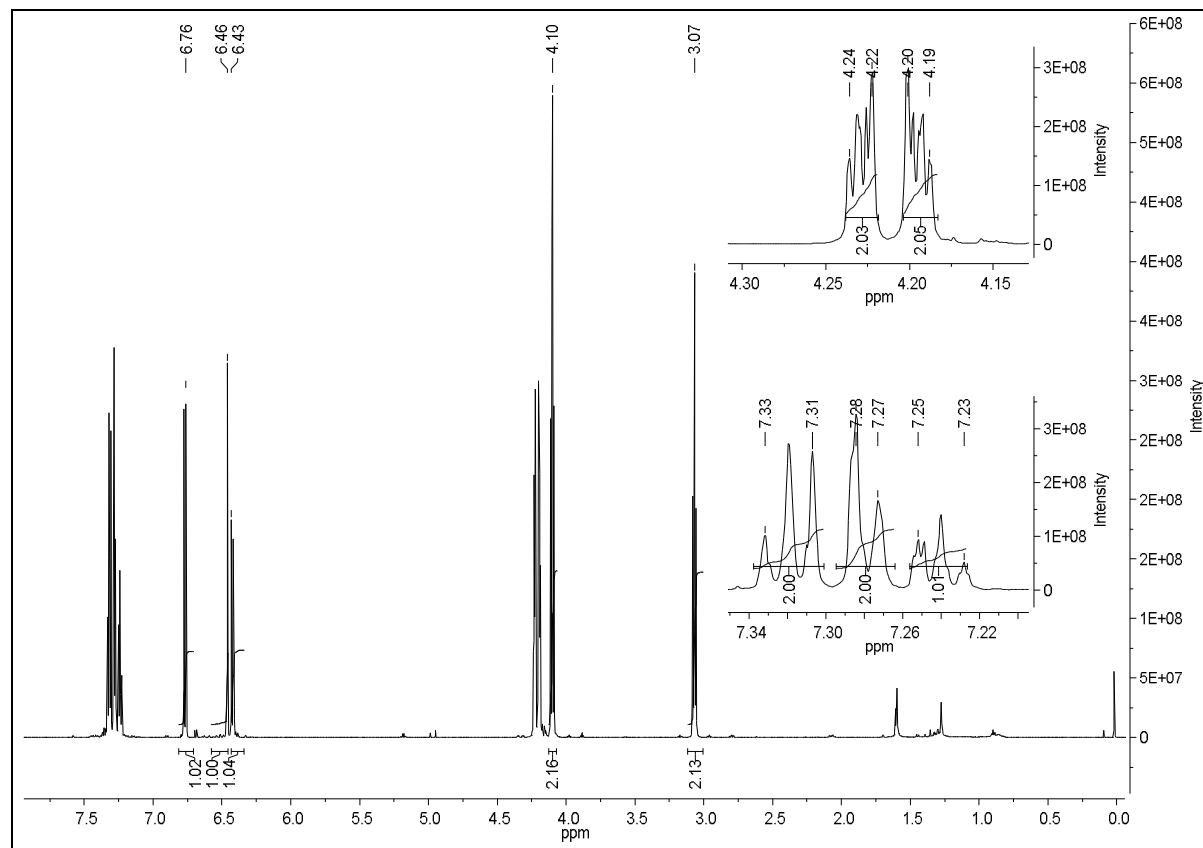


^{13}C NMR DEPT 135°

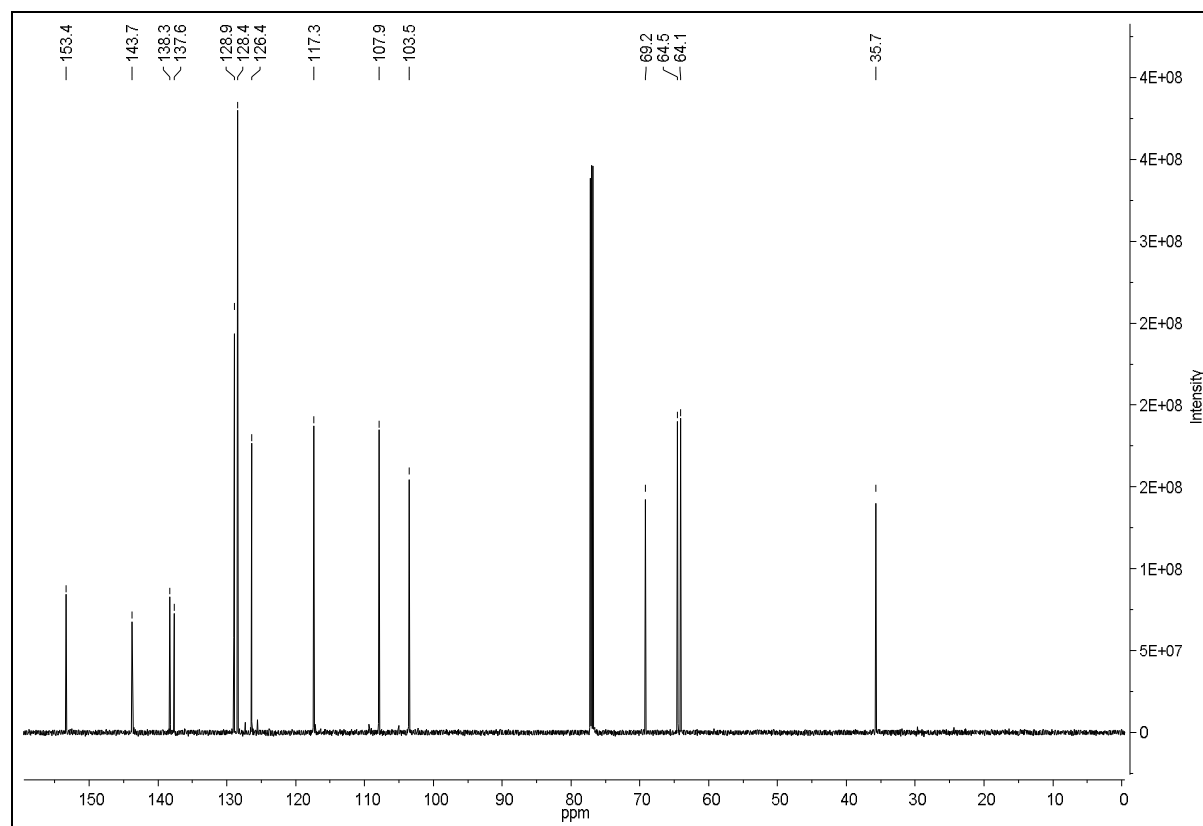


5d: 6-(2-Phenylethoxy)-2,3-dihydro-1,4-benzodioxine

¹H

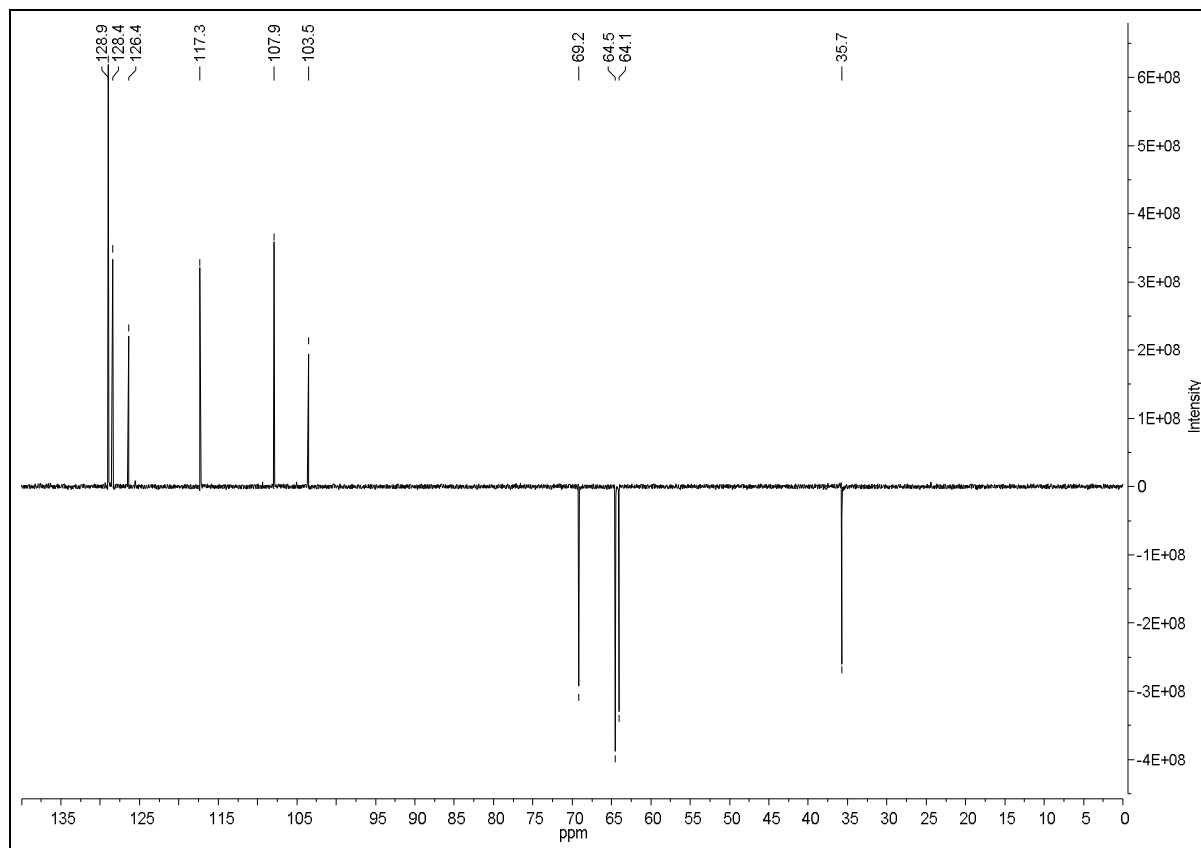


¹³C



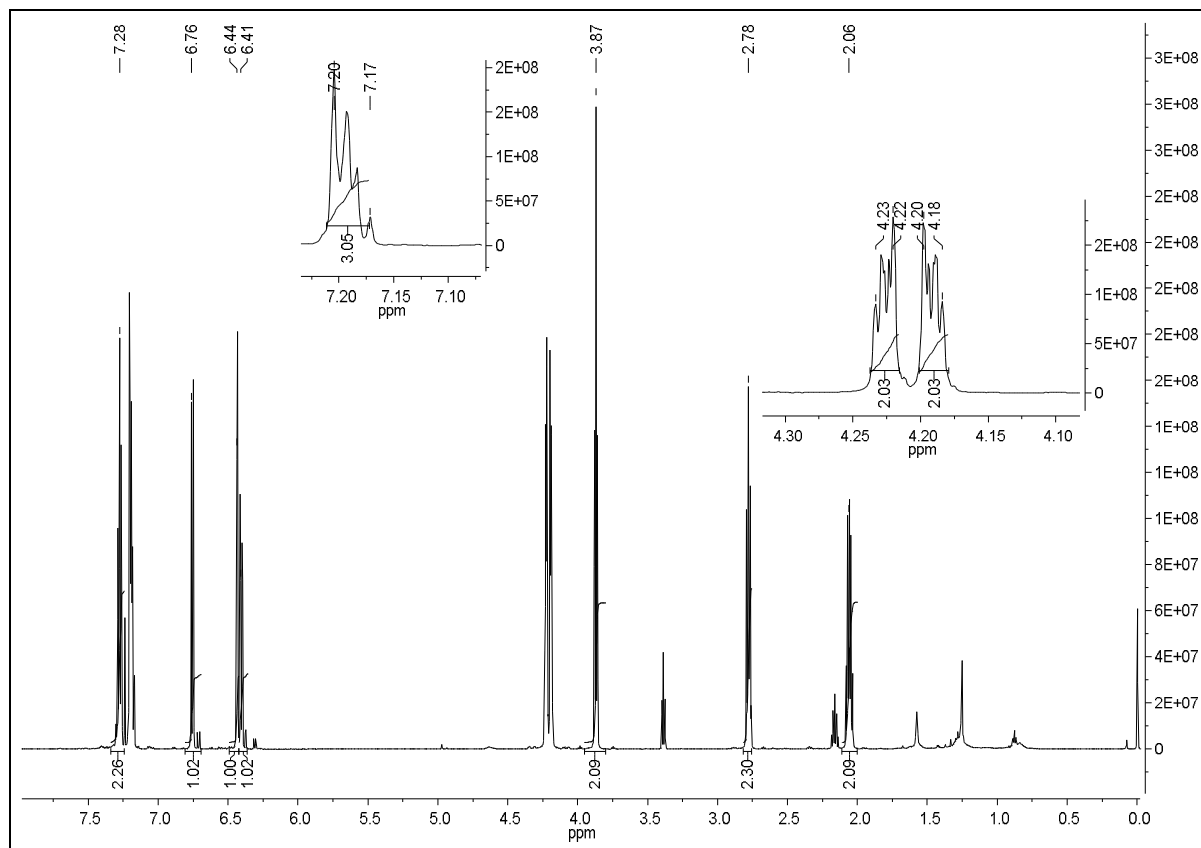
5d: 6-(2-Phenylethoxy)-2,3-dihydro-1,4-benzodioxine

^{13}C NMR DEPT 135°

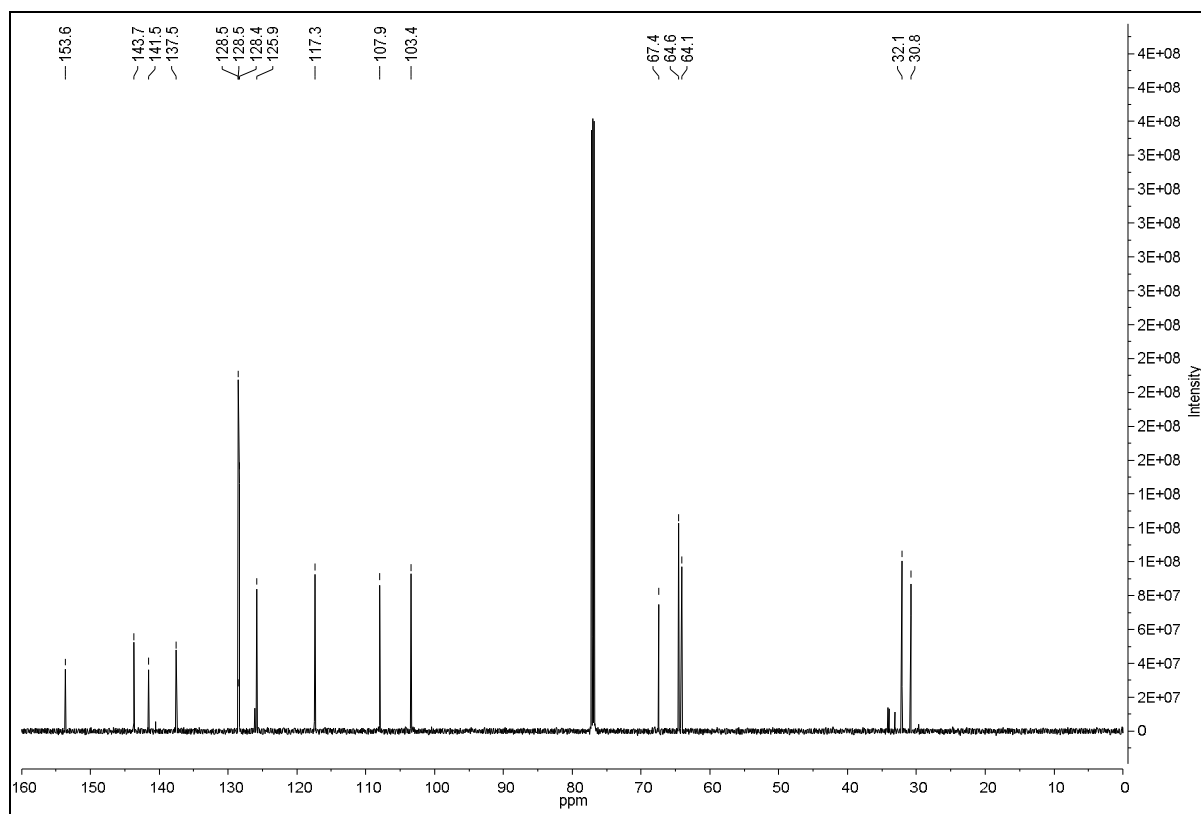


5e: 6-(3-Phenylpropoxy)-2,3-dihydro-1,4-benzodioxine

¹H

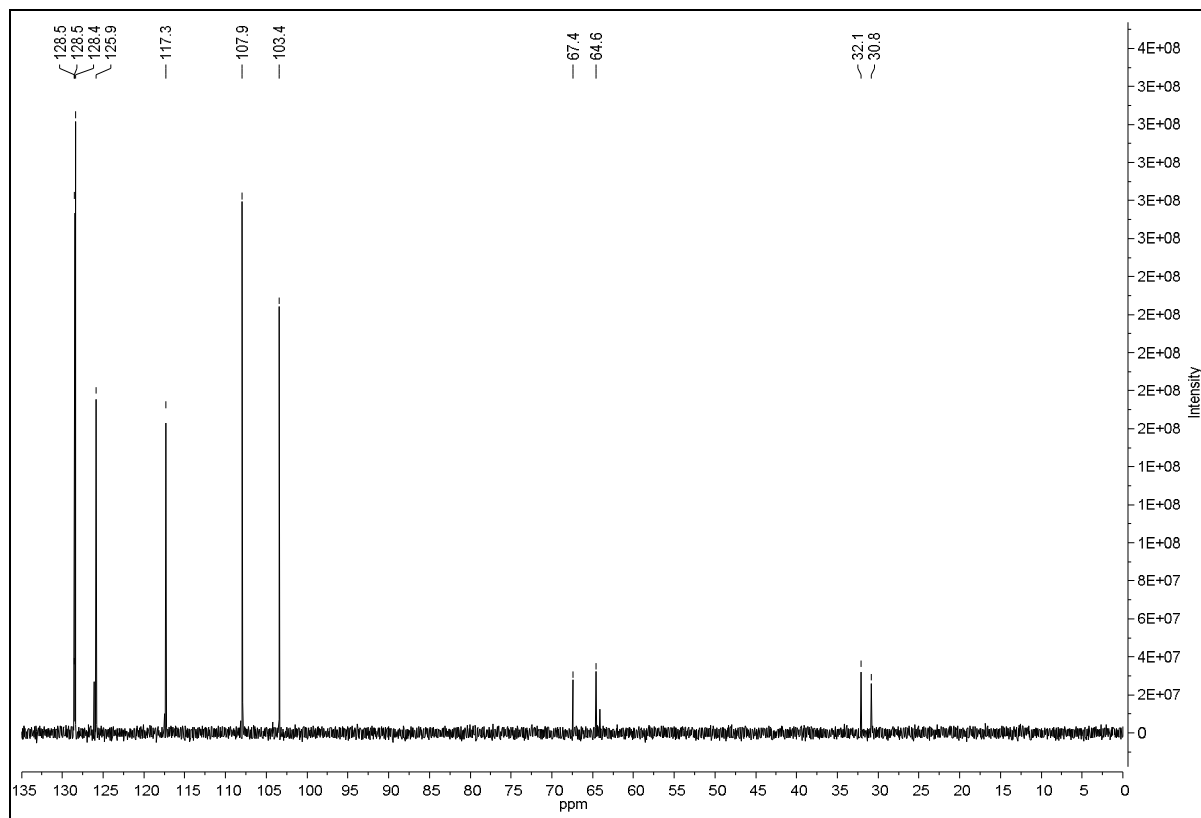


¹³C

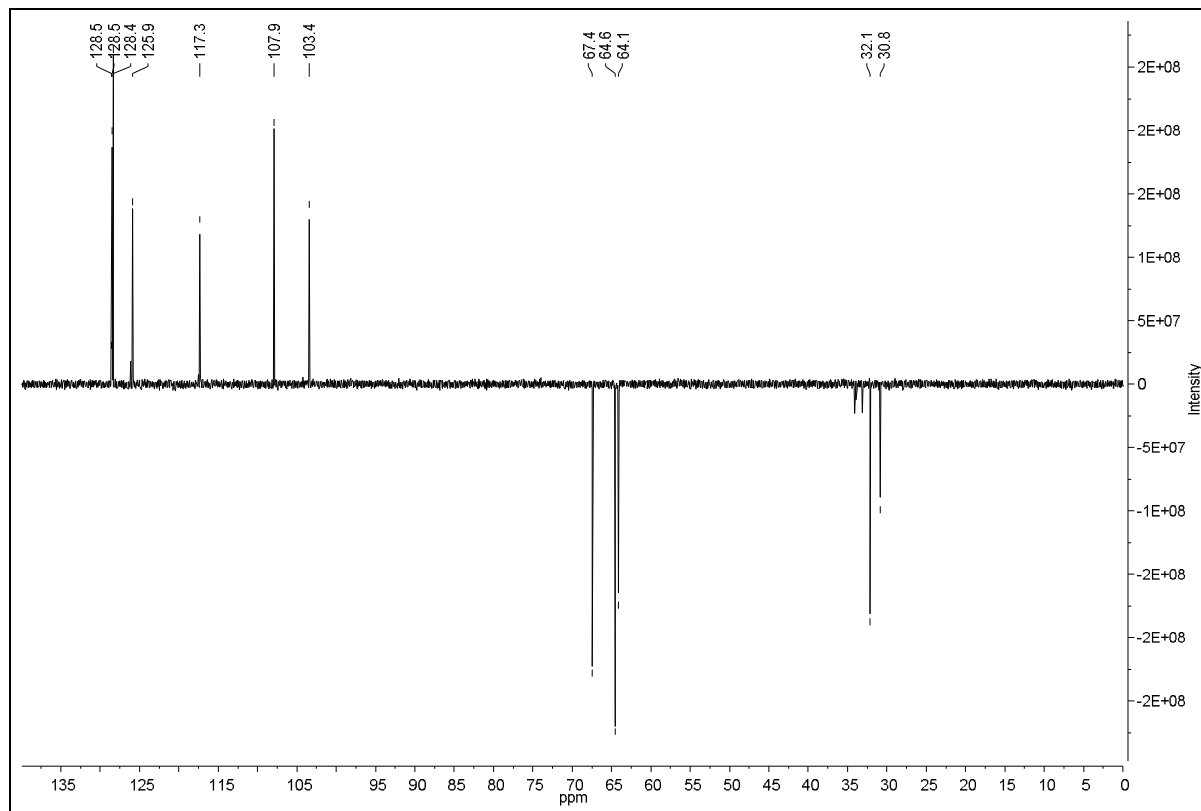


5e: 6-(3-Phenylpropoxy)-2,3-dihydro-1,4-benzodioxine

^{13}C NMR DEPT 90°

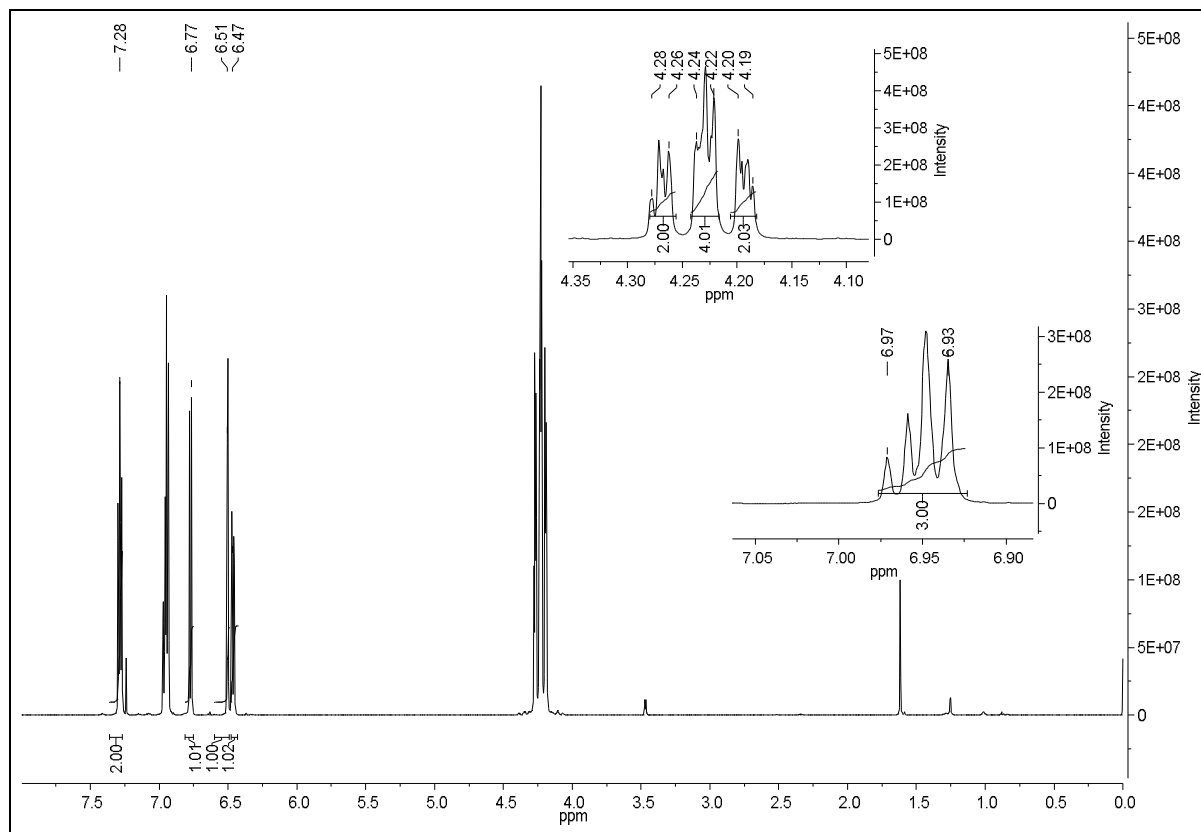


^{13}C NMR DEPT 135°

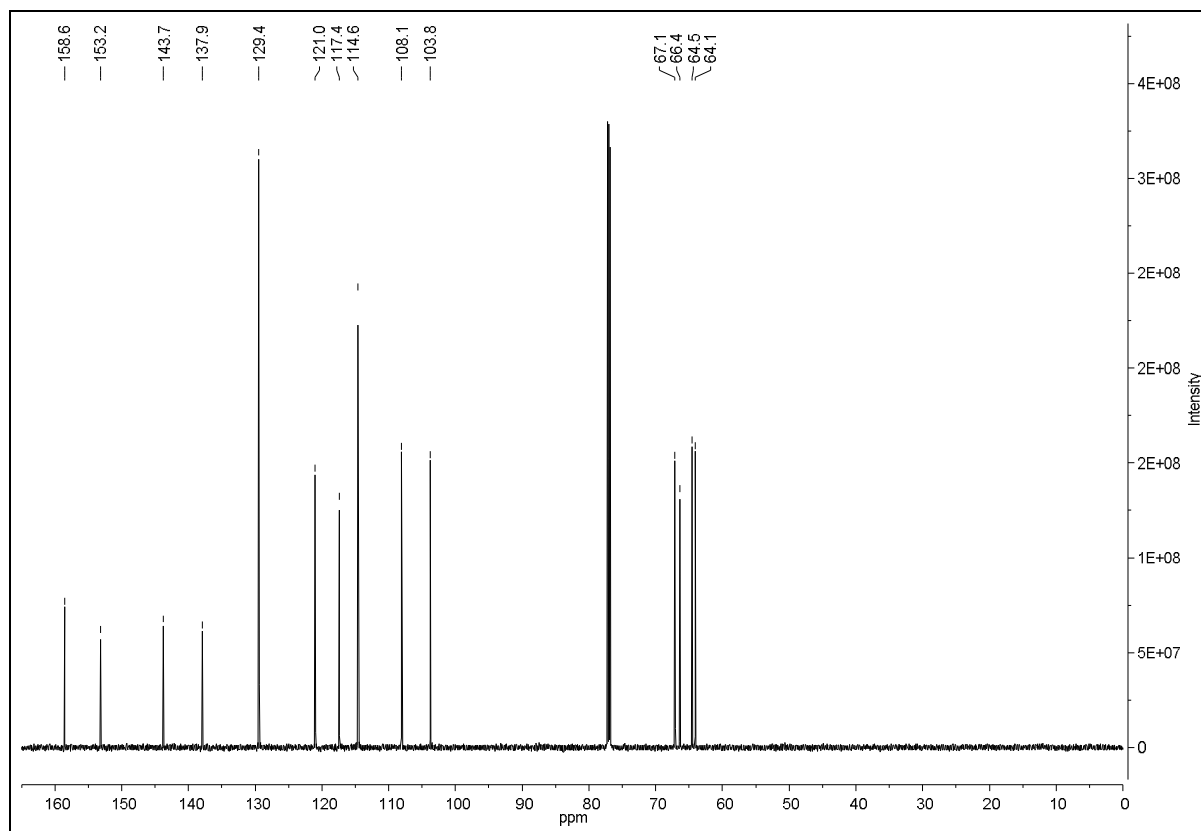


5f: 6-(2-Phenoxyethoxy)-2,3-dihydro-1,4-benzodioxine

¹H

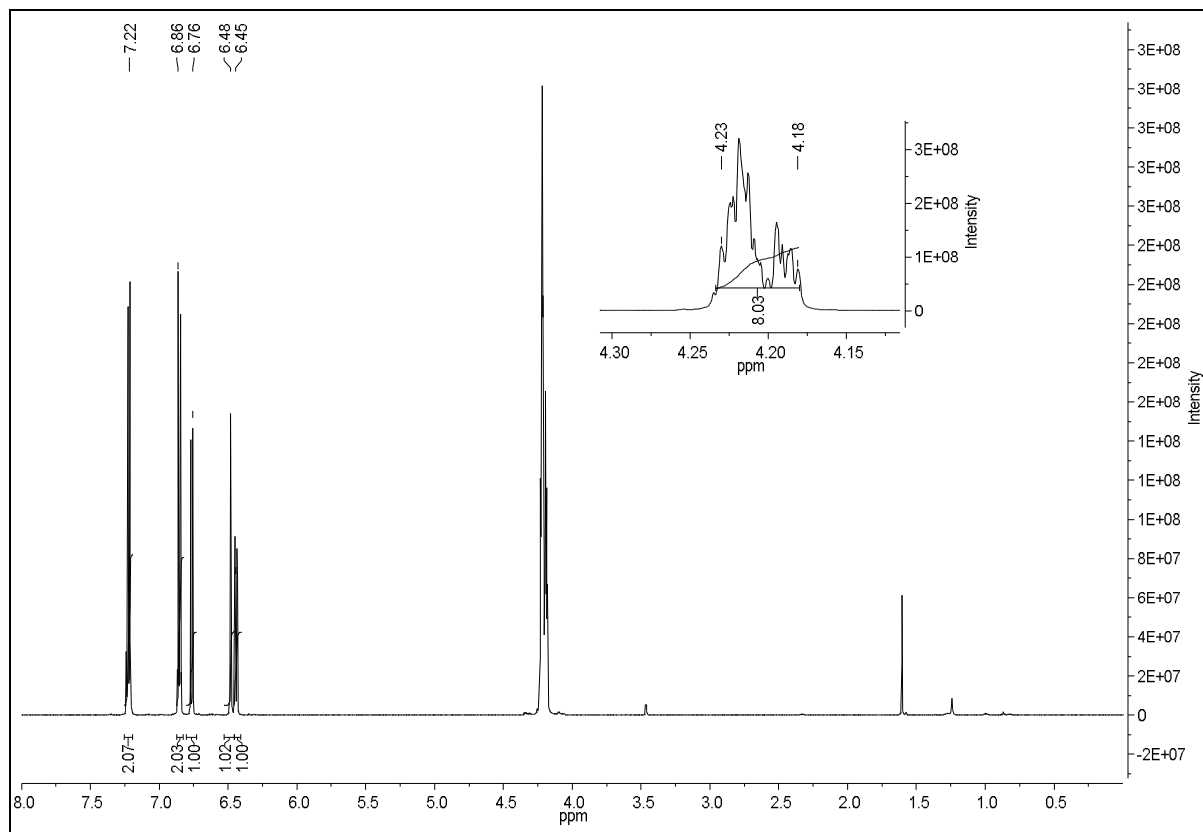


¹³C

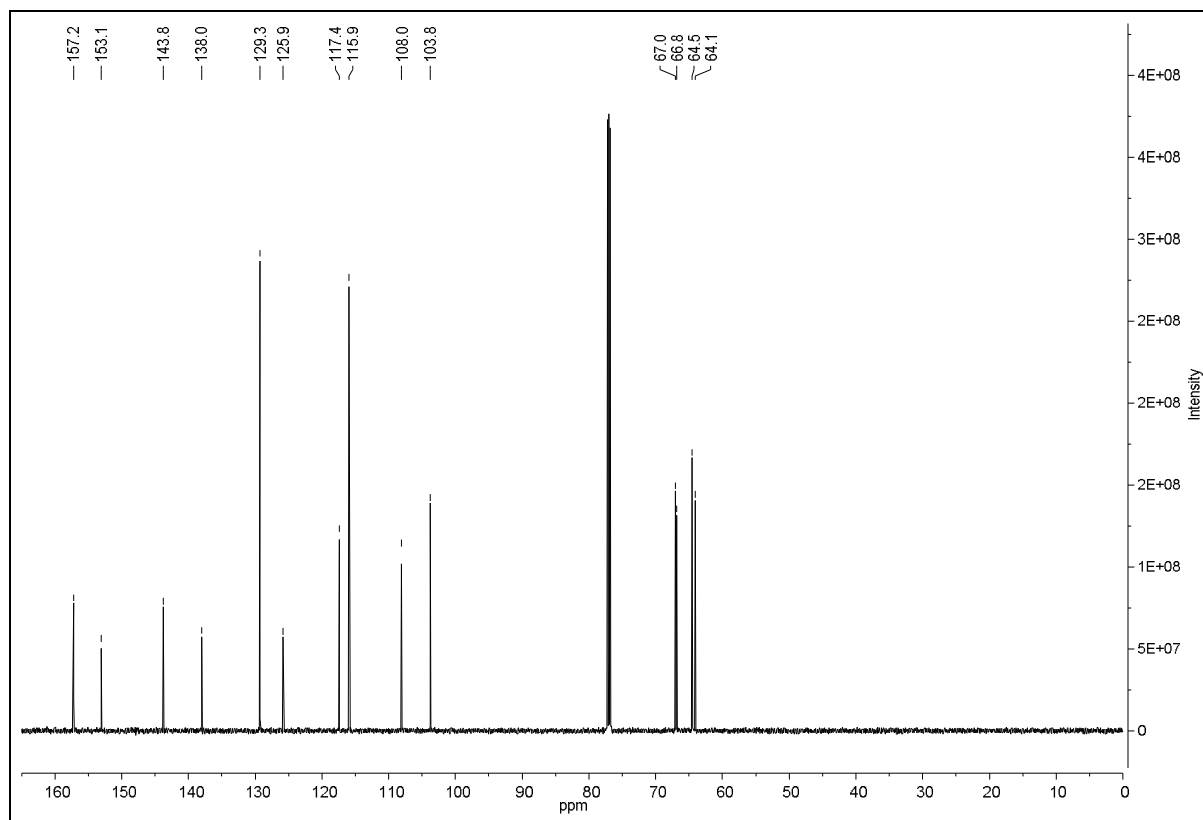


5g: 6-[2-(4-Chlorophenoxy)ethoxy]-2,3-dihydro-1,4-benzodioxine

¹H

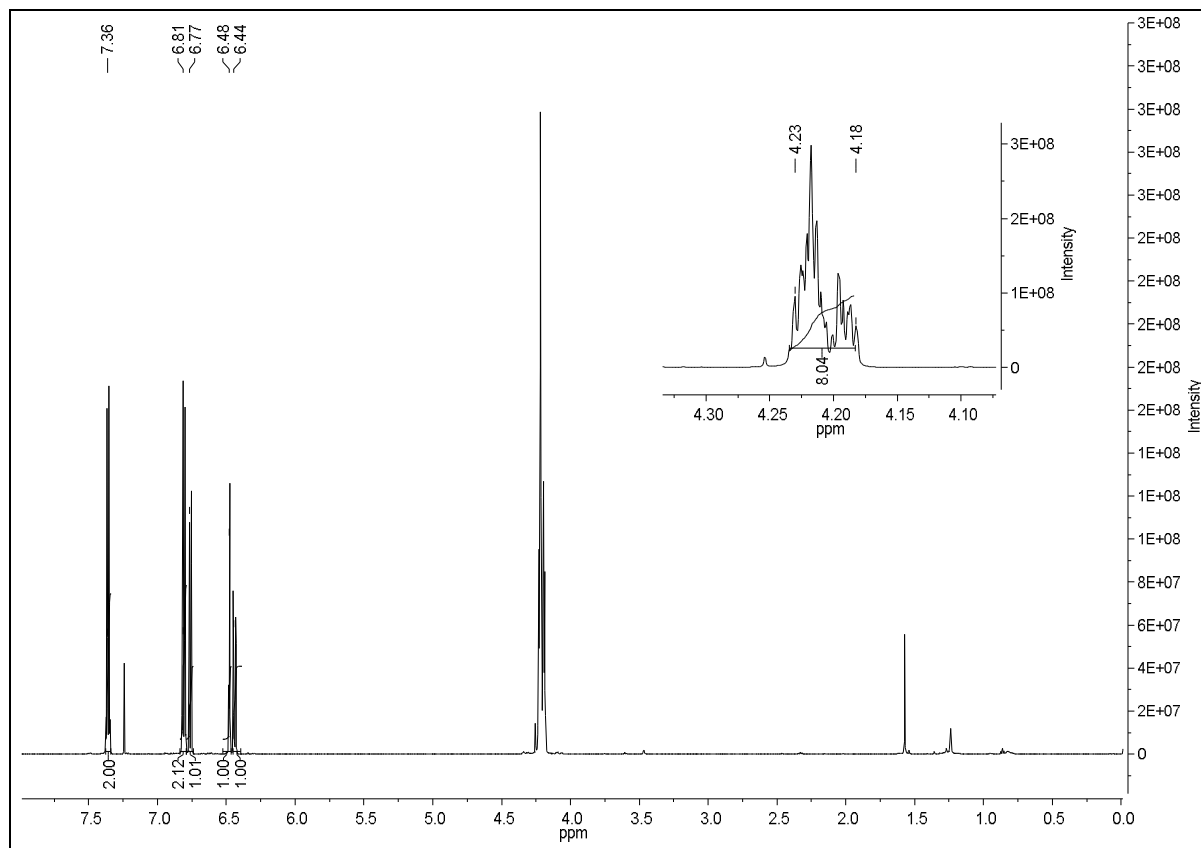


¹³C

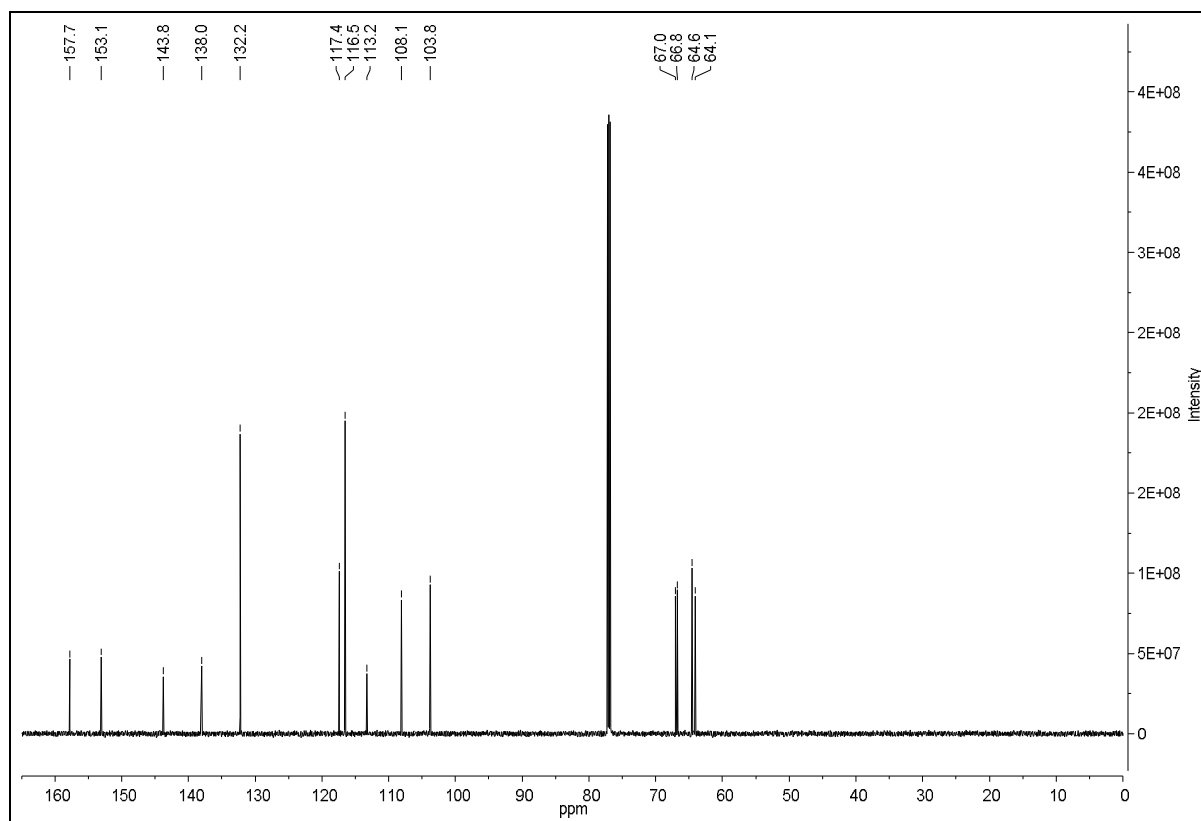


5h: 6-[2-(4-Bromophenoxy)ethoxy]-2,3-dihydro-1,4-benzodioxine

¹H

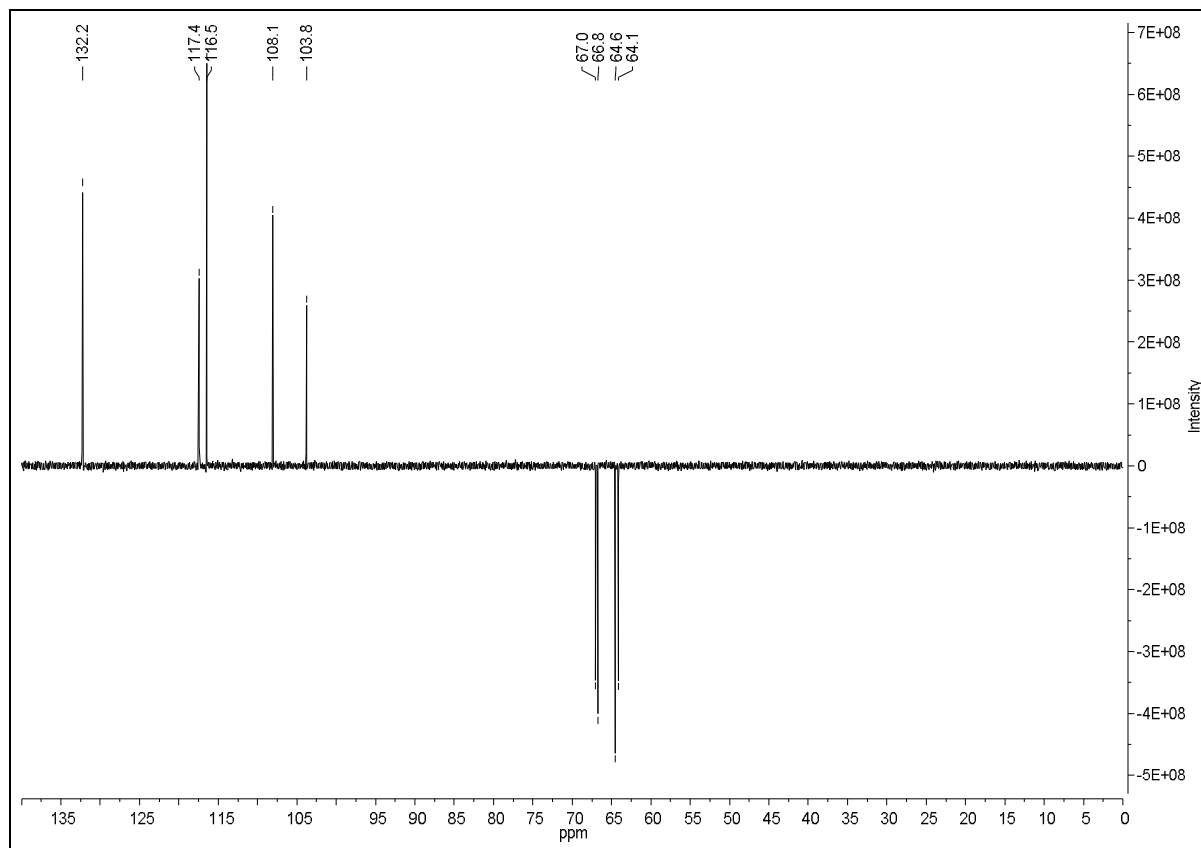


¹³C



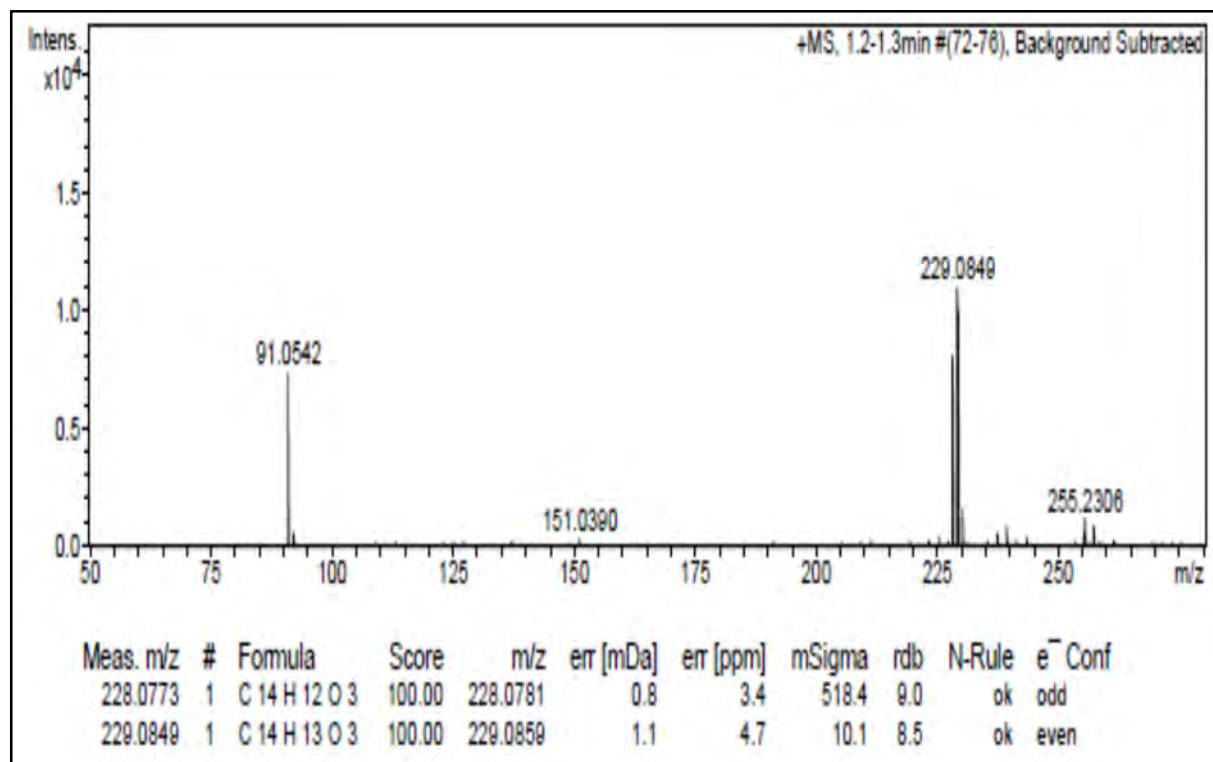
5h: 6-[2-(4-Bromophenoxy)ethoxy]-2,3-dihydro-1,4-benzodioxine

^{13}C NMR DEPT 135°

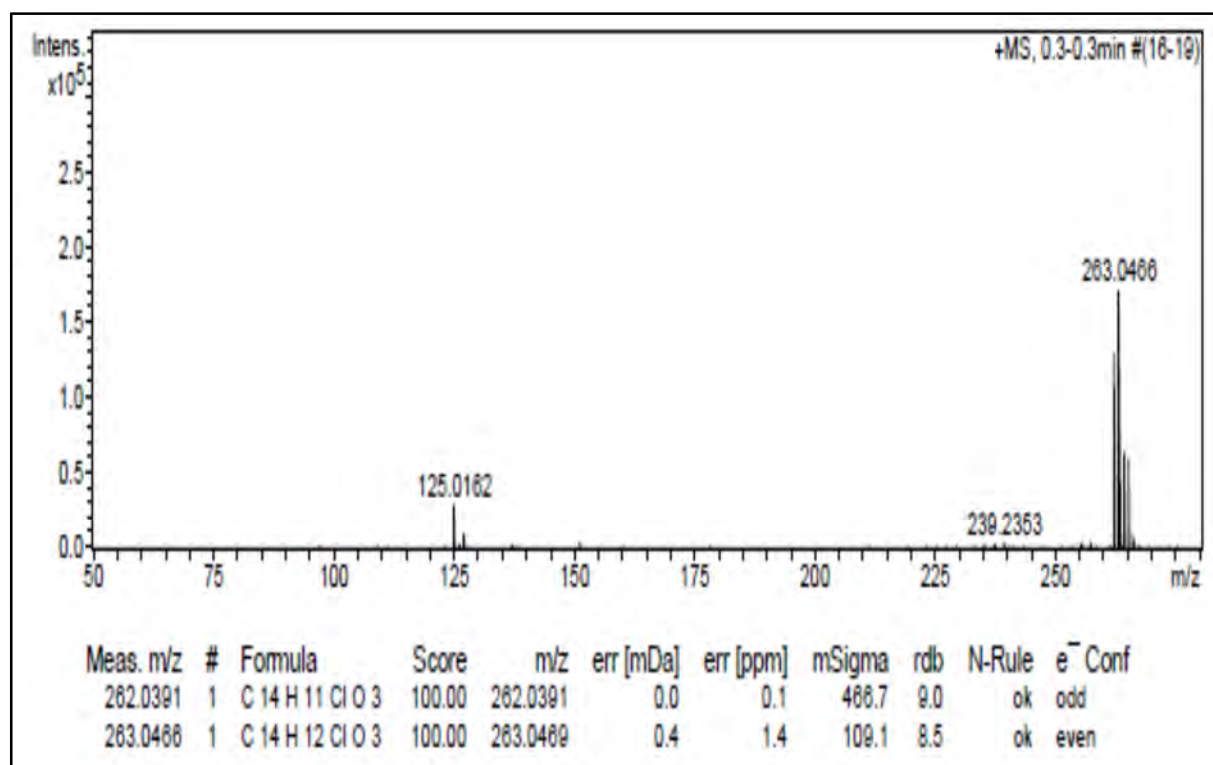


Section 2: Mass spectra

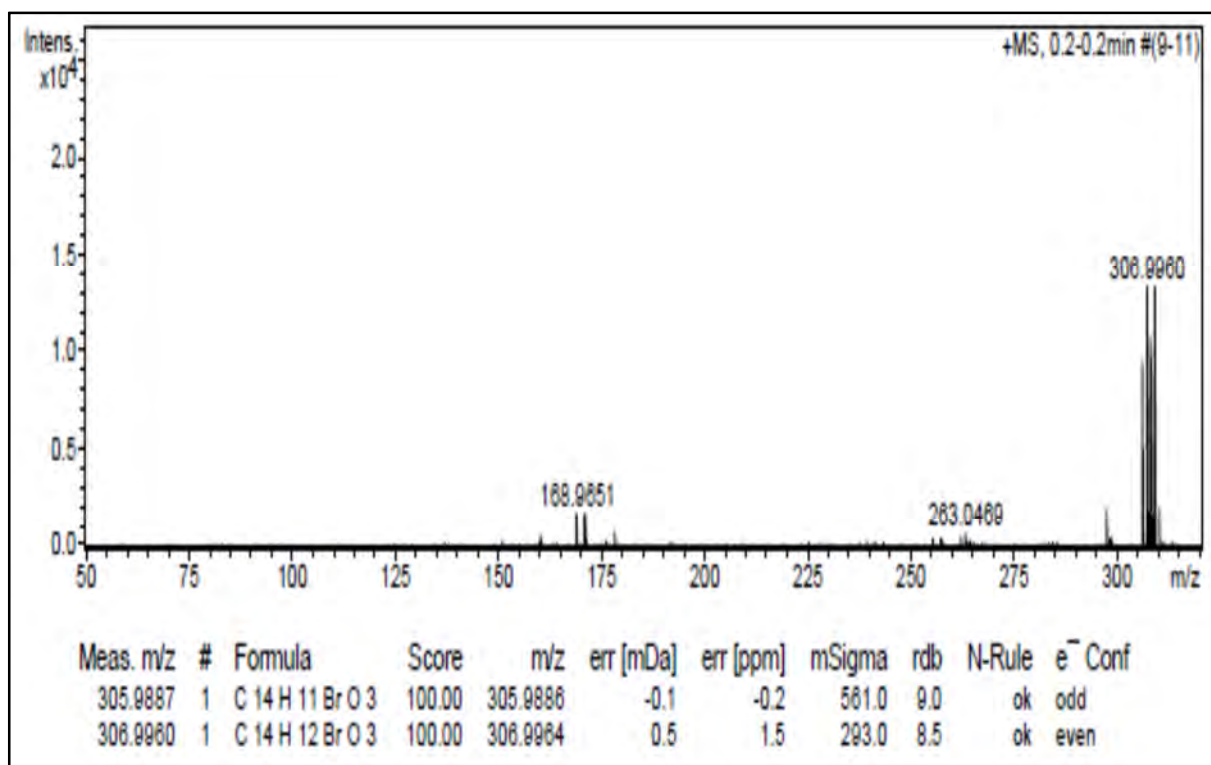
4a: 5-(Benzyloxy)-2H-1,3-benzodioxole



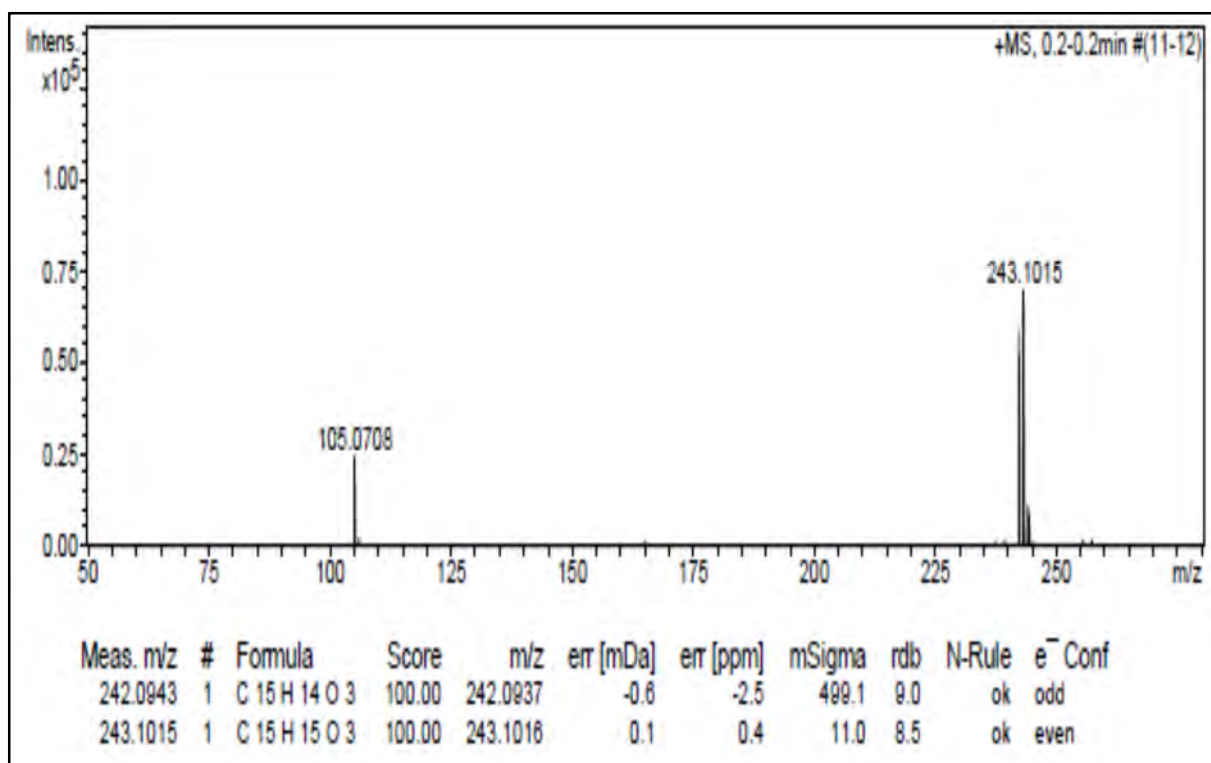
4b: 5-[(3-Chlorophenyl)methoxy]-2H-1,3-benzodioxole



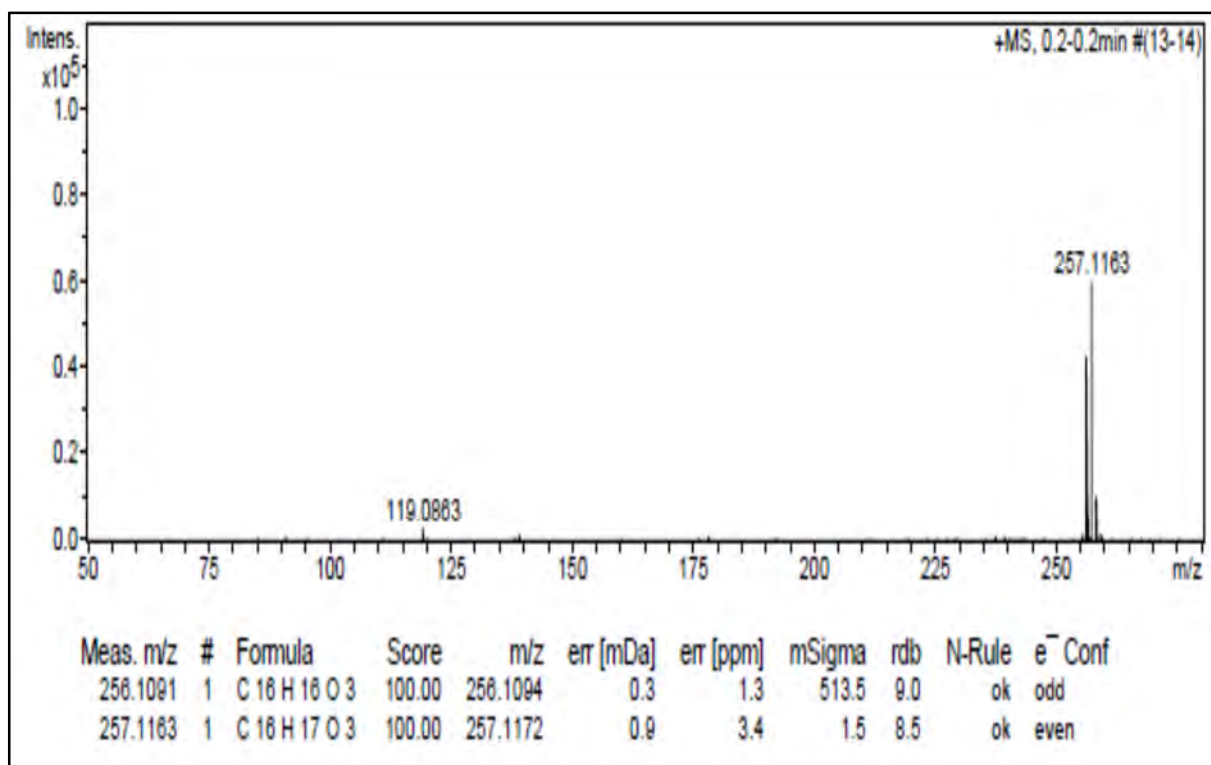
4c: 5-[(3-Bromophenyl)methoxy]-2H-1,3-benzodioxole



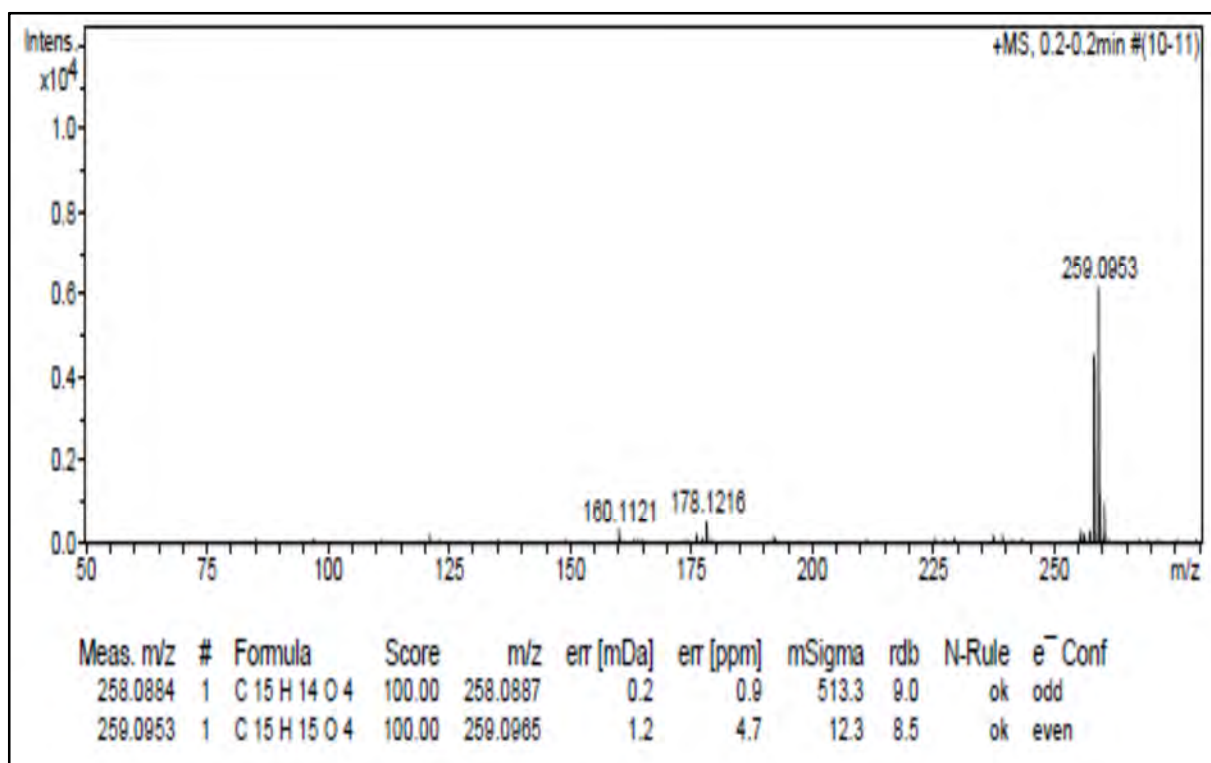
4d: 5-(2-Phenylethoxy)-2H-1,3-benzodioxole



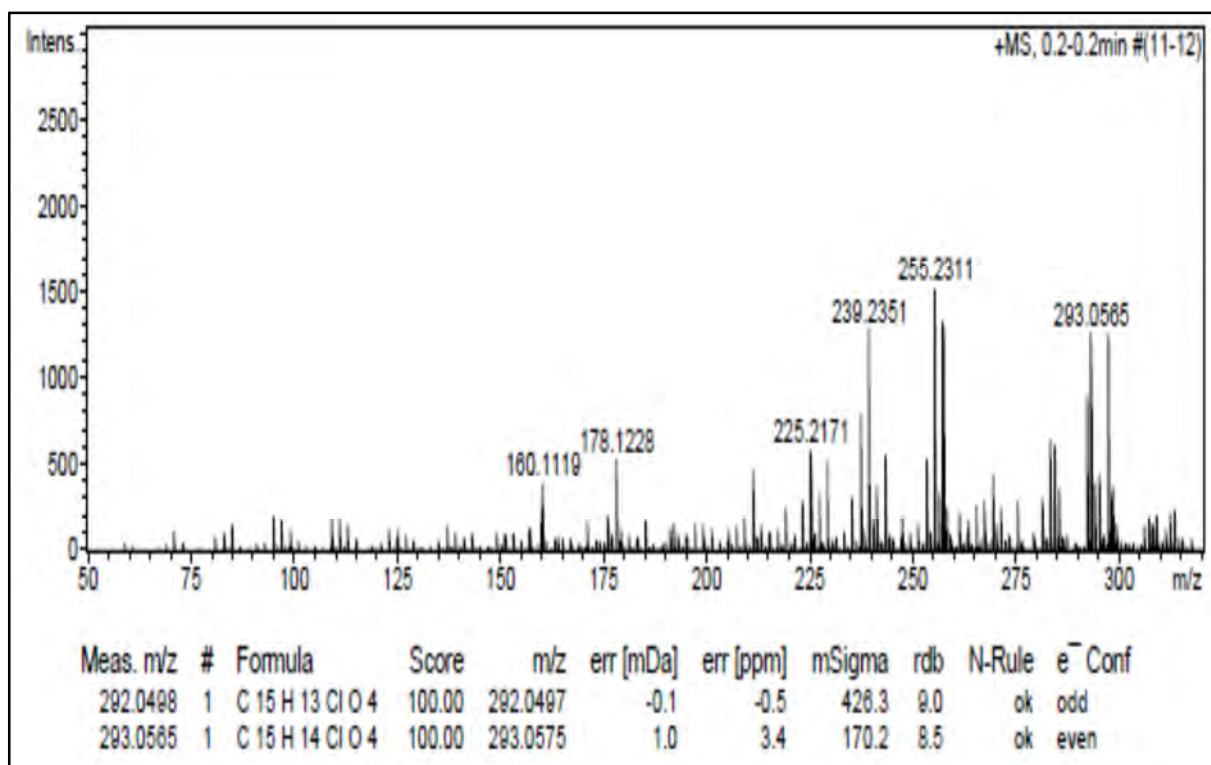
4e: 5-(3-Phenylpropoxy)-2H-1,3-benzodioxole



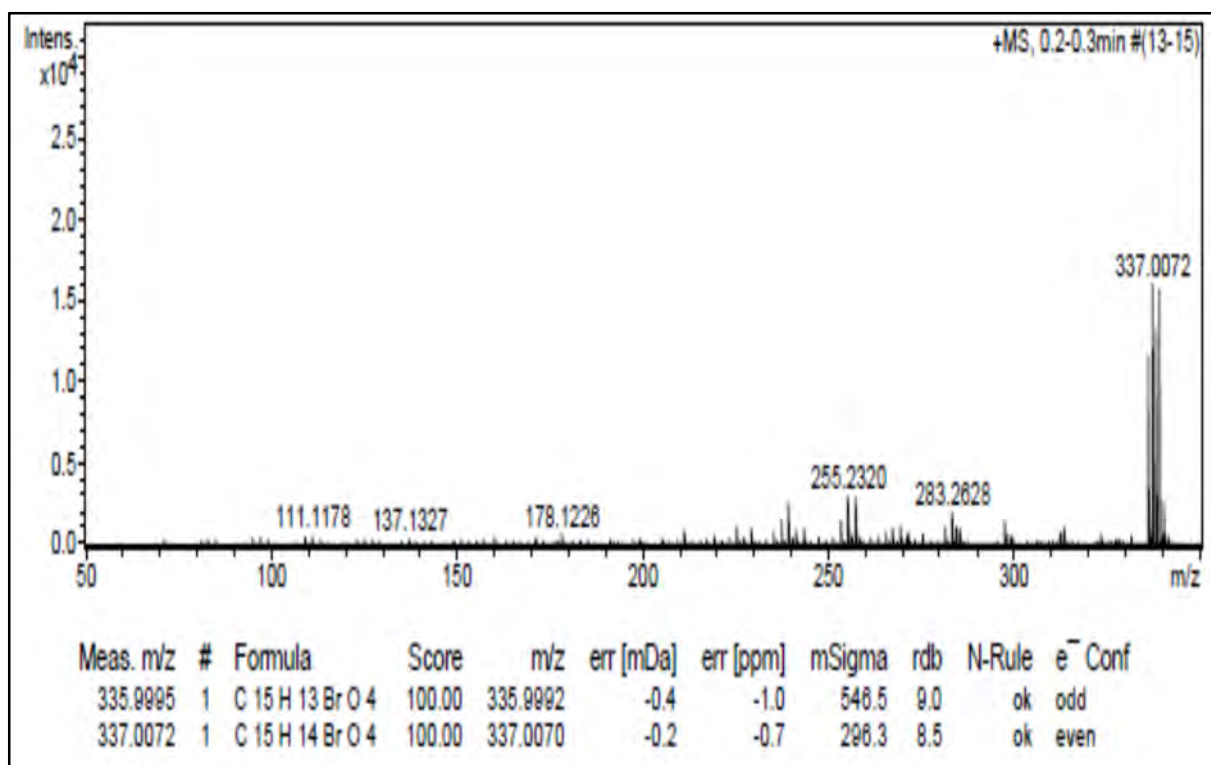
4f: 5-(2-Phenoxyethoxy)-2H-1,3-benzodioxole



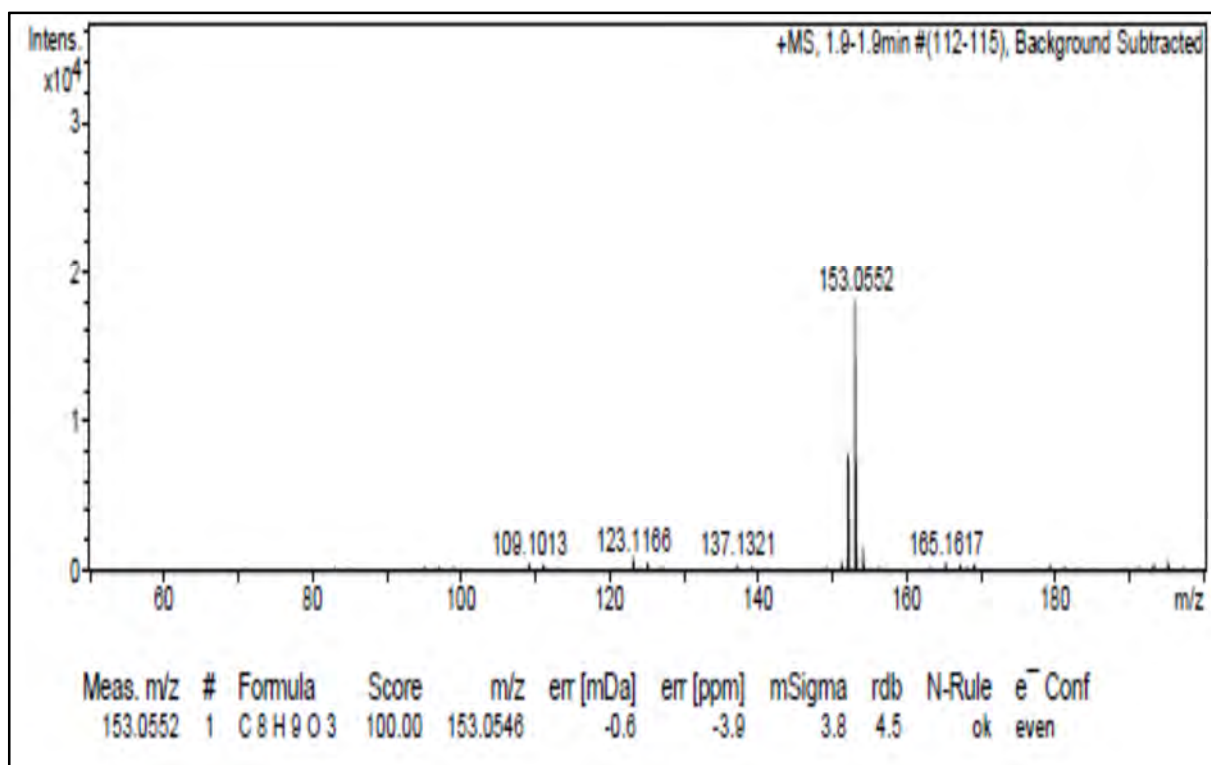
4g: 5-[2-(4-Chlorophenoxy)ethoxy]-2H-1,3-benzodioxole



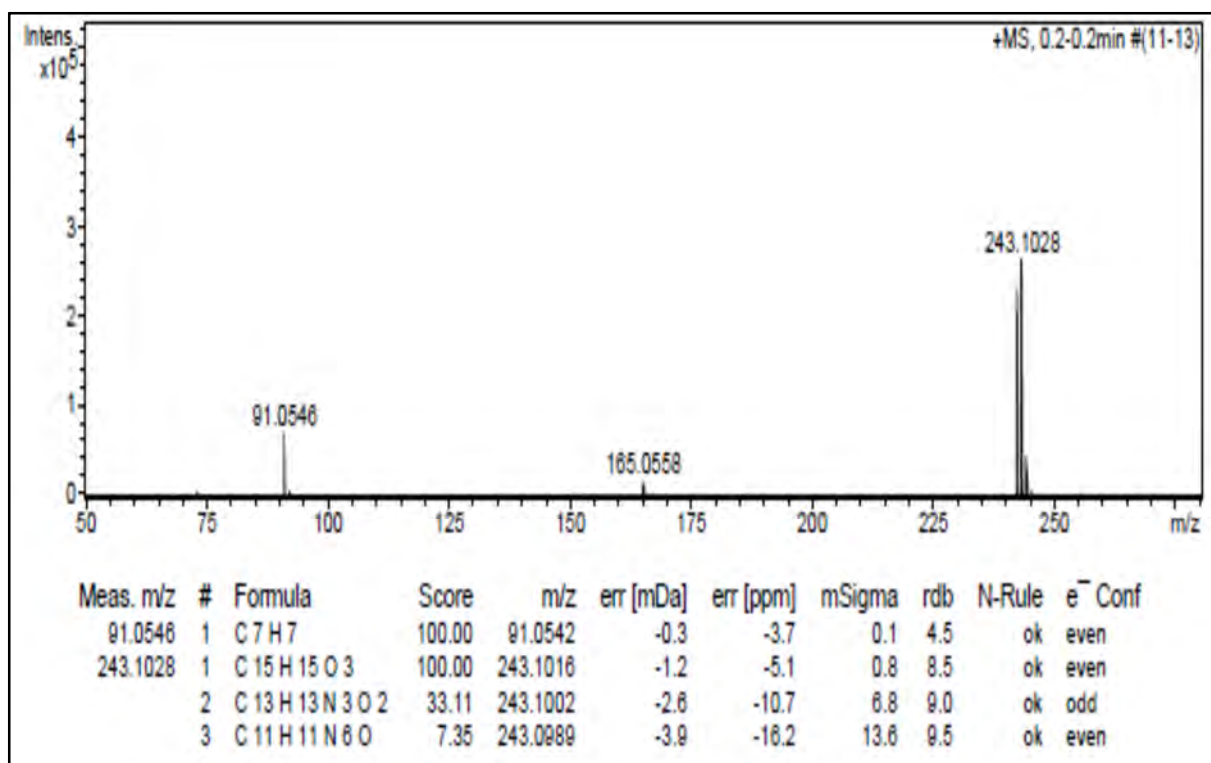
4h: 5-[2-(4-Bromophenoxy)ethoxy]-2H-1,3-benzodioxole



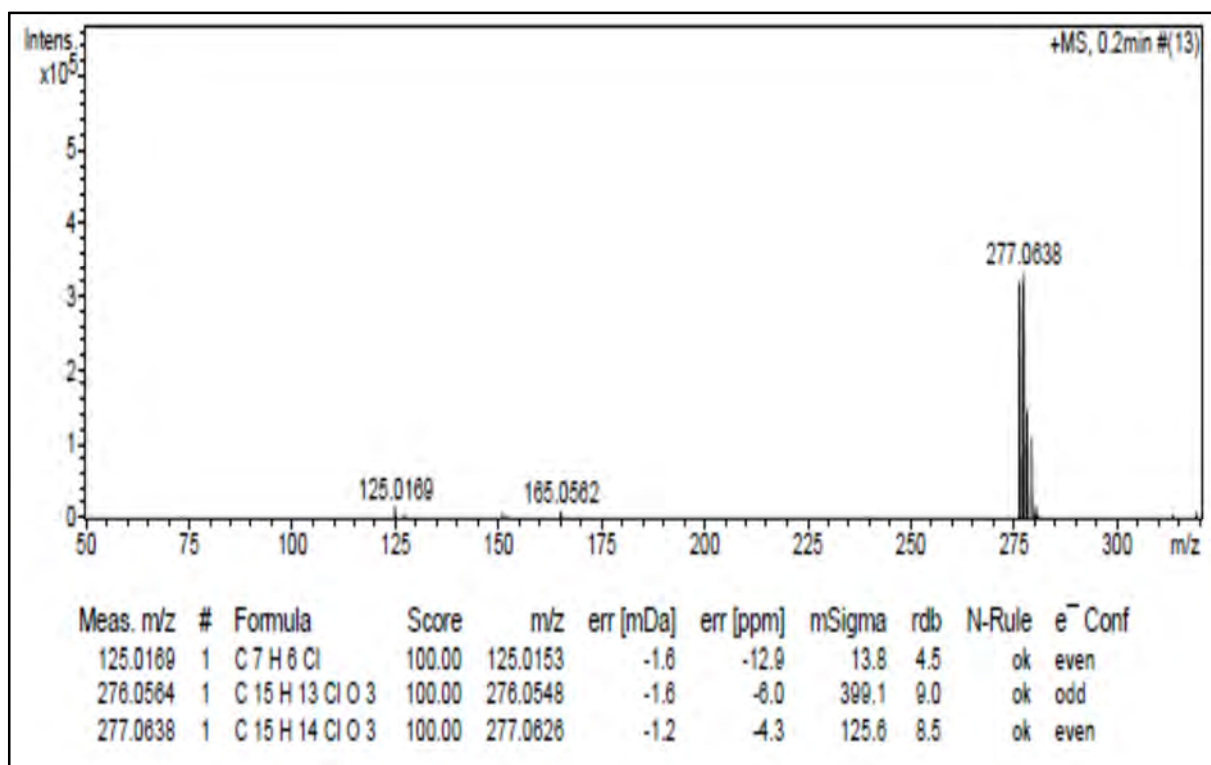
7: 6-Hydroxy-1,4-benzodioxane



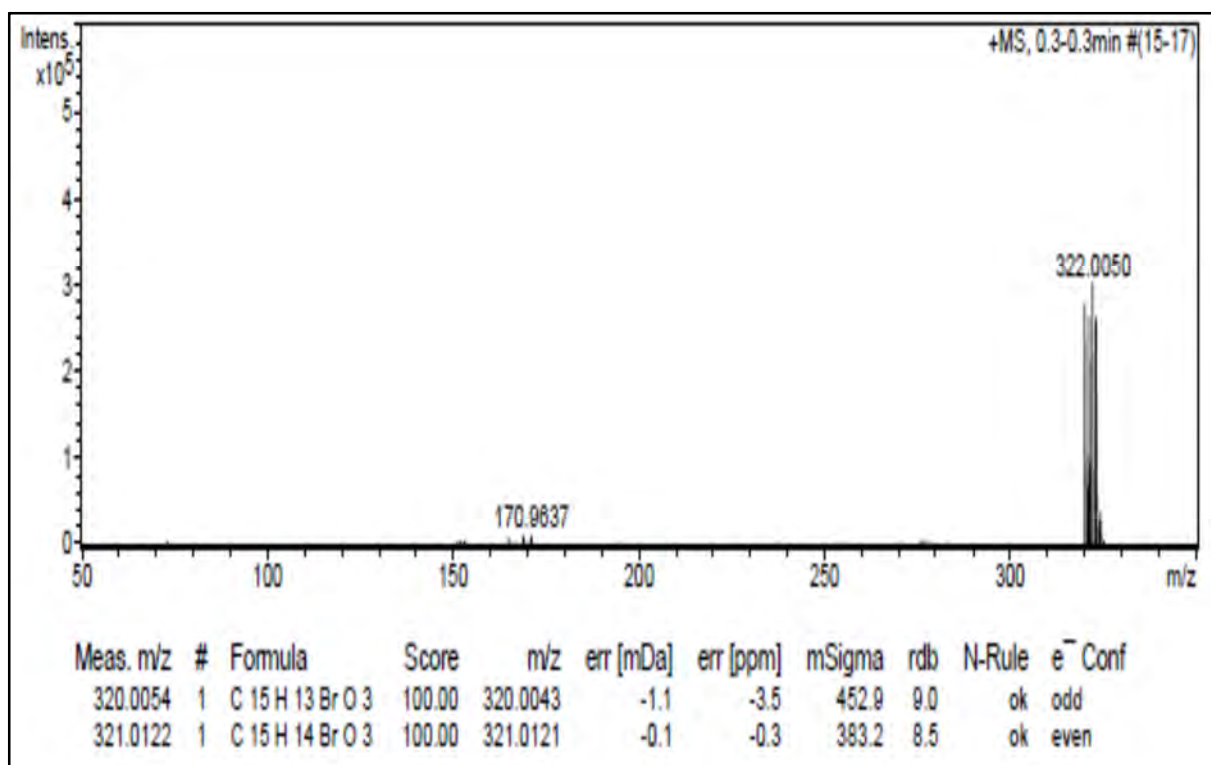
5a: 6-(Benzyloxy)-2,3-dihydro-1,4-benzodioxine



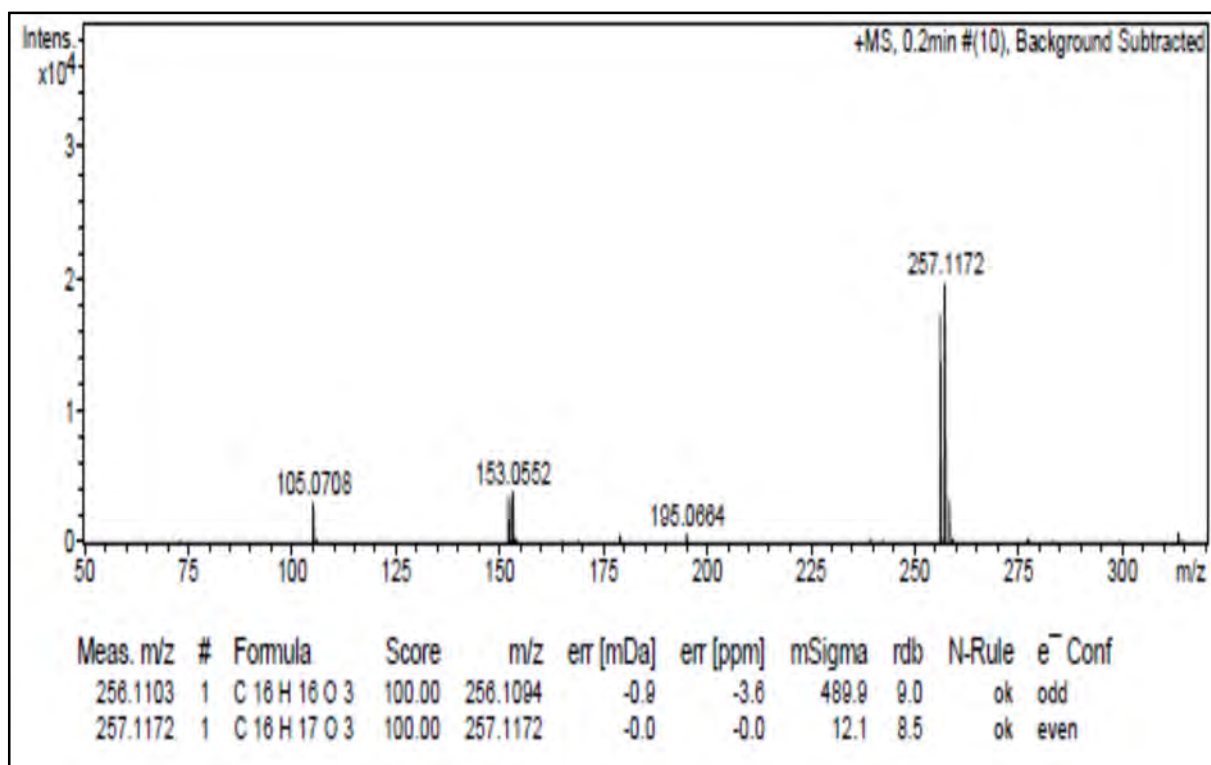
5b: 6-[(3-Chlorophenyl)methoxy]-2,3-dihydro-1,4-benzodioxine



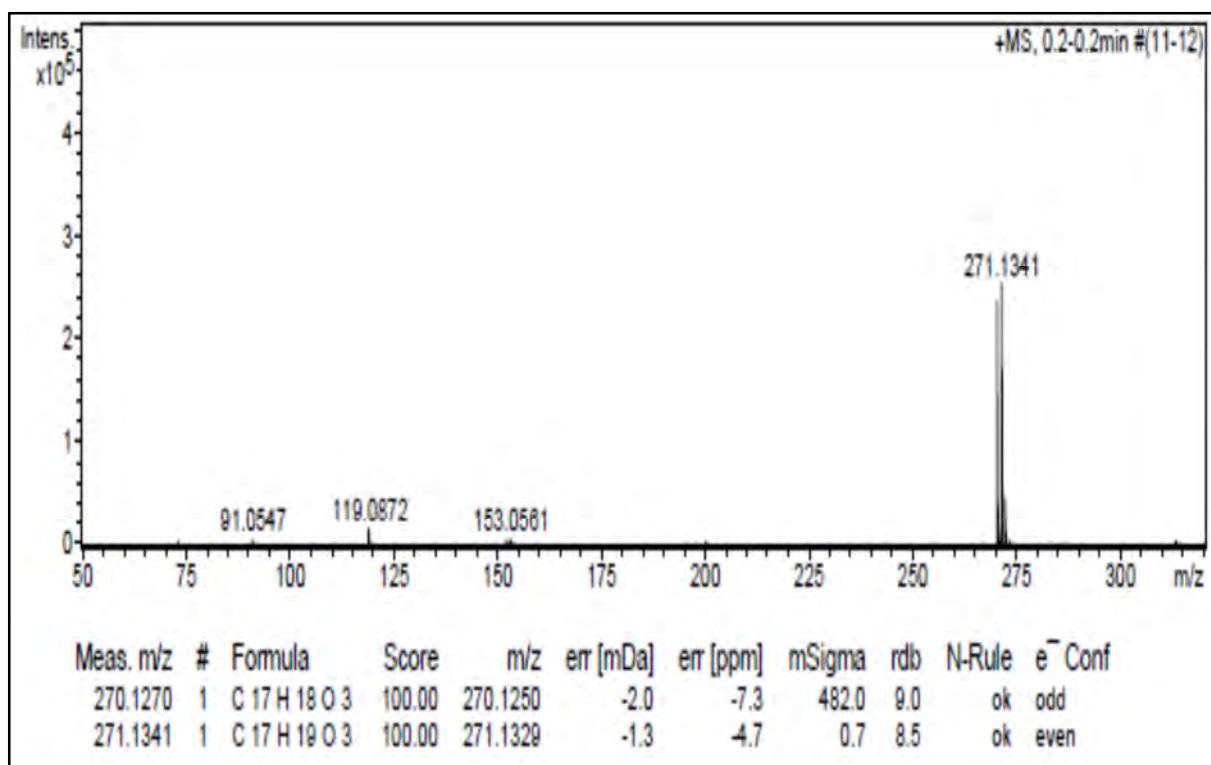
5c: 6-[(3-Bromophenyl)methoxy]-2,3-dihydro-1,4-benzodioxine



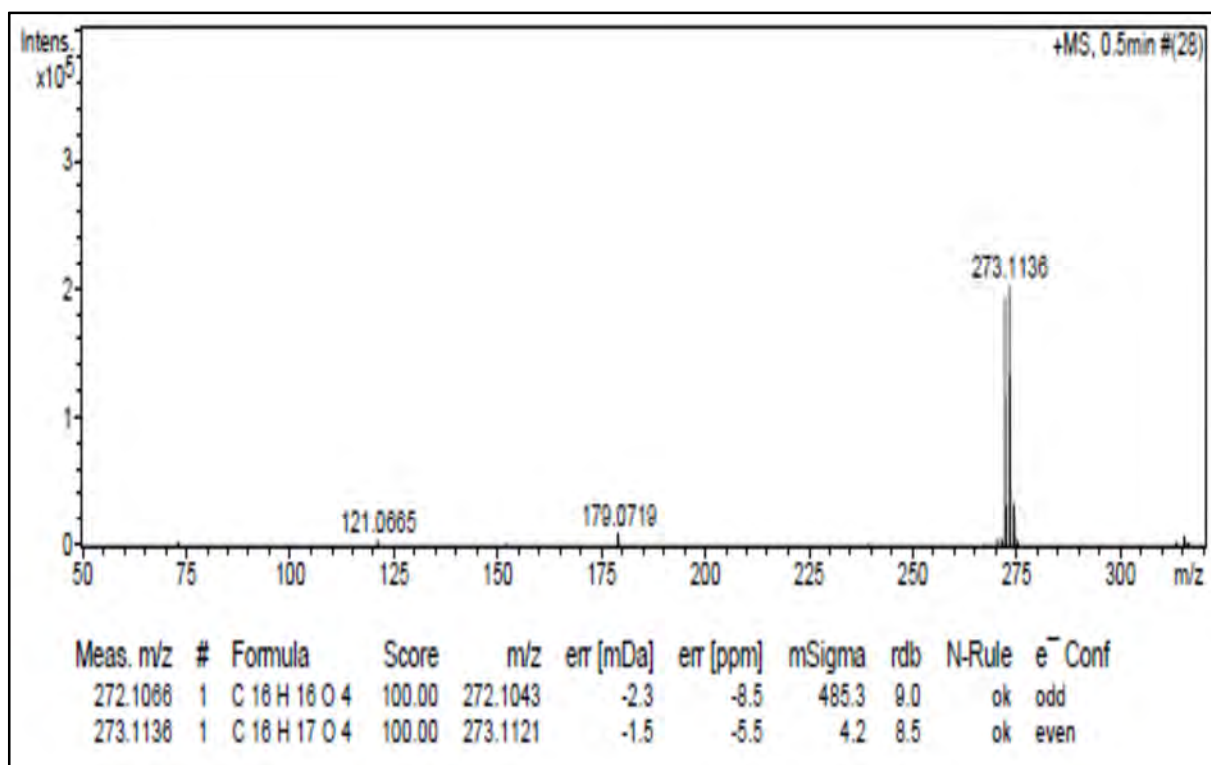
5d: 6-(2-Phenylethoxy)-2,3-dihydro-1,4-benzodioxine



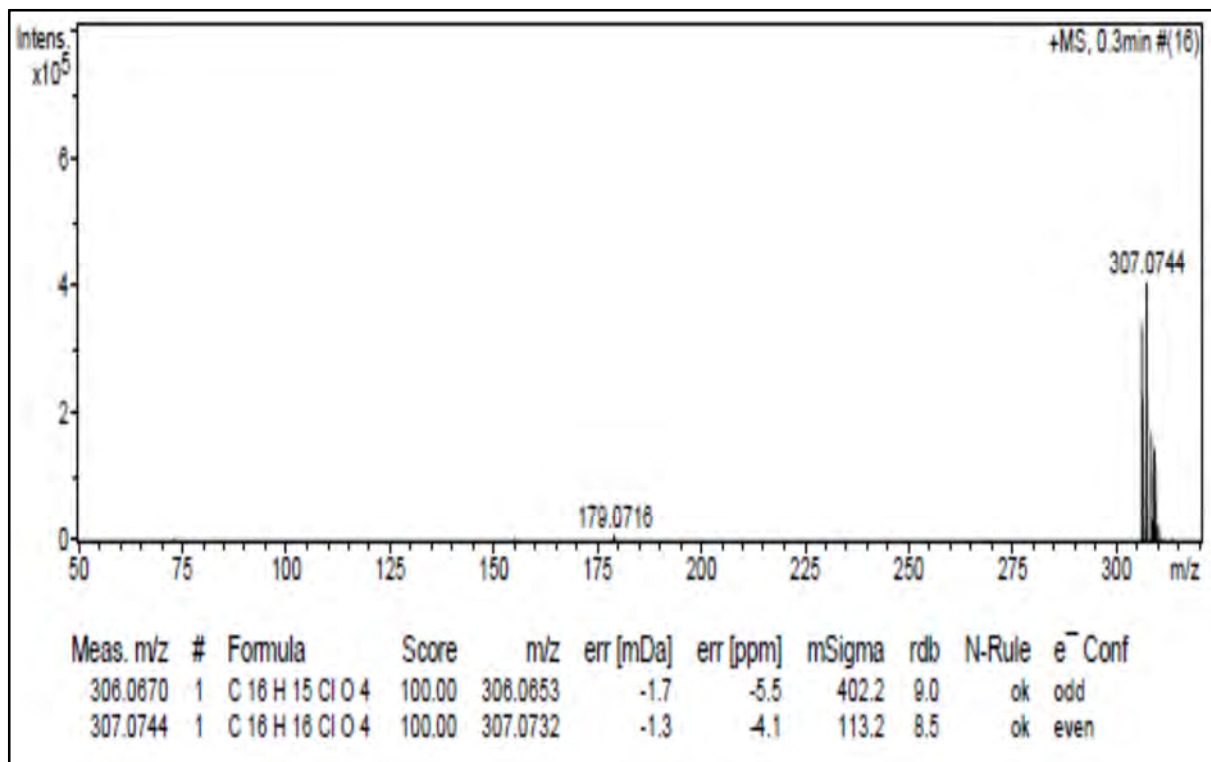
5e: 6-(3-Phenylpropoxy)-2,3-dihydro-1,4-benzodioxine



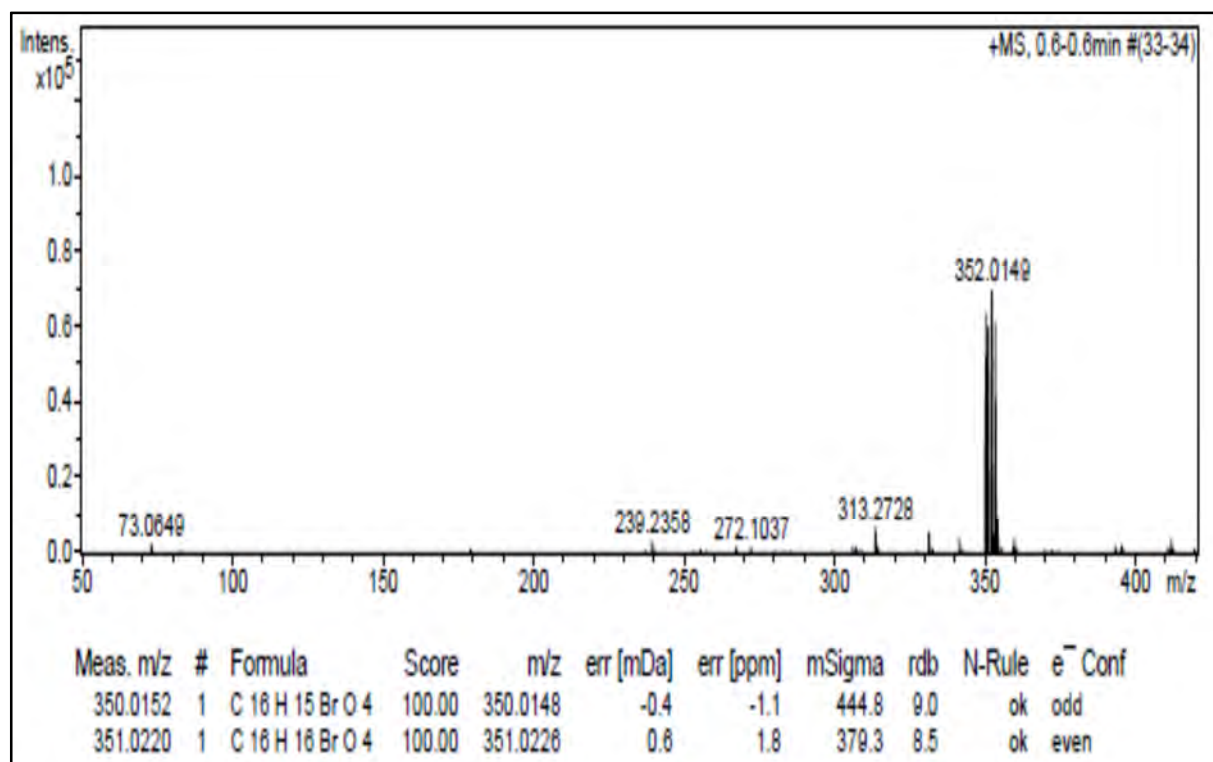
5f: 6-(2-Phenoxyethoxy)-2,3-dihydro-1,4-benzodioxine



5g: 6-[2-(4-Chlorophenoxy)ethoxy]-2,3-dihydro-1,4-benzodioxine

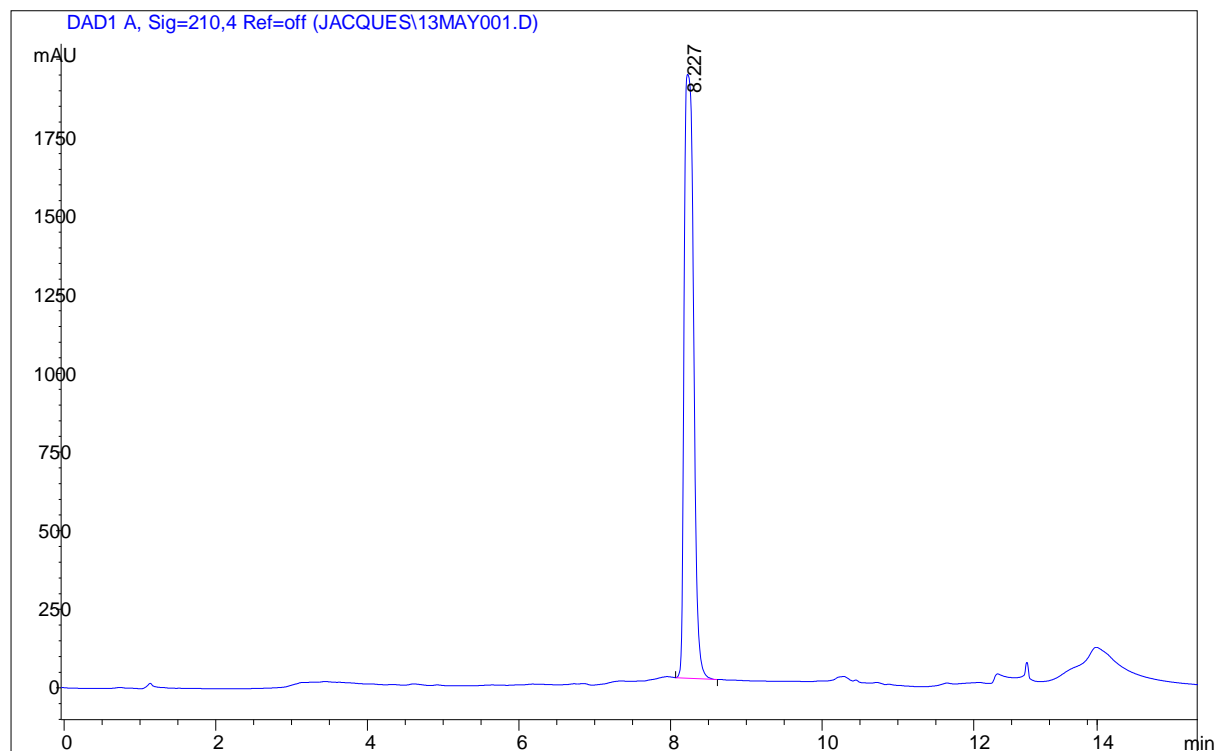


5h: 6-[2-(4-Bromophenoxy)ethoxy]-2,3-dihydro-1,4-benzodioxine

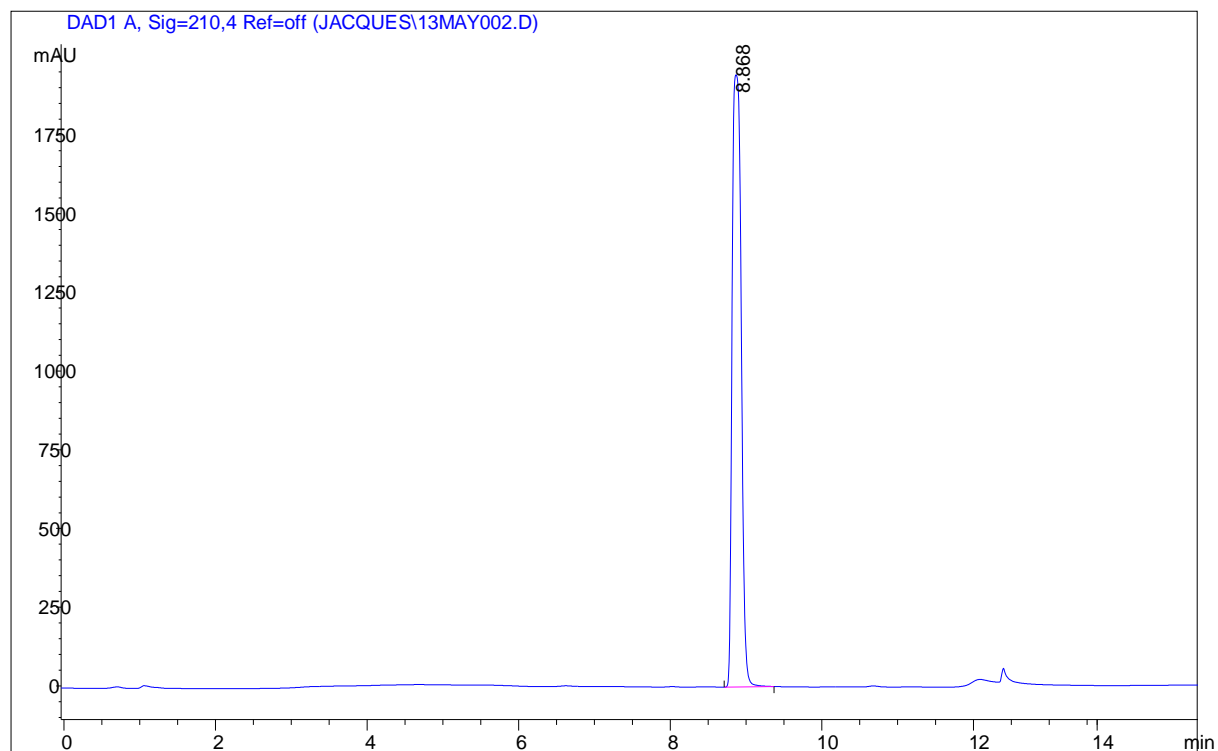


Section 3: HPLC chromatograms

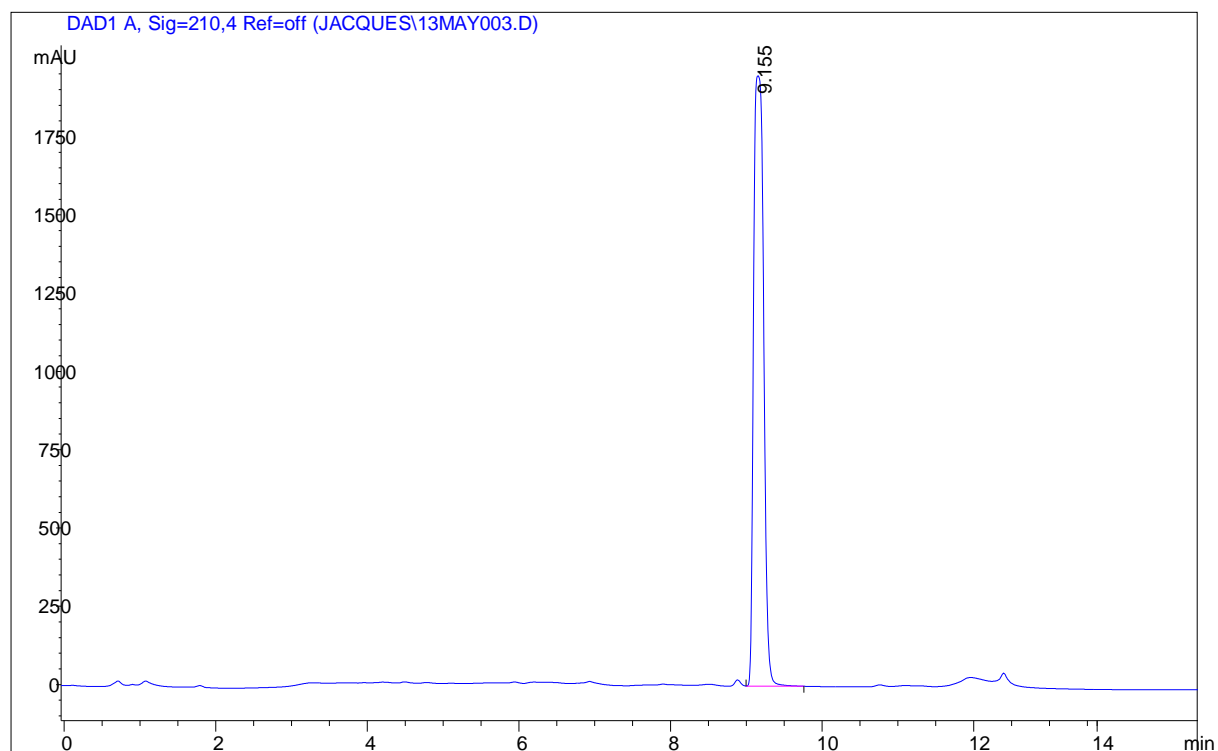
4a: 5-(Benzyloxy)-2H-1,3-benzodioxole



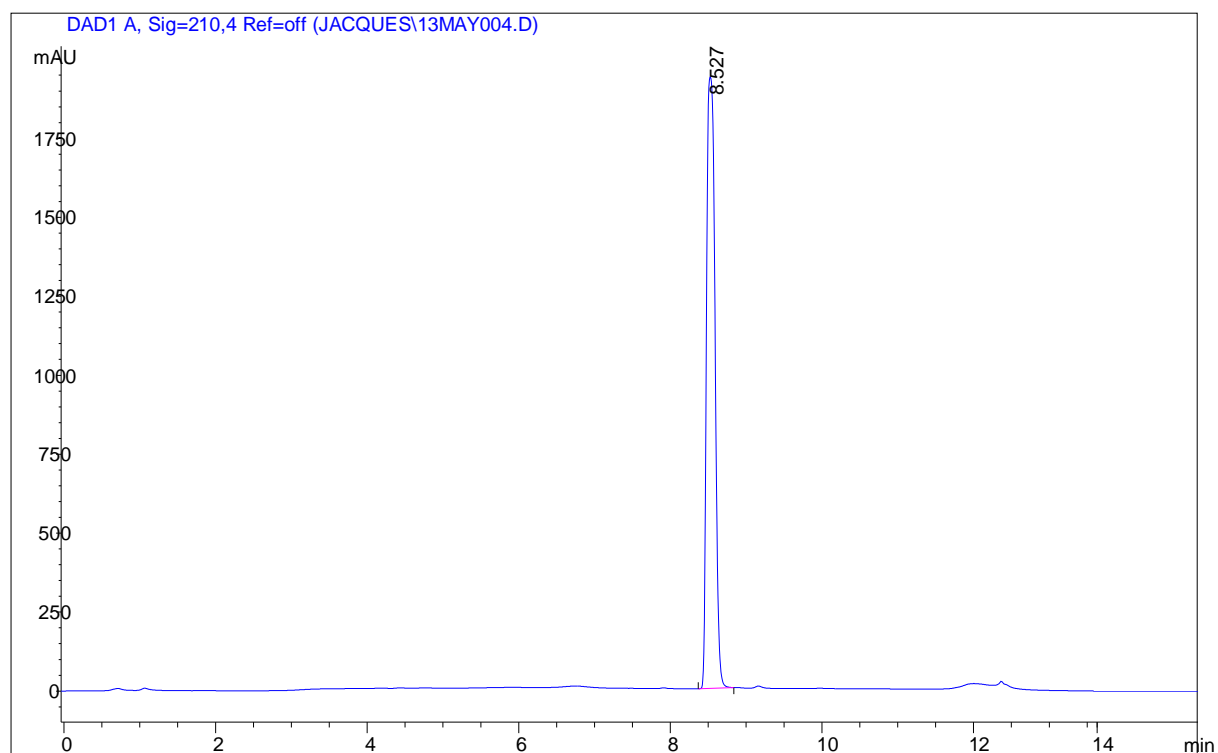
4b: 5-[(3-Chlorophenyl)methoxy]-2H-1,3-benzodioxole



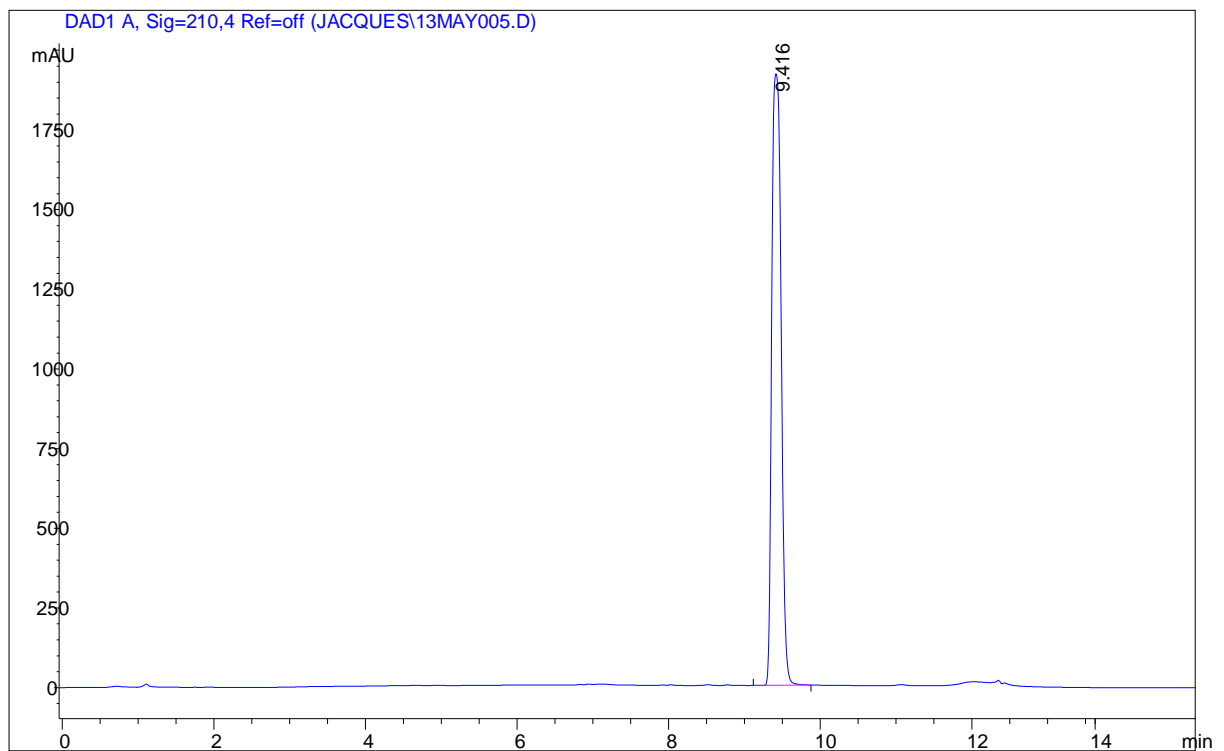
4c: 5-[(3-Bromophenyl)methoxy]-2H-1,3-benzodioxole



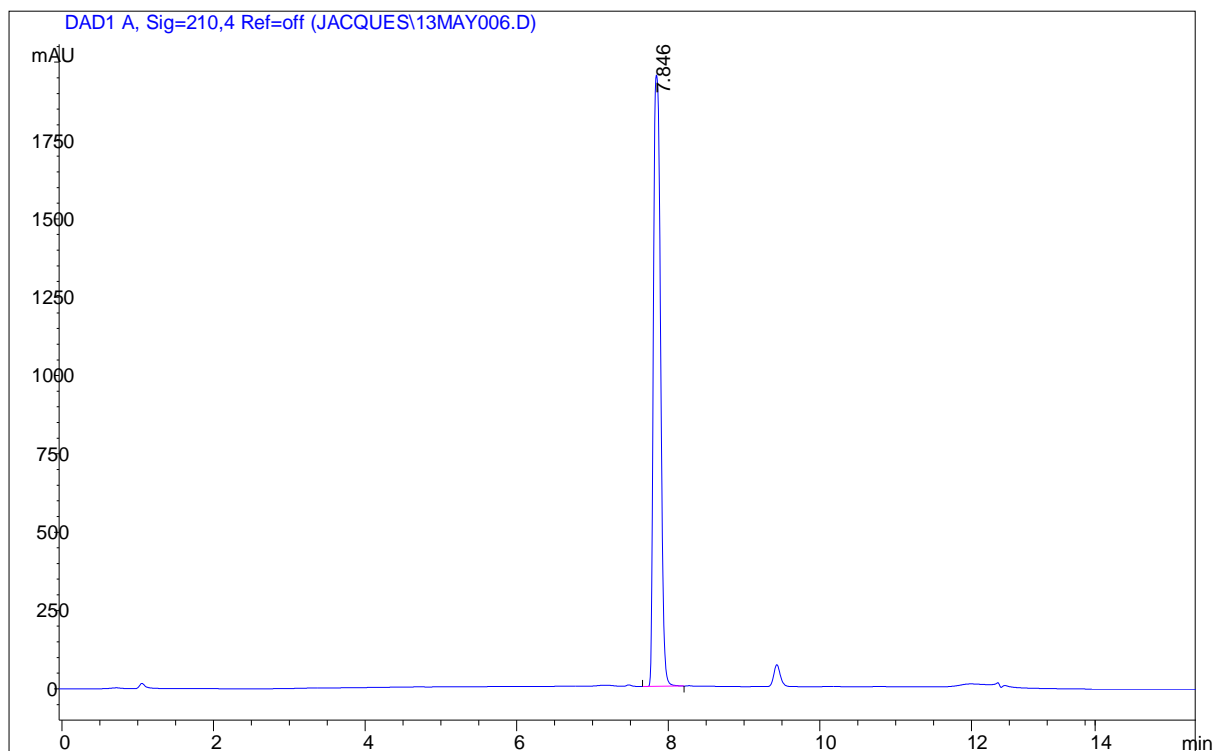
4d: 5-(2-Phenylethoxy)-2H-1,3-benzodioxole



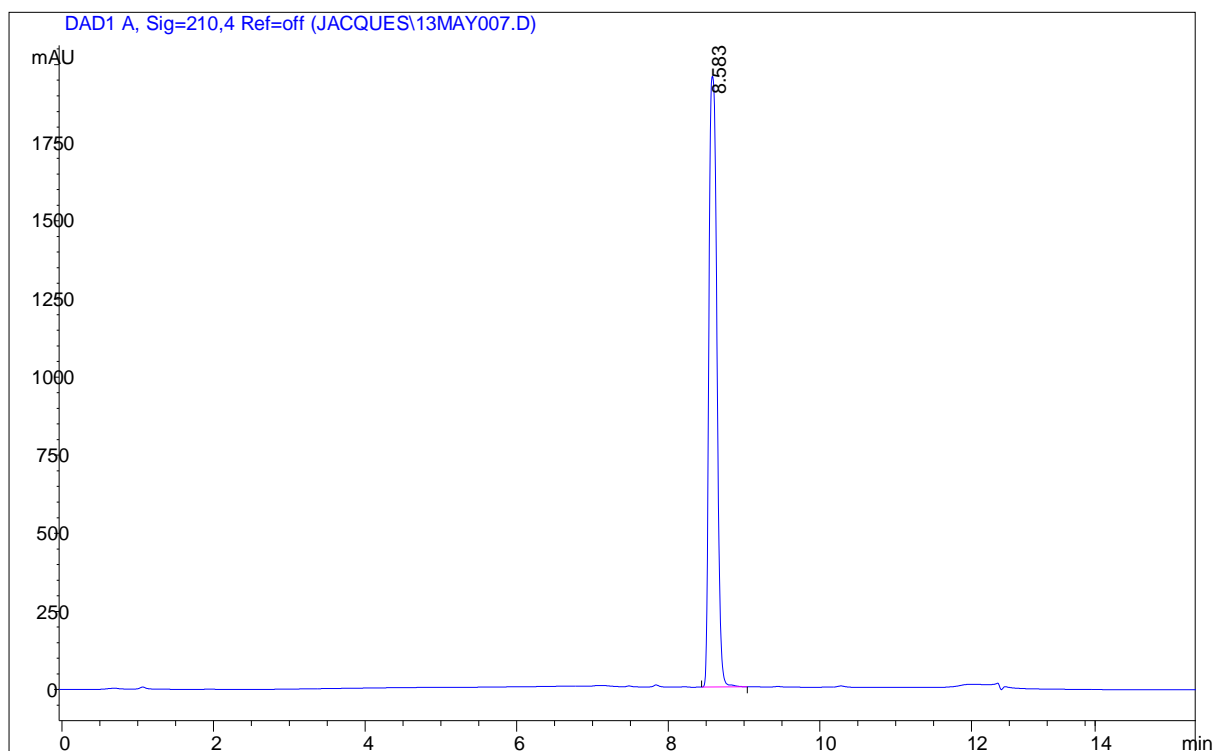
4e: 5-(3-Phenylpropoxy)-2H-1,3-benzodioxole



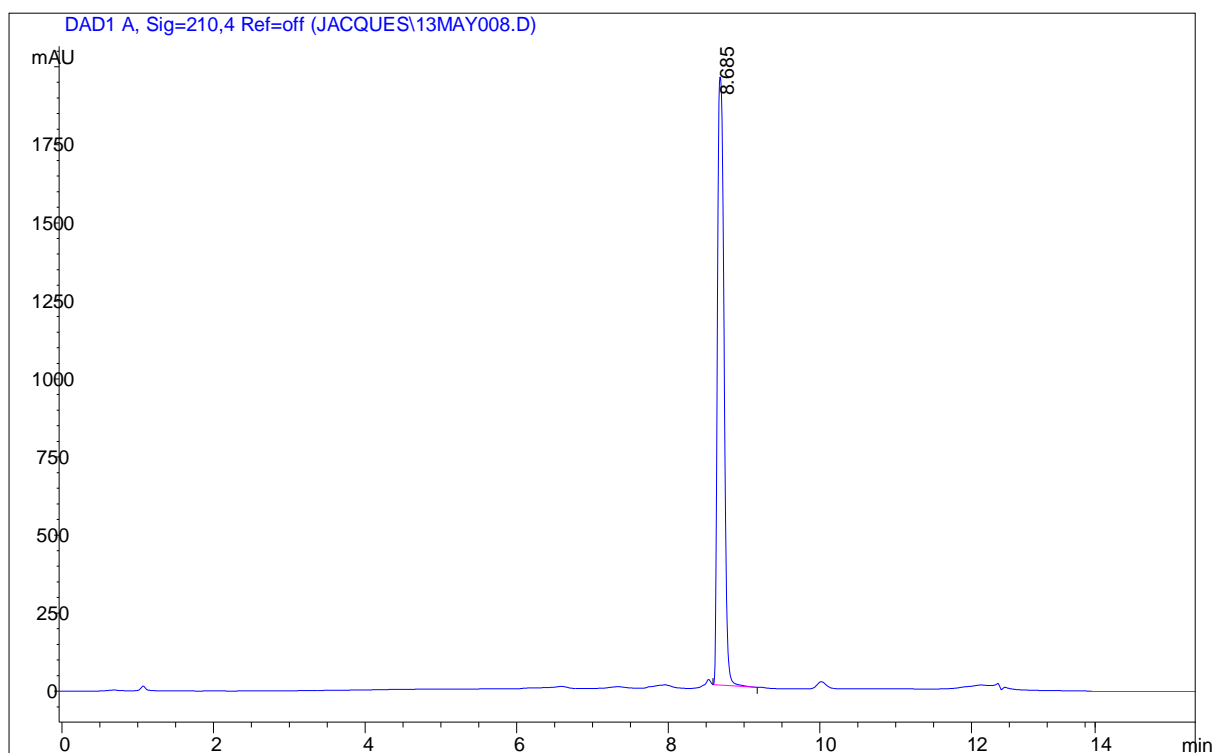
4f: 5-(2-Phenoxyethoxy)-2H-1,3-benzodioxole



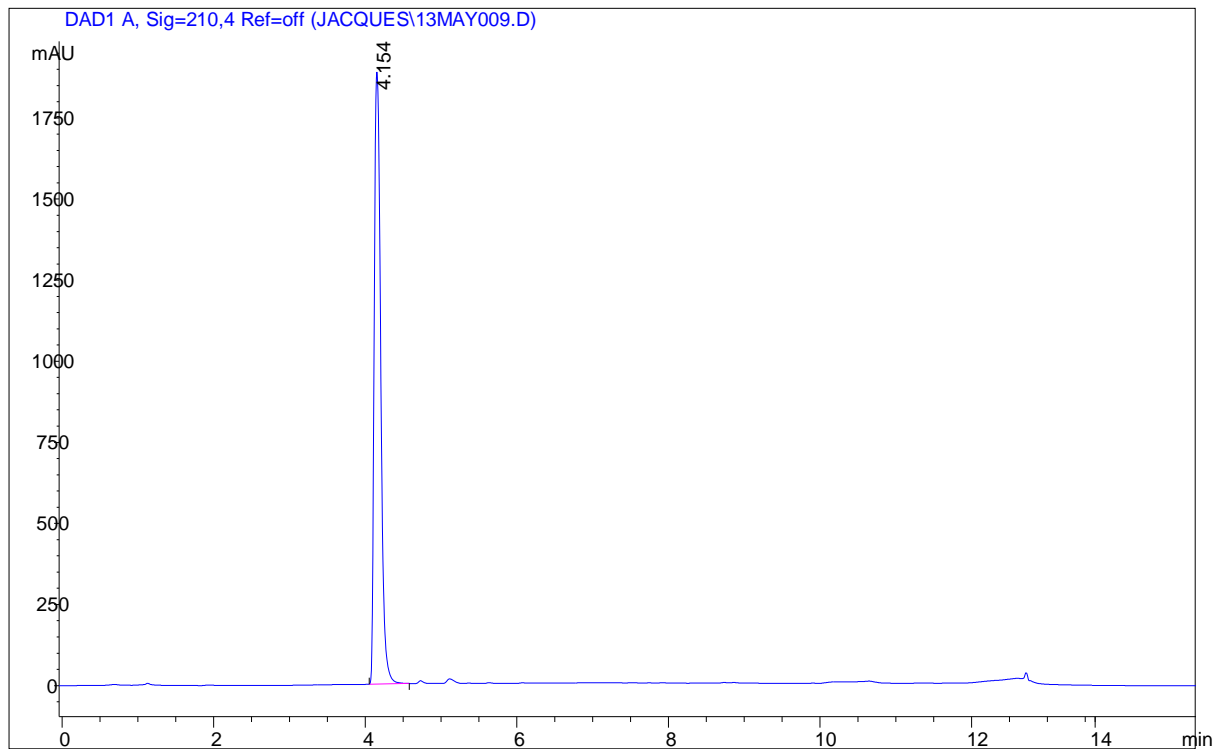
4g: 5-[2-(4-Chlorophenoxy)ethoxy]-2H-1,3-benzodioxole



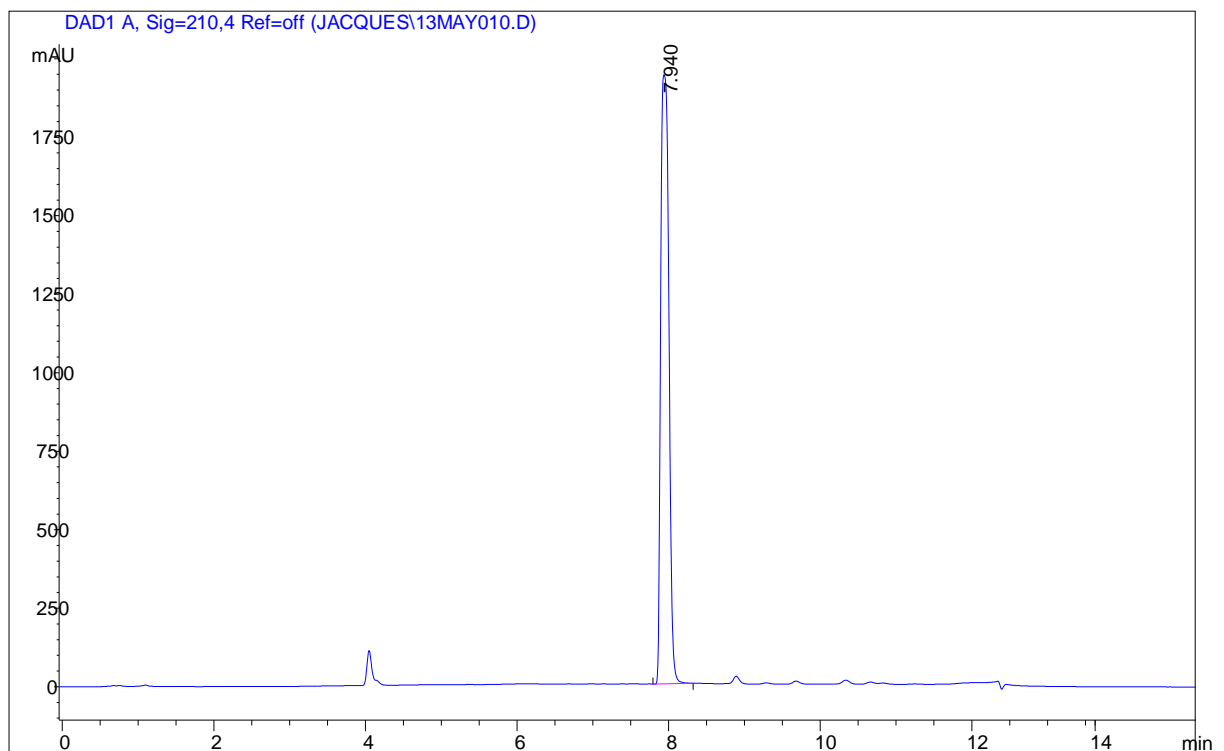
4h: 5-[2-(4-Bromophenoxy)ethoxy]-2H-1,3-benzodioxole



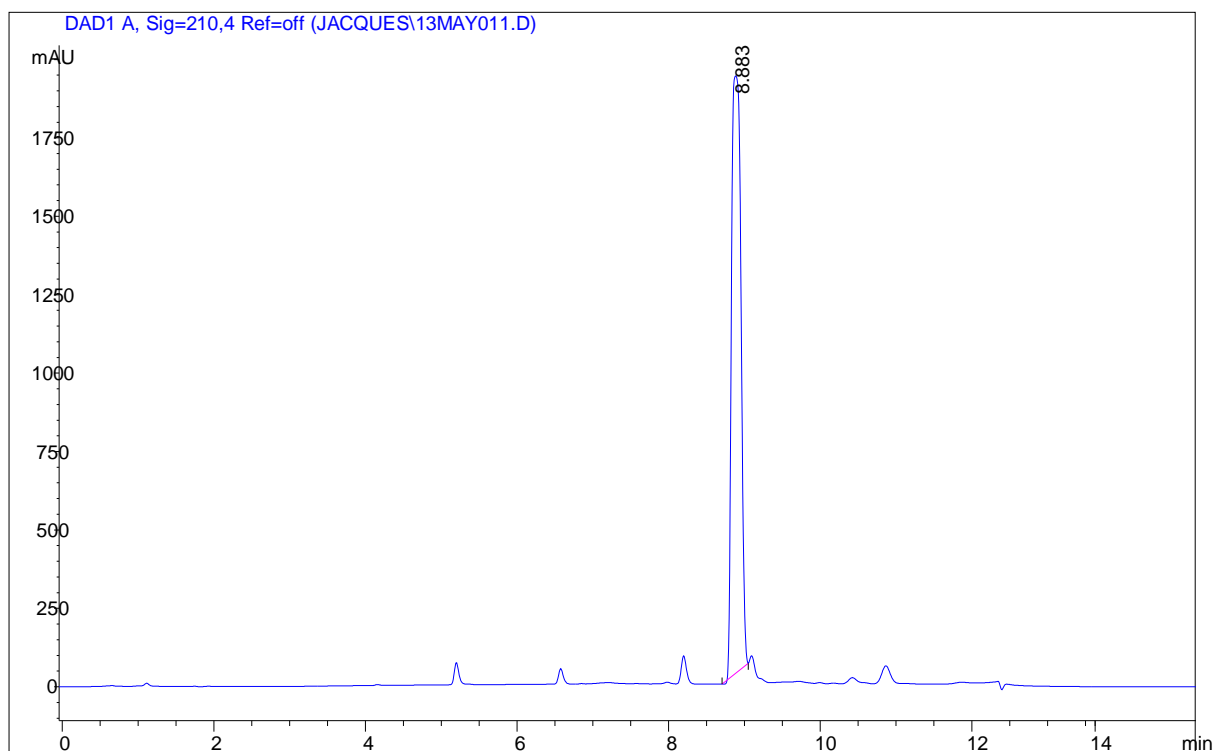
7: 6-Hydroxy-1,4-benzodioxane



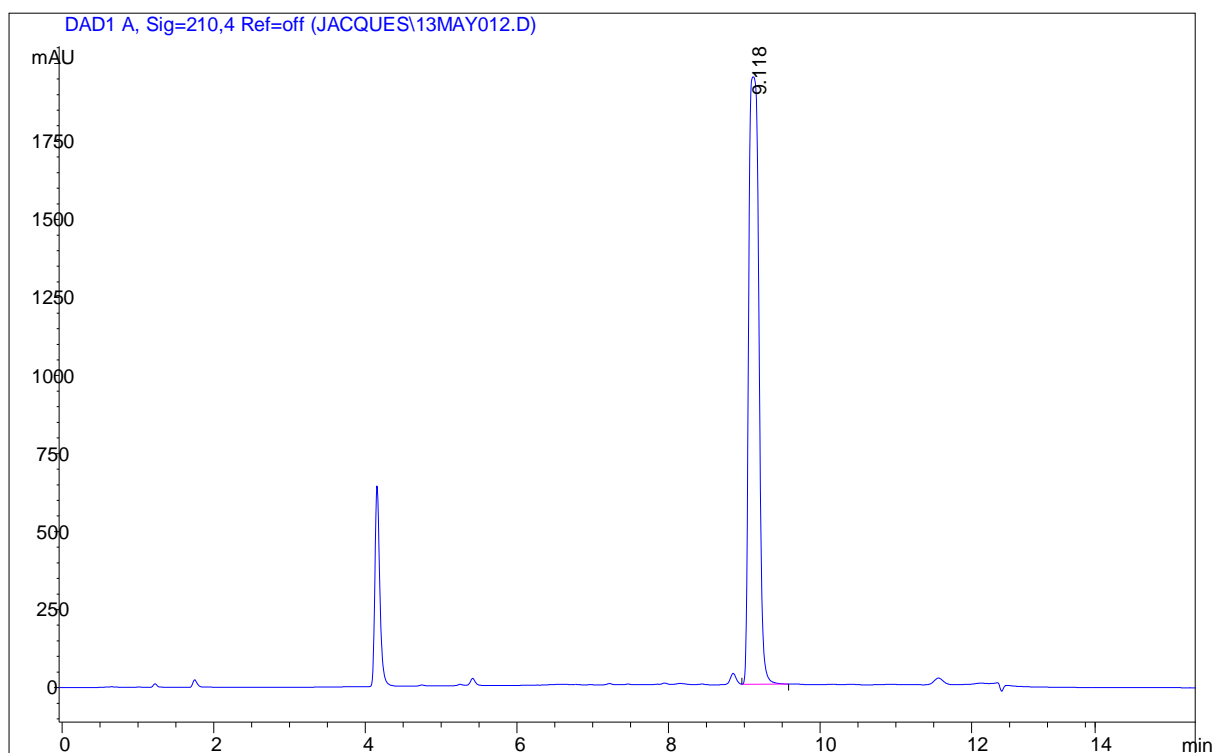
5a: 6-(Benzyloxy)-2,3-dihydro-1,4-benzodioxine



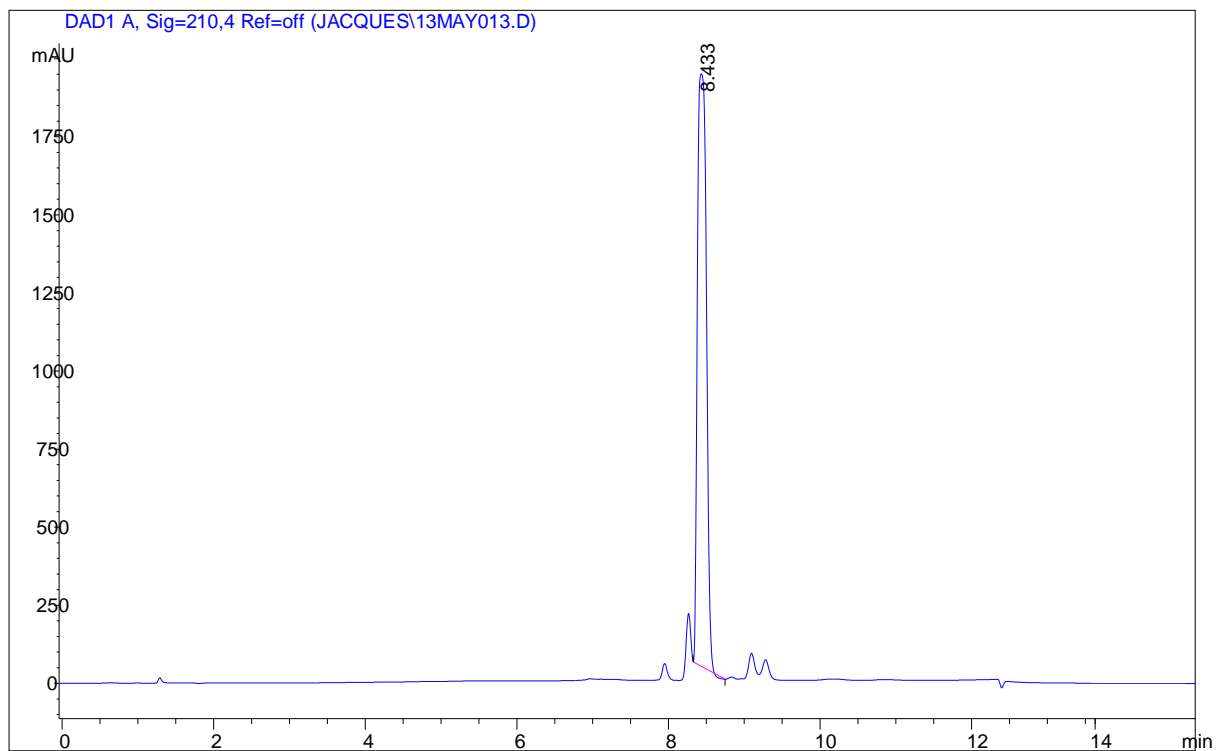
5b: 6-[(3-Chlorophenyl)methoxy]-2,3-dihydro-1,4-benzodioxine



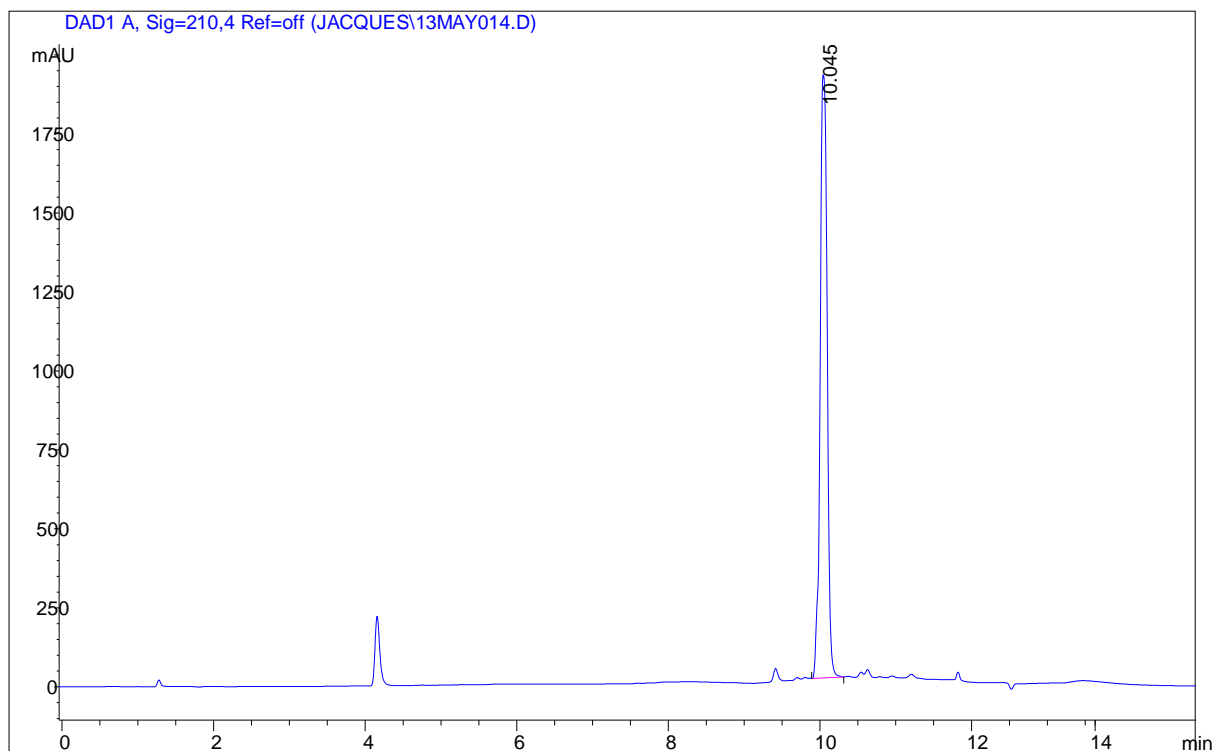
5c: 6-[(3-Bromophenyl)methoxy]-2,3-dihydro-1,4-benzodioxine



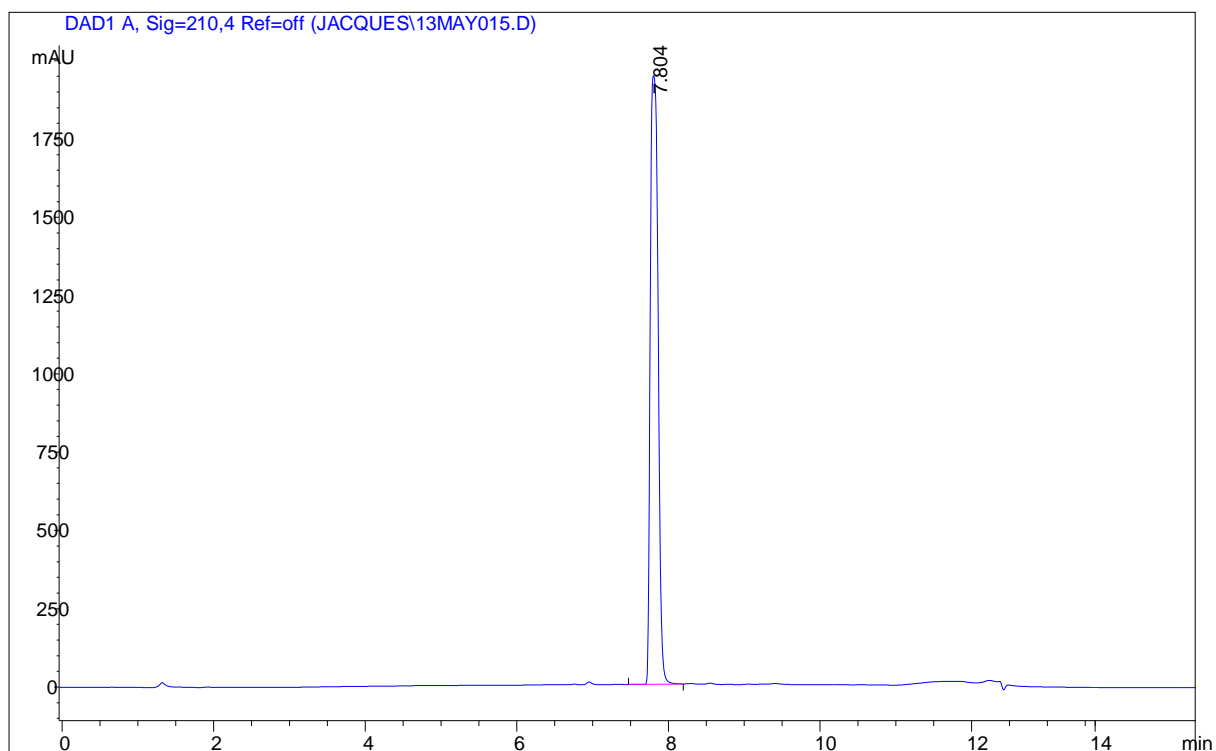
5d: 6-(2-Phenylethoxy)-2,3-dihydro-1,4-benzodioxine



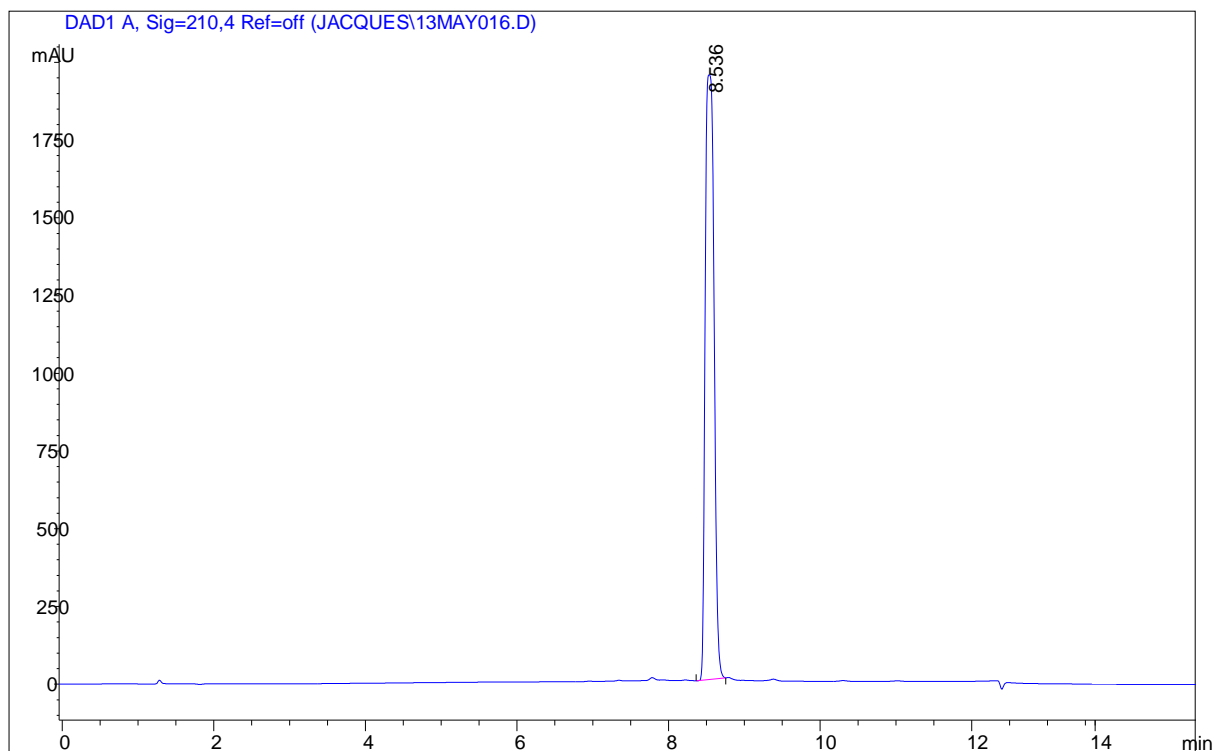
5e: 6-(3-Phenylpropoxy)-2,3-dihydro-1,4-benzodioxine



5f: 6-(2-Phenoxyethoxy)-2,3-dihydro-1,4-benzodioxine



5g: 6-[2-(4-Chlorophenoxy)ethoxy]-2,3-dihydro-1,4-benzodioxine



5h: 6-[2-(4-Bromophenoxy)ethoxy]-2,3-dihydro-1,4-benzodioxine

